Author:
Greening, Paul David

Title:
Dynamic finite element modelling and updating of loaded structures.

UNIVERSITY OF BRISTOL

DEPARTMENTS OF AEROSPACE AND CIVIL ENGINEERING

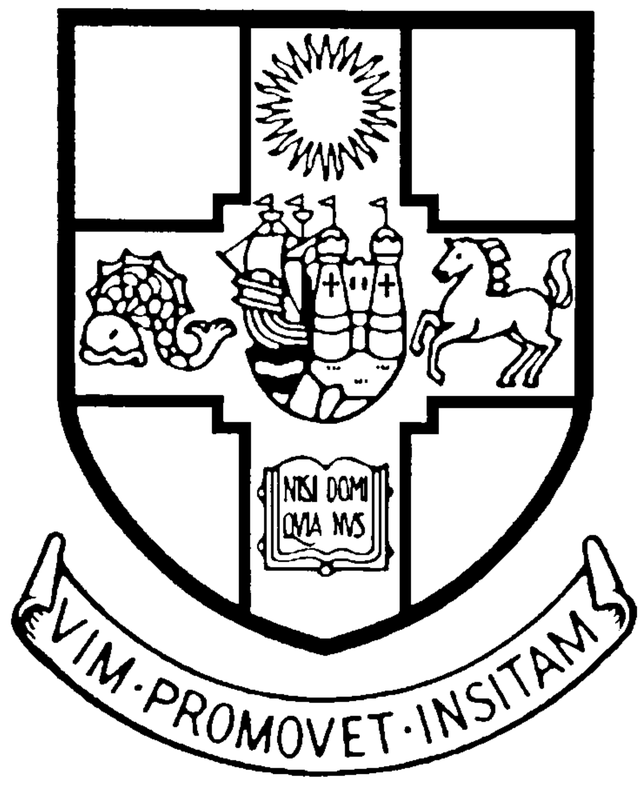

DYNAMIC FINITE ELEMENT MODELLING AND UPDATING OF LOADED STRUCTURES

Paul David Greening

A thesis submitted to the University of Bristol for the degree of Doctor of Philosophy in the Faculty of Engineering

March 1999

ABSTRACT

This thesis is concerned with the application of model updating techniques to structures whose dynamic performance is affected by static loading. The influence of structural loading is identified as important in dynamical terms. As a result, experimentally determined dynamic data should not necessarily be regarded as being uniquely representative of a structure. This observation has particular significance to the likelihood of success of model updating. Indeed the major source of error in dynamic finite element modelling may well be the omission of static loads. There are strong repercussions for schemes which use dynamic data for damage detection.

The methods for including load-effects in dynamic finite element models are outlined. A "static updating" technique which takes into account nonlinear geometry effects is demonstrated by means of experimental case studies. This technique is shown to produce finite element models of structures which match measured dynamic data.

Two new types of updating parameters are introduced in this thesis which allow the effects of loading to be accounted for in a finite element model. The parameters are shown to be suitable for implementation in the popular sensitivity based approach to updating. The first parameter accounts for the effects of stress stiffening in struts or beams and the second allows rigid body rotation of these types of elements. The changes made to beam type elements, while physically realistic, are shown not to be members of the generic beam element family.

The stress stiffening parameter is shown to allow loading in structural frames to be identified from dynamic data even with no *a priori* knowledge of load state. The rigid body rotation term is shown in the case of a 2D beam to allow identification of deformation given limited initial knowledge of the deflected shape. An extension of the latter technique is developed which allows the magnitude of pre-defined deflection shapes or "profiles" can be updated.

An experimental case study is presented in which success is achieved in updating a finite element model of the structure to account for load effects. Axial loads identified in a frame are shown to compare satisfyingly with static measurements of loading. The convergence is found to be reliable and robust, even when including other updating parameters.

A strategy for model updating is proposed which includes the effects of static loading. The approach should be adopted whenever static loading is suspected of influencing dynamic behaviour.

ACKNOWLEDGEMENTS

Thanks are first and foremost due to my advisor, Dr Nick Lieven for his unstinting enthusiasm and encouragement during the course of this project.

I would like to thank my aerospace contemporaries Drs Max Ratcliffe, Rob Levin and Tim Waters for their extensive assistance and advice. I would further like to express my gratitude to colleagues in the civil engineering department for providing a congenial and stimulating working atmosphere as well as offering much support and patience. Credit is also due to David Ward and Matthew Potts for their invaluable technical assistance.

I would especially like to acknowledge Dr Andy Vann and Dr David Wagg with whom I shared many a useful discussion at respectively the initial and final stages of this research.

Thanks are additionally due to the Engineering and Physical Sciences Research Council and the Earthquake Engineering Research Centre at the University of Bristol for their financial support.

DECLARATION

The work presented herein was carried out solely by the author, under the supervision of Dr. N.A.J. Lieven, in the Department of Aerospace Engineering at the University of Bristol, in partial fulfilment of the requirements for the degree of Doctor of Philosophy.

The ideas and results are original except where otherwise acknowledged or referenced, and no part of this work has been submitted previously to any university, college or other institution.

Note that the views expressed in this dissertation are those of the author, and are not necessarily those of the University of Bristol.

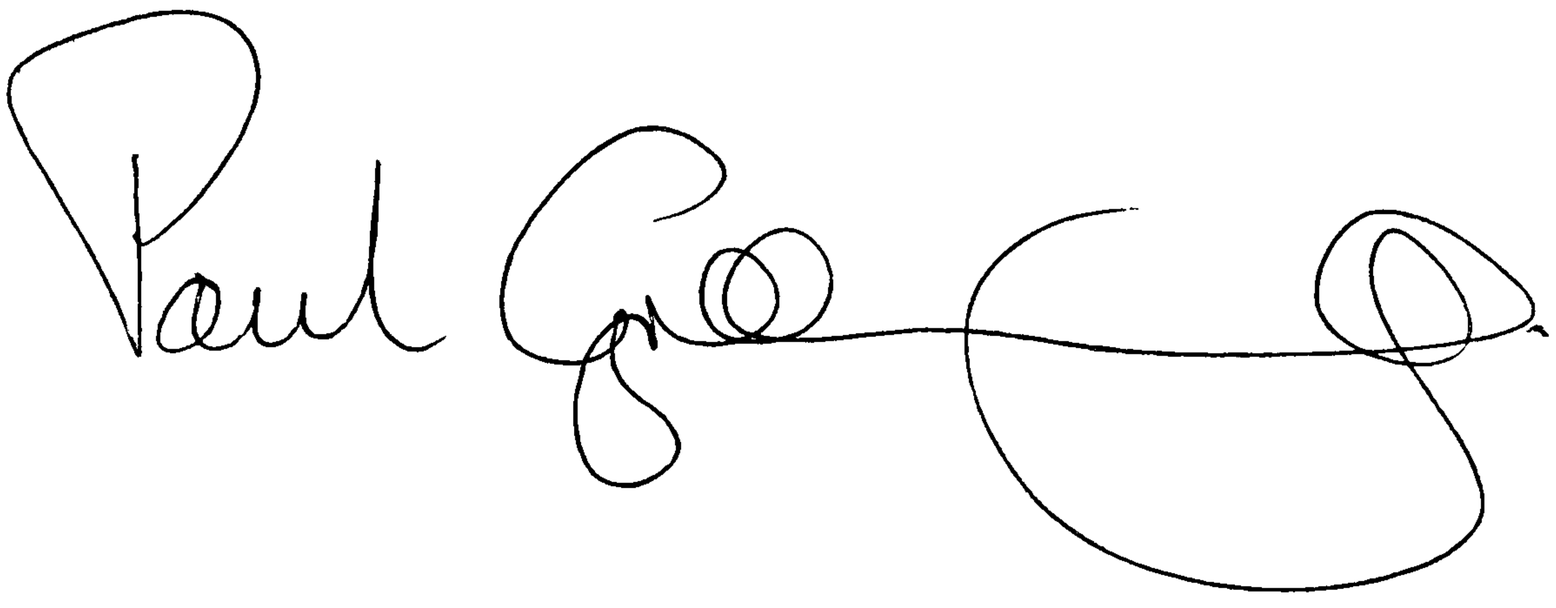

Paul David Greening

PERMISSION TO COPY

Paul David Greening

Adviser : Dr. N.A.J. Lieven

Department of Aerospace Engineering

University of Bristol

I, the undersigned, am willing that this thesis should be made available for consultation in Bristol University Library, for inter-library lending, for use in another library or for photocopy in part or in full - at the discretion of the librarian - on the understanding that users are made aware of their obligations under copyright.

Paul David Greening

$\{\ \}_{exp}$	Experimental vector
$[\ ]^{A}$	Analytical structural matrix
$[\ ]^{U}$	Updated structural matrix
$[\ ]_{e}$	Elemental structural matrix

Roman Letters

i,j,k	indices
x,y,z	co-ordinates
u,v,w	displacements
p	updating parameter
n_{modes}	Number of modes
n_{freq}	Number of frequency points
n_{dofs}	Number of degrees of freedom
n_{p}	Number of updating parameters
n_{e}	Number of elements
R	Residual

Greek Letters

$[\alpha]$	receptance matrix
$[\Psi]$	arbitrarily scaled mode shape matrix
$[\Phi]$	mass-normalised mode shape matrix
$\{\phi\}$	mass normalised mode shape vector
ω	frequency in rads s^{-1}
f	frequency in Hz
η	dimensionless distance along beam

NOMENCLATURE

Wherever possible notation has been defined in the text of the thesis. The following definitions are provided since they are used frequently but are not intended to be an exhaustive list of all notation used.

Abbreviations

FE	Finite Element
FEM	Finite Element Model
MAC	Modal Assurance Criterion
CMP	Correlated Mode Pair
COMAC	Co-ordinate Modal Assurance Criterion
FRAC	Frequency Response Assurance Criterion

Symbols

$\lvert\ \rvert$	magnitude
$\lVert\ \rVert_2$	p_2 (Euclidean) norm
$\lVert\ \rVert_\infty$	p_∞ norm
$\lVert\ \rVert_{frob}$	frobenius norm
$[\ ]$	matrix
$\{\ \}$	vector
$\{\ \}^*$	transposed complex conjugate
$[\ ]^T$	transpose of matrix
$[\ ]^+$	pseudo-inverse of a matrix
$\{\ \}_{FE}$	Finite element vector

$\{\ \}_{exp}$	Experimental vector
$[\ ]^{A}$	Analytical structural matrix
$[\ ]^{U}$	Updated structural matrix
$[\ ]_{e}$	Elemental structural matrix

Roman Letters

i,j,k	indices
x,y,z	co-ordinates
u,v,w	displacements
p	updating parameter
n_{modes}	Number of modes
n_{freq}	Number of frequency points
n_{dofs}	Number of degrees of freedom
n_{p}	Number of updating parameters
n_{e}	Number of elements
R	Residual

Greek Letters

$[\alpha]$	receptance matrix
$[\Psi]$	arbitrarily scaled mode shape matrix
$[\Phi]$	mass-normalised mode shape matrix
$\{\phi\}$	mass normalised mode shape vector
ω	frequency in rads s^{-1}
f	frequency in Hz
η	dimensionless distance along beam

TABLE OF CONTENTS

LIST OF FIGURES

CHAPTER 1

INTRODUCTION

"...the formulation of the mathematical model is the most critical step in any dynamic analysis, because the validity of the calculated results depends directly on how well the mathematical description can represent the behaviour of the real physical system"
Clough R. W., Penzien J. Dynamics of Structures [1]

1.1 Prologue

Computer models of structures provide the engineer with an extremely powerful tool for understanding their behaviour. A great deal of information about structural performance can potentially be obtained from simulations without the expense of undertaking structural testing of prototype structures. Unlike practical experimental testing, the number of scenarios which can be examined are almost boundless; it becomes possible to load a structure up to - and beyond - failure as often and in as many ways as the engineer desires!

The particular ability to model dynamic structural behaviour allows structures to be designed in the most cost effective and safe manner. This mitigates against the adverse effects of excessive vibration. There is, of course, an economic case for producing ever lighter, cheaper structures. However, this must not be achieved at the expense of safety, reliability and durability, each of which is strongly influenced by structural dynamic behaviour.

Computer-models can be built with some confidence from knowledge of the structure's geometry and material properties. This confidence in the quality of the model can be enhanced if the computer model can in some way be compared with experimental measurements from a prototype structure. A mismatch between experimental and analytical measurements motivates a process whereby the analytical model is altered to provide a closer agreement with experimental readings. The hope and expectation is that the altered model provides an improved representation of the prototype structure.

The ability to alter an *a priori* analytical model of a structure from test data further opens the possibility that the finite element model can be treated as a store of knowledge. This "encyclopaedia" of the structure's condition allows the computer model to be re-adjusted to account for time varying changes to structural response. In terms of structural monitoring, dynamic measurements can be thought of essentially as a signature of a structure. Thus, changes to this signature represent change to the structure itself.

1.2 Structural Modelling

A closed form differential equation approach to modelling the behaviour of structures is possible only in the simplest cases, such as beams and plates. In the late fifties an approximate approach involving discretisation of structures into a potentially large number of sub elements, whose behaviour is known, came to prominence. The so called finite element (FE) method allows the stiffness and mass distribution of a structure to be described in matrix terms with rows and columns representing the active degrees of freedom.

A finite element model of a structure can be used for calculating response to both static and dynamic loading. Many of the choices have to be made by an experienced engineer. Estimates of material properties will often be textbook values and geometric properties may be based upon the initial design rather than the measured configuration. The finite element model and associated predictions of static and dynamic behaviour of any structure is not unique. Indeed the well known DYNAS survey [2] and a more recent survey by Lloyd's Register [3] show large variations in prediction of dynamic structural behaviour by a number of finite element models of the same structure by different practitioners. Several important factors can be identified as being responsible for poor prediction of dynamic response. These principally include:

- mis-estimation of structural material properties;
- inaccurate modelling of structural geometry;

- poor choice of element type and quantity required; and
- difficulty in modelling complex structural components, the most common and widespread being the pitfalls which attend the modelling of structural joints.

Further errors in dynamic prediction of finite element models can arise due to model reduction. This is undertaken for FE models with very large numbers of degrees of freedom to reduce the size of the eigenvalue problem.

1.3 Dynamic Measurements

Vibration is a characteristic common to all engineering structures, from the smallest electrical components to the largest bridges and dams. The effect of vibration upon structural performance can be instrumental in causing fatigue, discomfort or ultimately structural failure.

The dynamic characteristics of a structure - even measured at few points spatially on a structure - offer a great deal of information about the structural form. Consequently, the use of dynamic data for characterising structural behaviour has long been popular. The well known example of striking solid train wheels and assessing their integrity based on the audible response of the wheel is a good example.

The field of modal analysis is concerned with characterising the dynamic behaviour of structures from experimental data. The methodology for dynamically testing structures and identifying modal behaviour is set out clearly in [4]. Dynamic test data are most commonly described in terms of a modal model consisting of resonant frequencies and mode-shapes. A process of modal identification is required to process raw measured data into this format. Corresponding predictions of dynamic behaviour can be determined from a finite element model using eigenvalue extractions techniques.

Comparison of experimental and FE data in the modal domain is used extensively in this thesis.

1.4 Correction of FE Model Using Dynamic Data

Every attempt should be made to use realistic, or better still, measured parameters in the process of building the finite element model as section 1.2 has indicated. However, there is still likely to be some error in the finite element model.

The comparison of predicted structural dynamic behaviour with experimentally measured data allows a great deal of insight into the likely sources of error in the finite element model. This has been motivated by the requirement to improve the finite element model of a structure. A large number of techniques have been developed whereby analytical FE models of structures are altered such that their dynamic characteristics become a closer match of experimentally determined behaviour.

Today, the "correction" of finite element models in this way is extremely widespread especially when the main purpose of the finite element model is to understand dynamic rather than static behaviour. A range of techniques exist for altering finite element models. At the most simple, it is very common to make a small number of changes to the overall properties of a finite element model in a number of iterations. This type of process involves a large amount of intervention from an engineer to assess the level of improvement in the dynamic predictions of the FE model. The engineer also has to ensure that changes made to the finite element model are realistic. While a perfectly acceptable approach, this manual technique is labour intensive and relies on the intuition of the engineer to identify possible sources of error in the finite element model. Finite element model updating is an alternative to these manual techniques. The methods allow changes to be made in an *automatic* sense. Several different approaches to model updating have been developed. Methods regarded as being of most use involve an optimisation scheme whereby a number of structural parameters (updating parameters) are altered to minimise an objective function. Limitations upon the amount of information available from experimentation curtail the number of updatable parameters. Factors upon elemental mass and stiffness are undoubtedly the most popular updating parameters. The procedure is iterative with changes made to the finite element model at

each step. The objective function is a formulation of the differences in dynamic behaviour between the experimental data and the finite element model. This is recalculated at each stage of the iteration. While continuing to be an active area of research, efforts to achieve robust model updating have achieved little success.

One important aspect of finite element model updating is that there exists much confidence in the experimental dynamic data and less in the finite element model itself. The concentration upon the finite element model as being in error stems partly from the fact that finite element modelling and modal analysis are often treated as separate disciplines. It is common for the two areas to be conducted by different departments in research and development organisations. An awakened interest in the possibility that any single set of dynamic data is not uniquely representative of the structure offers new challenges to model updating. This thesis takes up the mantle by considering how finite element model updating can be adapted to account for time varying (transient) changes in dynamic behaviour.

1.5 Variations in Dynamic Readings

Given the inevitable uncertainty in the veracity of the initial finite element model, the motivation for using experimental data to improve upon initial assumptions is clear. The experimental dynamic data are thus treated as being *uniquely* representative of the structure. Additionally, the collection of large numbers of sets of experimental data or the construction of a number of prototypes is an expensive undertaking. It is not surprising then that the potential variance in dynamic measurements either from:

(a) a single structure under a variety of conditions; or

(b) nominally identical structures;

have been given comparatively little attention. Fregolent *et al.* [5] specifically consider case (b). They provide a case study of using an FE model to characterise the behaviour

of a family of structures with nominally identical properties. Several papers by Imregun, for instance [6] and [7] consider a similar problem.

The experimental work presented by Fregolent *et al.*, as is common practice, seeks to test the experimental structure in very carefully controlled laboratory conditions. The purpose is to produce noise-free and consistent results. Generally, structures are tested in isolation from the surroundings. The quest for less obtrusive supporting conditions is an active research area; Carne and Dohrmann [8] for instance investigate the effect of supporting conditions in some detail.

The result of testing structures in free-free conditions is twofold. A good consistency of results can certainly be achieved. However, the results only represent the test structure under the specific conditions which exist at the time of testing.

In both the laboratory regime, and especially in more practical situations, the variation of dynamic data from the same structure - case (a) above - is increasingly being recognised as an important factor which must be considered. For instance, recent work by Woon and Mitchell [9] found that ambient laboratory temperature was responsible for subtly altering material properties and thus changing the dynamic behaviour of a simple plate specimen. At the other extreme engineers attempting to characterise the dynamic behaviour of large civil engineering structures such as bridges, buildings and dams frequently report differing dynamic behaviour being identified from the same structure at different times. Alampalli [10] for instance, presents widely variable baseline results from tests on a highway bridge under different conditions. The variation in measurements is attributed to the in-service environment, signal processing factors and variation amongst operators. The dynamic measurement of the bridge was motivated by the hope that changes to the vibration signature would enable areas of damage or deterioration to be located. Most disturbingly, it is reported that the variations in baseline modal data can be greater than the changes resulting from damage.

If the application of model updating strategies outside of the laboratory is to become practicable, a clear requirement exists for a unique baseline measurement of the

dynamic behaviour to be available or for the factors which alter the dynamic behaviour to be accounted for in finite element models.

1.6 Load Dependence of Dynamic Behaviour

Amongst the plethora of factors which effect dynamic behaviour, the effect of load upon structures stands out as being an important factor requiring closer consideration.

Structures by their very nature are called upon to carry loading. Table 1.1 for instance, sets out a selection of possible structural loading scenarios. The effect of loading is well known to cause changes to dynamic behaviour. The influence of axial load on a column's transverse vibration as well as the change in pitch of stringed instruments with wire tension are both good examples.

Load	Cause	Examples
External	Thermal	Space structures, bridges, aircraft, aeroengines
	Static steady state	All civil/mechanical structures
	Pseudo static	Aircraft manoeuvres, helicopter rotor blades
Internal	Manufacturing induced stress	machined component (grinding, milling, welding), composite materials (rates of cure), residual stress
	Lack of fit	Machined components with poorly defined tolerances
	Work hardening	Ageing aircraft

Table 1.1 - Sources of Static Stress in Structures

The specific effect of loading upon dynamic behaviour when comparing with finite element models appears to have been overlooked for several reasons. In laboratory conditions, every attempt is made to isolate a test structure from its surroundings, which results in no load being transmitted. For in-situ testing, there is a generally low expectation of accurate results leading to a culture where the reasons for discrepancies between expected and measured dynamic data are not specifically investigated.

1.7 Combined Static and Dynamic Load Identification

The consideration of the interaction between static and dynamic loading is particularly opportune since developments in sensor technology are fuelling interest in monitoring of both static and dynamic behaviour of *in-situ* structures. The ability to monitor structures in this way is principally bought about by improvements in strain gauge technology.

The use of piezoelectric transducers to measure strain to very high resolution is described in [11]. Such gauges have recently become available commercially, the performance of one such product is described in [12] where resolution of signals of an astonishing three orders of magnitude better than the common resistive type of gauges are quoted. While this type of gauge is currently very expensive it is clear that the future offers the possibility that strain will not continue to be the poor relation of translational quantities in terms of measurement fidelity.

The use of optical fibres for structural monitoring offers the opportunity to monitor structural behaviour at large numbers of locations about the structure, over a long period of time and at relatively modest cost. The specific use of this equipment to measure strain has received attention recently. A so-called Bragg grating system, for instance, involves treatment of short sections of a fibre optic cable which when bonded to a structure allows strain at that point to be determined remotely from processing of emitted and reflected light signals. Such a system comprising 64 strain gauge channels is described in [13]. The optical fibre in this case is mounted on the soffit of a bridge and allows the response of the bridge to be sampled at frequencies of up to 360Hz. This implies a useful range of up to 180Hz[1] although in this case resolution at a range of up to 45Hz was used.

---

[1] This is the Nyquist frequency. For this particular structure, the 0-180Hz range allows a great deal of the dynamic behaviour to be spanned. The sampling rate of strain data using this particular technique is a function of the number of gauging positions along each optical fibre.

A clear research opportunity exists to consider the interaction of the static and dynamic components of strain on structures so that the static effects can be accounted for during dynamic updating of finite element models. This area is investigated in this thesis.

1.8 Scope of Thesis

This thesis seeks to extend the possibility of using model updating techniques to structures whose dynamic behaviour is affected by the transient effects described in the preceding sections. Specifically the influence of structural loading is identified as a source of variability of dynamic behaviour. As well as demonstrating the effect of loading upon dynamic response, several methods of including this effect in finite element models are explored to help to improve the chances of successfully identifying permanent errors in the model.

The background to finite element model updating and in particular the evolution in choice of updating parameters is presented in chapter 2. A simple case study using measured experimental data is presented which allows some of the shortcomings of model updating to be demonstrated.

Chapter 3 introduces the changes to finite element modes which arise from static loading using a nonlinear geometric approach. The potential effects on dynamic readings due to static effects are also outlined.

The methods introduced in chapter 3 are implemented in chapter 4 with respect to measured static experimental data. The results are compared with experimental data. Loading is measured accurately but indirectly using strain gauges allowing the issue of load identification to be addressed practically. Additionally, the difficulty in identifying a set of unique modal data corresponding to zero loading is addressed.

Chapter 5 introduces a novel approach which allows load dependent structural properties to be updated from dynamic measurements. The methods are validated using a number of simulated experimental case studies.

A comprehensive experimental case study is presented in chapter 6 in which experimentally measured dynamic data is used to update a finite element model. A methodology is proposed for dynamic model updating in the presence of static structural loads. In addition, the author proposes a method for identifying static loads from dynamic data. The results are discussed in detail and directions for future research indicated.

1.9 Notes on Thesis

Nearly all of the finite element work described in this thesis was performed in MATLAB [14] using the finite element toolbox CALFEM [15] developed as a teaching tool at Lund University, Sweden. The basic package - developed for educational purposes - was augmented substantially by the author to include 3D stress stiffening effects and nonlinear geometry capabilities. Additional FE modelling work and validation of the MATLAB code was performed using ANSYS version 5.4 [16]

Throughout this thesis two example structures are introduced and revisited several times. While any particular experimental arrangement cannot be expected to be representative of all structures, the two experiments were designed to allow many aspects of the effect of loading on structures to be examined. Both arrangements are the subjects of extensive analysis which in turn is compared with a large volume of experimental work.

For reasons of brevity and simplicity, the numerical examples and experiments presented in this thesis relate to the study of frameworks made up of beam type elements. They are undoubtedly the most popular element type and particularly important in modelling of civil engineering structures. Where appropriate the application of the methods to other element types is described.

The first stage in the validation of new updating methods is generally carried out by simulating experimental data, with the use of experimentally measured data something of a rarity. Both methods are used in this thesis with the distinction being made as clear

as possible. Simulated experimental data are referred to by enclosing the word experimental in quotation marks. Whenever measured data is referred to, in all cases it derives from experimental modal analysis.

The standard notation for modal testing and analysis set out in [17] is used wherever possible throughout this thesis.

CHAPTER 2

FINITE ELEMENT MODEL UPDATING USING EXPERIMENTAL DATA

2.1 Introduction

As the previous chapter has outlined, the goal of finite element model updating is to use experimental data to improve the accuracy and hence quality of an analytical finite element model of a structure. Much work has been expended in the last twenty years in developing and improving methods to help to meet this target. While a vast amount of literature related to the mathematical treatment of the model updating problem exists, evidence of the use of updating techniques being applied to measured data to solve practical problems is - by contrast - scant.

The purpose of this chapter is to introduce some of the concepts which will be used later in the thesis as well as reviewing the state of the art in related fields. The following sections present a brief introduction to the finite element method and to modal testing. Developments in finite element model updating are then considered with particular reference to the evolution of parameters amenable to updating. A review of literature related to the use of measured experimental data to update finite element models is also presented.

The chapter is concluded by means of a simple case study which allows some of the topics related to conditioning of updating problems, choice of parameters and validity of the solution to be examined with reference to experimentally determined data.

2.2 The Finite Element Method

The development of the finite element method has its roots in the aircraft industry in the 1950s where the problem of analysing complex aeroplane structures stretched the

available analytical methods of the day. Courant [18] is generally credited with proposing a method which was destined to be highly suited for implementation on digital computers. Papers by Turner *et al.* [19] and Argyris and Kelsey [20] laid the foundations for the finite element method as it is used today. The term finite element was first used by Clough *et al.* in 1960 [21]. The use of finite element methods has burgeoned in the intervening period. Huge rises in the size and complexity of structural problems amenable to FE modelling as well as an increase in the variety of elements available to the engineer have been observed. Today a vast amount of literature is devoted to the subject; Zienkiewicz [22] and Bathe [23] for example provide a comprehensive coverage of the field.

The finite element method has been adopted by a number of areas of engineering such as heat transfer and magnetic field analysis. In this thesis, the original application of structural engineering is considered. In this domain, the technique broadly consists of discretising a structure into a number of small substructures. This allows the displacement or stress in these elements to be approximated, the latter being the most common approach. These elements must then be assembled in such a way that stresses are continuous across element interfaces and the internal stresses are in equilibrium both with each other and with the applied loads. The finite element method can thus be thought of as a two stage process, the first being the construction of finite elements and the second their assembly into structural matrices.

Many aspects of the finite element method can be best described by means of example. To this end the construction of 2D beam stiffness and mass elements are described in sections 2.2.2 and 2.2.4. The 2D beam element and its 3D counterpart are employed extensively in this thesis; however the method by which the elements are generated can be applied to a wide range of different element types. The following sections briefly outline other relevant aspects of the finite element method in particular the issue of transformation of finite element co-ordinates which forms the basis of a deformation updating technique presented in chapter 5.

2.2.1 Matrix Structural Analysis

The most common problem arising in structural analysis is to determine the deflection arising from a set of static loads. If the loads at a number of points about a structure - or *degrees of freedom* - are defined by a vector $\{F\}$ and the displacements at the corresponding points are similarly defined $\{x\}$, a matrix stiffness $[K]$ is required to relate the load and displacement.

$$\{F\} = [K]\{x\} \tag{2.1}$$

Of most interest to dynamicists is a similar formulation which includes inertia and damping terms

$$[M]\{\ddot{x}\} + [C]\{\dot{x}\} + [K]\{x\} = \{F\}, \tag{2.2}$$

where $[M]$ is the mass matrix describing the distribution of mass about the structural degrees of freedom and $\{\dot{x}\}$ and $\{\ddot{x}\}$ are the first and second derivatives of the displacement with respect to time. Note that the force applied to the system is now a function of time. While mass and stiffness of a structure are measured and relatively easily derived, the mechanism whereby energy is lost through damping is less easily modelled. The viscous damping model represented by matrix $[C]$ in equation (2.2) is commonly but by no means exclusively used[2], being proportional to velocity. Structural damping is an important area of structural dynamics which has deservedly received much attention. Of most importance is that damping dominates the *amplitude* of vibration around resonance [4]. Since this thesis is more concerned with modal *placement* than amplitude dependency the consideration of identification of damping parameters will not be discussed in any great detail herein.

---

[2] Hysteretic (or structural) damping is also commonly used, being represented by the matrix $[H]$ in the equation $[M]\{\ddot{x}\} + [H]\{x\} + [K]\{x\} = \{F\}$.

The *undamped* equation of motion from (2.2) is

$$[M]\{\ddot{x}\}+[K]\{x\}=\{F\}. \tag{2.3}$$

For free (unforced) vibrations the following relationship is obeyed

$$[M]\{\ddot{x}\}+[K]\{x\}=0, \tag{2.4}$$

the solution to which can be written in the form

$$\{x\}=\{\Psi\}_j e^{i\omega_j t}, \tag{2.5}$$

where the ω_j are the resonant frequencies. Substituting back into (2.4) leads to the well known eigenvalue problem

$$[K]\{\Psi\}_j=\lambda_j[M]\{\Psi\}_j, \tag{2.6}$$

where

$$\lambda_j=\omega_j^2, \tag{2.7}$$

and $\{\Psi\}_j$ can be thought of the *mode shapes* corresponding to the system natural frequencies $\{\omega\}_j$.

While the eigenvalues have an exact relationship with the resonant frequencies, the eigenvectors are arbitrarily scaled; it is common practice to define a uniquely scaled set of eigenvectors such that

$$[\Phi]^T[M][\Phi]=[I]. \tag{2.8}$$

This results in

$$[\Phi]^T[K][\Phi]=diag(\lambda), \tag{2.9}$$

where $[\Phi]$ is the matrix of *mass normalised* eigenvectors.

2.2.2 The Two Dimensional Beam

Elemental stiffness matrices are most commonly created using assumed displacement fields, the method for which is given in appendix A. The derivation presented therein is general and can be applied to any element type and proposed displacement field. The construction of the elemental stiffness matrices of a 2D beam is described in this section using the techniques and notation set out in appendix A.

Consider first the axial loading of such a beam, shown in figure 2.1. From equation (A.13) in appendix A, the displacement of a general point in the bar is related to the end displacements of the bar by the *shape function*.

$$\{u\} = [N]_e \{\Delta\}_e . \tag{2.10}$$

For the axial displacement of the beam, the shape function is trivial and can be inserted directly into (2.10) leading to

$$\{u\} = \begin{bmatrix} \frac{L-x}{L} & \frac{x}{L} \end{bmatrix} \begin{Bmatrix} \Delta x_1 \\ \Delta x_2 \end{Bmatrix}. \tag{2.11}$$

From equation (A.15) the *strain displacement* matrix - $[B]$ - is defined as

$$[B] = [\partial]^T [N], \tag{2.12}$$

thus for the 2D beam

$$[B] = \frac{\partial}{\partial x}\left(\begin{bmatrix} \frac{L-x}{L} & \frac{x}{L} \end{bmatrix}\right) = \begin{bmatrix} -\frac{1}{L} & \frac{1}{L} \end{bmatrix}. \tag{2.13}$$

The elemental stiffness matrix from (A.17) is

$$[K]_e = \int_V \left([B]^T [E][B]\right) dV = \int_0^L \begin{Bmatrix} -1/L \\ 1/L \end{Bmatrix} E \begin{bmatrix} -\frac{1}{L} & \frac{1}{L} \end{bmatrix} A dx = \frac{AE}{L} \begin{bmatrix} 1 & -1 \\ -1 & 1 \end{bmatrix}, \tag{2.14}$$

which is intuitively correct and could have been ascertained directly. However, it is the exception rather than the rule that elemental matrices can be constructed "by observation".

The lateral displacement of a beam undergoing shearing and rotational loading (shown in figure 2.2) can be shown from elementary theory to be of cubic order and hence the generalised expression for lateral displacement can be expressed as

$$u = \begin{bmatrix} N_1 & N_2 & N_3 & N_4 \end{bmatrix} \begin{Bmatrix} \Delta y_1 \\ \Delta \theta_1 \\ \Delta y_2 \\ \Delta \theta_2 \end{Bmatrix}. \tag{2.15}$$

A set of cubic functions [24] is required to express the shape functions N_i

$$N_1 = 1 - \frac{3x^2}{L^2} + \frac{2x^3}{L^3}, \tag{2.16}$$

$$N_2 = x - \frac{2x^2}{L} + \frac{x^3}{L^2}, \tag{2.17}$$

$$N_3 = \frac{3x^2}{L^2} - \frac{2x^3}{L^3}, \tag{2.18}$$

and

$$N_4 = \frac{x^2}{L} + \frac{x^3}{L^2}. \tag{2.19}$$

It is important to note that these expressions are assumed and are not necessarily exact or unique. Thus while leading to a viable finite element, the result will be one of an infinite number of similarly viable but subtly different elements, this non-uniqueness is exploited by so-called generic element updating parameters described in section 2.3.3 and subsequently in section 5.4.

The strain displacement matrix is therefore

$$[B] = [\partial]^T [N] = \begin{bmatrix} -\frac{6}{L^2} + \frac{12x}{L^3} & -\frac{4}{L} + \frac{6x}{L^2} & \frac{6}{L^2} - \frac{12x}{L^3} & -\frac{2}{L} + \frac{6x}{L^2} \end{bmatrix} \tag{2.20}$$

and the form of (A.17) which is applicable to beam elements [24] is

$$[K]_e = \int_V \left([B]^T EI [B] \right) dV. \tag{2.21}$$

Combining (2.20) and (2.21) and multiplying out gives

$$[K]_e = \frac{EI}{L}\begin{bmatrix} 12/L^2 & 6/L & -12/L^2 & 6/L \\ 6/L & 4 & -6/L & 2 \\ -12/L^2 & -6/L & 12/L^2 & -6/L \\ 6/L & 2 & -6/L & 4 \end{bmatrix}. \tag{2.22}$$

Combining (2.14) and (2.22) to find the elemental stiffness for a full 2D beam element which can resist shear and moment as well as axial load gives

$$[K]_e = \begin{bmatrix} \frac{AE}{L} & 0 & 0 & -\frac{AE}{L} & 0 & 0 \\ 0 & \frac{12EI}{L^3} & \frac{6EI}{L^2} & 0 & -\frac{12EI}{L^3} & \frac{6EI}{L^2} \\ 0 & \frac{6EI}{L^2} & \frac{4EI}{L} & 0 & -\frac{6EI}{L^2} & \frac{2EI}{L} \\ -\frac{AE}{L} & 0 & 0 & \frac{AE}{L} & 0 & 0 \\ 0 & -\frac{12EI}{L^3} & -\frac{6EI}{L^2} & 0 & \frac{12EI}{L^3} & -\frac{6EI}{L^2} \\ 0 & \frac{6EI}{L^2} & \frac{2EI}{L} & 0 & -\frac{6EI}{L^2} & \frac{4EI}{L} \end{bmatrix}. \tag{2.23}$$

This is the well known and very widely used Euler-Bernoulli formulation for a two dimensional cubic beam element.

2.2.3 Stress and Strain

Stress and strain are calculated by most finite element software as a function of nodal displacements. From equation (A.20) in appendix A, we recall that the general strain $\{\varepsilon\}$ is related to the nodal displacements $\{\Delta\}$ for a particular element by its strain displacement matrix $[B]$

$$\{\varepsilon\} = [B]\{\Delta\}. \tag{2.24}$$

The relationship between stress and strain for zero initial stress is given by (A.10) as

$$\{\sigma\} = [E]\{\varepsilon\} \tag{2.25}$$

and so from (2.24) and (2.25)

$$\{\sigma\} = [E][B]\{\Delta\}. \tag{2.26}$$

Required stresses are calculated element by element. Each point within the element will have a number of components of stress[3] associated with it and thus some user input is required to specify which stress is required. Stress can be defined in either local or global co-ordinates depending on the element type. For instance, the stress caused by beam flexure is given in the element's local co-ordinates since this type of stress is, by definition, in the direction of the beam's axis.

Returning to the example of the 2D beam, the standard equation for flexural stress is given by

$$\sigma_{flexural} = \frac{My}{I}, \tag{2.27}$$

where y is the distance from the beam's neutral axis and I is the second moment of area of the section. Recalling that the product of the strain displacement matrix and the elemental nodal displacements gives the curvature, then the following relationship can be written

$$M = EI\frac{d^2v}{dx^2} = EI[B]\{\Delta\}. \tag{2.28}$$

From (2.27) and (2.28) it can be seen that

$$\sigma_{flexural} = E[B]\{\Delta\}y\,. \tag{2.29}$$

This formulation for stress is used to estimate the stress on the outer surface of a beam element and will be used as a comparative measure with the experimental observations in chapter 4.

---

[3] Three for a 2D element and 6 for a 3D element.

2.2.4 Construction of Mass Matrices

Using finite elements for dynamic analysis requires consideration of inertial forces which arise from mass undergoing acceleration. Traditionally mass was considered as discrete particles distributed about a structure, resulting in lumped mass matrices an approach which results in a non-continuous inertia distribution. A consistent formulation of the mass matrix [25] can be shown to be

$$[M]_e = \int_V \rho [N]^T [N] dV \tag{2.30}$$

where ρ is the material density and other symbols are defined in appendix A.

Substituting the shape functions for the 2D beam (2.11) and (2.16)-(2.19) into (2.30) and integrating over the volume leads to the elemental mass matrix

$$[M]_e = \frac{\rho AL}{420}\begin{bmatrix} 140 & 0 & 0 & 70 & 0 & 0 \\ 0 & 156 & 22L & 0 & 54 & -13L \\ 0 & 22L & 4L^2 & 0 & 13L & -3L^2 \\ 70 & 0 & 0 & 140 & 0 & 0 \\ 0 & 54 & 13L & 0 & 156 & 22L \\ 0 & -13L & -3L^2 & 0 & 22L & 4L^2 \end{bmatrix} \tag{2.31}$$

2.2.5 Co-ordinate Transformation

The formulation of the elemental matrices described above has - for convenience and generality - been relative to a set of axes local to the element itself. To convert elemental stiffness matrices from the local set of co-ordinates $(\bar{x}, \bar{y}, \bar{z})$ within which they were formulated into the global co-ordinates (x, y, z) of the structure of which they must form a part a transformation is required. This is given by

$$\begin{Bmatrix} \bar{x} \\ \bar{y} \\ \bar{z} \end{Bmatrix} = [T]\begin{Bmatrix} x \\ y \\ z \end{Bmatrix} = \begin{bmatrix} \frac{\partial \bar{x}}{\partial x} & \frac{\partial \bar{x}}{\partial y} & \frac{\partial \bar{x}}{\partial z} \\ \frac{\partial \bar{y}}{\partial x} & \frac{\partial \bar{y}}{\partial y} & \frac{\partial \bar{y}}{\partial z} \\ \frac{\partial \bar{z}}{\partial x} & \frac{\partial \bar{z}}{\partial y} & \frac{\partial \bar{z}}{\partial z} \end{bmatrix}\begin{Bmatrix} x \\ y \\ z \end{Bmatrix}. \tag{2.32}$$

Figure 2.3 shows the local and global axes of a three dimensional bar or beam type of element.

Forces in elemental co-ordinates can similarly be transformed:

$$\left[\overline{F}\right]^T = [T][F] \tag{2.33}$$

Equating work done in the local co-ordinates with that done in global co-ordinates, it can be shown that

$$[F]^T[\Delta] = \left[\overline{F}\right]^T\left[\overline{\Delta}\right] = [F]^T[T]^T[T][\Delta]. \tag{2.34}$$

The transformation matrix, T, can then be seen to be orthogonal, i.e.

$$[T]^T[T] = [I] \tag{2.35}$$

Considering work done once more and now including the local elemental stiffness $\left[\overline{K}\right] = \left[\overline{F}\right]\left[\overline{\Delta}\right]^{-1}$ and global elemental stiffness $[K]$

$$\left[\overline{\Delta}\right]_e^T\left[\overline{K}\right]_e\left[\overline{\Delta}\right]_e = [\Delta]_e^T[K]_e[\Delta]_e = \left[\overline{\Delta}\right]_e^T[T]^T\left[\overline{K}\right]_e[T]\left[\overline{\Delta}\right]_e, \tag{2.36}$$

therefore

$$[K]_e = [T]^T\left[\overline{K}\right]_e[T]. \tag{2.37}$$

It can be shown [26] that the elements of $[T]$ are the trigonometric identities for direction cosines. Thus for the two dimensional beam example, the transformation $[T]$ is given by

$$[T]_{2Dbeam} = \begin{bmatrix} \Lambda & 0 \\ 0 & \Lambda \end{bmatrix}, \tag{2.38}$$

where

$$\Lambda = \begin{bmatrix} n_{x\bar{x}} & n_{y\bar{x}} & 0 \\ n_{x\bar{y}} & n_{y\bar{y}} & 0 \\ 0 & 0 & 1 \end{bmatrix}, \tag{2.39}$$

the terms of which are the elemental direction cosines such that

$$n_{x\bar{x}} = n_{y\bar{y}} = \frac{x_2 - x_1}{L}, \tag{2.40}$$

and

$$n_{y\bar{x}} = -n_{x\bar{y}} = \frac{y_2 - y_1}{L}. \tag{2.41}$$

If the angle between the local x-axis and global x-axis is θ then the transformation matrix becomes

$$[\mathrm{T}]_{2Dbeam} = \begin{bmatrix} \cos(\theta) & \sin(\theta) & 0 & 0 & 0 & 0 \\ -\sin(\theta) & \cos(\theta) & 0 & 0 & 0 & 0 \\ 0 & 0 & 1 & 0 & 0 & 0 \\ 0 & 0 & 0 & \cos(\theta) & \sin(\theta) & 0 \\ 0 & 0 & 0 & -\sin(\theta) & \cos(\theta) & 0 \\ 0 & 0 & 0 & 0 & 0 & 1 \end{bmatrix} \tag{2.42}$$

The transformation matrix for a three dimensional beam is found in a similar manner to be given by

$$[\mathrm{T}]_{3Dbeam} = \begin{bmatrix} \Lambda & 0 & 0 & 0 \\ 0 & \Lambda & 0 & 0 \\ 0 & 0 & \Lambda & 0 \\ 0 & 0 & 0 & \Lambda \end{bmatrix}, \tag{2.43}$$

where

$$\Lambda = \begin{bmatrix} n_{x\bar{x}} & n_{y\bar{x}} & n_{z\bar{x}} \\ n_{x\bar{y}} & n_{y\bar{y}} & n_{z\bar{y}} \\ n_{x\bar{z}} & n_{y\bar{z}} & n_{z\bar{z}} \end{bmatrix}, \tag{2.44}$$

with the direction cosines having the same definition as in the two dimensional beam case.

2.2.6 Construction of Global Matrices

Once transformed into global axes, elemental structural matrices can be constructed into global structural matrices where each row and column in the global matrices represents a degree of freedom of the modelled structure. For connectivity of elements some overlap of elemental matrices will occur in the global matrices. For more comprehensive details the reader is referred to an elementary text on finite element implementation such as [22] or [23].

The most recent model updating technologies display a trend towards altering parameters at an elemental level. Therefore, it is important to consider the model in terms of elemental matrices and their connectivities since the latter are lost once the transformation into global matrices has been performed. The storage space and processing time involved in storing the structural matrices is insignificant compared with the matrix inversions and eigen-solutions which are commonly performed a number of times during updating.

2.2.7 Finite Element Modelling for Model Updating

The philosophy of model updating is to improve finite element models of structures. However, the functionality of the finite element method itself is largely overlooked in the literature. Therefore, the procedural aspects of the finite element method have been dwelt upon in the previous sections.

With ever increasing computer power and the cost of storing data dropping the size of finite element models are increasing. It is not uncommon for a finite element model to contain several hundred thousand degrees of freedom. Most of the credible examples of model updating however (section 2.6), consist of making changes to relatively simple FE models whose construction is trivial and does not require the power of a commercial FE package.

Updating of real-life finite element models which might well consist of tens of thousands of degrees of freedom requires that only a limited amount of structural information can be stored and processed at once.

As later sections will demonstrate, the only involvement of the commercial FE package in the model updating process is to generate the initial structural matrices. It is the opinion of the author that future model updating techniques should enjoy a more intimate relationship with the finite element method. To this end, the use of finite element methods to identify loading on structures and to determine accurate deflected shapes of real structures as part of a model updating strategy are investigated in the forthcoming chapters.

2.3 Model Updating Technologies

The following sections outline and explore some of the main issues relating to the current state of the art. They are concerned with the application of updating procedures to practical situations with particular reference to choice of updating parameters. It is not the intention to give a comprehensive review of the field. For this the reader is directed to review papers such as those by Natke [27], Visser and Imregun [28] and Mottershead and Friswell [29] as well as a book by Friswell and Mottershead [30]. These give more comprehensive coverage of the very large amount of literature related to model updating.

2.3.1 Direct Methods

The earliest methods which fall under the model updating heading are known as *direct methods*. The first advocates of these were Berman and Nagy [31] and Baruch [32]. These methods consist of updating a set of structural matrices by making change to *any* of the terms in a single step. The result is that while the updated finite element model will exactly reproduce the experimental results, there is no guarantee that the model will correctly predict the structural response in other loading or testing configurations. This

is inevitable since the changes have not been made with reference to the physical relevance of the structural matrices.

Levin *et al.* [33] have recently examined in some detail the effect of making *ad hoc* changes to a set of structural matrices. They conclude that the inclusion of such terms is likely to result in the representation of a structure containing grounded springs which can have a profound and unrealistic effect on dynamic response.

Direct methods have been largely superseded by sensitivity and other forms of optimisation methods. The resulting updated models are constrained to be physically realisable and are outlined in the following sections.

2.3.2 Sensitivity Methods

Another generation of methods requires the determination of the sensitivity of a set of updating parameters to differences in dynamic behaviour between analytical and experimental dynamic data. The techniques yield an expression of the form

$$[S]\{\Delta p\} = \{\Delta obs\}. \tag{2.45}$$

where $\{\Delta p\}$ are a set of alterations to a set of updating parameters upon which the structural matrices are dependent, $\{\Delta obs\}$ are a set of differences in dynamic behaviour between an analytical model and experimental observations and $[S]_{ij}$ is the sensitivity of observation i to change in updating parameter j.

The form of $[S]$ depends on the choice of updating parameter (section 2.3.3). Apart from certain exceptional cases, the changes in parameter value have nonlinear relationships with the changes in observed dynamic behaviour. In such cases a first order approximation of $[S]$ is used and the best choice of $\{\Delta p\}$ to match the $\{\Delta obs\}$ are found iteratively.

These methods can be subdivided into techniques which use modal data and those which use frequency response functions as the system descriptor. The methods both continue to enjoy popularity and are examined practically in section 2.7. Furthermore

the ability of the eigenvalue sensitivity method of model updating to account for the effect of load on structures is described in chapters 5 and 6.

2.3.2.1 Methods using Eigenvalues and Eigenvectors

The comparison of observed resonant frequencies and - to a lesser extent - mode shapes with their analytical counterparts pre-dates model updating as the most obvious and direct method of comparing analytical predictions of dynamic behaviour with experimental observations. Indeed, manual methods of altering aspects of the analytical model to bring predictions of resonant frequencies into agreement with observed values was and is standard practice. It is logical then that early methods of updating should seek to find the sensitivity of system eigenvalues to changes in certain structural parameters.

The rate of change of eigenvalues with respect to structural parameters, p_j, can be derived as follows [34]. Considering λ_i and $\{\phi\}_i$ which are the solutions to the equation (2.6) derived in section 2.2.1.

$$([K]-\lambda_i[M])\{\phi\}_i=\{0\}, \tag{2.46}$$

where the eigenvectors are mass-normalised such that

$$\{\phi\}_i^T[M]\{\phi\}_i=1. \tag{2.47}$$

If either or both of the structural matrices is a function of a parameter p_j, differentiating (2.46) with respect to p_j gives

$$\left(\frac{\partial}{\partial p_j}[K]-\frac{\partial\lambda_i}{\partial p_j}[M]-\lambda_i\frac{\partial}{\partial p_j}[M]\right)\{\phi\}_r=-([K]-\lambda_i[M])\frac{\partial\{\phi\}_r}{\partial p_j}. \tag{2.48}$$

Pre-multiplying by $\{\phi\}_i^T$ makes the right hand side of (2.48) vanish due by an orthogonality argument. Re-arranging leads to

$$\frac{\partial\lambda_i}{\partial p_j}=\{\phi\}_i^T\left(\frac{\partial}{\partial p_j}[K]-\lambda_i\frac{\partial}{\partial p_j}[M]\right)\{\phi\}_i, \tag{2.49}$$

which is the rate of change of the i^{th} system eigenvector to the j^{th} updating parameter. This relationship is used extensively in chapters 5 and 6 of this thesis.

Methods have also been developed which also employ discrepancies in eigenvectors. This is partly to address the problem that only a relatively small number of resonant frequencies are available for updating. The use of eigenvectors to update structures suffers from their being relatively insensitive to structural modifications as well as the level of uncertainty in their value when determined experimentally.

2.3.2.2 Methods Using Frequency Response Data

To address the issue of lack of information provided by the potentially small number of resonant frequencies in a measured frequency range, researchers have turned to using the response data directly. This has the additional benefit that there is no requirement for time consuming and potentially inaccurate modal identification to be performed. A further feature of the method is that some residual information from frequencies outside the measured range is implicit within the experimental data.

The development of the so-called response function method of model updating is generally attributed to Lin and Ewins [35] with a significant later contribution from Fritzen [36]. The method employs the sensitivity of structural parameters to differences in experimental measurements and analytical predictions of frequency response functions. The sensitivity matrix relates the structural updating parameters to the changes in receptance by

$$[S(\omega)]\{p\} = \{\Delta\alpha(\omega)\}, \tag{2.50}$$

where the change in receptance term on the right hand side is defined as

$$\{\Delta\alpha(\omega)\} = \{\alpha(\omega)\}_{FE} - \{\alpha(\omega)\}_{exp}. \tag{2.51}$$

The sensitivity of the receptance at the i^{th} degree of freedom to the j^{th} updating parameter p_j at a given frequency point can be shown [37] to be

$$S(\omega)_{ij} = \{\alpha\}_{FE}^{T}\left(\left[-\omega^2 \frac{\partial}{\partial p_j}[M] + \frac{\partial}{\partial p_j}[K]\right]\{\alpha\}_{exp}\right). \tag{2.52}$$

An appropriate choice of updating parameter leads to an iterative solution to find the set of values which minimise the difference between experimental and FE predictions of receptance at given frequency points.

A number of sensitivity matrices at as many frequency points as one wishes to compare between experimental and analytical models can be constructed and stacked as

$$\begin{bmatrix} S(\omega_1) \\ S(\omega_2) \\ \vdots \\ S(\omega_n) \end{bmatrix}\{p\} = \begin{Bmatrix} \Delta\alpha(\omega_1) \\ \Delta\alpha(\omega_2) \\ \vdots \\ \Delta\alpha(\omega_n) \end{Bmatrix} \tag{2.53}$$

to produce $n_{dof} \times n_{freqs}$ equations in n_p unknowns where n_{dof}, n_{freqs} and n_p are respectively the number of degrees of freedom at which responses are available, the number of frequency points and the number of (unknown) parameter values.

At first glance, the generally greatly overdetermined system of equations given by (2.53) allows a large number of parameters to be updated with some confidence. In practice there is a large amount of inter-dependence of the rows of the sensitivity matrix. A number of techniques exist for selecting the most useful frequency points for instance [38]. It is the opinion of the author however, that the extra information yielded from considering differences in response is not significantly greater than that from changes in eigenvalues.

2.3.3 Selection of Updating Parameters

The issue of choice of updating parameter is crucial in the development of finite element model updating. The brief history of the subject is punctuated by the introduction of different updating parameter schemes. It is a general topic which applies to whatever choice of comparison between experimental and analytical data is made. Chapter 5 of

this thesis investigates new types of updating parameter. It is important to understand the motivation and requirements which determine the choice of these parameters.

Considering a Taylor expansion about the original structural matrices in terms of a set of updating parameters, the j^{th} of which is defined as p_j. A first order approximation for the updated systems matrices is found to be

$$[K]_U \approx [K] + \sum_{j=1}^{n_p} \delta p_j \frac{\partial}{\partial p_j} [K]_e \tag{2.54}$$

and

$$[M]_U \approx [M] + \sum_{j=1}^{n_p} \delta p_j \frac{\partial}{\partial p_j} [M]_e . \tag{2.55}$$

where the summation sign represents matrix building[4]. If the first order derivative of the structural matrices with respect to the chosen updating parameters can be found then an approximation to the changes required to the structural matrices can be derived. A best solution for p_j can be established by a process of optimisation of a generally over-determined yet ill-conditioned problem (commonly by using singular value decomposition described in section 2.4).

A particular case which has commonly been applied in model updating is to define the updating parameters as factors of individual or groups of elemental stiffness or mass matrices. The updated structural matrices are given by

$$[K]^U = [K] + \sum_{j=1}^{n_p} p_j [K]_{e\,j} \tag{2.56}$$

and

$$[M]^U = [M] + \sum_{j=1}^{n_p} p_j [M]_{e\,j} , \tag{2.57}$$

where $[K]_{e_j}$ and $[M]_{e_j}$ are, respectively, the j^{th} elemental stiffness and mass matrices.

---

[4] This equation is strictly true for elemental matrices having the same dimensions as the global value.

It is common for the updating parameters to be chosen to factor a group of elements – or super-element. This is because the number of individual elements in an FE model may be very large and the amount of data available to inform the choice of updating parameters relatively small.

Mottershead *et al.* [39] have considered a different approach whereby *geometric properties* of elements are updated principally to enable identification of joint behaviour. Joints are known to be a likely source of error in the FE model. Specialised finite elements have been developed in which the elemental formulation is recast in terms of a structural parameter change. This is likely to account for differences between experimental and analytical models. For instance the flexural and shear stiffness of a 2D beam (equation (2.22)) is modified to include a flexible length l and a rigid part a and is given by [40] as

$$[K]_e = \frac{EI}{L^3}\begin{bmatrix} 12 & 6l+12a & -12 & 6l \\ & 12a^2+12al+4l^2 & -12a-6l & 6al+2l^2 \\ & & 12 & -6l \\ sym & & & 4l^2 \end{bmatrix}, \tag{2.58}$$

with the corresponding mass matrix given by

$$[M]_e = \frac{\rho AL}{420}\begin{bmatrix} 156 & 156a+22l & 54 & -13l \\ & 156a^2+44al+4l^2 & 54a+13l & -13al-3l^2 \\ & & 156 & -22l \\ sym & & & 4l2 \end{bmatrix}. \tag{2.59}$$

The offset parameter - a - therefore becomes the updating parameter. It is noted that while varying the value of a apparently has little effect on the stiffness matrix, the flexibility (to which the lower modes of vibration are most sensitive) is changed significantly by perturbations of the offset parameter.

A similar method involving the development of specialised finite elements to update a particular model of a rubber seal is described by Ahmadian et al [41]. A finite element model of the rubber component is built from first principles. Its dependence upon a number of user-defined parameters (in this case two) can then be updated.

A more general approach for parameter selection, also motivated by the perceived requirement to update structural joints, has been suggested by Gladwell and Ahmadian [42]. They consider families of elemental stiffness and mass matrices that are physically realisable and which will alter the overall dynamic characteristics of a structure of which they are a part. Thus the *generic element* is any element of a family which has certain properties in common with an initial elemental matrix. This approach allows a great deal of scope in the changes one can make to elements while ensuring that the element remains physically realisable. It is therefore very attractive. A comparison of generic updating parameters with load-dependent updating parameters is undertaken in chapter 5 (section 5.4).

While the generic element method appears to be deservedly gaining in popularity, many practitioners continue to factor elemental stiffness and mass matrices as described by equations (2.56) and (2.57). Given that information available to inform the updating process is scarce, the choice of suitable and sensible parameters for model updating is of paramount importance.

2.4 The use of Singular Value Decomposition in Model Updating

Singular value decomposition (SVD) is a very powerful tool in the consideration of the equations which arise in the formulation of model updating problems. In the following sections the use of SVD for optimising over and under determined multiple parameter problems is considered. In addition the method is applied to estimate the conditioning of sensitivity equations.

The method is described in [43] and its use in optimisation in dynamical systems is comprehensively set out by Maia [44]. The singular value decomposition comprises recasting a matrix into the product of two orthogonal matrices [U] and [V] as well as a set of singular values $[\Sigma]$ thus:

$$[A]_{n_r \times n_c} = \left[\{u\}_1 \{u\}_2 \ldots \{u\}_{n_r}\right]_{n_r \times n_r} [\Sigma]_{n_r \times n_c} \left[\{v\}_1 \{v\}_2 \ldots \{v\}_{n_c}\right]^T_{n_c \times n_c} = [U][\Sigma][V]^T \quad (2.60)$$

The columns of $[U]$ and $[V]$ are respectively said to be the left and right singular vectors of $[A]$.

The matrix $[\Sigma]$ consists of a set of $\min(n_r, n_c)$ singular values $\sigma_1, \sigma_2, \ldots$ arranged in descending order along the leading diagonal,

$$[\Sigma] = \begin{bmatrix} \sigma_1 & & & 0 \\ & \sigma_2 & & \\ & & \ddots & \\ 0 & & & \end{bmatrix}. \tag{2.61}$$

It is very common for updating procedures - and certainly those employed in the later stages of this thesis - to require the solution of an equation of the form

$$[A]\{x\} = \{b\} \tag{2.62}$$

where $\{b\}$ is a set of measured values and $[A]$ is a set of sensitivities of the measured values $\{b\}$ to changes in a set of parameters $\{x\}$. If the rank of $[A]$ is greater than the number of elements in $\{x\}$ the problem is overdetermined. Since in the case of updating problems, both $[A]$ and $\{b\}$ contain experimental data or derivatives of it, an exact solution to $\{x\}$ is unlikely to be obtainable. In such cases other criteria must be used to select a set of values of $\{x\}$. While a set of equations for determination of updating parameters can appear over-determined, the sets of equations are likely to be nearly linearly dependent on one another. In other words the whole problem is *ill-conditioned*. The SVD allows a quick insight into the rank of an updating problem. It can be shown [43] to be r where

$$\sigma_1 \geq \sigma_2 \geq \ldots \geq \sigma_r \geq \sigma_{r+1} \geq \ldots \geq 0 \tag{2.63}$$

and

$$\sigma_{r+1} < \varepsilon \tag{2.64}$$

where ε is a small threshold value below which sets of equations can be thought of as not contributing usefully to the overall solution. A comparison of the ratio of the k^{th}

singular value to the first in practical terms gives an indication of the practical rank of the problem.

Turning to the solution of (2.62) the clearest choice is to minimise the value of the *residual*, R, defined as

$$R = \|\{b\} - [A]\{x\}\|_{\mu} \tag{2.65}$$

where the parameter μ indicates that several different residuals can be defined based upon type of norm. Most commonly the two norm or the so called Frobenius norm are employed.

Golub and Van Loan [43] show that for any problem of the type, including the underdetermined case, there exists exactly one $\{x\}$ which minimises the sum of the squares of the residuals,

$$\min(R_{LS}^2) = \|\{b\} - [A]\{x\}\|_2^2 . \tag{2.66}$$

They show that for

$$A = \sum_{i=1}^{rank(A)} \sigma_i u_i v_i^T , \tag{2.67}$$

the least squares estimate of $\{x\}$ is given by

$$\{x\}_{LS} = \sum_{i=1}^{rank(A)} \left(\frac{u_i^T b}{\sigma_i} \right) v_i , \tag{2.68}$$

resulting in

$$R_{LS}^2 = \sum_{i=rank(A)=1}^{n_c} \left(u_i^T b \right)^2 . \tag{2.69}$$

The vector $[A]\{x\}_{LS}$ can be thought of as a predictor of $\{b\}$ and is the orthogonal projection of $\{b\}$ onto the range of $[A]$.

The pseudo inverse matrix $[A]^+$ where

$$\{x\}_{LS} = [A]^+ \{b\} \tag{2.70}$$

can be found to be

$$[A]^{+} = [V][\Sigma]^{+}[U]^{T} \tag{2.71}$$

where

$$[\Sigma]^{+} = \begin{bmatrix} \frac{1}{\sigma_1} & & 0 \\ & \frac{1}{\sigma_2} & \vdots \\ & & \ddots \\ 0 & \cdots & 0 \end{bmatrix} \tag{2.72}$$

The pseudo inverse of $[A]$ is the unique Frobenius norm of the residual

$$\min_{[X]\in\Re^{n\times m}} \left\| [A][X] - [I]_m \right\|_{frob}. \tag{2.73}$$

Furthermore, if the rank of $[A] = n_r$ then

$$A^{+} = \left([A]^{T}[A] \right)^{-1}[A]^{T}, \tag{2.74}$$

clearly for the particular case $n_r = n_c$

$$[A]^{+} = [A]^{-1}. \tag{2.75}$$

2.5 Issues Related to Using Experimental Data

The details of experimental dynamic testing of structures and the subsequent identification of a dynamic model of a test structure will not be covered in detail here. A comprehensive coverage of the area can be found in [4]. The extent to which a single set of identified data can be thought of as uniquely defining a structure is currently an area of active research. The variance of predictions of dynamic data from nominally similar[5] structures falls within this definition. The effects of essentially transient changes to a structure's dynamic behaviour resulting from loading - which is the principal topic of this thesis - being an important example.

---

[5] The expression *nominally similar* is used a number of times throughout this thesis and refers to the fact that a single FE model will be used to represent a single structure under any conditions as well as any identically manufactured structure.

The effect of "noise" on experimental data along with the other well known difficulties such as lack of frequency bandwidth and limitations on the number of measurement locations is blamed extensively for any lack of success in using measured data to update finite element models. The term can be used as something of a catch-all into which any number of unidentified factors whose effect is to hinder successful model updating using experimental data can be thrown. Different predictions of dynamic behaviour can occur from the same structure at different times or from nominally identical structures. However, the factors which cause this variation have only recently received some attention and are discussed below.

Cafeo *et al.* [45] set out to consider the variability of test measurements in a methodical manner, their motivation being the reduction of tests required while maintaining confidence in the results. They observe that the variability in modal test data results from either inconsistencies in the modal/test analysis procedure or in the structure that is being tested. The former is investigated with reference to a set of 9 tests on 7 vehicles. Specifically the test/analysis procedure is subdivided into the following:

(a) Linearity Considerations;

(b) Shaker Attachment Method;

(c) Measurement System;

(d) Accelerometer Placement; and

(e) Signal Processing Considerations.

The study of these individual components of a dynamic test provides the basis for a thorough investigation in to the causes for test-to-test error. While they are not studied in any great detail, the dynamic behaviours of the seven nominally identical vehicle specimens are seen to vary quite considerably. Further investigation of the test-to-test variability problem [46] leads to some very useful guidelines on methods to avoid variability of measurements resulting from inconsistencies in the measuring and analysis of structures.

Balmès [47] considers the problem of a single FRF model being required to represent a real structure. He notes that the behaviour of a single structure can be altered by time varying factors such as ageing, temperature effects, loading conditions. Also, he states that variation amongst a population of nominally identical structures can occur due to manufacturing tolerances, residual stresses and welding point positions. The results of the "GARTEUR" round-robin exercise whereby a number of laboratories tested a single structure each with their own testing equipment are examined. The relative simplicity of the model and the availability of free-free testing in laboratory conditions led to the observation that differences in dynamic readings arose from slight differences in test equipment and procedures.

De Clerck [48] notes the difficulty of comparing multiple sets of nominally similar data and describes a method which statistically compares a number of sample modal analyses. A relatively simple formulation involving the term by term comparison of the i^{th} sample eigenvector $\{\phi\}_i$ with the average of the population is given by

$$\{\phi\}_{i_{EAV}} = \frac{1}{n}\sum_{i=1}^{n}\{\phi_i\}_n \,. \tag{2.76}$$

A more sophisticated method involves the singular value decomposition (SVD) which is covered more fully in section (2.4) below. The SVD of the set of eigenvalues is taken

$$SVD\left(\left[\{\phi\}_{i_1}\{\phi\}_{i_2}..\{.\phi\}_{i_n}\right]\right) = [U]_i[S]_i[V]_i^T \tag{2.77}$$

and the average of the n eigenvectors in this way is given by

$$\{\phi\}_{i_{SAV}} = \{U\}_{i_1} \tag{2.78}$$

with the maximum normalised singular vector,

$$\frac{S_{11}}{n^2} \tag{2.79}$$

shown to give a measure of the consistency between a set of measured modal data. The remaining singular values are found to represent the spatial variance of the set of eigenvectors.

This approach allows the variation of mode shapes with respect to variability of components of the model to be considered. The usefulness of these methods was proved with a simple FE model whose characteristics could be changed and dynamic response re-calculated many times and there appears to be a clear requirement to test the effectiveness of the method in a real-life situation.

Ziaei-Rad and Imregun [6] appear to be amongst the first to consider the specific area of understanding what level of noise in the experimental data can still allow a finite element model to be successfully updated. They describe the problem in terms of the range of error arising from the measurement of a single specimen. They acknowledge that the method is equally valid in considering the variability in dynamic behaviour between nominally identical structures. The method considers the response function method of section 2.3.2.2 with a noise model of the form

$$[\alpha_{exp}] = ([Z_{FE}] + [\Delta Z_{FE}])^{-1} + [\varepsilon], \tag{2.80}$$

where the dynamic stiffness matrix $[Z]$ is given by

$$[Z] = ([K] - \omega^2 [M]) \tag{2.81}$$

and the subscripts FE and exp denote analytical (FE) prediction and experimental measurement respectively. An upper bound upon the error matrix is found to be given by

$$\|[\varepsilon]\| << \|[\Delta Z_{FE}]\| / \|[Z_{FE} + \Delta Z_{FE}]\|^2, \tag{2.82}$$

where $\|[\varepsilon]\|$ in this case denotes the Frobenius norm of the error matrix. This expression indicates that the level of noise in the experimental data (or discrepancy between test to test measurements) which can be tolerated by the response function updating technique is a function of the type of mathematical model employed.

The common choice of updating factors of elemental mass and stiffness matrices (equations (2.56) and (2.57)) lead to a formulation of the sensitivity equation (2.45) which includes terms from the error matrix

$$([S]+[S_\varepsilon])\{p'\}=[\Delta\alpha]+[\Delta\alpha_\varepsilon], \tag{2.83}$$

where $\{p'\}$ are noise affected p-values. The solution is found by finding the pseudo inverse (described in section 2.4 and denoted '$^+$') of the sensitivity matrix

$$\{p'\}=([S]+[S_\varepsilon])^+[\Delta\alpha]+[\Delta\alpha_\varepsilon]. \tag{2.84}$$

Ziaei-Rad and Imregun show that for the case of the norm of the sensitivity error matrix being much smaller than that of the sensitivity matrix itself then a solution is possible. For the converse case they show that the extent of the noise leads to equation (2.84) becoming increasingly ill-conditioned. This method allows a statistical consideration of the variability in experimental data to be used to assess the likelihood of success in performing model updating.

2.6 Updating Applied to Real Structures

Despite the large amount of literature published on the subject of finite element model updating, there is a relatively small amount of information describing the experiences of applying such techniques to measured data. Instead many of the methods devised have been demonstrated and validated using only simulated experimental data - that is to say that the data originate from an analytical model rather than from a real structure. The use of simulated data offers the analyst the chance to assess in a systematic and rigorous way the effects of various perceived aspects of experimental data. Many of the limitations which apply to experimental data can be accounted for and investigated in simulations. These include:

- truncation of experimental data in the frequency range; and
- limitation on the number of measurement points upon a structure.

Other factors however can be less well understood by means of the use of simulated case studies - for instance:

- interaction between the test structure and excitation and measurement equipment; and
- noise resulting from the experimental process.

The importance of these factors is well known as is their detrimental effect upon the success of any model updating strategy.

A number of authors have described experiences in applying *automatic* model updating techniques in practical situations; a review of the literature follows. Much literature uses the word updating to describe processes which amount to little more than manual alterations to structural matrices. The following examples differ in that the updating is *automatic* in that structural parameters are altered in a number of steps according to *pre-determined* set of rules.

Hoff and Natke [49] appear to be amongst the first to apply model updating techniques to practically measured experimental data in 1988. A radar tower was modelled using 3D beam elements and a lumped parameter model of the foundation behaviour resulting in some 52 degrees of freedom. Unsurprisingly, calculations showed that eigenvalues and eigenvectors were most sensitive to the stiffness in the region of the tower's foundation. These were used as updating parameters and converged updated values for these parameters were obtained from eight identified resonant frequencies.

Imregun *et al.* [50] considered a box like structure in 1993. The response function method (RFM) was used to update the finite element model of a sheet metal box comprising 716 active degrees of freedom. Some of the material properties of the finite element model were altered manually at the correlation stage. A limited number of responses (one direction only) were used to update the properties of two of the sides of the box but with limited success despite the choice of multiple sets of frequency points. The authors concluded that the scale of the discrepancy between measured and predicted FRFs was beyond that which could reasonably be reconciled.

At around the same time, Lammens *et al.* [51] considered the use of measured experimental data for model updating. They took the cautious approach of using very simple models - namely a PVC plate and a small frame structure. A method employing the difference between pairs of frequency response functions was used to update a small number of elementary updating parameters. The influence of frequency point selection was considered practically as well as the use of including damping in the analytical model. While finding that updating using real experimental data is possible - at least at a very simple level - they arrive at a number of interesting conclusions. Firstly that the choice of frequency points is important in influencing the likelihood of a successful update. Secondly it was observed that the amount of information available from the structure limits the number of updating parameters which can be updated. They also found that zero damping in the analytical model produces more robust convergence than attempting to include damping parameters in the updating process.

Imregun *et al.* [7] investigated both the response function method and the eigen-sensitivity methods of model updating using experimental data from five nominally identical L-shaped plates with spot welded connections. A significant observation from this work is that the five specimens exhibited remarkably different dynamic behaviour. The assumption that the global correction matrices can be found by multiplying individual element matrices by scaling factors (equation (2.56) and (2.57)) is used. Updating is performed using both the response function method (section 2.3.2.2) and an eigen-sensitivity method (2.3.2.1). The eigen-sensitivity method was found to fare better when augmented in a two stage approach with certain constraints. While the method based on response function also produced satisfactory results, the choice of frequency points was found to have a strong influence on the likelihood of success. The choice of FRF estimator led to the response being ill-defined around resonance and therefore not contributing to a well conditioned problem.

A further set of experiments was presented by Imregun *et al.* [52] with two nominally identical structures built to compare with a simple FE model. The correlation between

one of the sets of data and the finite element model was found to be very poor and hence was not used in the subsequent model updating procedures – a worrying observation. Updating was performed using the response function method with converged results only occurring after rejecting noisy experimental FRFs and rejecting the use of damping parameters. It was noted that a number of sets of p-values led to converged solutions clearly demonstrating that the solution is non-unique. The computational effort is investigated and shown to require the least square inversion of a matrix of size $(n_{dof} \times n_f) \times n_p$ and the inversion of a matrix of size $n_{dof} \times n_{dof}$ n_f times where n_{dof} equals the number of degrees of freedom, n_f the number of frequency points considered and n_p is the number of p-values. It is noted that this amount of heavy computation is practical only for very small models.

The application of model updating techniques has not been confined to small structures tested under laboratory conditions. Imregun and Agardh [53] considered responses measured from a three span road bridge. Sixty five measurement positions were employed and 12 modes were extracted in the 0-40 Hz frequency range and compared with results on a 1050 degree of freedom finite element model with reasonably good correlation found between pairs of modes. The noisy nature of the data led to the decision to use the eigen-sensitivity method to update elemental stiffness factors (equation (2.56)) with successfully converging solutions. The conclusions are upbeat suggesting that the method could be used for damage detection. The authors note that the use of dynamic data has become popular as a method for monitoring bridges and other large structures for signs of damage. The finite element model of a structure can then be thought of as a repository of information regarding current levels of damage and deterioration which can be periodically updated using dynamic test data.

Waters [54] concluded an in depth study of the FRF sensitivity method by using high quality experimental data from a plate wing model. High order frequency responses were used and frequency points were selected to be away from resonance to avoid ill-conditioning. The plate was initially cantilevered but the clamping arrangement and the

bench upon which the specimen was mounted were found to influence the dynamic response so free-free testing was used instead. The effect of interaction of the structure and the shaker and stinger was also found to significantly pollute the experimental data. The stiffnesses and masses of groups of elements as well as an element representing the mass of the force transducer were updated and convergence was achieved.

Mottershead [55] summarised several case studies of application of updating of the geometric joint properties described in section 2.3.3 to practical situations. The finite element of a welded joint was successfully updated by increasing the initial offset parameter by 3%. In a variation upon this theme a specialised element for modelling the rubber interface between a car window and adjacent bodywork was developed and two of the elemental parameters adjusted to give the closest fit to a set of experimental data. The veracity of the updated rubber seal model was tested by re-testing the seal with a metal sheet replacing the car window. The closeness of the agreement gives much confidence in the accuracy of the updated model in a way that is not generally available.

Mottershead and James [40] considered both joint geometry and generic elements to update a three storey aluminium space frame structure. The sensitivities of resonant frequencies to three elemental eigenvalues were considered. These contributions from these updating parameters, however, added exclusively positive values to the overall sensitivity matrix. Since the experimental results did not lie exclusively above or below the finite element model prediction, no combination of the elemental eigenvalues could adjust the resonant frequency prediction of the finite element model. To address this problem the mass of the structure adjacent to its joints was also considered although it is acknowledged that there was no reason to suppose that the mass was in any way mis-modelled in the original model.

More recently Imamovic [56] considered the practicality of updating FE models using measured experimental data in some detail. He concluded that methods employing sensitivity of parameters to eigenvalues offer the best prospect of updating finite element models of structures using measured experimental data. Several practical case

studies are considered. Experimental data from a cantilever plate[6] mounted in a large rubber block was obtained from several sources and the average experimental data were used and compared with a finite element model of the structure where the principal plate component was modelled using 60 plate elements. For the first seven correlated modes, the initial finite element model produced resonant frequencies which were of greater magnitude than their experimentally observed counterparts by factors of between 7 and 27%. Due to the limited availability of resonant frequencies observed, the stiffnesses of five plate elements closest to the grounded end of the cantilever were used as updating parameters with a converged solution arising. Alterations to the stiffnesses of these elements of between –40% and +20% are required to bring the FE prediction into agreement with the observed data. The author inferred that much of the discrepancy lay in the modelling of the joint between plate and foundation. While this may be true it is also clear that resonances of the cantilever (as opposed to the low magnitude resonances resulting from the straining the rubber foundation) are most sensitive to the stiffnesses of this part of the structure. They would thus be changed most readily by the updating method whether or not they actually contribute to the discrepancies between FE prediction and measured dynamic data.

A further study involved a very large (92 000 DoF) model of an aeroplane engine casing. Firstly a set of super-elements was chosen where elements were considered to share properties. Multiple combinations of stiffness factors were considered with some 300 of these producing converged solutions. The best solution was chosen based on issues such as good modal assurance criterion (MAC) [57] values between correlated mode pairs (CMPs) and improvement in the agreement of modes not included in the updating process.

These applications of model updating procedures to experimental data represent a useful attempt to apply immature technologies in the hostile environment in which they must

---

[6] The test data derived from a simple structure designed and built by Lloyds Register and tested by three independent companies

eventually operate. The mismatch between the amount of information from a modal test and the range of possible parameters in a finite element model still appears to be the largest obstacle. Some converged solutions suggested in the literature appearing at best to be rather arbitrary. It is the opinion of the author that the limited scope for change of finite element models common to all of the examples described above means that the wrong problem is being solved. Specifically, the choice of updating parameter is crucial. Specialised updating parameters which allow the scope to alter a finite element model to represent any possible structural configuration appear to present a route to successfully implementing model updating in practice. This area of research is pursued in chapters 5 and 6 of this thesis. In the mean time, a case study is presented which allows some of the issues raised in this section to be demonstrated.

2.7 Case Study

As an introduction to the consideration of using experimental data to update finite element models a simple case study is presented here. This is included to highlight the more general features and drawbacks of model updating. The test data derive from a real structure tested on several occasions. The use of real experimental data allows some conclusions to be drawn about the requirement for repeatability of results.

It is prudent that in considering the possibility of updating real structures one should start with a very simple structure allowing the areas of uncertainty to be isolated and studied in detail.

The experimental specimen is a narrow mild steel plate of dimension 850 × 100 × 5mm. Further work on this structure is described in chapter 4; a full description of the experimental data collection techniques is deferred until that point. The tests upon the narrow plate described in this section essentially validate the FE model.

Dynamic measurements were taken with the plate hanging in free-free conditions, the experimental arrangement is shown schematically in figure 2.4. The response of the plate was measured along the centre line of the plate using a scanning Doppler Laser

Velocimeter. Excitation was applied at a point 250mm from one end. Frequency response functions between the load point and up to 18 response points along the length of the plate were calculated.

2.7.1 Identified Resonant Frequencies

Dynamic measurements were conducted on three independent occasions. The same equipment was used during each test but was disassembled in between sessions. The tests will be referred to as A, B and C. The three test programmes differed in several ways, a combination of point measurements[7] and complete measurements were taken during the three sets of tests and during test B point FRFs were measured at different levels of forcing. Tests A and B involved measurements in the 0-800 Hz frequency range while test C considered the range 0-400 Hz.

Two different modal identification methods were used. The global method outlined by Fillod et al. [58] was employed to analyse the full sets of 18 FRFs while a line fitting method [59] was used to identify frequencies from single point measurements. In addition to using a large set of response measurements the global method also allows identification of multiple modes. The line fit method by contrast might be used where a single response is available and modes are sufficiently spaced that interaction is minimal. The global method would be expected to provide the better quality estimate of resonance frequencies since most information is used. While these two modal identification methods are common and representative, they are both members of an increasingly large family of such methods. For a comprehensive and recent review of the field one should turn to chapter 4 of [60].

Table 2.1 summarises the tests conducted as well as showing the results of modal analyses performed on data from the structure. The two pairs of resonant frequency data gained using the global method were extracted from the same data but at different times.

---

[7] Measurement point and excitation point are coincident

Test A			Test B				Test C		
18 FRFs			4 Point FRFs at Different Loading				18 FRFs		
0-800 Hz			0-800Hz				0-400Hz		
Global Method	Global Method	Line Fit	Line Fit	Line Fit	Line Fit	Line Fit	Global Method	Global Method	Line Fit
37.73	36.83	37.18	37.68	36.54	36.97	35.25	36.84	36.92	36.91
101.00	100.86	100.98	100.78	100.83	100.98	100.17	100.90	100.90	100.86
197.73	197.69	197.78	197.70	197.76	197.86	197.86	198.10	197.88	197.86
328.78	328.80	328.61	327.75	327.91	327.67	327.97	328.22	328.11	328.08
492.20	492.23	492.25	491.46	491.56	491.82	491.54	-	-	-
688.92	688.98	688.97	688.97	688.67	688.80	688.75	-	-	-

Table 2.1 – Identified Resonant Frequencies

The mean and standard deviation[8] of the value estimated for each resonant frequency are shown in table 2.2. The scarcity of data and the relative inter-dependence of readings[9] relating to the circumstances of their collection makes it difficult to draw very firm conclusions regarding the variability of data. It is however interesting to note that any one of the modal analyses would have allowed the modal analyst to be very confident that the correct readings for the plate had been attained.

---

[8] mean = $\frac{\sum_{i=1}^{n_{obs}} X_i}{n_{obs}}$ and standard deviation = $\sqrt{\frac{\sum_{i=1}^{n_{obs}} (X_i - \bar{X})^2}{n_{obs} - 1}}$, where X_i is the i^{th} observation and n_{obs} is the number of observations.

[9] Each column for instance should be treated as independent of the other columns since the readings were taken and to a lesser extent the modal analyses were performed at the same time.

	Experimentally Identified Resonance Frequency (Hz)			
Mode Number	**Mean**	**Min**	**Max**	**Standard Devation**
1	36.89	35.25	37.73	0.69
2	100.83	100.17	101.00	0.24
3	197.82	197.69	198.10	0.12
4	328.19	327.67	328.80	0.41
5	491.87	491.46	492.25	0.36
6	688.87	688.67	688.98	0.12

Table 2.2 – Comparison of Variation of Experimental Modal Analyses

The data suggest that certain modes can be extracted with some more consistency than others, the standard deviation of the prediction of modes 3 and 6 is 20% of the standard deviation of the first mode. This difference in consistency could result from a combination of a number of factors such as noise in certain parts of the frequency range, close modes, lower levels of response etc. It is not intended to pursue the consideration of the reasons for inconsistency of extraction of modal parameters.

2.7.2 Finite Element Modelling of Beam

The behaviour of the narrow plate which has been discussed in the previous section is modelled as a set of two dimensional beam elements of the type described in sections 2.2.2 and 2.2.4 to keep the problem at a relatively elementary level. The principal parameters used in the finite element model are shown in table 2.3.

Parameter	Value Chosen
Young's Modulus	2.11×10^{11} Nm^{-2}
Density	7850 kgm^{-3}
Second Moment of Area (I)	1.04167×10^{-9} m^4

Table 2.3 - Material and Geometric Properties Chosen in Updating

The predictions of resonant frequencies yielded by this simple method are shown in table 2.4 along with the average experimental observations for comparison. The plate was modelled with 17 two dimensional Euler-Bernoulli beam elements such that the node points matched the measurement points on the structure described above. Additionally the plate was modelled with twice as many beam elements and further with 34 elements the results are shown in table 2.4 along with the closed form prediction [61]. The analytical readings, like the identified experimental readings, show some variety.

	Experimentally Identified Resonance Frequencies (Hz)			Analytical Natural Frequencies (Hz)		
Bending Mode	**Min**	**Mean**	**Max**	**FE – 17 Beam Elements**	**FE – 34 Beam Elements**	**Closed Form**
1	35.25	36.89	37.73	36.82	36.60	34.00
2	100.17	100.83	101.00	101.48	100.88	93.73
3	197.69	197.82	198.10	198.99	197.79	183.75
4	327.67	328.19	328.80	329.07	327.03	303.74
5	491.46	491.87	492.25	491.86	488.65	453.73
6	688.67	688.87	688.98	687.56	682.72	633.73

Table 2.4 – FE Predictions of Resonant Bending Frequencies

The coarsest discretisation using 17 elements each of length 50mm produces excellent agreement with the experimental data. This would be regarded as a good starting point for model updating. It is shown in section 2.2.2, however, that the finite element method using elements derived from the displacement method described in appendix A will *always* produce an overestimate of resonant frequencies. This is acknowledged and in at least one case it has been studied [62]. However, the cause of mismatch between finite element prediction and experimental observation is rarely taken into account. This is because improving the finite element prediction dramatically increases the processing time required to extract the eigen-solution. Some practitioners [63] employ a rule of thumb that the first third of the resonant frequencies produced by a finite element

model can be regarded as mesh convergant. The similar FE model with double the number of elements gives a very slightly lower prediction of the resonant frequencies as one would expect. However, one might argue that the elemental formulation is less valid when elemental length is less than width.

2.7.3 Updating of Finite Element Model

As the proceeding sections have described, there is some uncertainty about which experimental data should be used for updating. Furthermore the choice of parameters to be updated is by no means simple. In this case the test structure is sufficiently uncomplicated that any error in the finite element model is expected to lie in global properties such as mass and stiffness or in the added mass of the shaker and force transducer arrangement.

To assess the effectiveness of updating using experimental data, the stiffness of the beam between 200 and 250mm from one end (element 5 of the 13 beam element model) was reduced by 23.1%. This value of artificial error implies that a factor of exactly 1.3 must be applied to the stiffness of this area to bring it to the same value as the rest of the beam. The artificial error is analogous to an initial mis-modelling but allows the usefulness of updating strategies to be quantitatively examined.

Eight updating runs were performed with the effect of some of the principal factors varied. Three sets of experimental data were used, the description of each updating run is given in table 2.5. It is important to note that each of the different problems are realistic and that *any* could be chosen in practice.

Run	Experimental Data Set	Experimental Modes	FE Model	Updating Parameters
1	Mean	1-6	17	3,5,7
2	Min	1-6	17	3,5,7
3	Max	1-6	17	3,5,7
4	Mean	1-6	17	3-10
5	Min	1-6	17	3-10
6	Max	1-6	17	3-10
7	Mean	1-3	17	3,5,7
8	Mean	4-6	17	3,5,7

Table 2.5 – Initial Parameters For Experimental Data Updating

The three sets of experimental data referred to are the mean and extreme identified resonant frequencies shown in table 2.4.

Only stiffness parameters are updated with the updated stiffness matrix being given by

$$[K]^U = \sum_{j=1}^{n_p}(1+p_j)[K]_{e_j}^A + \sum_{k=1}^{n_e-n_p}[K]_{e_k}^A \tag{2.85}$$

where the second summation represents the elements which are not factored by the n_p updating parameters p_j.

Since only six resonant frequencies were available, updating of any more parameters than this number of (independent) parameters leads to an underdetermined problem. Two sets of updating parameters were chosen, the three stiffnesses of respectively elements 3, 5 and 7 leading to an overdetermined problem and stiffness of elements 3 through 10 leading to an underdetermined problem.

Updating was carried out using the eigenvalue sensitivity method described in section 2.3.2.1

Convergence was assumed to have occurred when the largest change in any of the updating parameter dropped below 1% of their original value and was achieved in each case within five or six iteration representing quite robust convergence.

Figure 2.5 shows the value of the residual with each iteration. The residual is defined in general terms in section 2.4, in this context it is defined as

$$R = \left\| \{\lambda\}_{FE_k} - \{\lambda\}_{exp} \right\|_2 \tag{2.86}$$

where $\{\lambda\}_{FE_k}$ are the six values of system eigenvalue at the k^{th} updating iteration. The residual is therefore an indication of the extent to which the updated model matches the experimental data. The least successful updating run is seen to be number 7, the large error arises since it is does not attempt to minimise the difference between experimental and finite element predictions of modes 4, 5 and 6. Updating run 8 on the other hand which should suffer from the same problem matches all of the frequencies. While a very simple example this is phenomena is likely to occur in practice when only a small number of modes are available. Of the sample of measured resonances those occuring at higher frequencies are seen to be much more useful in making changes to the finite element model than the lower order modes.

The choice of updating parameters is also seen to be important in reducing the residual. The under-determined runs 4 to 7 which alter 8 elemental stiffnesses using the six resonant frequencies are successful as is run 8 which only alters modes 3, 5 and 7 using modes 4, 5 and 6. The latter result suggests that attempting to minimise the difference between the FE and experimental predictions of higher order modes is more useful than using all of the modes.

A range of updating parameters arise from the eight runs and are displayed in figure 2.6 with the target value of stiffness shown as a dashed line. The updated parameter values are seen to vary widely.

The variation of experimental data is seen not to affect the converged solution for the overdetermined cases (1 to 3) although the final parameter values in the other cases are seen to alter dramatically as a result of data variation.

One might argue that the variation in updated parameter values is to be expected from altering a parameter which was not thought to be in error. This problem with the initial

FE model being artificially damaged is completely analogous to the problems encountered in reality. If the stiffness of one element of the beam had indeed been mis-estimated the insight into the level of correctness of the initial FE model would not be available.

On a more positive note, most of the updating runs successfully identified the location of error in the initial finite element model with the overdetermined data producing the consistently better results

2.8 Concluding Remarks

The background to the generation of finite elements using the displacement method based on the theory of minimum displacement has been set out. It has been argued that an understanding of the construction of elements from first principles is vital. The method of estimating stress at locations about a structure from elemental displacements has been demonstrated and will be employed to useful effect in the following chapter.

The transformation of elements from local to global co-ordinates has been set out. The application of this simple congruent transformation can account for structural deformations and this transformation is considered as an updating parameter in chapter 5.

The reasons for variability in observed experimental data have been discussed. Literature on the subject has been reviewed and a number of approaches to quantification of test-to-test error have been described. The review of the field of variability of experimental data reveals that a methodical approach to the consideration of the factors which cause sets of data from nominally similar structures to differ will continue to provide a very fruitful line of research.

The development of model updating techniques has been briefly reviewed. Emphasis has been placed on sensitivity methods with the eigenvalue sensitivity method and the response function method outlined in detail. The use of Singular Value Decomposition

to solve the equation relating small changes in observed dynamic behaviour to changes in updating parameter has been advocated and described.

The selection of updating parameters is considered in some detail. There has been some conservatism in the choice of updating parameters. Recent methods which update geometric parameters appear to offer a more versatile method of changing finite element models, particularly in specific regions such as joints. This versatility comes at the expense of considerable engineering judgement being required to assess the number, location and type of updating parameters to use on a case-by-case basis.

A review of the application of *automatic* model updating methods to practical real-life situations has been presented. It has been observed that practitioners have generally been able to alter FE models such that they bring FE predictions of dynamic behaviour into close agreement with *observed* behaviour. However, the updated solutions have been seen to be far from unique. Disparity between sets of experimentally collected data from nominally identical structures has been observed. In addition a discussion of the difficulty in discerning which amongst a large population of sets of parameter values make the best changes to the finite element model has been included. This leads to the conclusion that the updated models are rather arbitrary and may only fare better than the original model in matching the observed dynamic data.

Some studies which test the usefulness of the updated model by using tests which are independent of the updating process have been reported. These give rise to optimism that the wealth of experience in developing finite element updating techniques can eventually be successfully be translated into the practical arena.

A practical case study has allowed some of the issues related to applying updating procedures to measured experimental data to be examined. By creating a known error in the initial finite element model, it has been possible to show that experimental data can be used to correctly make alterations to the finite element model. It was shown however that the nature of the updated model is very sensitive to the updating parameters chosen.

Variation in experimental data is seen not to decrease the chance of obtaining a converged and plausible updated model. The variability, choice of updating parameter and number of modes all appear to have a similar effect in leading to non-uniqueness of the solution.

Higher order modes have been seen in the experimental case to provide the most useful information in updating elemental stiffness parameters.

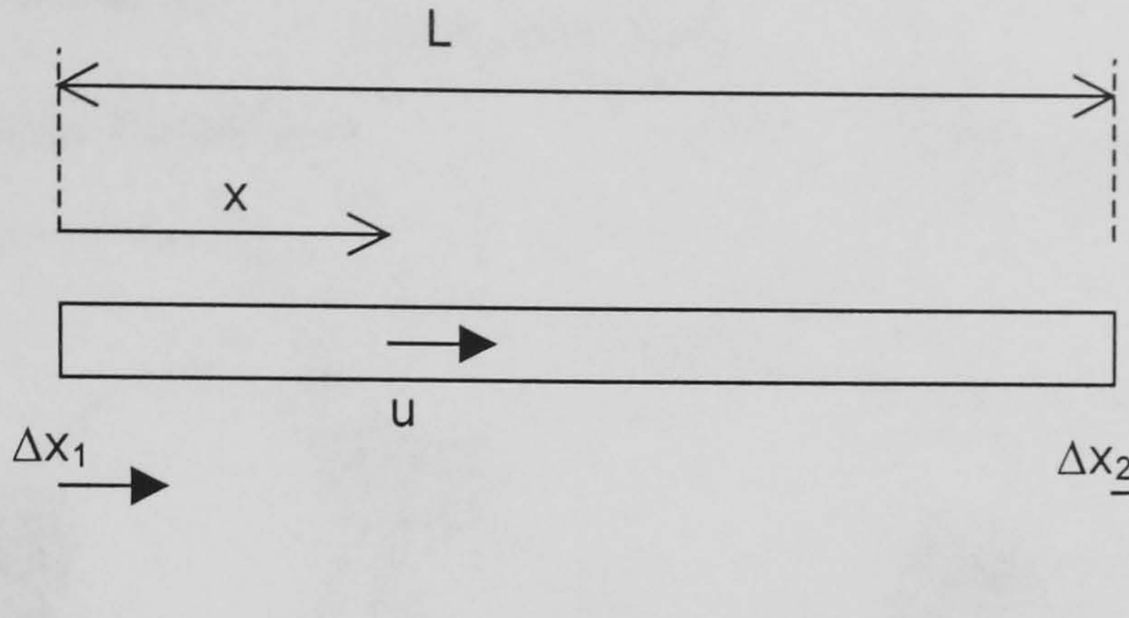

Figure 2.1 – Beam Under Axial Load

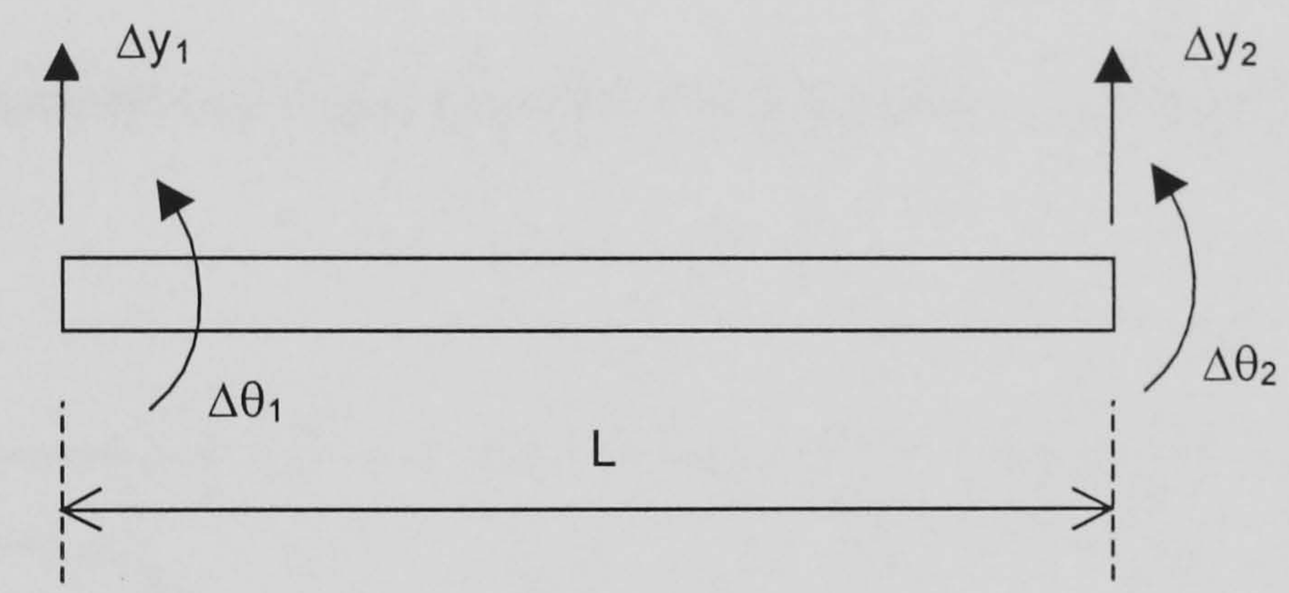

Figure 2.2 – Beam Under Shear and Rotational Loading

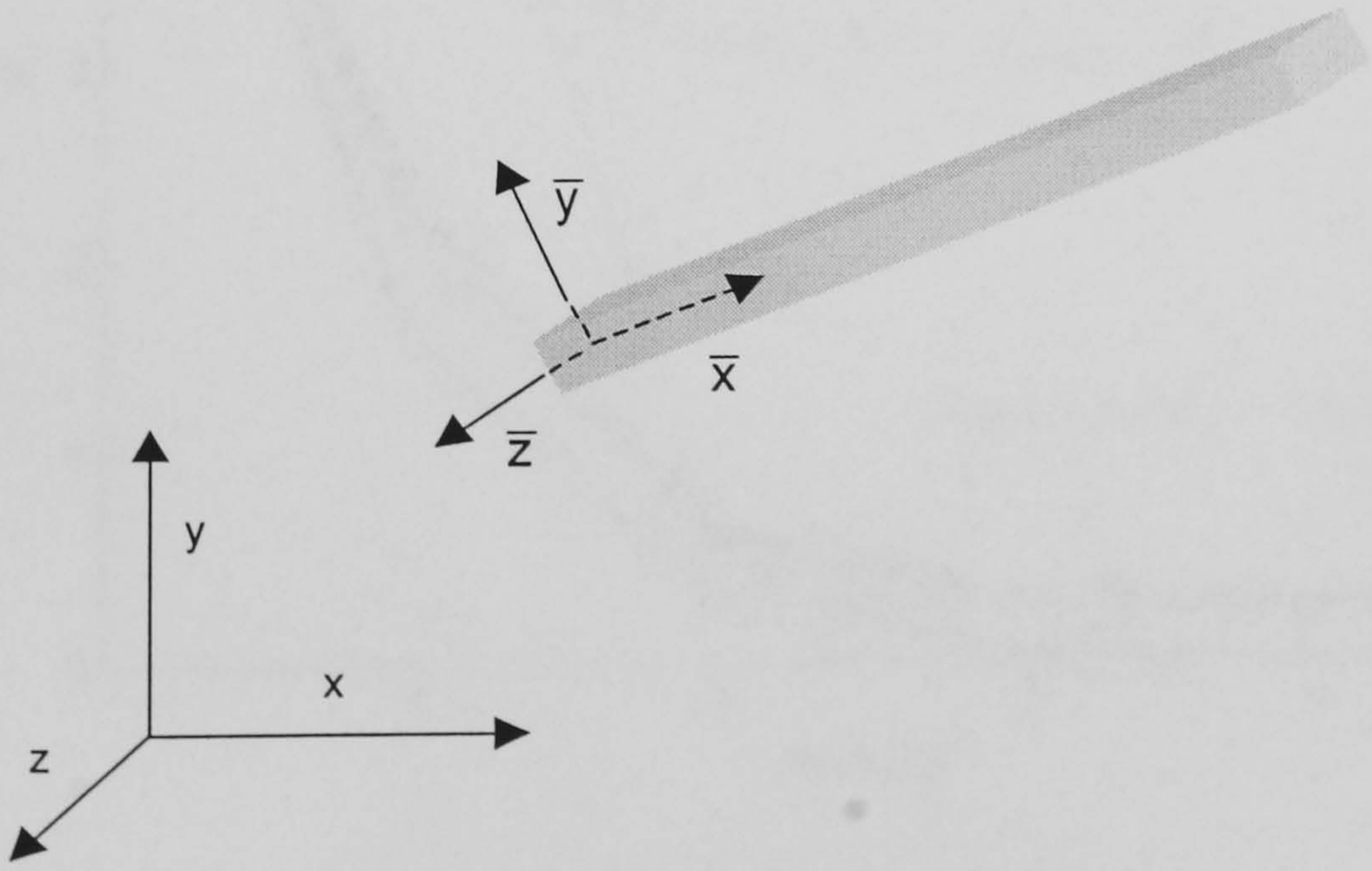

Figure 2.3 – Transformation of Axes

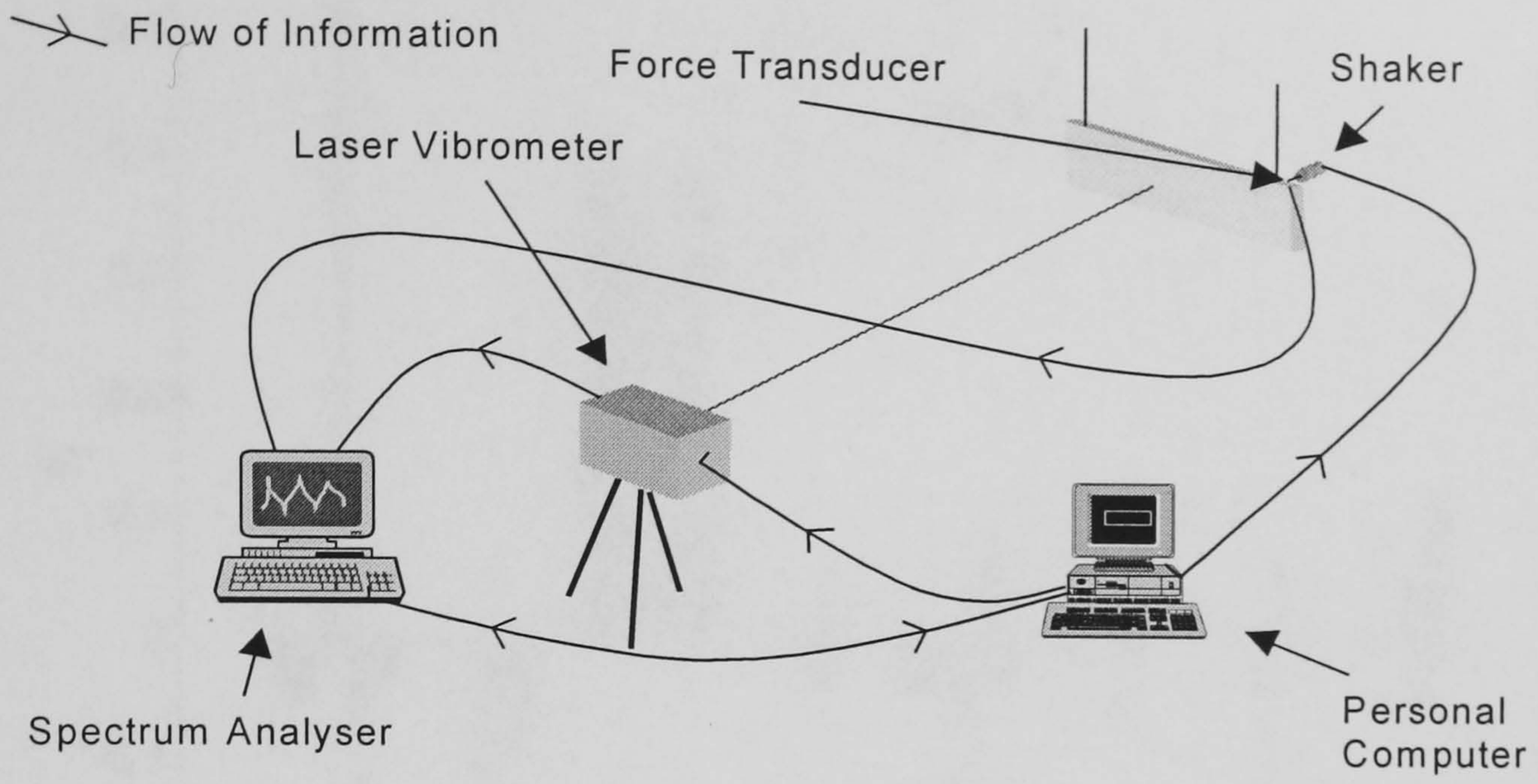

Figure 2.4 – Schematic of Experimental Arrangement; Testing of Narrow Plate

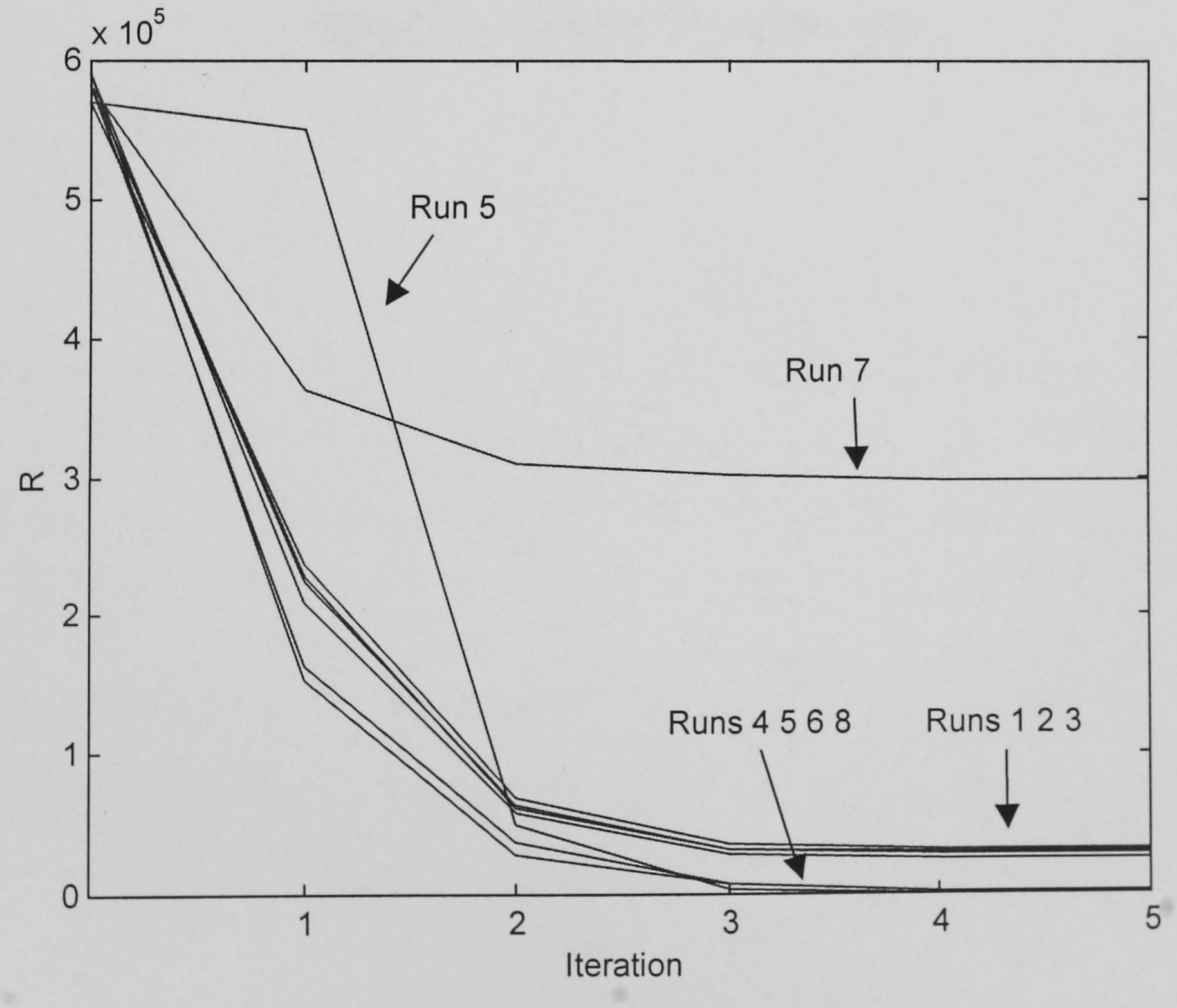

Figure 2.5 – Residual Values

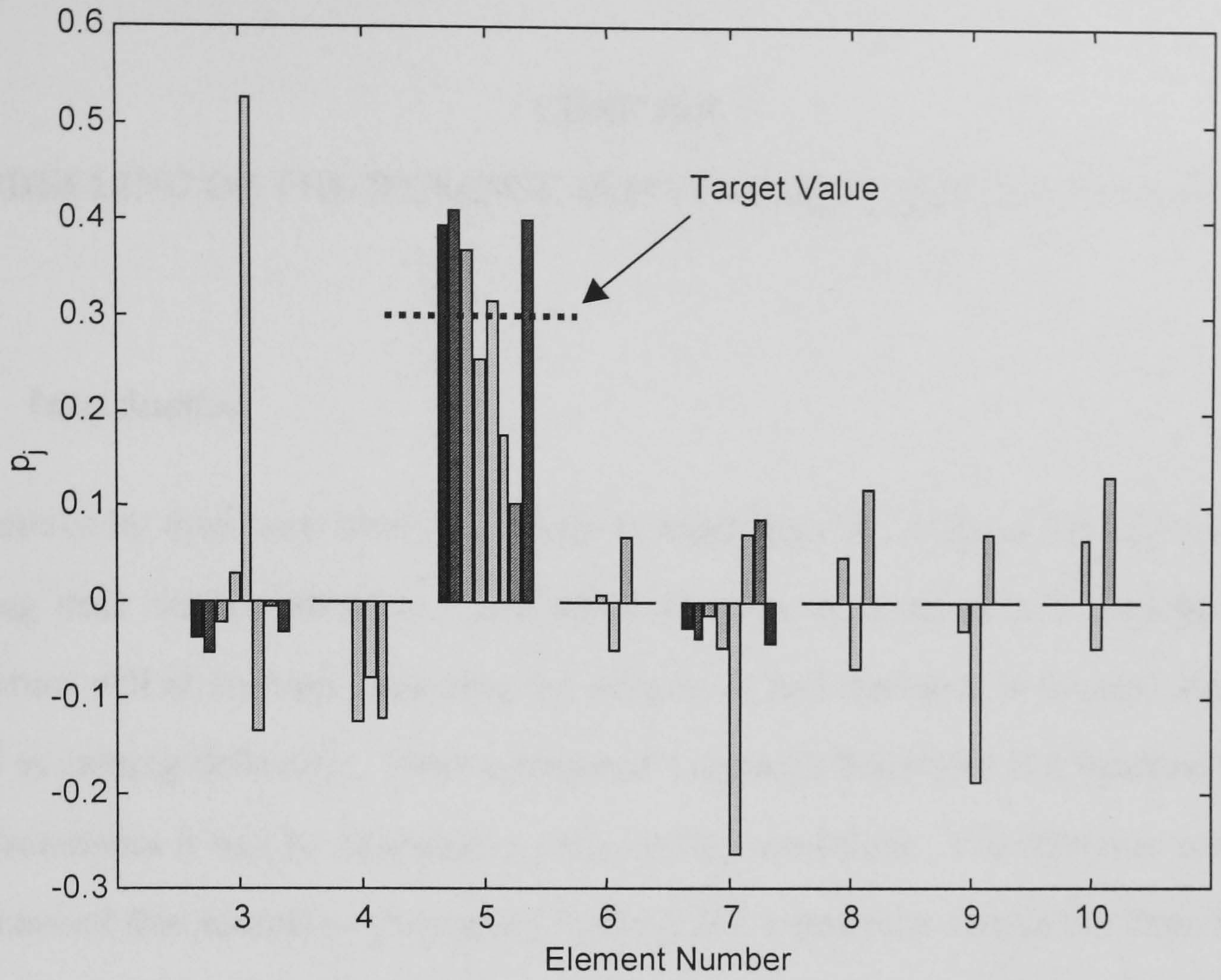

Figure 2.6 – Updated Parameter Sets

CHAPTER 3

MODELLING OF THE DYNAMIC BEHAVIOUR OF LOADED STRUCTURES

3.1 Introduction

Structures by their very nature are likely to experience a variety of loading conditions during their service lifetimes. The effect of static or quasi-static[10] loading upon a structure will at the very least alter the magnitude and direction of internal stresses as well as causing deflection. Since a structure's dynamic behaviour is a function of these characteristics it will be dependant on the loading conditions. It is therefore commonly understood that structures undergoing loading will experience changes to their dynamic behaviour. This very phenomenon is exploited when tuning a stringed instrument for example, as the pitch of a tensioned wire is observed to change with its axial loading.

The common practice of modal testing of structures in unconfined 'free-free' conditions minimises the interaction of structural components with the outside world. The consequence is that the dynamic behaviour of the test structure itself can be considered in isolation. The result of this approach is that the effect of load-dependence of dynamic behaviour upon validation and updating of finite element models has been largely overlooked. Given that structures are likely to experience a range of loading, we take as premises that:

(a) loading can effect dynamic readings; and

(b) the structural changes which result from loading can be accounted for in a finite element model.

---

10 This implies that while loading might change during time, the rate of change is sufficiently small that inertial forces need not be taken into account when considering equilibrium. This definition applies whenever static loading is referred to later.

Thus, it is incumbent upon the engineer to investigate the possibility of altering finite element models to reflect the loading conditions.

Two principal factors altering the dynamic response of loaded structures will be considered in this chapter, they both fall under the general heading of *geometric nonlinearities*. The first is stress (or geometric) stiffening in which axial load in slender beams and membrane forces in thin plates or shells interact with small out of plane deflections. The second concerns[11] a structure's form while under static loading which will deflect and hence alter the response. While it is not inconceivable that static loading will affect the dynamic response of a structure in other ways - for instance the damping at joints - these are less easily defined and modelled and will not be considered in this thesis.

It is important to note that although the consideration of large displacements falls into the category of nonlinear geometry, this term refers to the *overall* relationship between force and displacement. The solution method itself involves approximating the nonlinear relationship by a number of linear steps. The validity of performing an eigenvalue analysis upon a structure which has been altered in the nonlinear sense still holds. Figure 3.1 shows schematically that for levels of dynamic loading which are small compared with the static loading, the stiffness of the structure can accurately be represented by the *tangent stiffness*. In the experimental studies in the following chapers the amplitude of the dynamic load is of the order of 0.1% of the static loading.

Both stress stiffening and large deformation can be accounted for in finite element analyses. They each require at least a single reformulation of the finite element structural matrices. For large load levels, flexible structures, or if high solution accuracy is required, the structural matrices might require reformulation a large number of times.

---

[11] A third factor concerning the 'bowing' of structural members (or finite elements) completes a trio of factors quoted by most authors, and is investigated in detail in [64]. This deformity necessarily involves large elemental strains. In the context of finite element modelling this effect is an extension to discretisation inaccuracies and thus while its effect is noted it is regarded as being insignificant compared to stress stiffening and geometry changes.

Each of these actions potentially increases the cost of performing the analysis. It is interesting to note that in the field of validating and updating finite element models using dynamic data, facilities for including the effects of nonlinear geometry in modal analyses offered by most commercial finite element packages are rarely[12], if ever, used.

As the previous chapters have discussed, finite element model updating seeks to make changes to a finite element model. These result in the finite element model not only producing a closer dynamic response to the measured behaviour but being a closer facsimile of the structure itself. More specifically, the types of updating parameters which can be changed by finite element updating schemes have evolved to address the supposed sources of error in the FE model (see chapter 2). This chapter investigates the changes in FE models required to account for loading so that they can be included in the arsenal of updating parameters. The implementation of alterations to finite element models to account for loading upon a practical experimental example is described in chapter 4.

The phenomena of stress stiffening and large deflections are described in detail in the following sections. The derivation of the finite element formulation of each effect is demonstrated and their interdependence is described. The remainder of the chapter discusses the influence of these effects on dynamic modelling of structures and the practicalities of their inclusion in validation and updating procedures.

3.2 Stress Stiffening

Stress stiffening arises due to the interaction of an axial load on a thin structural member[13] with transverse motion. Lateral deflections are assumed to be sufficiently small that the axial load can be regarded as constant throughout the transverse motion.

---

[12] The author has been unable to find references for instances where the finite element model of a structure is altered prior to dynamic validation.

[13] Generally applicable to beams and plates. In the latter case it is a membrane load which interacts with transverse movement.

The influence of stress stiffening in the area of stability analysis of columns and shells as well as the vibration of slender structures is well established. Euler [65] took an interest in the subject in the mid eighteenth century; the ultimate load sustainable by a perfect slender column which bears his name results from a consideration of stress stiffening. The formulation is a function of the geometry of the slender structure and of the axial/membrane force itself but *not* of the elastic properties of the structure.

The importance of the phenomenon in a structural dynamics context is also well known. Lurie [66], for instance, explored the relationship between lateral vibration and the elastic stability of beams and plates in 1952. The relationship between frequency and end load were investigated experimentally on both struts and plates. In the former case the behaviour of two simple frameworks were examined.

The use of vibration data to assess the loading conditions and fixity of columns has been of perennial interest to engineers. Stephens [67] appears to be the first to consider the problem presenting a paper which claims that both parameters can be identified from the first resonant frequency although some corrections to Stephen's work were made some years later by Lurie [68]. Closer to the present day Plaut and Virgin [69] consider the steady state linear response to transverse harmonically varying load. The influence of an axial load specifically on the response is investigated for several boundary conditions.

The work of Lurie and others pre-dated the widespread use of the matrix methods in structural analysis and in particular finite element methods. Therefore, the complexity and range of structures which were amenable to analysis using simplified governing differential equations of motion were rather limited. The widespread implementation of the finite element method has revolutionised the size of problems upon which the effects of stress stiffening can be determined. As the following sections (principally section 3.2.2) will show, stress stiffening can be incorporated in the finite element method by the addition of extra terms to elemental stiffness matrices.

The following sections firstly derive the influence of axial loading on the closed form solution. This is followed by a description of the technique that implements the effect in

the finite element method. In common with previous and subsequent chapters both methods will be illustrated by means of the Euler-Bernoulli beam.

3.2.1 Closed Form Solution

Before investigating how stress stiffening effects are accounted for in the finite element method it is instructive to demonstrate how the effect can be included in closed form solutions. Note that the range of structural forms whose behaviour can be modelled using closed form differential equations is limited. The following relates to the development of the Euler-Bernoulli beam.

The basic governing equation for a beam can be found for instance in [70]. The loads acting on a small section of beam of length dx are shown in figure 3.2. Taking moments about the point marked P gives

$$S\delta x + M - \left(M + \frac{\partial M}{\partial x}\delta x \right) = 0\,, \tag{3.1}$$

where S is the shear force and M the bending moment. This leads to

$$S = \frac{\partial M}{\partial x}. \tag{3.2}$$

Continuing by resolving vertically yields

$$\frac{\partial S}{\partial x} = \rho A \frac{\partial^2 v}{\partial t^2}. \tag{3.3}$$

Also recall that a simplified relationship[14] between bending moment and curvature can be expressed as

$$M = -EI \frac{\partial^2 v}{\partial t^2}. \tag{3.4}$$

---

[14] This formulation neglects the influence of shear strain, the result being the so called Euler-Bernoulli beam model. If more accuracy is required an approach which considers the shear strain results in the Timoshenko beam formulation.

Combining (3.2), (3.3) and (3.4) leads to the familiar partial differential equation describing the dynamic behaviour of a straight two dimensional beam without external loading.

$$\frac{\partial^2}{\partial x^2} EI \frac{\partial^2 v}{\partial x^2} + \rho A \frac{\partial^2 v}{\partial t^2} = 0 \tag{3.5}$$

For a uniform beam this can be further simplified to

$$EI \frac{\partial^4 v}{\partial x^4} + \rho A \frac{\partial^2 v}{\partial t^2} = 0 \,. \tag{3.6}$$

This can be solved for various boundary conditions. Substituting $v(x,t)$ as the product of shape $V(x)$ and harmonic component $\sin(\omega t + \alpha)$ gives

$$v(x,t) = V(x)\sin(\omega t + \alpha) \tag{3.7}$$

substituting (3.7) in (3.6) leads to

$$\frac{d^4 V}{dx^4} - \frac{\rho A \omega^2}{EI} V = 0 \,. \tag{3.8}$$

Substituting

$$V = Be^{\lambda_0 x} \tag{3.9}$$

provides a suitable solution for (3.8) if

$$\lambda_0^4 = \frac{\rho A \omega^2}{EI} \tag{3.10}$$

which has the four roots $\lambda_0 = \pm\lambda$ and $\lambda_0 = \pm i\lambda$ where

$$\lambda = \left(\frac{\rho A \omega^2}{EI} \right)^{\frac{1}{4}} \,. \tag{3.12}$$

The general equation of motion is therefore

$$V = B_1 \sin \lambda x + B_2 \cos \lambda x + B_3 \sinh \lambda x + B_4 \cosh \lambda x \tag{3.13}$$

The unknowns, $B_1,...,B_4$, can be determined by applying the boundary condition constraints.

Equation (3.2) can be modified relatively simply to take account of the effect of a *time invariant* axial load, N shown in figure 3.3. This assumes that the transverse deflections during vibration are small enough that no time varying axial load needs to be considered:

$$S = -N\frac{\partial v}{\partial x} + \frac{\partial M}{\partial x} \tag{3.14}$$

Using this modified version of shear force we obtain a new partial differential equation describing the motion of a bar experiencing an axial load:

$$EI\frac{\partial^4 v}{\partial x^4} + N\frac{\partial^2 v}{\partial x^2} + \rho A\frac{\partial^2 v}{\partial t^2} = 0 \tag{3.15}$$

Exact solutions are only available for certain end conditions. If, for instance, the ends of the beam are considered as being pinned then

$$v(x,t) = B\sin\left(\frac{n\pi x}{L}\right)\sin(\omega_n t + \alpha) \tag{3.16}$$

is a solution to (3.15) provided

$$EI\left(\frac{n\pi}{L}\right)^4 - N\left(\frac{n\pi}{L}\right) - \rho A\omega_n^2 = 0\,. \tag{3.17}$$

The ability of the time dependent term in equation (3.16) to satisfy the modified differential equation of motion shows that the axial load does not affect the simple harmonic nature of the solution. However, the natural frequencies are altered with the n^{th} resonant frequency being given by

$$\omega_n = \left(\frac{n\pi}{L}\right)^2\left[\frac{EI}{\rho A}\left(1 - \frac{NL^2}{n^2\pi^2 EI}\right)\right]^{\frac{1}{2}}. \tag{3.18}$$

The resonant frequencies are seen to be a function of the axial load N. Substituting the well-known Euler buckling load

$$N_{Euler} = \frac{n^2 \pi^2 EI}{L^2}, \tag{3.19}$$

leads to

$$\omega_n = \left(\frac{n\pi}{L}\right)^2 \left[\frac{EI}{\rho A}\left(1 - \frac{N}{N_{Euler}}\right)\right]^{\frac{1}{2}}. \tag{3.20}$$

The relationship between transverse vibration and elastic stability becomes very clear. It is seen that

$$\omega_n^2 \propto N. \tag{3.21}$$

The mode shapes can also be shown to be affected by stress stiffening. Experimental results by Lurie [66] show close results for tests on beams. For a plate[15] he finds significant nonlinearity which he surmises is a result of initial curvature of the test specimen[16]. Massonnet [71] experienced similar results when considering the effect of circumferential loading of circular plates. He concludes that the perturbation to resonant frequencies are influenced by initial deformation.

Many authors consider only the change in the first resonant frequency with a view to studying the stability of the structure. Indeed the literature related to estimation of buckling load from frequency characteristics appears to concentrate exclusively upon the first mode of vibration. To the modern structural dynamicist, perturbations to any frequencies are of importance. The observation that *all* of the flexural modes will be affected by axial load as shown in (3.21) bodes well for including loading effects in updating procedures.

---

[15] This need not apply to exclusively to plates, a 3D beam with low second moment of area in one axis would demonstrate the same behaviour.

[16] The initial out-of-shape of structures is considered in a practical sense in chapter 4.

3.2.2 Finite Element Formulation

The closed form solution described in the previous section provides great insight into the influence of axial load upon simple structures. The inclusion of these effects into matrix methods of structural analysis allows stress stiffening effects to be considered for much more complex structures.

The application of the phenomenon described in the previous section was applied to the matrix method of structural analysis of both plates and beams by Gallagher and Padlog [72]. Continuing to consider the example of beam-type elements, a method for determining the stress stiffening effects on finite beam elements is described in [25]. The strain of a beam in bending, with only the normal stresses taken as contributing to the energy stored is given by

$$\varepsilon_{xx} = \frac{\partial u_0}{\partial x} - \frac{\partial^2 v}{\partial x^2} y + \frac{1}{2}\left(\frac{\partial v}{\partial x}\right)^2 \tag{3.22}$$

where u_0 is the axial change in length, $v(x)$ is the transverse displacement and y is the distance from the neutral axis. The first term of (3.22) is the axial strain term, the second term is familiar from beam theory relating to the energy stored in the beam in curvature while the third term expresses the lengthening of the beam element due to its rigid body rotation.

The strain energy is given by

$$U_i = \frac{E}{2}\int_V \varepsilon_{xx}{}^2 dV \,. \tag{3.23}$$

Substituting (3.22) into (3.23) leads to

$$U_i = \frac{E}{2}\int_V \left[\frac{\partial u_0}{\partial x} - \frac{\partial^2 v}{\partial x^2} y + \frac{1}{2}\left(\frac{\partial v}{\partial x}\right)^2\right]^2 dV \,. \tag{3.24}$$

For constant cross sectional area, A, expanding and omitting higher order terms gives

$$U_i = \frac{EA}{2}\int_0^L \left(\frac{\partial u_0}{\partial x}\right)^2 dx + \frac{EI}{2}\int_0^L \left(\frac{\partial^2 v}{\partial x^2}\right)^2 dx + \frac{EA}{2}\int_0^L \frac{\partial u_0}{\partial x}\left(\frac{\partial v}{\partial x}\right)^2 dx . \tag{3.25}$$

Recalling the relationship between general lateral displacement, v, and end displacements from equations (2.16) - (2.19)

$$\{v\} = \begin{bmatrix} 1-\frac{3x^2}{L^2}+\frac{2x^3}{L^3} & x-\frac{2x^2}{L}+\frac{x^3}{L^2} & \frac{3x^2}{L^2}-\frac{2x^3}{L^3} & \frac{x^2}{L}+\frac{x^3}{L^2} \end{bmatrix} \begin{Bmatrix} v_1 \\ \theta_1 \\ v_2 \\ \theta_2 \end{Bmatrix} \tag{3.26}$$

differentiating with respect to x gives

$$\frac{\partial v}{\partial x} = \begin{bmatrix} \frac{6x}{L^2}+\frac{6x^2}{L^3} & 1-\frac{4x}{L}+\frac{3x^2}{L^2} & \frac{6x}{L^2}-\frac{6x^2}{L^3} & \frac{2x}{L}+\frac{3x^2}{L^2} \end{bmatrix} \begin{Bmatrix} v_1 \\ \theta_1 \\ v_2 \\ \theta_2 \end{Bmatrix}, \tag{3.27}$$

and further

$$\frac{\partial^2 v}{\partial x^2} = \begin{bmatrix} \frac{6}{L^2}+\frac{12x}{L^3} & \frac{4}{L}+\frac{6x}{L^2} & \frac{6}{L^2}-\frac{12x}{L^3} & \frac{2}{L}+\frac{6x}{L^2} \end{bmatrix} \begin{Bmatrix} v_1 \\ \theta_1 \\ v_2 \\ \theta_1 \end{Bmatrix}. \tag{3.28}$$

Substituting (3.27) and (3.28) into (3.25) and minimising the total potential energy with respect to the nodal displacements leads to the elemental beam stiffness previously derived in chapter 2 – equation (2.23) - plus the stress stiffness matrix

$$[K]_e^{ss} = \frac{F}{L}\begin{bmatrix} 0 & 0 & 0 & 0 & 0 & 0 \\ & \frac{6}{5} & \frac{L}{10} & 0 & -\frac{6}{5} & \frac{L}{10} \\ & & \frac{2L^2}{15} & 0 & -\frac{L}{10} & -\frac{L^2}{30} \\ & & & 0 & 0 & 0 \\ & sym & & & \frac{6}{5} & -\frac{L}{10} \\ & & & & & \frac{2L^2}{15} \end{bmatrix}, \tag{3.29}$$

where F is the axial load. Like the formulation for the 2D beam element derived in the previous chapter, the formulation is not a unique representation of the effect of stress stiffening but is commonly used in commercial FE software.

If torsional stress stiffening is ignored, a similar expression can be gained for the modification to a three dimensional beam element using a symmetry argument.

$$[K]_e^{ss} = \frac{F}{L}\begin{bmatrix} 0 & 0 & 0 & 0 & 0 & 0 & 0 & 0 & 0 & 0 & 0 & 0 \\ & \frac{6}{5} & 0 & 0 & 0 & \frac{L}{10} & 0 & -\frac{6}{5} & 0 & 0 & 0 & \frac{L}{10} \\ & & \frac{6}{5} & 0 & -\frac{L}{10} & 0 & 0 & 0 & -\frac{6}{5} & 0 & -\frac{L}{10} & 0 \\ & & & 0 & 0 & 0 & 0 & 0 & 0 & 0 & 0 & 0 \\ & & & & \frac{2L^2}{15} & 0 & 0 & 0 & \frac{L}{10} & 0 & \frac{L^2}{30} & 0 \\ & & & & & \frac{2L^2}{15} & 0 & -\frac{L}{10} & 0 & 0 & 0 & -\frac{L^2}{30} \\ & & & & & & 0 & 0 & 0 & 0 & 0 & 0 \\ & & & & & & & \frac{6}{5} & 0 & 0 & 0 & -\frac{L}{10} \\ & & & & & & & & \frac{6}{5} & 0 & \frac{L}{10} & 0 \\ & & sym & & & & & & & 0 & 0 & 0 \\ & & & & & & & & & & \frac{2L^2}{15} & 0 \\ & & & & & & & & & & & \frac{2L^2}{15} \end{bmatrix}. \quad (3.30)$$

3.2.3 Implementation of Stress Stiffening

Most commercial packages allow the implementation of stress stiffening although it is not generally applied by default since modification to the stiffness matrix after at least one initial load step is required to determine axial loading. The perturbation of natural frequencies can easily be determined by modifying elemental stiffnesses by the expressions such as those given in equations (3.29) and (3.30), for a 2D and 3D beam respectively.

There is no limit to the range of loading to which the technique accurately applies although the derivation holds only for small rotations from the original element shape. For situations where significant elemental rotation occurs the change in geometry of the structure must be taken into account; this is investigated in section 3.3.

The question of whether the extra processing time and hence expense involved in including stress stiffening effects has occupied a number of authors. Ryu *et al.* [73] reviewed methods for determining whether stress stiffening effects should be included in dynamic simulations of rotating multi-body structures. The method proposed was intended for assessing whether stress stiffening reaches levels where static buckling is likely and is therefore not sensitive enough for assessing slight frequency perturbations.

Finite element model updating is a computationally intensive procedure. Therefore the extra cost in performing a loading step and subsequent eigenvalue analysis does not represent a significant extra cost and is an effective and useful exercise. This is particularly true in situations where dynamic data from a loaded structure are used to validate or update an FE model.

The engineer must consider all possibilities of loading to the structure including thermal effects.[17] The application of the worst case of loading (as one would perform in the design process) should include stress stiffening effects. The resulting system matrices would lead to an eigen-solution to determine the dynamic behaviour. This will enable the sensitivity of frequency response with respect to loading conditioning to be reasonable easily assessed. This information allows the engineer to discern whether the perturbations to resonant frequencies are of a scale which might affect a subsequent validation exercise. If the resonant frequencies are found to be sensitive to the loading level then the analyst must consider how best to monitor the load on a structure. This enables the effect of load to be taken into account. Issues relating to the identification of loading and the sensitivity of resonant frequencies to load are investigated in the following chapter.

---

[17] If the structure being tested is likely to experience a range of temperatures then the thermal expansion coefficient for all structural materials should be determined and included in the structure's properties in the finite element model.

3.2.4 Updating of Stress Stiffening Effects Using Conventional Parameters

As the term *stress stiffening* implies, the effect of an axial load is to change apparent transverse stiffness. The changes to structural matrices required to model the stress stiffening effects correctly cannot be accounted for by conventional finite element updating parameters. Therefore, the updated model may exhibit the correct modal and response properties, but on a physically unjustifiable basis [74].

A simple case study allows the effect of stress stiffening on conventional model updating procedures to be investigated. Consider the beam structure shown in figure 3.4 consisting of 13 elements modelled with simple 2D beam elements. The section and material properties are the same as the narrow plate structure described in the previous chapter (section 2.7). The structure has fixed ends and the whole beam is subjected to an axial load of 5kN[18]. The first four bending resonant frequencies of the beam predicted by finite element modelling are shown in table 3.1 along with the corresponding frequencies from an unloaded beam.

Unloaded Resonant Frequencies (Hz)	5kN Load Resonant Frequencies (Hz)	Absolute Decrease (Hz)	Percentage Decrease
63.1	55.1	8.0	12.7
173.9	163.4	10.4	6.0
340.9	329.6	11.3	3.3
563.7	552.0	11.7	2.1

Table 3.1 – Change in Resonant Frequency Under Loading

The bending frequencies are seen to be shifted by the approximately the same absolute value. It is well known that altering the overall structural stiffness on the other hand increases (or decreases) all frequencies by a common *factor*.

A rudimentary model update using the sensitivity of the first resonant frequency to the overall stiffness leads to the observation that the stiffness of the initial finite element

---

[18] The Euler buckling load in this case is 20.5kN.

model needs to be decreased by around 25% (or the mass increased by 25%). Figure 3.5 shows the point receptances (the excitation point being shown in figure 3.4) arising from matching the first resonant frequency of the updated structure with the "experimental" counterpart. It is very clear that the updated model - while meeting the single criterion set out in the updating procedure - is a significantly worse dynamic representation of the structure than the original finite element model. This is the "worst case scenario" and the inconsistency of the updated dynamic behaviour with the higher experimentally observed frequencies would be noted. If the first four frequencies are used to update the overall stiffness a reduction of 5% is reported, the resulting receptance is shown in figure 3.6.

In practice if more than one frequency is used to update the overall mass or stiffness of the structure, a poor final residual value should indicate that the observed frequency perturbations do not derive from mis-modelled overall stiffness.

3.3 Large Deformations

When structural loading is sufficiently large (or the structure particularly flexible) that the geometry of the structure changes during the load step, the stress stiffening approximation to the structures loaded characteristics may not be sufficient. To account for the deformity, equilibrium equations must be written with respect to the deformed geometry *which is not known in advance*. Although it is assumed that no components of structures undergoing modal testing will stray into plastic ranges, the solution procedure for geometric nonlinearities shares some similarities with the treatment of material nonlinearity.

Commonly the structural deflection is determined in a single step from the structural matrices and loading. The stiffness matrix - which was constructed from the initial estimates of geometry and material properties - is assumed to describe adequately the stiffness distribution representative of the structure for the entire load step. Cases exist where combinations of large loading and structural flexibility make it difficult to

determine the deflected geometry particularly accurately. In instances such as these the assumption that the stiffness remains constant throughout the load step might be inadequate.

An important concept is introduced at this point. The displacements experienced by an element can be split into those which cause straining of the element and those which cause rigid body motion of the element. That is

$$\{u\}^{total} = \{u\}^{rigid} + \{u\}^{strain}. \tag{3.31}$$

This is a simple yet important relationship. The rigid body displacement $\{u\}^{rigid}$ of any finite element consists of both translation and rotation components although only the latter has any effect on the elemental matrices. Therefore, the geometry for each element is a relatively simple rotational transformation. Figure 3.7 shows the rigid body and straining deformations for a two dimensional beam where the accurate determination of the rigid body rotation θ_r is the most important term since it defines the deformed shape and thus the dynamic response.

Most commercial finite element packages allow the implementation of both material and geometric nonlinear techniques. Indeed some packages, for instance ANSYS [16], have developed code to address this problem.

3.3.1 Finite Element Formulation

The simplest way to model the nonlinearity resulting from static loading is to discretise into a number of linear steps. This involves recalculation of the structural matrix at each point as suggested by Turner *et al.* [75]. The displacement at the $(n+1)^{th}$ load step is given by

$$\{u\}_{n+1} - \{u\}_n = [K]_n^{-1}\left(\{F\}_{x_{n+1}} - \{F\}_{x_n}\right) \tag{3.32}$$

The effect of loading upon an element can be included after the first load step and thus the effect of stress stiffening can be included in the nonlinear analysis. Improved results

can be obtained by increasing the number of load steps. An example of this approach for a single degree of freedom system is shown in figure 3.8 where the upper dotted line shows the result of recalculating the stiffness parameter at several discrete points. It is clear that a purely iterative approach can lead to a relationship between stiffness and deflection which diverges from the 'true' relationship. As the size of the load step decreases towards zero however the predicted line will converge upon the true one.

Another approach which is set out by Jennings [76] is to combine the previously described incremental approach with a series of equilibrium iterations.

A very large amount of literature is published on the subject. Much of this - [77] being a good example - is related to determining accurately the force displacement relationship for very large elemental rotations. This situation is most likely to occur near collapse. As far as the current discussion is concerned, the interest is not in extreme deformations but small deformations to which the dynamic behaviour of the structure can be sensitive. In this case elemental rotations while needing to be determined accurately are not of a large magnitude.

For illustrative purposes, a method for establishing the nonlinear relationship between load and displacement will be described. The method is an iterative solution and involves moving co-ordinates. It is clearly set out by means of an example in [26].

Considering a structure exhibiting small deflections under the action of small loads

$$[K]\{\Delta X\} = \{\Delta F\}, \tag{3.33}$$

where $\{\Delta X\}$ are sufficiently small changes in deflection that $[K]$ is linear. The forces comprise the specified loading plus loading applied at nodes by elemental distortion. For equilibrium we must achieve

$$\{\Delta F\} = 0. \tag{3.34}$$

At this point, the example of stiffness changes to a 2D beam will be considered in detail; note however that the method is general. The straining displacement of such a 2D beam

can be described by two end rotations and an axial displacement relative to suitable local axes

$$\{u\}^{strain} = \{0 \quad 0 \quad \theta_1 \quad e \quad 0 \quad \theta_2\}^T \tag{3.35}$$

where definitions of θ_1 and θ_2 are shown in figure 3.7. The loading upon a single element resulting from the deformations are found to be

$$\{f\} = -[K]_e \{x\}. \tag{3.36}$$

Summing over all elements and substituting into (3.32) to find the global displacements gives

$$\{\Delta X\}_{i+1} = [K]_i^{-1} \left(\{F\} - \sum_{j=1}^{n_{elems}} [K]_{e_j} \{x\}_j \right), \tag{3.37}$$

where $\sum_{j=1}^{n_{elems}}$ represents matrix building of n_{elems} elements rather than straight summation and $\{F\}$ is the external static loading on the structure. The overall structural deformations are updated at each step using the relation

$$\{X\}_{i+1} = \{X\}_i + \{\Delta X\}_{i+1}. \tag{3.38}$$

The most convenient convergence criterion is to consider the incremental displacements. Bergan and Clough [78] recommend that convergence should be based on the ratio:

$$r = \left| \{\Delta X\}_i / \max(\{X\}_i) \right|, \tag{3.39}$$

where $\max(\{X\}_i)$ is the maximum displacement of the same type as $\{X\}_i$. The lower this value is set, the tighter the convergence. The choice of convergence criteria requires engineering judgement. If the deformed structural matrices are to be used to perform a subsequent dynamic analysis, then the sensitivity of eigenvalues and possibly mode shapes to small changes in structural geometry must be considered.

Nonlinear geometry methods that take account of large deflections are a superset of those described in the previous section. These account for the stress stiffening effect.

That is, the stress stiffening elemental stiffness modifications can be included in the iterative procedure. These account for the transverse lack of stiffening affecting both the static solution and the subsequent resonant frequency.

3.3.2 Effect of Boundary Conditions

The influence of deformation of structural members upon vibration characteristics is itself very strongly influenced by the boundary conditions. This can be demonstrated by means of a simple simulation based on a real situation. A plate such as the one described in section 2.6 was ordered from a standard supplier and found to contain a noticeable camber arising from the manufacturing process. The plate deflection is plotted with equally scaled axes in figure 3.9. It can be seen that while discernible, the camber is far from spectacular. The maximum deflection is 4mm over the span of 850mm.

The plate was modelled using seventeen 2D beam elements as described in chapter 2, with and without the deformation included and with clamped and free boundary conditions. The results are shown in table 3.2 from which it can be seen that there is no difference to the frequency perturbation for the free plate but a considerable (33%) increase in the fundamental resonant frequency for the completely fixed situation. The increase in the first natural frequency with amount of deformation is shown in figure 3.10.

	Fundamental Natural Frequency (Hz)	
	Flat	Deformed
Free-Free	36.88	36.87
Clamped-Clamped	36.88	47.94

Table 3.2 – Interaction of Boundary Conditions and Deformity

The observation ties in with early analytical work on the vibration of curved bars [79,80] showing that for a beam with symmetrical curvature the first mode of vibration is most strongly altered.

This observation has interesting and significant repercussions on the process of validation of finite element models of substructures. If the plate is tested independently of a structure into which it will eventually form a part, the response of the deformed plate will be indiscernible from that of the straight structure. However, if the deformity of the plate exists when assembled into the superstructure, the stiffness of its constraints will affect its dynamic response considerably.

Generalising from this simple case by considering a more complex structure containing components which are deformed. The deformation could be the result of any one of a number of factors such as manufacturing imperfections or simply in response to in-service static loading. The dynamic behaviour is likely to be altered but unlike the simple beam example described above whose first mode is sensitive to the deformation, a wider range of modes are likely to experience perturbations. This hypothesis is tested by means of an experimental case study in the following chapter (section 4.3).

3.4 Effect Upon Validation / Updating

As the foregoing discussion has shown, the effect of stress stiffening upon structures is to alter the apparent transverse stiffness of structures subject to axial loading. The result is that all of the *flexural* resonant frequencies are shifted in the same direction while extensional frequencies are not altered.

The changes to elemental matrices to account for the change in behaviour derived in section 3.2.2 cannot be included in an updated finite element model using any conventional updating parameter. Limiting the modifications to elemental stiffness, density, or cross sectional area is inadequate.

The highly underdetermined nature of updating parameters is such that a huge number of sensible changes to arbitrary sets of updating parameters will result in an apparently successfully updated model. However, if loading is present in a structure then modifying its dynamic behaviour through a model update is invalid. The stress stiffening matrix alterations necessary for making justifiable changes to the original finite element model are omitted.

The same observation can be made for the transformation resulting from the large-deflection transformation. In this case the transformation consists of a rigid body rotation. To take account of the changes to an elemental matrix caused by loading in an updating procedure the updated matrix would take the form

$$[K]_e^u = [T]^T \left\{ [K]_e + [K]_e^{ss} \right\} [T], \tag{3.40}$$

where $[T]$ is a rotational transformation of the type described in chapter 2. The simplicity of this relationship belies the computational effort which is required to derive $[T]$ and $[K]_e^{ss}$. This is significant and the relationship is exploited in chapter 5 which considers the use of these quantities as updating parameters.

3.5 Concluding Remarks

The factors which are responsible for changes to dynamic behaviour of structures have been set out. Methods for incorporating these techniques into finite element models have been outlined. The specific case of the 2D beam element is considered in some detail.

The relative importance of two phenomena, namely stress stiffening and structural deformity, in altering dynamic behaviour of structures has been investigated.

The apparent stiffness of boundary conditions are shown to be crucial in influencing the extent to which the dynamic behaviour of a deformed structural component is altered. It is shown that the a deformed component tested in free-free condition displays much the same dynamic characteristics as its undeformed counterpart.

The phenomena which result in changes to dynamic behaviour under loading have been shown to be encapsulated by relatively simple alterations to finite element structural matrices. Conventional model updating techniques using elemental mass and stiffness used to update loaded structures are invalid.

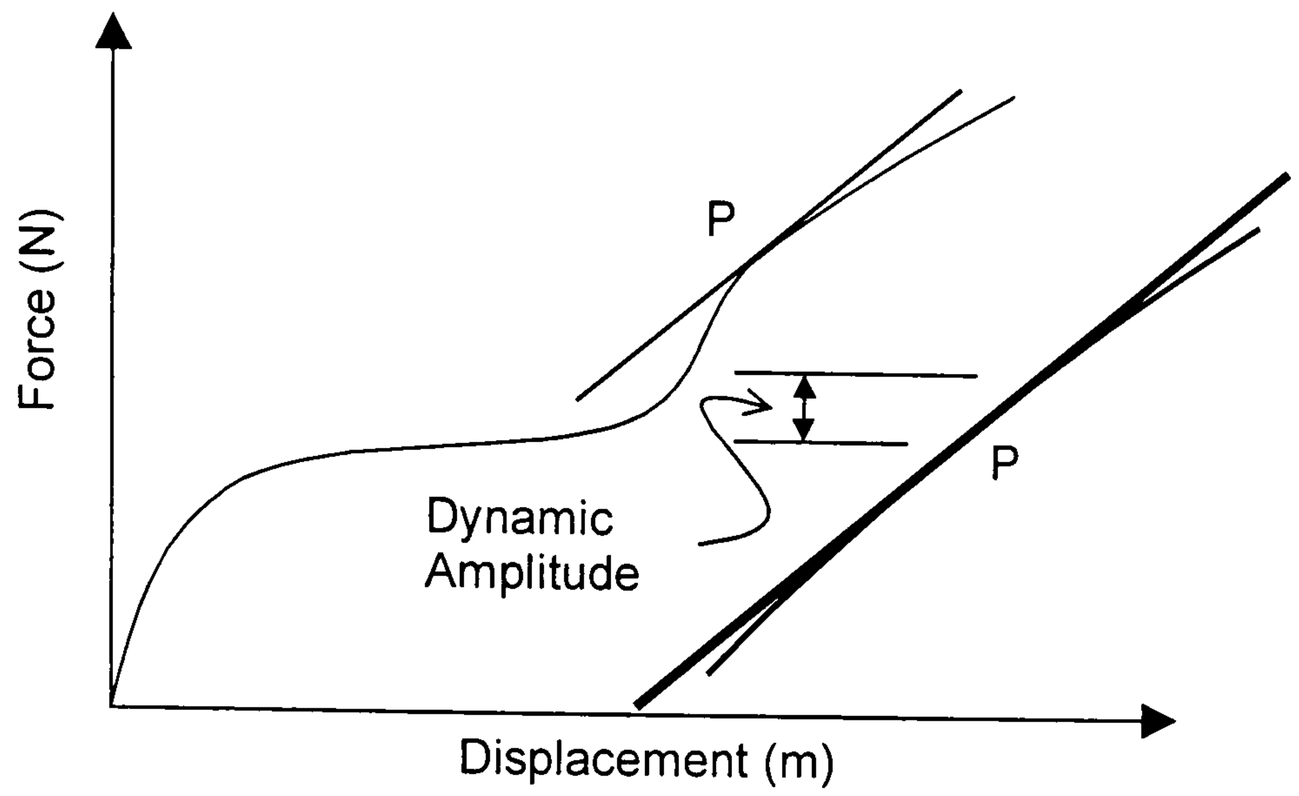

Figure 3.1 – Tangent Stiffness

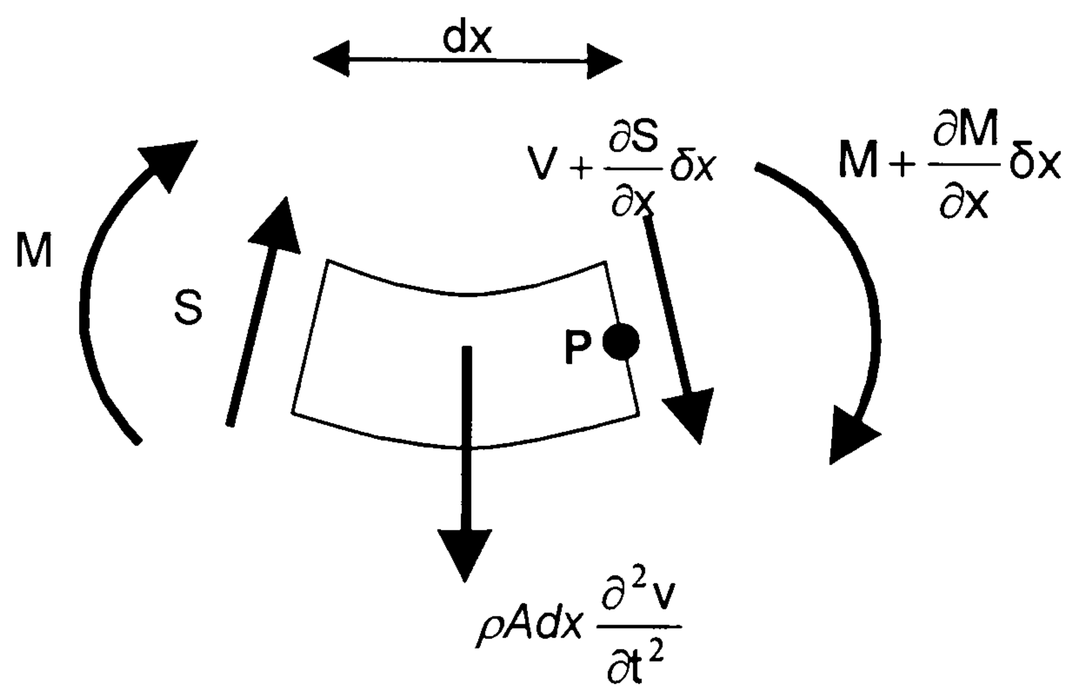

Figure 3.2 – Forces Acting on A Small Portion of Beam

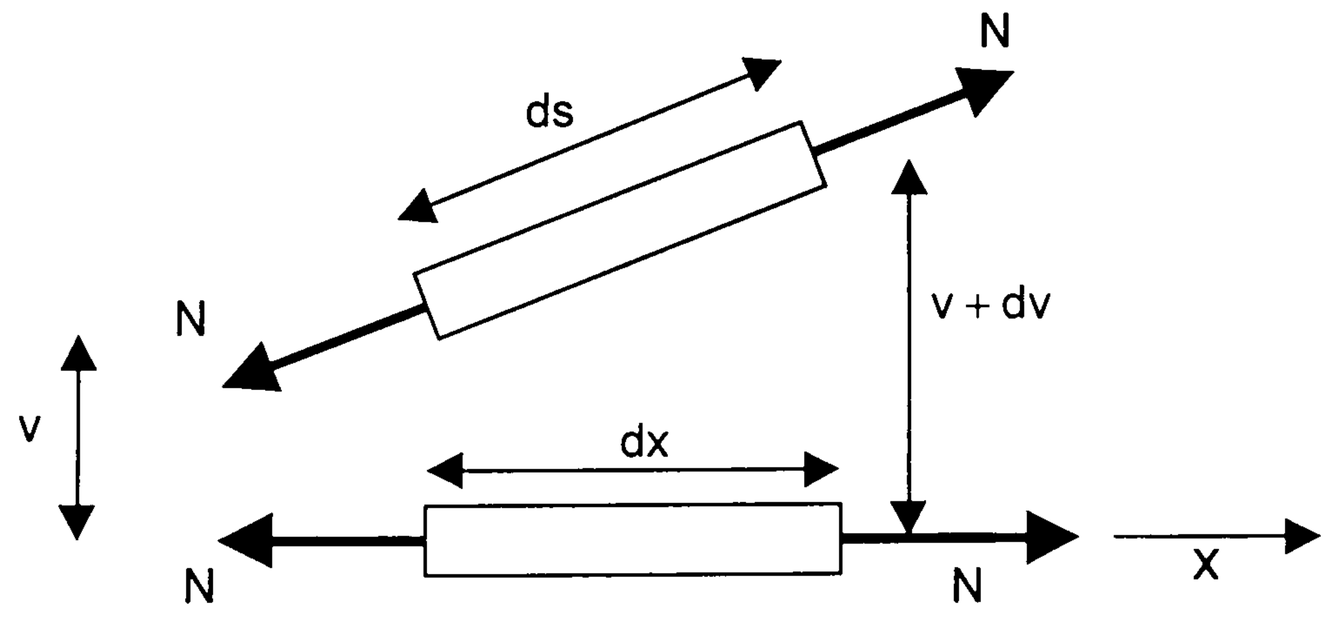

Figure 3.3– Lateral Movement of Small Beam Element Under Constant Axial Load

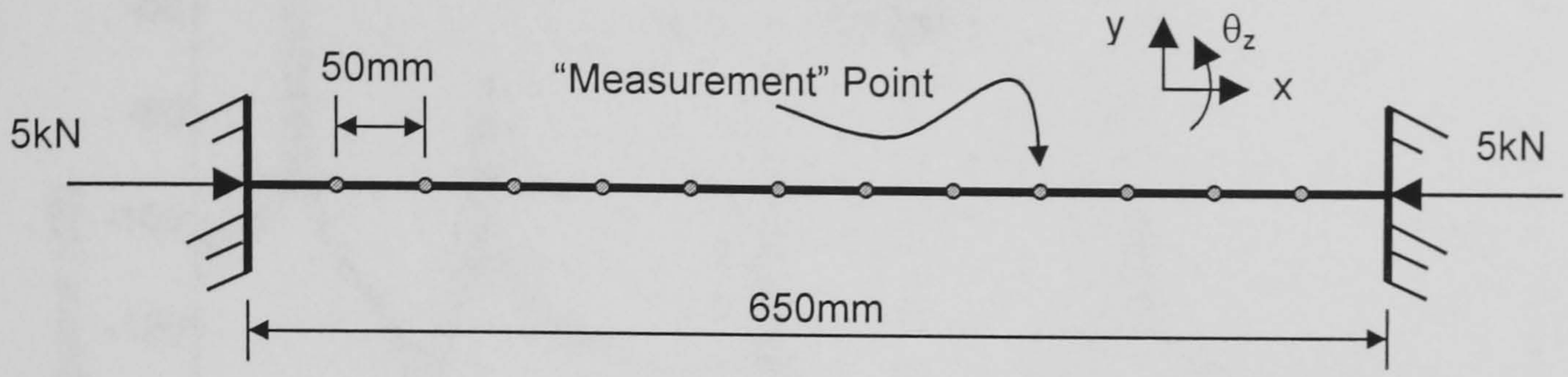

Figure 3.4 – Fixed-Fixed 13 Element Beam

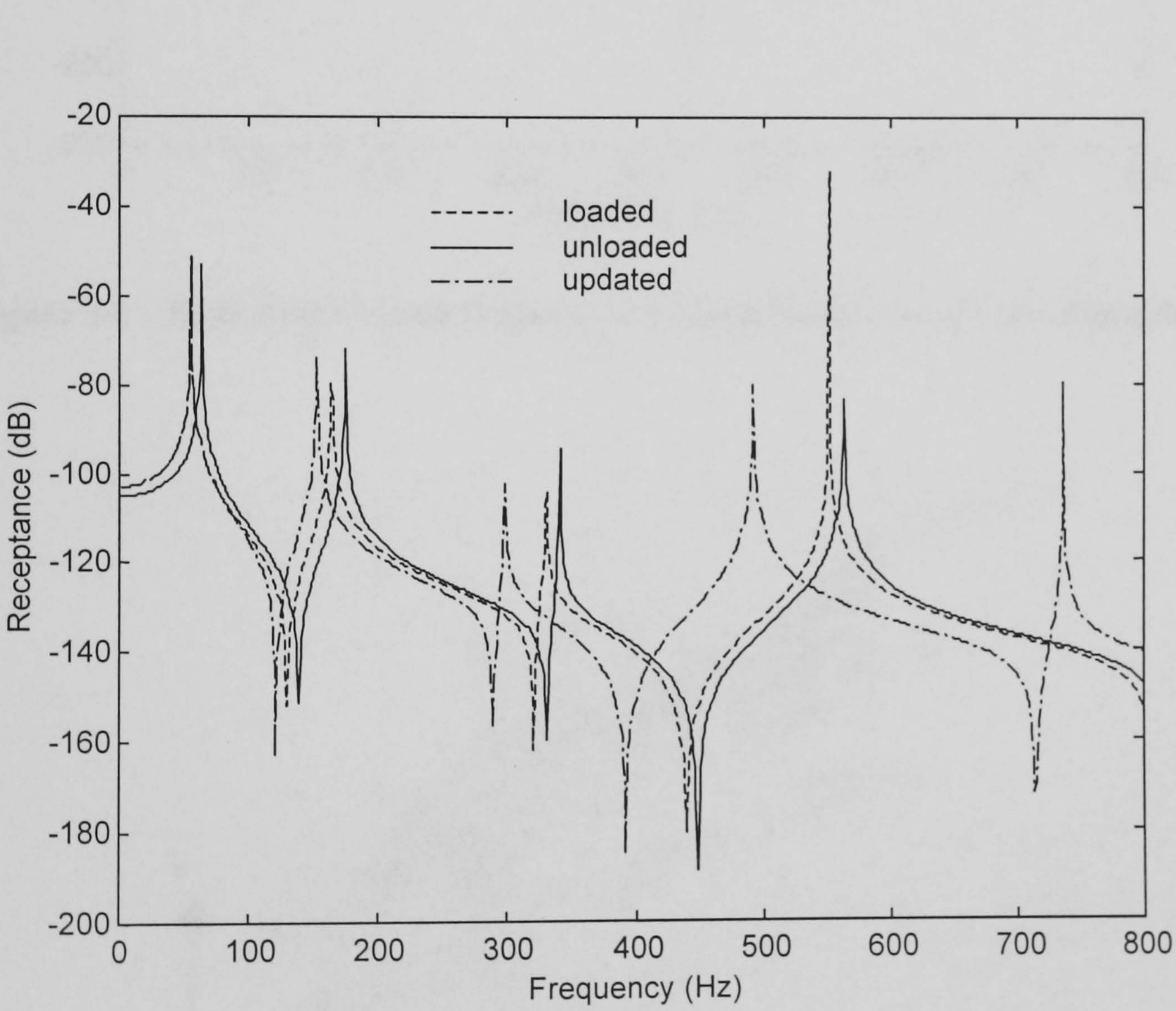

Figure 3.5 – Updating Overall Stiffness of Loaded Beam Using First Eigenvalue

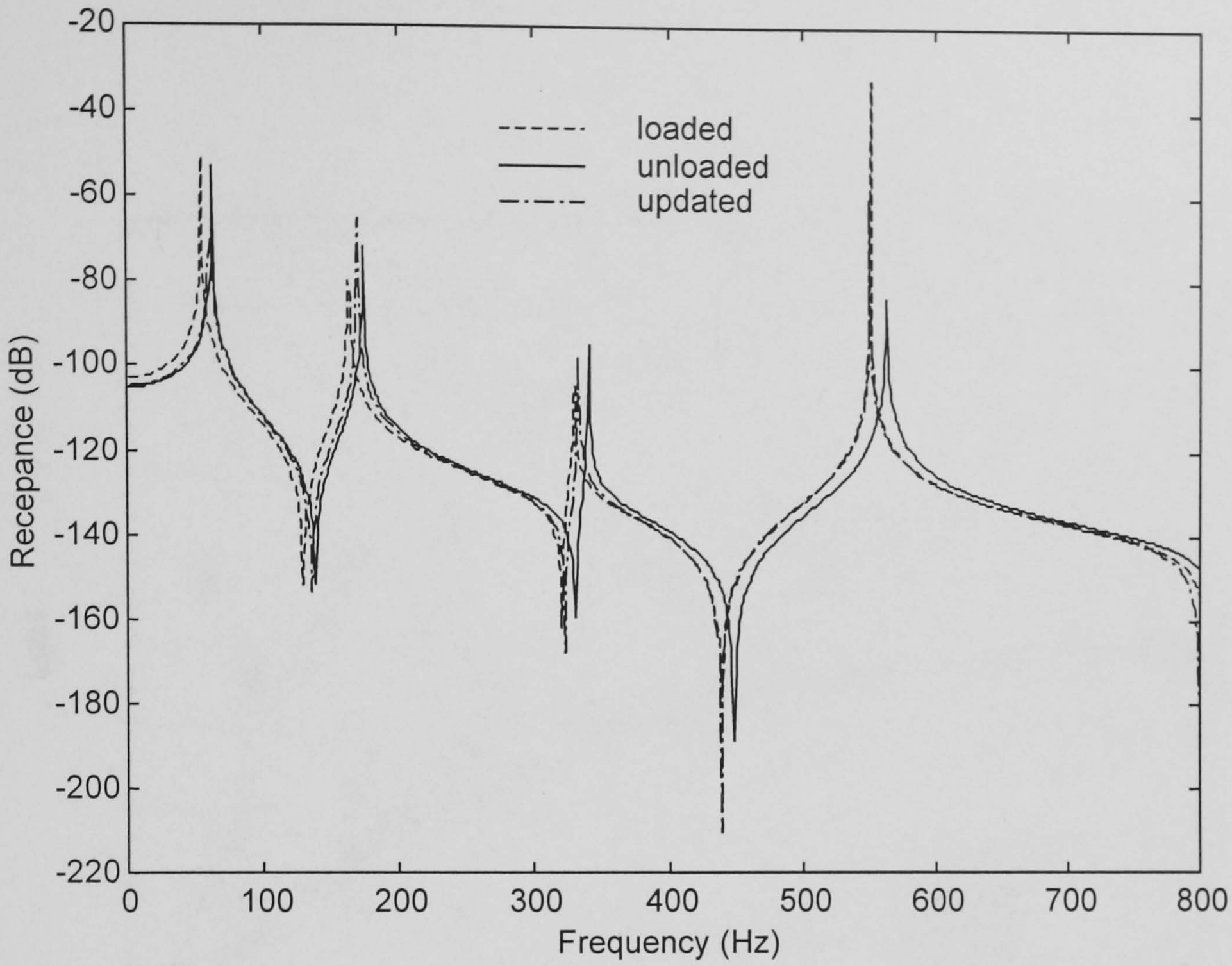

Figure 3.6 – Updating Overall Stiffness of Loaded Beam Using Four Eigenvalues

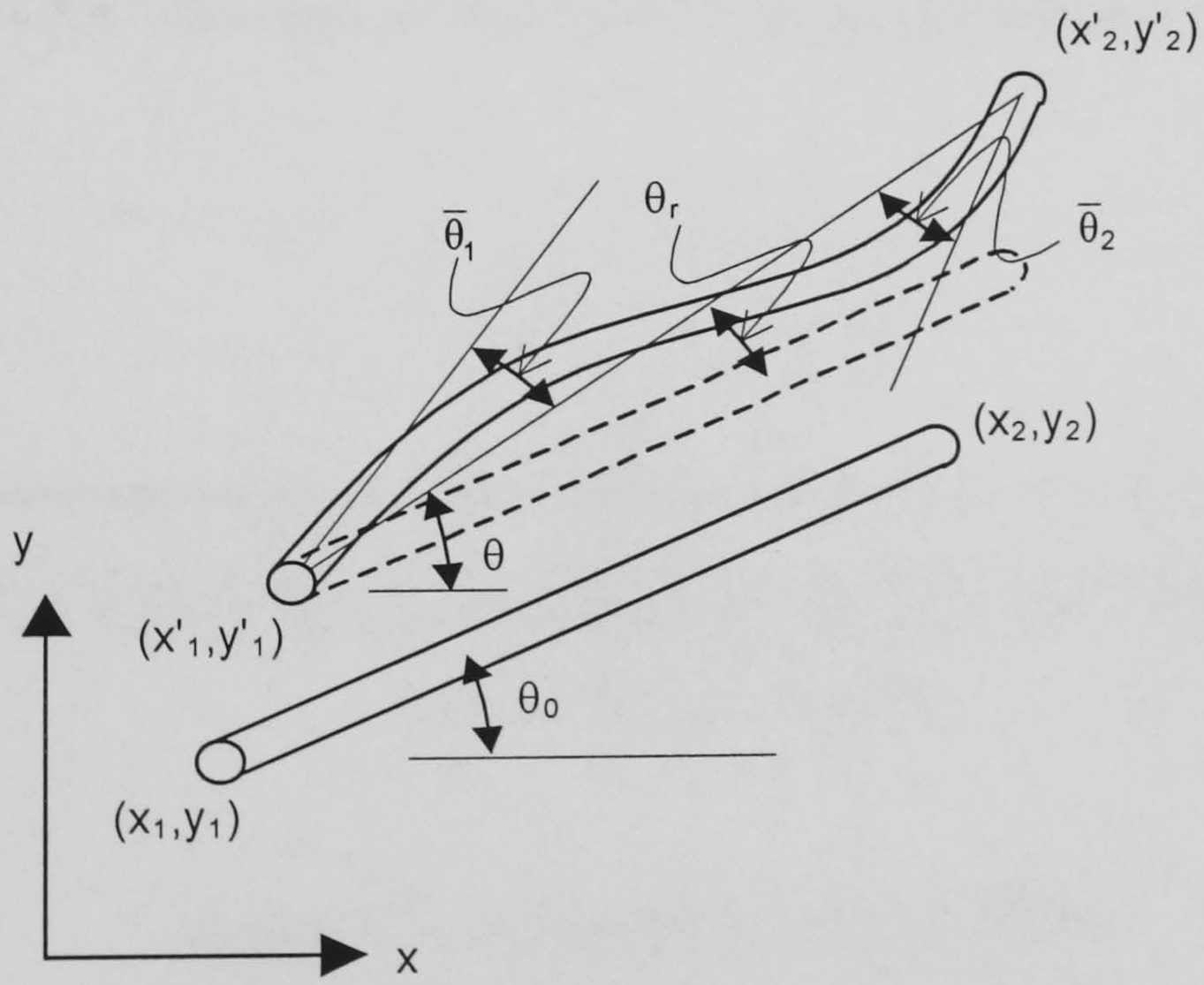

Figure 3.7 – Rigid Body and Straining Displacements of 2D beam

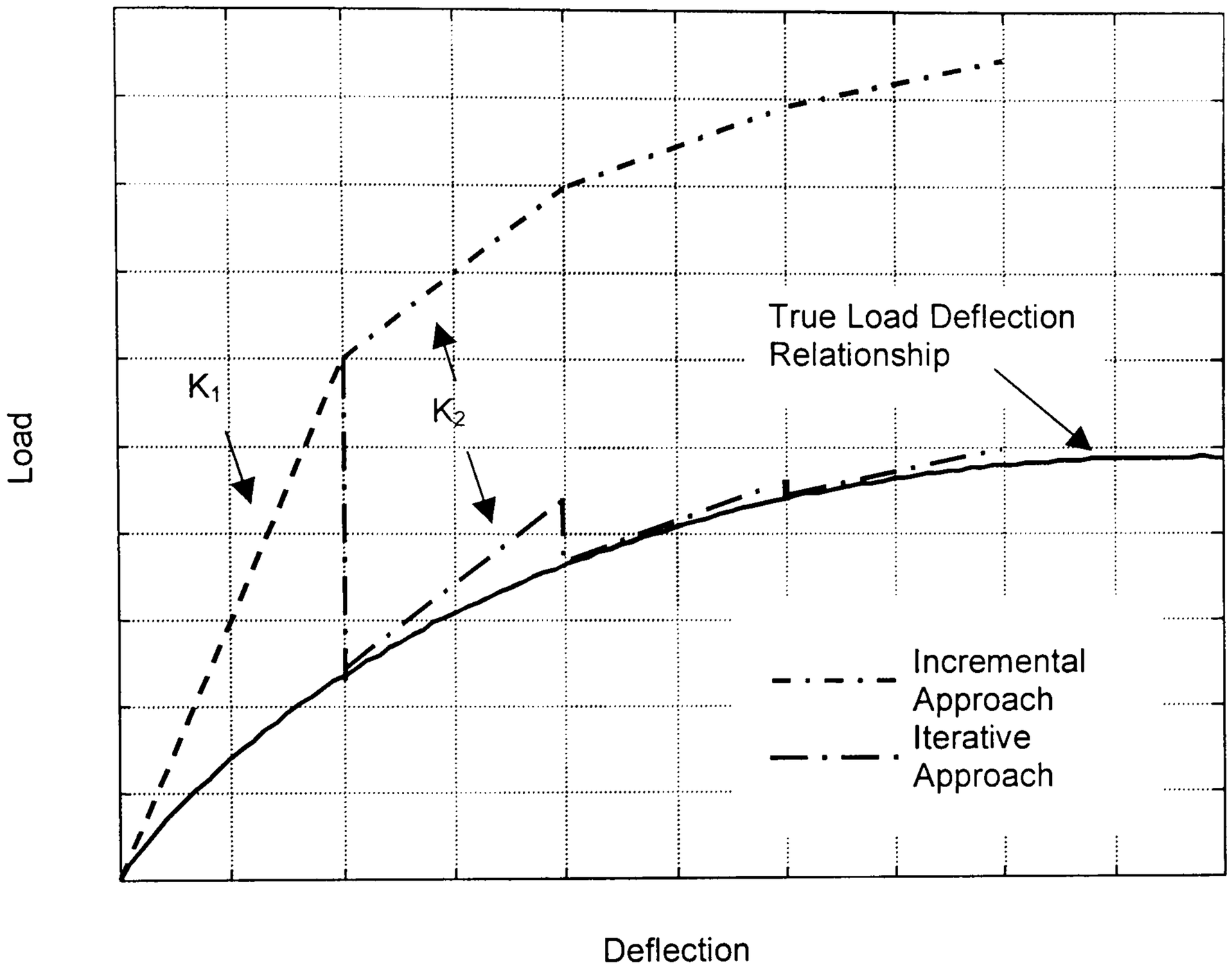

Figure 3.8 – Iterative vs. Incremental Tangent Stiffness Calculation

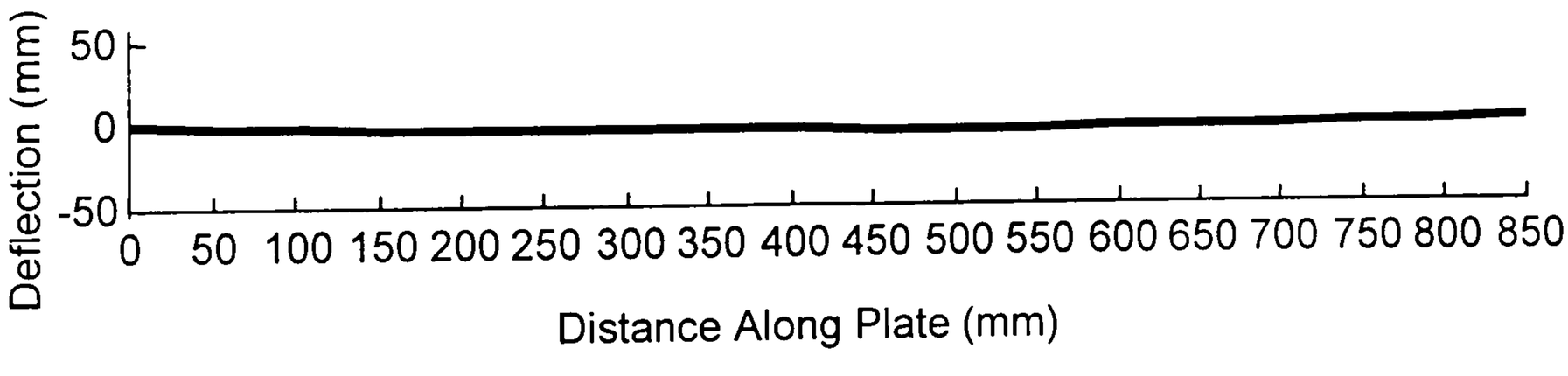

Figure 3.9 – Measured Deflection of Plate

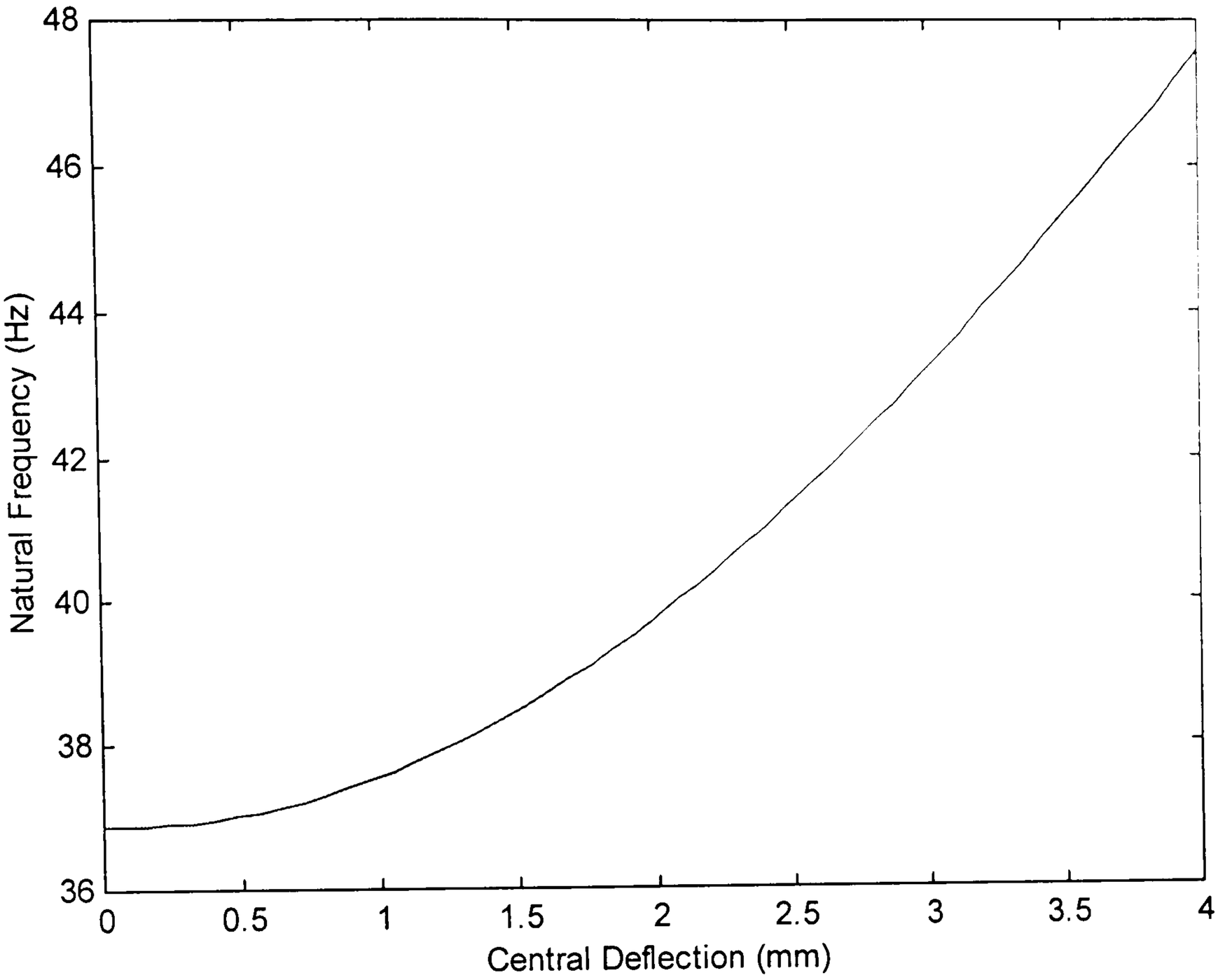

Figure 3.10 – Change in Natural Frequency Magnitude of Deformation

CHAPTER 4

EXPERIMENTAL STUDY OF THE DYNAMIC BEHAVIOUR OF LOADED STRUCTURES

4.1 Introduction

The previous chapters have discussed how changes to dynamic behaviour resulting from loading to structures can occur. Finite element techniques for taking account of the changes to structures due to loading have been developed. To assess the validity of finite element models which have been altered in this way, some practical validation of the "statically updated" finite element model is required. To this end, this chapter presents two experimental case studies in which the dynamic behaviour of structures subjected to controlled loading is investigated. The results are compared with the FE modelling techniques described in the previous chapter.

The first case involves the consideration of a slender structure whose state of loading can be altered due to its inclusion in a relatively substantial testing structure. This arrangement is directly analogous to the situation where a structural component – or substructure[19] - is tested and its FE model validated in free-free conditions before being included in a larger assembly.

The direct identification of static loading to a structure is likely to be impractical in a real-life situation. This is because the loading can arise as a result of such wide range of factors. The experimental study describes a method of identifying load indirectly from surface mounted strain gauges. The example shares clear similarities with methods which measure bridge strain using optical fibres [81].

---

[19] A sub-structure is a constituent part of a larger structure some of whose properties are determined independently of its parent structure.

The second experimental example allows the influence of loading to be investigated in isolation. The acquisition of spatial data enables some conclusions to be drawn about the influence of the loading on mode shapes. Direct identification of loading is possible in the second experimental set-up.

4.2 Test on Narrow Steel Plate

A test rig was designed and constructed [82] to apply loads to certain simple structures. This section considers the behaviour of a narrow steel plate under loading. The free-free behaviour of the plate has previously been studied in chapter 2, being mild steel and measuring 100mm wide by 5mm deep and 850mm long. The shape was chosen such that the structure could reasonably be modelled using either plate or more elementary beam finite elements.

The narrow plate underwent dynamic testing under several static loading regimes. The test allowed some of the issues related to the determination of loading in real structures to be investigated. The study demonstrates why the resulting changes to the structure should be accounted for in a subsequent dynamic analysis.

4.2.1 Application and Identification of Loading

A schematic of the experimental arrangement is shown in figure 4.1. Loads are induced in the test structure by changing the position of the end masses relative to the adjustment bars by means of nuts on the threaded ends of these bars. The 100mm at each end of the plate were clamped within the two large masses which comprise the test rig producing an encastré connection. The test rig was designed to be sufficiently stiff that the test specimen experienced boundary conditions approaching fixity. The two end masses weigh 100kg each and the adjustment bars are solid and measure 40mm in diameter.

As in most situations where direct experimental determination of loading onto individual components is impractical or impossible, the loading on the structure within the testing rig needs to be determined indirectly. To this end, small single-element

electrical resistance strain gauges were placed at a number of locations along either side of the plate. These allowed the longitudinal strain - and hence stress - distribution on each surface of the structure to be assessed. This in turn permitted identification of loading applied to the plate relative to an initial set of conditions. The strain gauges and associated wiring were sufficiently unobtrusive to have little effect on the plate's stiffness. As chapter 1 has outlined, this type of instrumentation strategy would offer a versatile method of instrumenting pre-existing structures to help to characterise their loading regimes through time. More specifically, substructures tested with free-free boundary conditions could be instrumented to determine loading introduced though boundary conditions. The measured loads could then be used for dynamic validation of the in-situ finite element model.

Figure 4.2 shows the location of the strain gauges along the plate. It also indicates the co-ordinate system and the single point at which excitation was applied and dynamic response was measured. The strain gauges were placed in pairs on opposite sides of the plate. Strain readings were logged continuously throughout the testing programme, beginning with the plate "resting" in an entirely unconfined state and ending in the same condition. Four different load regimes were introduced in to the specimen by adjusting the length of the bars joining the masses. The four load cases will henceforth be referred to as cases A, B, C and D. Note that case A was intended to represent the plate with zero loading. The discrete points in figure 4.3 show the measured stress distribution along the top and bottom of the plate in each of the four load cases assuming a linear relationship between stress and strain.

Identification of the loading applied to the plate from a knowledge of the stress distribution is not a trivial task. The strong nonlinearity of the stress distributions raises some doubt about whether the use of a simple linear model to estimate the stress - from bending moment and axial load - would produce a sufficiently accurate prediction of loading. The most rigorous method available using the finite element method is to determine the deflected shape of the plate accurately using a nonlinear geometric

techniques described in the chapter 3. The consideration of less computationally intensive methods of determining loads from the measured stress distribution are described at the end of this section.

The plate was modelled in MATLAB [14] using a finite element toolbox - CALFEM [15] - with thirteen 2D Euler-Bernoulli beam elements (described in chapter 2). Elemental stress is determined from the displacements of the nodes of each beam element. The relationship is set out in equation (2.29)

$$\sigma_{flexural} = E[B]\{\Delta\}y\,, \tag{4.1}$$

where E is the Young's modulus of the material, $[B]$ is the strain displacement matrix, $\{\Delta\}$ are the nodal shearing and rotational displacements and y is the distance from the neutral axis at which the stress is required.

Recall that one of the premises of the finite element method is that the stress is assumed to vary linearly between elemental nodes. For the two dimensional beam element the flexural stresses are given by

$$\left[-\frac{6}{L^2}+\frac{12x}{L^3} \quad -\frac{4}{L}+\frac{6x}{L^2} \quad \frac{6}{L^2}+\frac{12x}{L^3} \quad -\frac{2}{L}+\frac{6x}{L^2}\right]\begin{Bmatrix} v_1 \\ \theta_1 \\ v_2 \\ \theta_2 \end{Bmatrix} Ey\,. \tag{4.2}$$

Rotation of the central axis of the beam allows the flexural stress to be cast entirely in terms of two rotations

$$\left\{\left(-\frac{4}{L}+\frac{6x}{L^2}\right)\bar{\theta}_1+\left(-\frac{2}{L}+\frac{6x}{L^2}\right)\bar{\theta}_2\right\}Ey\,, \tag{4.3}$$

where the rotations are now relative to the local axis passing though both ends of the deformed element. The local rotations $\bar{\theta}_1$ and $\bar{\theta}_2$ can be seen in figure 3.7 from the previous chapter. The longitudinal axial stress resulting from the x-direction displacements of the ends of the element is known to be given by

$$\sigma_{axial} = \frac{AE}{L}\Delta u \tag{4.4}$$

where

$$\Delta u = u_2 - u_1 . \tag{4.5}$$

Since the estimation of stress is not absolute[20], any attempt to determine loading and resulting deflected shape of the structure will also be non-absolute. To establish an estimate of the absolute loading and hence the structure's dynamic behaviour some extra information is required. This would then enable identification of the deflected shape Using only static observations two possibilities presented themselves; the first is to regard case A - where the test rig was adjusted so that the end blocks were parallel and thus the plate was close to being flat - as the datum. The alternative was to take readings relative to the entirely unconfined plate. The unexpectedly large loading observed in case A (top graph in figure 4.3) led to the adoption of the latter scheme.

The magnitude of the initial deflection was surveyed and found to be a smooth but non-symmetrical curve with maximum eccentricity of 2.4mm. The measured shape of the plate was included in an initial FE model which then corresponded closely to the state of the plate at the point of assumed zero strain. A Nelder-Mead[21] simplex direct search method [83] was used to vary two bending moments M_1 and M_2 and the axial load F_{axial} - shown in figure 4.4 - applied to the ends of the FE model. The minimisation was applied to the difference between analytical and experimental stresses. The objective function was taken as the 2-norm of the vectorised difference

$$\Delta\sigma = \left\| \{\sigma\}_{\mathrm{FE}} - \{\sigma\}_{\mathrm{exp}} \right\|_2 , \tag{4.6}$$

where $\{\sigma\}_{FE}$ and $\{\sigma\}_{\mathrm{exp}}$ are the finite element and experimental stress distributions. These were defined at n corresponding positions so that

---

[20] The strain gauges can only give an indication of the change in strain relative to the condition of the gauges point when monitoring begins.

[21] Different optimisation routines are not discussed herein since it is generally accepted that the conditioning of the problem - and clearly the number of parameters - are more important influences on the speed of convergence than the choice of optimisation routine chosen.

$$\{\sigma\} = \begin{Bmatrix} \sigma_1 \\ \sigma_2 \\ \vdots \\ \sigma_n \end{Bmatrix}. \tag{4.7}$$

The iterative approach to determining the effects of large deformations described in chapter 3 was used with the displacement convergence (equation (3.39)) set at 1×10^{-6}. The result is a close match of the stress plots for each case. The longitudinal stress distributions of along the length of the top and bottom of the plate arise from the identified loading regimes. These are shown as lines in figure 4.3 with the experimental readings appearing as discrete points. The closeness of the agreement gives much confidence in the validity of the identified loads. This observation takes on particular importance when considering the comparison of the FE prediction of loaded dynamic behaviour with experimental observations. The end moments (M_1 and M_2) and axial load (F_{axial}) giving rise to these distributions are shown in table 4.1, below.

	Case A	Case B	Case C	Case D
M_1 (Nm)	5.8	-26.2	-41.4	-16.9
M_2 (Nm)	-9.6	-26.7	-33.3	3.5
F_{axial} (N)	-7700	-5700	-12800	-7200

Table 4.1 – Identified Loading

The maximum overall deflections are determined by the nonlinear finite element analysis to be 1, 3, 5 and 6mm respectively. The greatest of these is a mere 1% of the overall length of the narrow plate specimen which is likely to be well within the serviceability tolerance of most structures.

While producing coherent estimates of loading, the method of indirect determination is far from efficient and probably not practical for application on real structures. Several simpler methods of deriving stress distributions from loading provide different estimates of the loading. The simplest route is via consideration of a linear stress distribution. Considering the plate specimen as a single beam finite element, the bending load and

the axial load become uncoupled. A more involved method is to use the full finite element model. This is achieved by applying the bending moments and subsequently the axial load, with the finite element model being reformulated after each step but without considering equilibrium iterations. This will be referred to as the two step approach. Note that both methods are special cases of the nonlinear geometrical method described previously. The loads identified by application of these two schemes to the data from case B are set out in table 4.2. The last two columns show the effect of not including the knowledge of the initial deformity of the plate.

The number of individual arithmetic operations required for the identification of loading by each scheme are also shown to give some comparison of the relative computational efficiency. Whilst noting that the number of operations is a function of the starting point of the minimisation process it is clear that a vast increase in computing power is required to implement the more accurate schemes. The resonant frequencies which would arise from each set of identified loads are calculated using the full nonlinear analysis with tight convergence criteria and are also presented in table 4.2.

				Include Initial Shape		Omit Initial Shape	
		Original	Simple	Two Steps	Full Equilibrium	Two Steps	Full Equilibrium
Flops:		-	$O(10^5)$	$O(10^7)$	$O(10^9)$	$O(10^7)$	$O(10^9)$
Loading	M_1 (Nm)	-	-26.0	-25.6	-26.2	-25.7	-27.8
	M_2 (Nm)	-	-27.0	-26.5	-26.7	-26.6	-24.7
	F_{axial} (N)	-	-5100	-6940	-5600	-6830	-6000
Bending Modes	1 (Hz)	63.0	65.0	64.2	65.2	64.2	69.5
	2 (Hz)	173.9	166.3	162.6	165.4	162.8	164.6
	3 (Hz)	340.9	329.6	325.4	328.5	325.6	327.7

Table 4.2 – Identified Loading and Resonant Frequency Predictions for Case B

There is certainly some variation in the prediction of loading which in turn results in some inaccuracy in the prediction of resonant frequency. However, from these observations and from the resulting stress distributions which are shown in figure 4.5, it

is clear that - for this particular specimen - the expense of matching the stress to a large amount of accuracy is not justifiable.

The results indicate that a rudimentary match of strain is required. Once loading is identified the accuracy of the statically updated finite element model should be calculated to as much accuracy as can be afforded. It is particularly important to note that the spatial distribution of strain gauges is a crucial factor in allowing the stress distribution to be characterised accurately.

4.2.2 Modal Analysis of Plate Specimen

Excitation was applied normal to the plane of the plate at the point shown in figure 4.2 by a small electro-magnetic shaker resting on a foam foundation. The response for each of the four cases was measured at the same point in the same direction by means of a laser velocimeter. It was not the intention to consider changes to mode shape resulting from loading in this instance[22]. Figure 4.6 shows the FRFs in the form of point receptances,

$$\alpha(f) = \frac{x(f)}{F(f)}, \tag{4.8}$$

taken from the plate under the four loading conditions.

The H_1 FRF estimator was used to experimentally determine mobility. As a result some definition is lost at resonance. Some evidence of interaction of the specimen with the mechanical shaker is also evident. Considering only the four clear resonances, the first corresponds to the first bending mode while following modes are the second bending, first torsion and third bending modes respectively. For comparison with the natural frequencies predicted by the loadable two dimensional beam model, only the bending modes are examined in the following discussions. A single input single output (SISO)

---

[22] Recent work by Link [84] lends weight to the view that mode shapes cannot be identified consistently accurately enough to be considered as representative of a structure.

line fitting modal identification algorithm [59] was used to determine the bending resonant frequencies. The results of the analysis are set out in table 4.3.

Resonant Bending Modes	Resonance Frequencies (Hz)			
	Case A	Case B	Case C	Case D
1	47	58	63	76
2	153	159	154	155
3	312	318	307	315

Table 4.3 – Experimental Resonant Frequencies

There is clearly a large amount of variation in the measured responses resulting from the loading process, particularly of the lowest natural frequency.

The choice of a method for comparing the sets of data is not a simple one, insufficient spatial data exists to enable consideration of the variation in Modal Assurance Criterion (MAC) [**57**] values between these sets of data. However, an alternative criterion, the Frequency Response Assurance Criterion FRAC [85], has been suggested as a means of assessing the similitude of the data by comparing frequency domain responses. The FRAC formulation is analogous to the MAC and has similarities to the COMAC [86] in that each value compares co-ordinate response. It is given by

$$FRAC = \frac{\left|\left\{\alpha(\omega_i)^p\right\}.\left\{\alpha(\omega_i)^q\right\}^*\right|^2}{\left(\left\{\alpha(\omega_i)^p\right\}.\left\{\alpha(\omega_i)^p\right\}^*\right).\left(\left\{\alpha(\omega_i)^q\right\}.\left\{\alpha(\omega_i)^q\right\}^*\right)}, \tag{4.9}$$

where the superscripts p and q refer to two response functions defined at frequencies ω_i. The star symbol (*) represents the conjugate transpose. While the receptances $\alpha(\omega_i)$ in (4.9) are single row (or column) complex quantities it is suggested in [85] that it might be necessary to replace these quantities with their absolute values.

It is suggested that a factor on either set of frequencies, β, can be included to account for a systematic mis-estimation of stiffness in an analytical prediction of $\alpha(\omega_i)^p$. The modified FRAC becomes

$$FRAC = \max_{\beta}\left(\frac{\left|\left\{\alpha(\beta\omega_i)^p\right\}.\left\{\alpha(\omega_i)^q\right\}^*\right|^2}{\left(\left\{\alpha(\beta\omega_i)^p\right\}.\left\{\alpha(\beta\omega_i)^p\right\}^*\right).\left(\left\{\alpha(\omega_i)^q\right\}.\left\{\alpha(\omega_i)^q\right\}^*\right)}\right). \qquad (4.10)$$

Figure 4.7 shows the result of applying different values of β to the FRAC between receptances from case 1 and case 2, formulating the FRAC using both the complex receptances and absolute values. The observation that an overall change in stiffness is required to maximise the level of FRAC is counter intuitive and arises since the magnitude of the response of the first mode dominates the formulation. Figure 4.8 indicates this clearly on a plot of the absolute values of point receptance for cases A and B against a linear scale. If the factor is included the responses can be clearly seen to be very different. However, it is noticeable that the first mode of the stiffened response converges on the mode of the response to which it is being compared (figure 4.9 and figure 4.10).

This observation has some repercussions upon updating methods which use the difference between response data (chapter 2 section 2.3.2.2). If the first mode of a real structure – a bridge for instance – was to experience frequency shifts under loading then a dilemma arises: if the differences in low order responses are included then there is a risk of erroneously stiffening the entire structure. However, if they are ignored the effect of loading will not be included in the updated finite element model.

Formulating the FRAC with a logarithm of the response leads to a value of $\beta = 1$ as one would expect (figure 4.11). The result of using the familiar representation of the receptance in decibel units is that the FRAC in all cases is very close to unity as table 4.4 clearly shows. The FRAC values are shown as percentages of unity for clarity.

		Load Case			
		A	B	C	D
Load Case	A	100.0	99.8	99.4	99.2
	B	99.8	100.0	99.6	99.4
	C	99.4	99.6	100.0	99.6
	D	99.2	99.4	99.6	100.0

Table 4.4 – % FRAC Values Based on dB Receptance

Table 4.5 shows the corresponding FRAC values for the absolute values of the receptances from the four load cases.

		Load Case			
		A	B	C	D
Load Case	A	100.0	47.6	24.7	15.9
	B	47.6	100.0	40.8	25.2
	C	24.7	40.8	100.0	36.0
	D	15.9	25.2	36.0	100.0

Table 4.5 – % FRAC Values Based on Absolute Receptance

Given the experience with determination of the stiffness factor, it is understood that the first mode contributes heavily to the low level of agreement between the pairs of responses from different load cases. In such cases the use of FRAC values should be treated with extreme caution.

The preceding paragraphs effectively demonstrate some of the problems which arise when attempting to compare response data from nominally identical structures. A comparison of resonant frequencies represents an alternative comparison. Accordingly the implementation of methods which compare sets of identified resonant frequencies are investigated in the following sections - principally in section 4.2.4.

4.2.3 Comparison of Measured Dynamic Behaviour with FE Modelling

The loads identified in section 4.2.1 (see table 4.2) were applied to the 2D beam representation of the narrow plate using the nonlinear geometric approach described in chapter 3. An eigen-solution of the resulting set of transformed structural matrices results in a set of resonant frequency predictions which are shown in table 4.6 along with the experimental measurements.

Resonance Bending Modes	Frequencies (Hz)							
	Case A		Case B		Case C		Case D	
	FE	Exp	FE	Exp	FE	Exp	FE	Exp
1	51	47	65	58	78	63	100	76
2	157	153	165	159	162	154	160	155
3	323	312	328	318	317	307	327	315

Table 4.6 – Analytical Predictions and Experimental Observations of Resonant Bending Frequencies

It is noted that the finite element predictions consistently overestimate the experimental data. Several factors are likely to result in the differences between the predicted and observed resonances. The first is the effect of the discretised nature of the finite element model which has been discussed previously. Additionally the lack of complete fixity provided by the experimental supporting structure will have a significant effect on the experimental resonances. These effects make it more difficult to assess to what extent the changes to the analytical model reproduce the experimental behaviour.

It is clear however, that a similarly large amount of variation is manifest in the finite element prediction as was measured experimentally. The following section develops a method which facilitates an easier comparison between the sets of data.

4.2.4 Identification of Zero-Load Resonant Frequencies

An understandable comparison of experimental and analytical results can be ascertained if the experimental dynamic behaviour of the unloaded structure is available. For this

experimental case - as with many industrial cases - it is almost impossible to recreate the situation corresponding to the unloaded FE model. For the narrow plate currently under consideration this would involve end constraints which straighten out the initial deformity in the plate without introducing axial load.

This section sets out a technique for estimating the zero-load experimental load from the FE model of the structure and several sets dynamic measurements under various loading conditions.

If the i^{th} experimental resonant frequency from the j^{th} loading case is written ${}_iE_j$ and the corresponding analytical prediction ${}_iA_j$ then the increase in the p^{th} identified resonant frequency from the q^{th} load case over the corresponding mode in the unloaded case is given by

$$ {}_q\mathrm{E}_p - {}_0\mathrm{E}_p \tag{4.11} $$

with a similar expression for the analytical case

$$ {}_q\mathrm{A}_p - {}_0\mathrm{A}_p, \tag{4.12} $$

where the 0 subscript refers to the zero load case. It is common to consider percentage increases between corresponding resonant frequencies. Therefore, the normalised experimental frequency increase can be considered. This is

$$ \frac{{}_q\mathrm{E}_p - {}_0\mathrm{E}_p}{{}_0\mathrm{E}_p}. \tag{4.13} $$

For a given frequency from a single load case, a prediction of the corresponding zero-load resonant frequency can be found by minimising the differences between the normalised increases with respect to ${}_0E_p$

$$ \left| \frac{{}_q\mathrm{E}_p - {}_0\mathrm{E}_p}{{}_0\mathrm{E}_p} - \frac{{}_q\mathrm{A}_p - {}_0\mathrm{A}_p}{{}_0\mathrm{A}_p} \right|. \tag{4.14} $$

For a set of n_{loads} load cases the p^{th} zero-load resonant frequency can be found by minimising

$$\sum_{q=1}^{n_{loads}} \left| \frac{{}_{q}\mathrm{E}_{p} - {}_{0}\mathrm{E}_{p}}{{}_{0}\mathrm{E}_{p}} - \frac{{}_{q}\mathrm{A}_{p} - {}_{0}\mathrm{A}_{p}}{{}_{0}\mathrm{A}_{p}} \right| \tag{4.15}$$

with respect to ${}_{0}\mathrm{E}_{p}$ where $p = 1 \ldots n_{freqs}$. This can be performed on each frequency in turn or the global sum over all n_{freqs} measured identified frequencies

$$J = \sum_{p=1}^{n_{freqs}} \sum_{q=1}^{n_{loads}} \left| \frac{{}_{q}\mathrm{E}_{p} - {}_{0}\mathrm{E}_{p}}{{}_{0}\mathrm{E}_{p}} - \frac{{}_{q}\mathrm{A}_{p} - {}_{0}\mathrm{A}_{p}}{{}_{0}\mathrm{A}_{p}} \right|. \tag{4.16}$$

Using this method with all four sets of data yields predictions of bending resonant frequencies shown in table 4.7 along with their FE counterparts. The result of minimising absolute frequency differences is also tabulated but can be seen not to be significantly different.

Resonant Bending Modes	Unloaded Resonant Frequencies (Hz)		
	FE	Exp (norm)	Exp (abs)
1	63	52	51
2	174	167	168
3	340	329	330

Table 4.7 - Estimated Experimental Resonant Frequencies

The percentage increase of each natural frequency relative to the unloaded values are displayed in figure 4.12. The minimisation procedure described above ascribes equal importance to the perturbation of all of the modes. The results indicate that the zero-load resonant frequencies are estimated so that the perturbation to the higher order modes most accurately matches the finite element model prediction. This phenomenon is understandable in light of the observation that the first mode is most sensitive to slight alterations in loading. Hence the prediction of this mode would be expected to be less accurate. Other factors which lead to lack of agreement between dynamic and experimental measurements and finite elements predictions are described in the following section.

The technique presented here - while simple - has considerable practical appeal. Given knowledge or possibly estimation of structural loading at the time of several runs of modal testing, it is possible to estimate the set of resonant frequencies which *uniquely* represent the loaded structure. These are referred to as the *zero-load resonant frequencies* in forthcoming chapters.

4.2.5 Investigation of FE – Experimental Mismatch

The previous sections give confidence that the loading upon the plate is the primary factor in causing the observed perturbations to resonant frequencies. Several other factors whose influence causes inconsistency between the experimental and FE models must also be addressed.

Firstly, as the previous sections have acknowledged, the test rig not being infinitely massive will interact with the plate to some degree. To investigate the influence of the test rig on the dynamic behaviour of the plate, a simplified finite element model was used with each the end blocks represented by four solid "brick" finite elements. The plate specimen and each of the adjustments bars were modelled with 5 3D beam elements.

As one would expect, the loss in apparent[23] stiffness at the supports results in lower predictions of resonant frequency. Table 4.8 shows that the effect upon the first three bending modes.

Bending Resonant Frequencies	Fixed Plate	Plate in Test Rig	Estimated Zero-load Measure
1	63.1	58.2	52
2	174.4	161.7	167
3	343.9	320.0	329

Table 4.8 – Experimental Modes Identified

[23] This refers to the stiffness of supports "perceived" by the plate specimen.

While the result is a closer agreement between the analytical and experimentally determined values of resonant frequency at zero load, some disagreement between the measured zero-load resonant frequencies and the FE predictions is still evident. Several other factors seem likely to be to blame.

The previous sections have assumed that the loading applied to the plate consists of only axial and bending loads. While this was the intention during testing, the design of the rig makes it difficult to prevent some component of torsional loading to be experienced by the specimen.

A further source of error will arise from the stiffness of the physical connection between the plate and the large restraining blocks.

4.3 Small Framework

To address some of the issues raised by the initial experimental investigation and to circumvent some of its shortcomings, a second test was devised involving a cross braced frame structure. The structure was supported in free-free conditions for dynamic testing thus obviating the requirement of accounting for potentially complex interaction with boundary conditions. An adjustable strut in the framework allowed loading to be introduced into the structure in a controlled and directly measurable manner.

The following sections present several sets of dynamic readings taken from the framework under different load levels and investigate some of the aspects of the changes in dynamic characteristics. A more comprehensive study of three nominally identical frameworks is undertaken in chapter 6. At this stage the use of model updating strategies to alter the finite element model of the structure will be studied.

4.3.1 Arrangement of Framework

An exploded view of the truss is shown in figure 4.13; the overall dimensions (between joint centres) are 300mm by 500mm. The truss was constructed from 6 × 15mm mild

steel section spars which were bolted at their joints. Figure 4.14 shows the points at which the structure was tested as well as the numbering and co-ordinate system. Three strain gauging locations (also shown in figure 4.14) were used with the instruments positioned in pairs on either side of the spars. These gauges were oriented to measure the longitudinal strain. The framework was supported from two flexible strings to minimise interaction of the test structure with the supporting structure.

The framework was deliberately designed to contain a single redundancy if considered as a two dimensional pinned structure. However, it was anticipated that the non-coincidence of the centre lines of the constituent spars would result in bending moments being transmitted at the joints. This leads to the requirement that the structure be modelled in three dimensions. The practical observation was that tension induced in the adjustable spar led readily to noticeable deflection of spars 1, 2, 3 and 4, allowing the effects of deformity in addition to axial spar loads to be investigated.

4.3.2 Experimental Results

Four sets of dynamic readings were taken in the out-of-plane z-direction at different levels of loading. Strain gauges on spar 5 adjacent to the turnbuckle indicated that axial load in this strut were 440N, 820N and 1230N relative to the initial case. These load cases will be referred to as cases 1, 2 and 3 with the zero-load initial conditions being case 0. Experience gained in the previous experimental investigation (section 4.2.1) has shown that difficulties can arise from judging an initial load case to represent zero loading. In this situation the turnbuckle slackened noticeably when no load was induced in the axial member. The strain gauges were zeroed with the turnbuckle in this state. The bolted nature of the joints did not preclude the possibility of some loading and deformity being locked into the structures. However, this was thought not to be significant compared to the known loading levels applied with the turnbuckle.

Broadband random excitation was applied to node 26 – shown in figure 4.15 - in the z-direction with a small electro-dynamic shaker via a flexible rod or *stinger* and a force

transducer. Response (mobility) was measured in the same direction at the 24 points shown in figure 4.14 in the 0-400Hz range.

Modal analysis was performed using the MODENT program within the ICATS [87] suite of software. The global method [58] of analysing multiple frequency response functions was used to extract natural frequency and mode shape estimates.

Figure 4.16 shows the point receptances measured from the extremal load cases 0 and 3. The dynamic behaviour of the frame is seen to change dramatically under the loading. The identified resonant frequencies from all of the load cases are shown in table 4.9. Note however that the rows of the table do not necessarily imply correspondence of modes. The identified modes shown in the table are the result of an extensive examination of the sets of responses. It was observed that the "prominence" of modes altered noticeably with the level of loading. Two of the modes, shaded in table 4.9, were particularly difficult to identify in the unloaded case.

Mode Number	Resonant Frequencies (Hz)			
	Case 0	Case 1	Case 2	Case 3
1	44.3	42.0	40.6	40.1
2	70.5	82.7	87.3	91.3
3	90.6	92.0	93.3	94.4
4	123.4	119.7	115.0	111.5
5	133.4	141.8	147.4	154.6
6	178.2	178.1	179.6	177.9
7	186.5	185.3	183.8	182.3
8	210.7	224.6	230.2	233.6
9	229.2	233.2	234.5	236.4
10	249.3	247.8	245.6	243.7
11	309.9	306.1	302.8	298.8
12	347.3	342.8	338.8	334.9

Table 4.9 – Experimental Modes Identified

A graphical representation of these results is given in figure 4.17. This shows each of the rows of table 4.9 as a line against the values of identified load in the adjustment bar.

The graph gives some confidence in the table's rows representing correlated modes. Of most significance is that all of the resonant frequencies of the structure identified in the 0-400Hz range are perturbed a great deal, by different amounts and *in different directions*. The pairs of modes two and three as well as eight and nine are observed to be converging upon one another. Also of interest is the observation that the scale of the perturbation in absolute terms for each identified resonant frequency is of a similar order. This observation is borne out in table 4.10 which shows the absolute and percentage difference in the identified value of each mode between load cases 0 and 3.

Case 0	Abs Increase (Hz)	% Increase
1	-4.2	-9.4
2	20.8	29.4
3	3.9	4.3
4	-11.9	-9.7
5	21.2	15.9
6	-0.3	-0.2
7	-4.2	-2.3
8	22.9	10.9
9	7.1	3.1
10	-5.6	-2.3
11	-11.1	-3.6
12	-12.4	-3.6

Table 4.10 – Differences Between Identified Frequencies - Case 0 and Case 3

The mode shapes corresponding to each of the resonant frequencies are shown in figure 4.18. As one would expect some modes - for instance two and three - are dominated by resonance of a subset of the total number of members. Others represent more global displacement patterns, for example modes one and six. Employing the modal assurance criterion to compare the sets of experimental data yields interesting results. Figure 4.19 shows the MAC of the mode shapes identified in case 0 with those in case 3 and indicates that there is good correlation between the pairs of modes numbered one to five

and ten to twelve. The correspondence between pairs six and seven and particularly eight and nine show less clear correlation. This observation suggests that the deformities to the structure and the state of internal stress resulting from loading can have a considerable effect on some of the mode shapes. The following sections allow the phenomena to be investigated in more detail with reference to the finite element model of the structure.

4.3.3 Finite Element Modelling

The framework was modelled using the ANSYS [16] commercial finite element package. Three dimensional cubic beam elements were used exclusively to model the structure. The model consists of a total of 34 elements and 192 degrees of freedom. Soft grounded springs were 'attached' to the top corners of the framework to prevent numerical instability arising from calculation of eigenvalues corresponding to rigid body modes of vibration. The node points at each of which there are six degrees of freedom are shown in figure 4.15.

As the exploded view of the framework in figure 4.13 clearly shows, the struts which constitute the truss lie in several layers. The co-ordinate system is shown in figure 4.15, the z axis has its zero value at the mid-depth of back-most spar, 6. Table 4.11 summarises the relative location of all of the spars.

Spar	z (mm)
1	6
2	18
3	6
4	18
5	12
6	0

Table 4.11– Relative Depth of Spar Elements

This non-coincidence of the lines of action of the spars under loading was accounted for by including stiff beams with axes parallel to the global z axes.

An eigen-solution of the finite element model results in fifteen resonant frequencies in the range 0-400Hz whose values are shown in table 4.12.

Mode Number	Frequency (Hz)
1	46.69
2	87.50
3	95.21
4	130.29
5	140.34
6	185.74
7	199.52
8	212.73
9	226.42
10	239.65
11	246.01
12	270.99
13	301.55
14	331.91
15	368.91

Table 4.12 – Resonant Frequencies Predicted By FE Model (Zero Load)

The mode shapes corresponding to these modes are shown in figure 4.20.

The mode shapes predicted by the FE model were compared with the experimentally determined values from case 0 using the MAC. The results of this standard procedure are shown in figure 4.21. The results show that while for some of the modes at each end of the frequency range of interest show good agreement, several modes around 180-220Hz do not agree with one another with any certainty. Figure 4.22 shows the agreement of modes between the case 0 readings and the FE prediction in terms of MAC values above 0.9, above 0.7 and above 0.5. Only seven of the twelve identified modes

can be readily matched with analytically derived mode shapes leaving considerable uncertainty about the correlation of the remaining five modes.

Some insight into the poorly correlating modes is afforded by considering the auto-MAC[24] of the FE mode shapes. The results shown in figure 4.23, indicate that there is a great deal of similarity between the very modes which had previously failed to correlate well with experimental data. Figure 4.24 illustrates the auto-MAC more clearly, showing the locations of MAC values greater that 0.8 with the shaded points indicating multiple mode correspondence. It is seen that the mode shapes of modes 6 and 9 are both of a similar form to mode 7; additionally modes 8 and 12 are seen to be much alike.

While the behaviour of the closely correlating modes is a matter of some interest, for the purposes of using dynamic data to characterise a structure, the modes which correspond to FE modes 6, 7, 8, 9 and 12 can be justifiably overlooked. For the purposes of the current study, the closely correlating modes 1 through 5 will be considered in isolation.

The loading upon the structure was applied to the ANSYS model with both the stress stiffening and large-deformation effects described in chapter 3 taken into account. The effect of loading the frame by shortening spar 5 was accounted for in ANSYS in two stages as shown in figure 4.25. Spar 5 was loaded in tension separately from the rest of the frame with the load resulting from the shortening of this spar being applied to the frame independently of the spar itself. The elemental stiffness and mass matrices from the two sub-models were output from ANSYS and combined in the MATLAB environment.

Loads from 0 to 1200N were applied to the finite element model in this way. The variation of the first five resonant frequencies for which good correlation between finite element and experimental modes exists are shown in figure 4.26 along with the

---

[24] The auto-MAC is the special instance of the MAC where two identical sets of mode shapes are compared and is thus symmetrical.

experimental readings. The trends in both sets of data appear to be qualitatively similar which inspires confidence that the changes to the structure caused by the loading are accounted for by the changes to the finite element model resulting from the nonlinear analysis.

To allow the accuracy of the finite element model to be determined, pairs of corresponding modes from the zero load case experimental readings and the finite element model are set out in table 4.13. These lower order modes conform to the expectation that the finite element model discretisation will lead to over-estimates of resonant frequency. The larger error observed in the prediction of mode two is explained by the fact that this mode consists predominantly of flexure of the adjustable spar which contains the turnbuckle device whose characteristics were not included in the simple model.

Case 0 Modes	Frequency (Hz)	FE Modes	Frequency (Hz)	% Increase
1	44.3	1	46.7	5.4
2	70.5	2	87.2	24.1
3	90.6	3	95.2	5.1
4	123.4	4	130.3	5.6
5	133.4	5	140.3	5.2

Table 4.13 – Corresponding Modes Zero Loading

While giving encouraging agreement with the experimental data qualitatively, there is clearly some error between the zero-load FE model and experimental measurements whose causes must be investigated. The framework example is revisited in chapter 6 where the techniques described in chapters 3 and 4 are joined by a dynamic updating technique to account for the effects of loading in the structure.

4.4 Concluding Remarks

The state of loading in two experimental case studies has been found to alter significantly the dynamical behaviour of the structures. The techniques described in chapter 3 account for both the deformation and stress stiffening resulting from loading. These produced perturbations to predicted resonant frequencies consistent with observed values.

An instance which demonstrates the indirect identification of loading using strain gauges has been investigated. Several methods of employing the *a priori* finite element model of a substructure to help to identify loading from discrete strain measurements have been investigated. Deformations which are likely to give rise to changes in dynamic readings have been seen to lead to nonlinear stress distributions. Therefore, an appropriately large number of strain gauges must be used to characterise this type of stress distribution.

The problem of determining the dynamic behaviour characteristics of the unloaded state of a structure has been investigated. This scenario could quite plausibly be encountered in a real-life situation. A new method for identifying the zero-load dynamic behaviour of a structure has been introduced. The technique uses several sets "loaded" data and allows the identification of loading using a finite element model of the structure.

The sensitivity of mode shapes to static loading has been studied in a specific experimental case study. The *a priori* finite element model allows the vibration modes with sensitive mode shapes to be excluded from validation exercises.

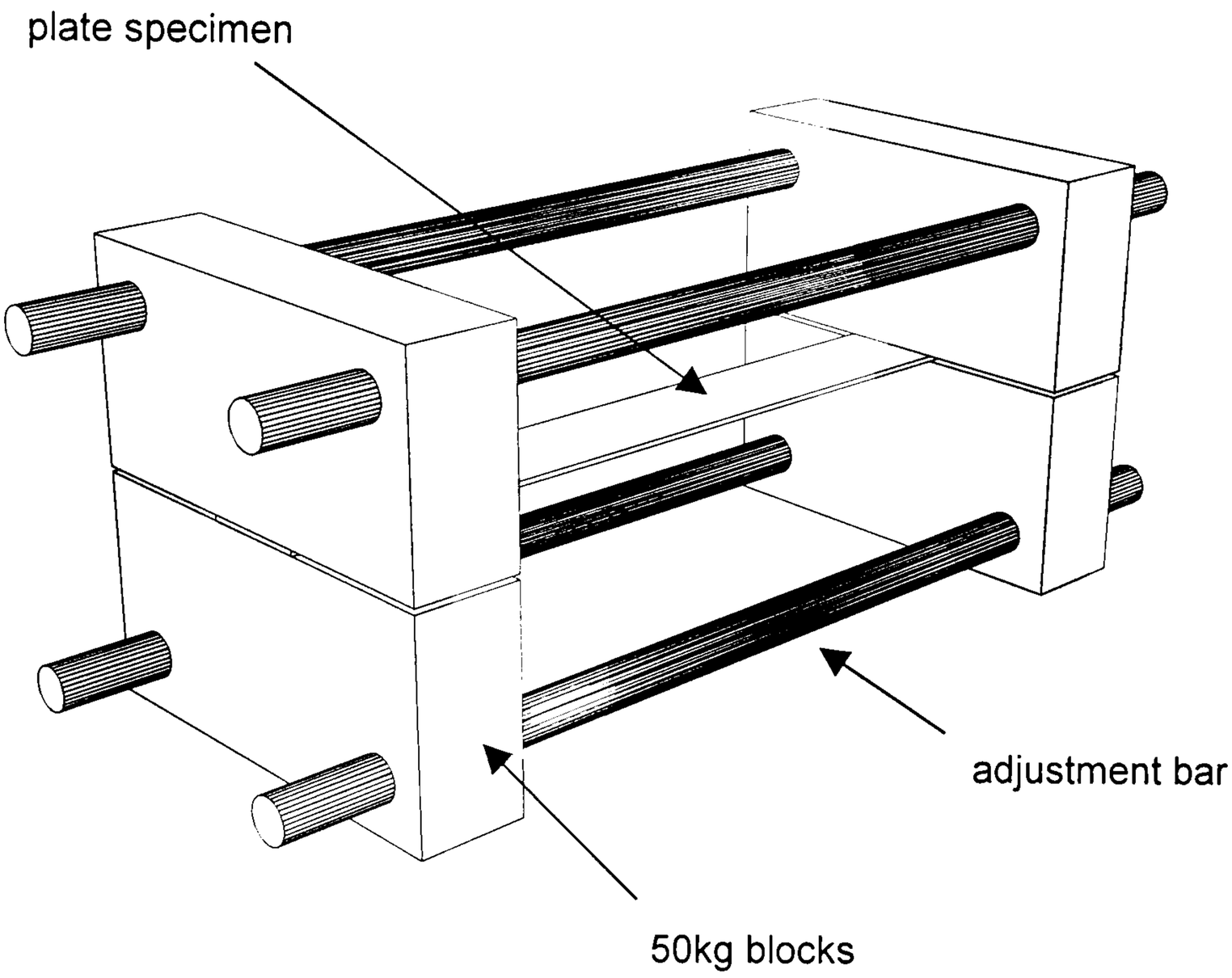

Figure 4.1 - Experimental Arrangement

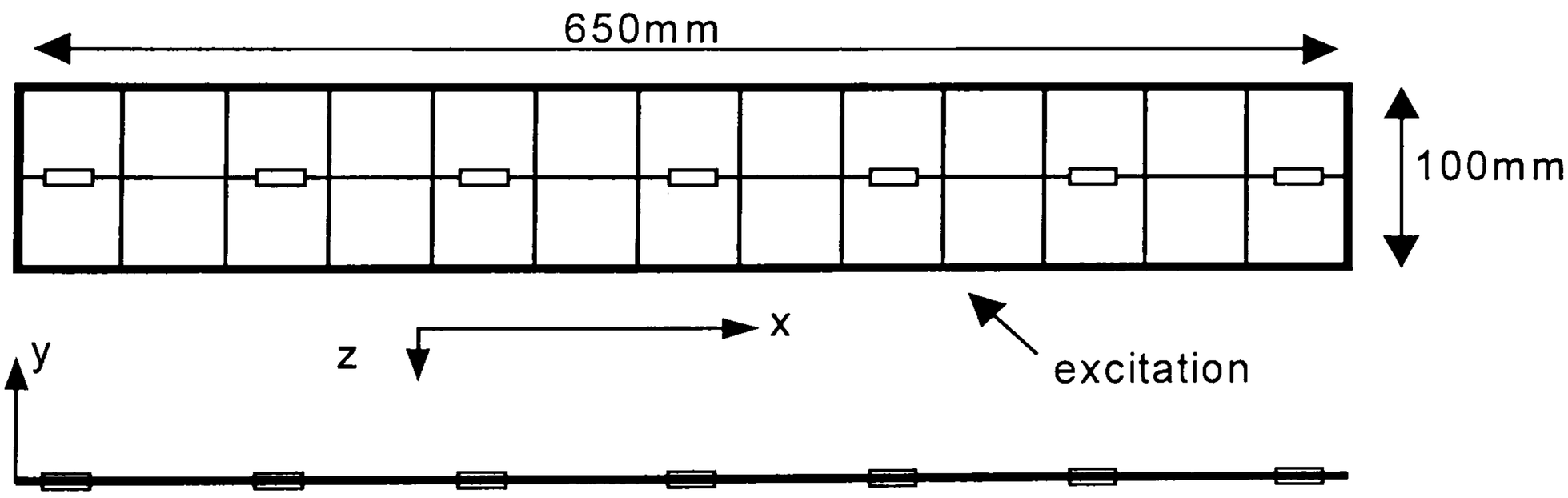

Figure 4.2 - Co-ordinate System and Strain Gauge Locations on Plate

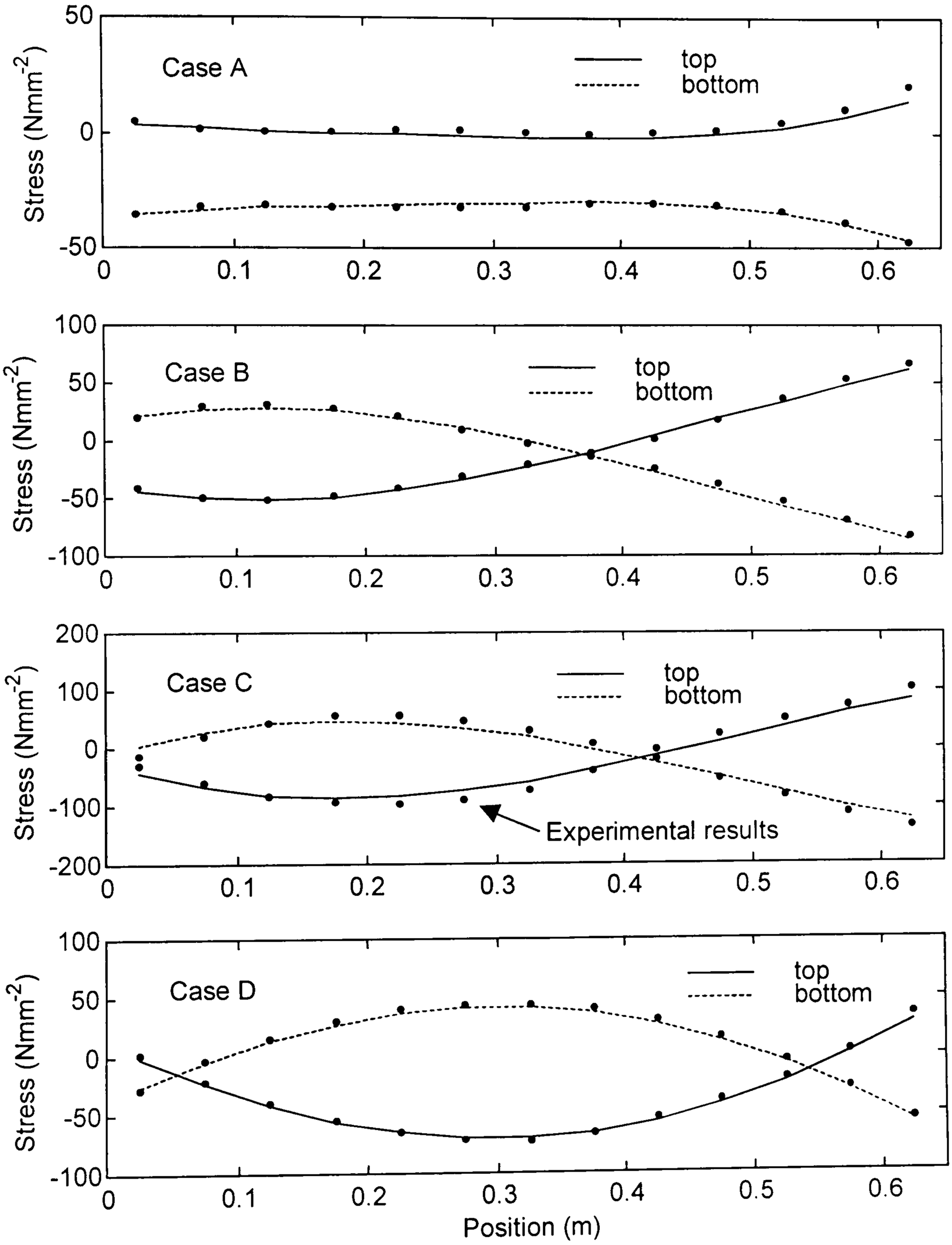

Figure 4.3 - Observed Stresses Distributions on Plate – Cases A to D

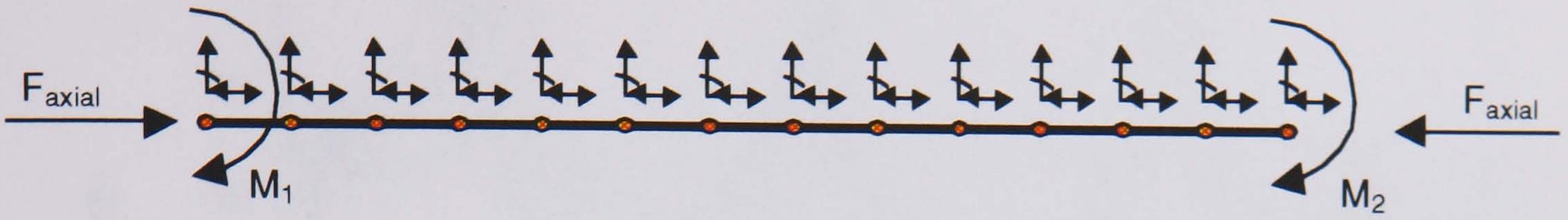

Figure 4.4 – Application of Load to Finite Element Model

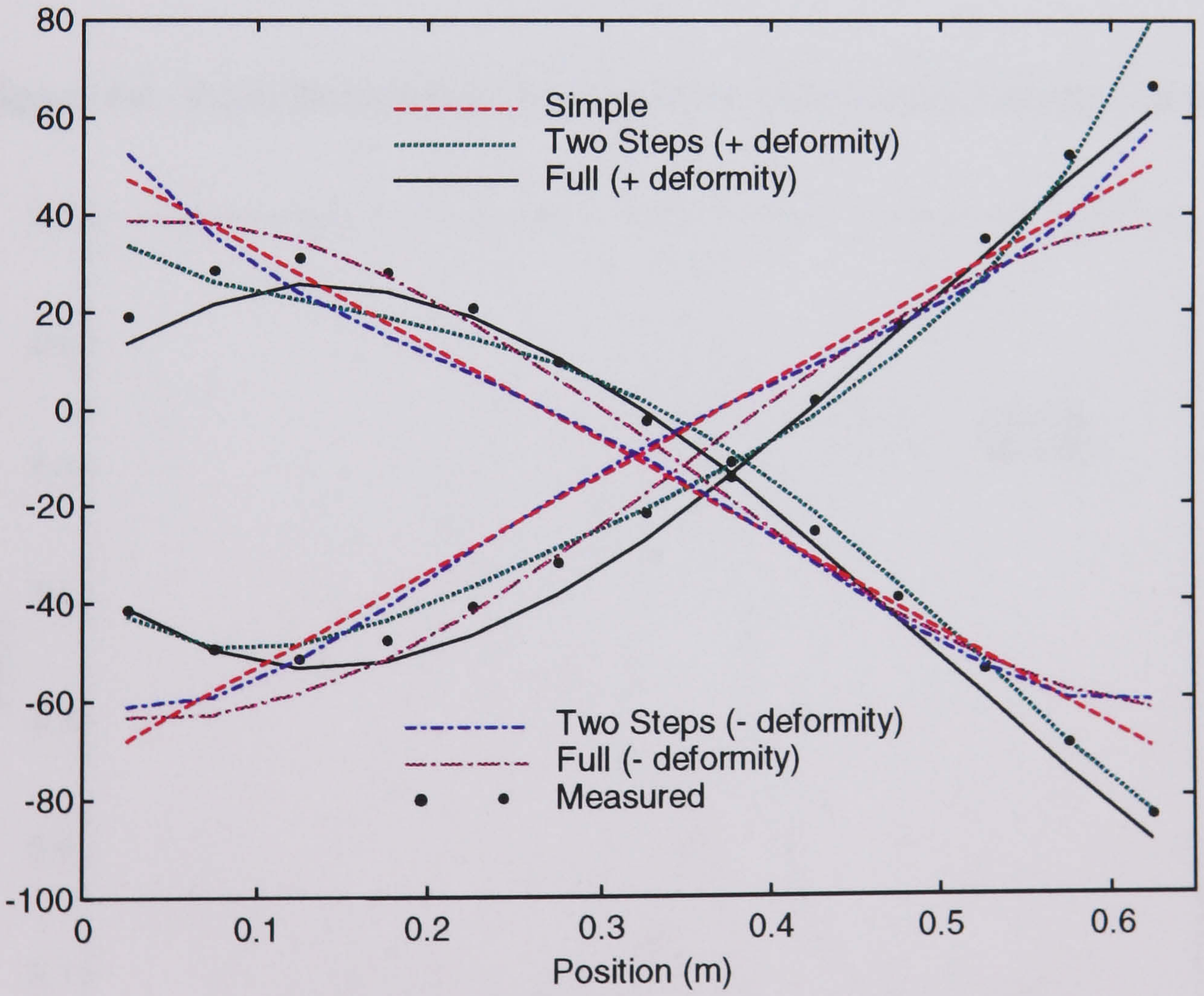

Figure 4.5 – Stress Distributions from Different Stress Models

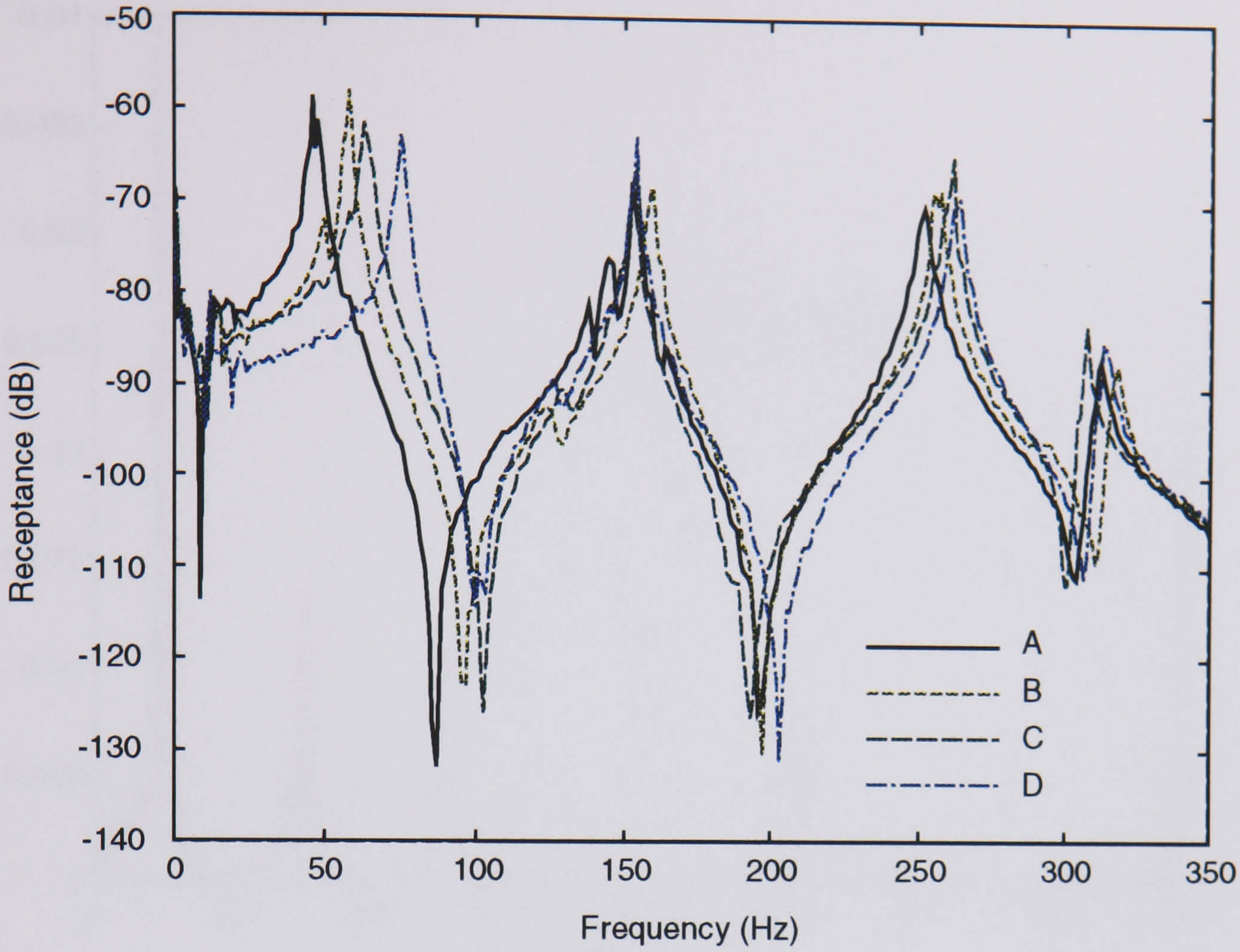

Figure 4.6 - Point Receptances from Narrow Plate Under Varying Loading

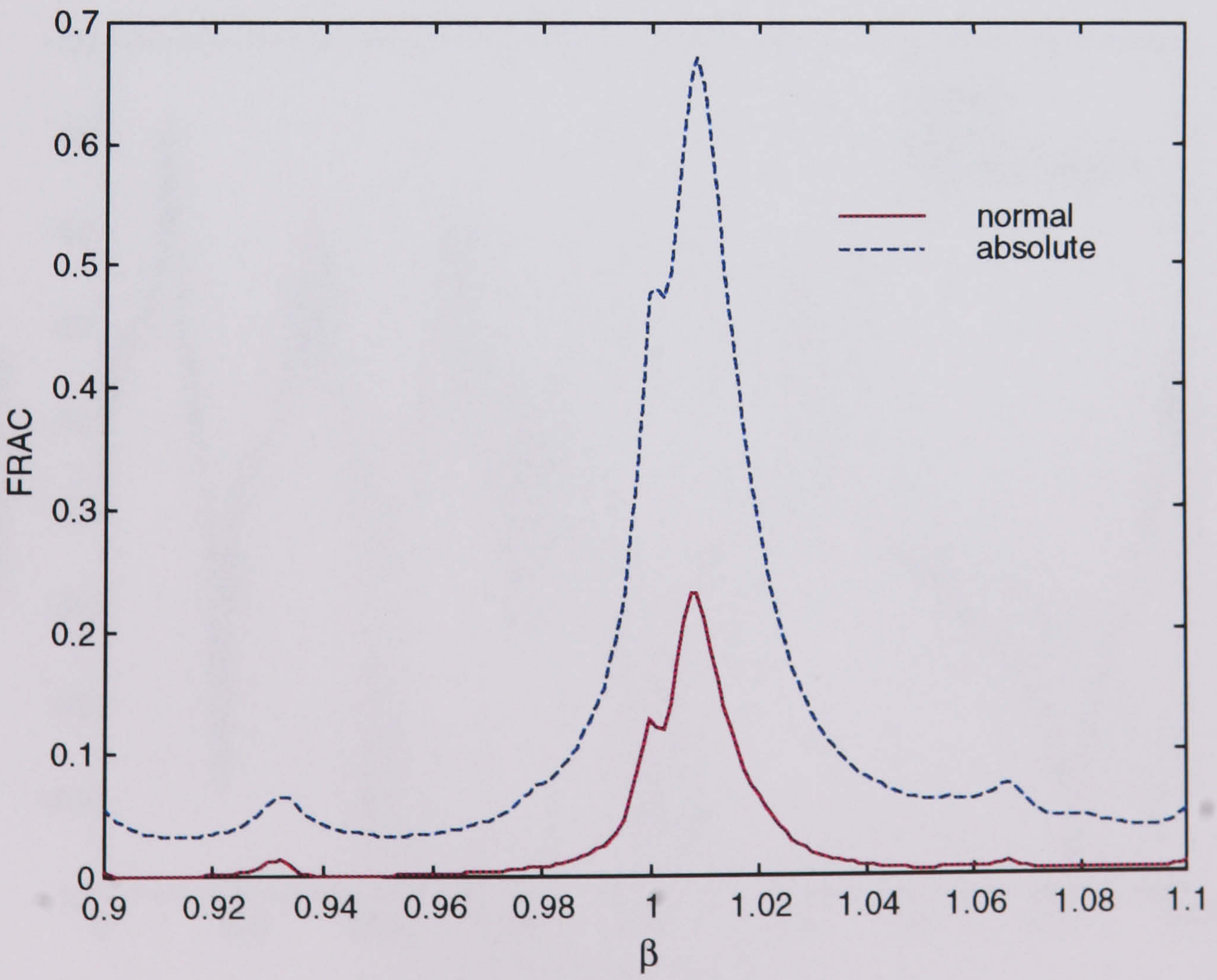

Figure 4.7 – FRAC Between Load Cases 1 and 2 Varying β

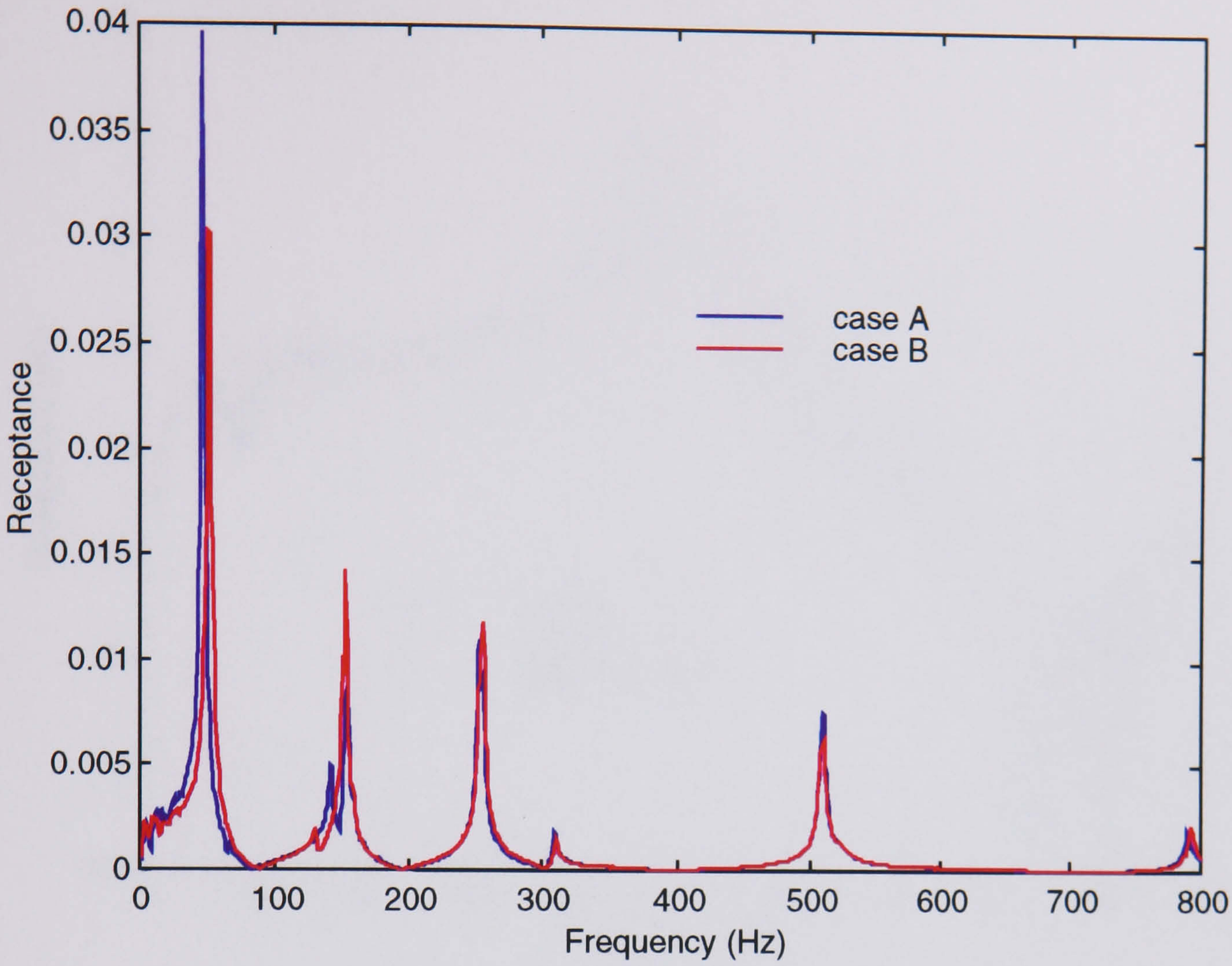

Figure 4.8 – Linear Receptance Case A and Case B

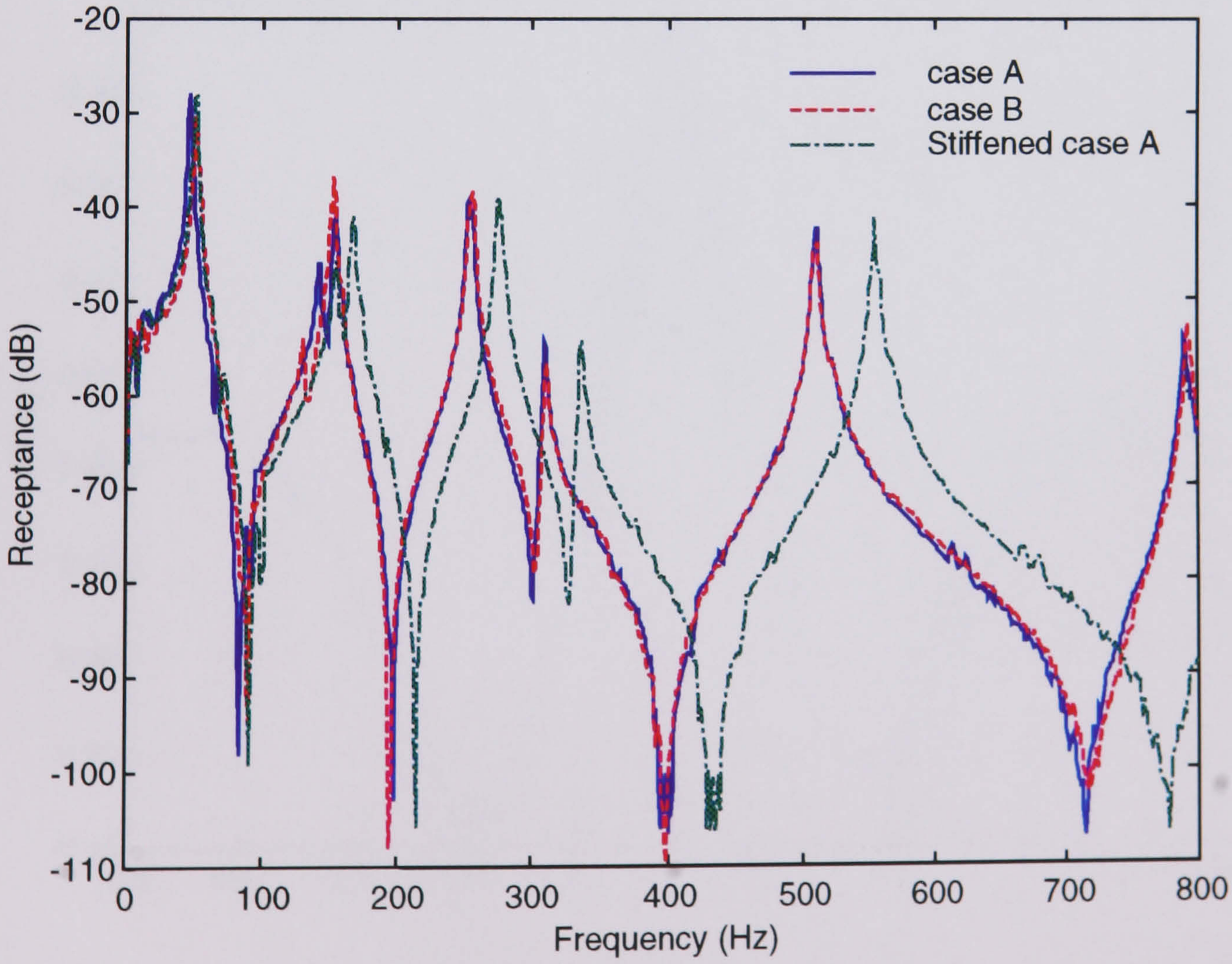

Figure 4.9 – Frequency Shifted Receptances 0-800Hz

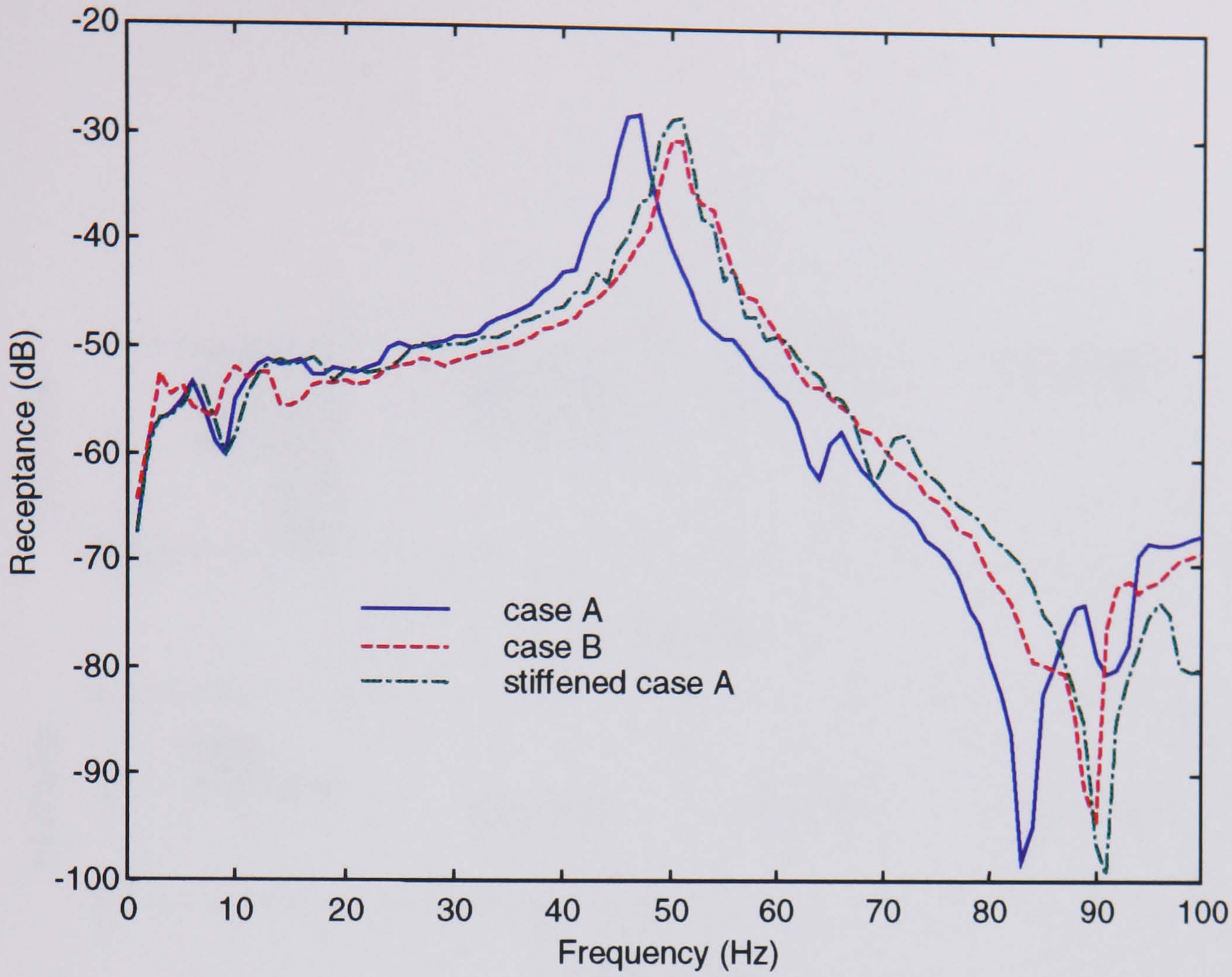

Figure 4.10 – Frequency Shifted Receptances, First Mode

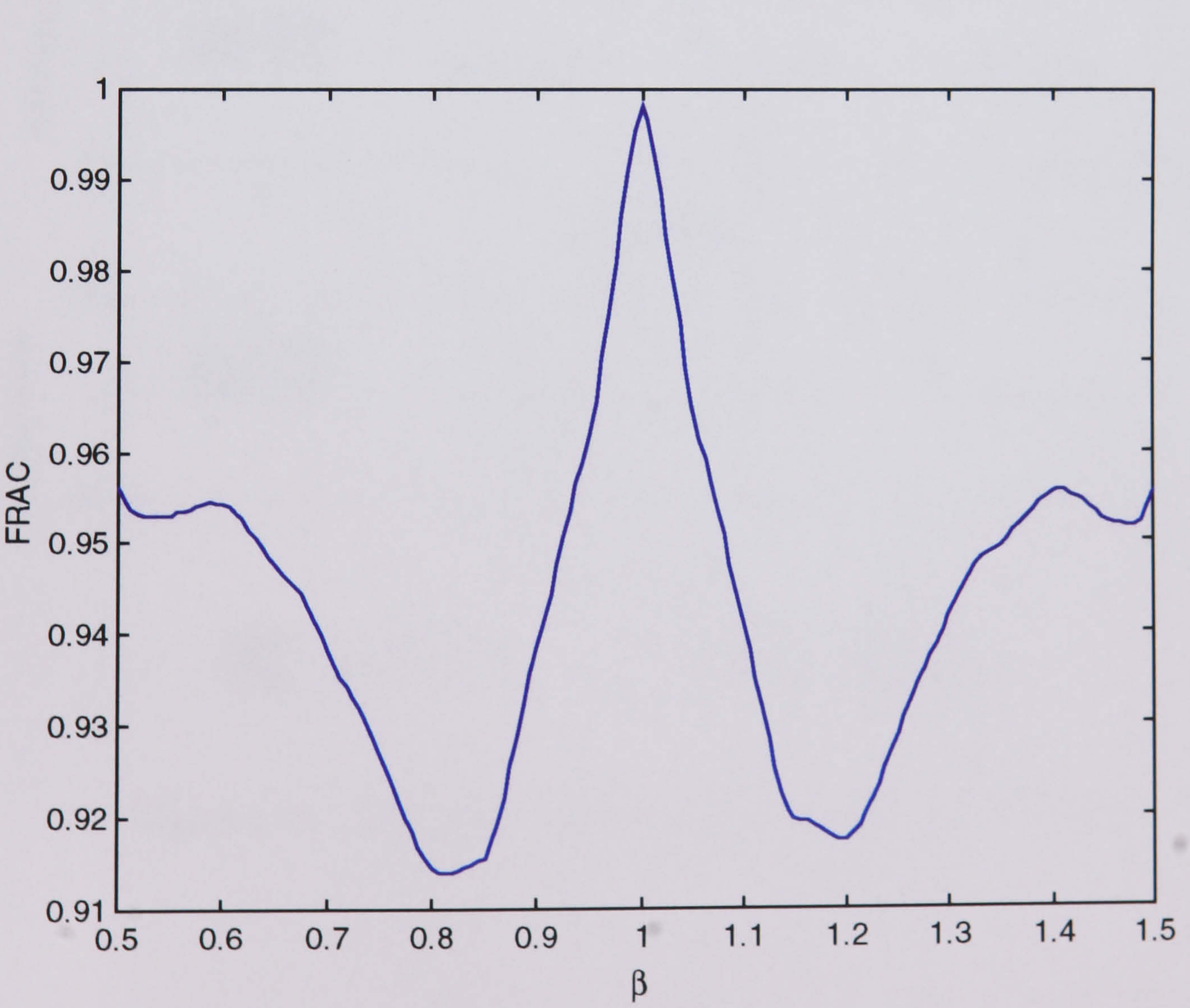

Figure 4.11 – Effect of β on FRAC of Case A and Case B Using Log Receptance

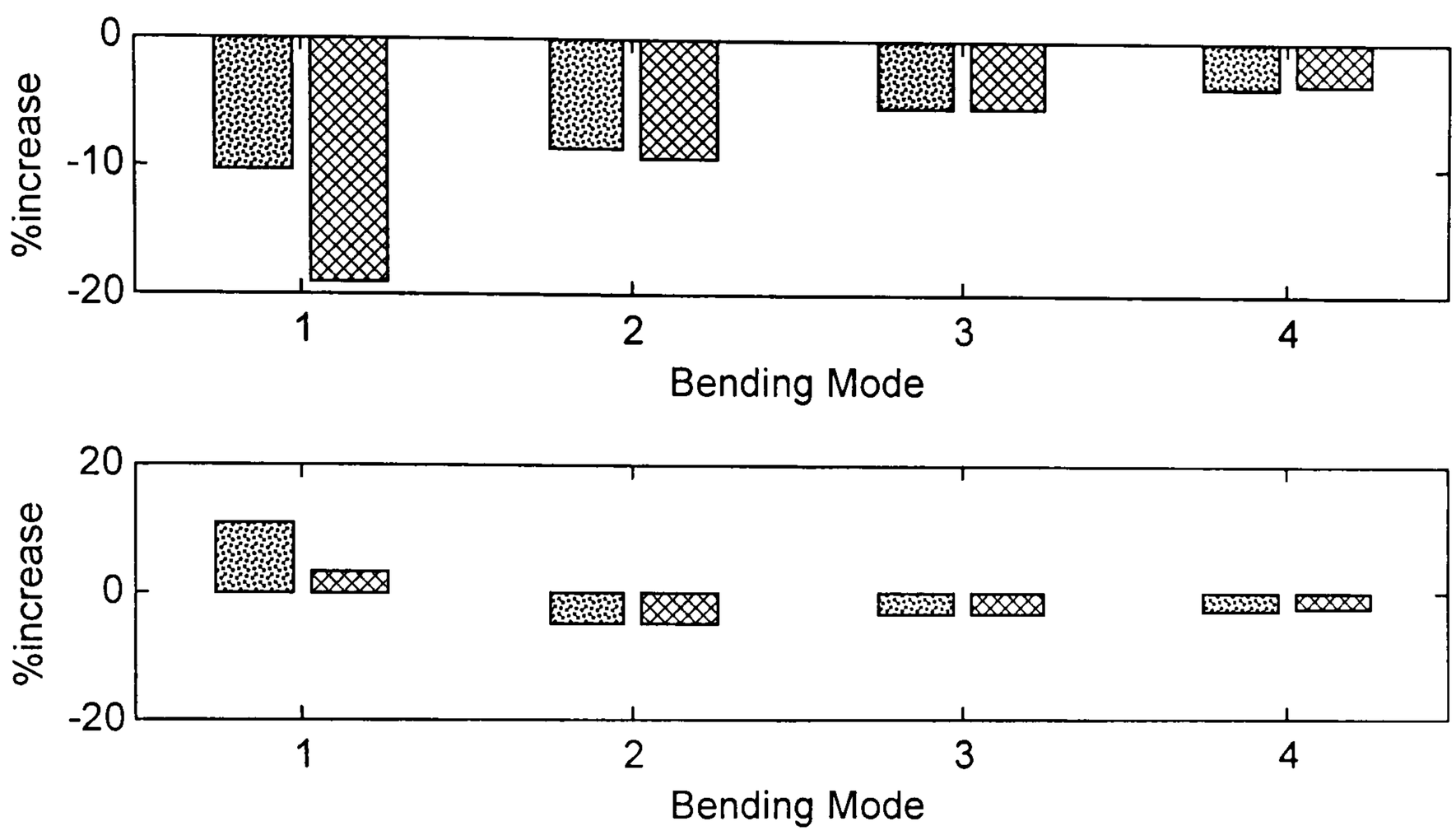

Figure 4.12 - Percentage Increase From Nominal Zero Load

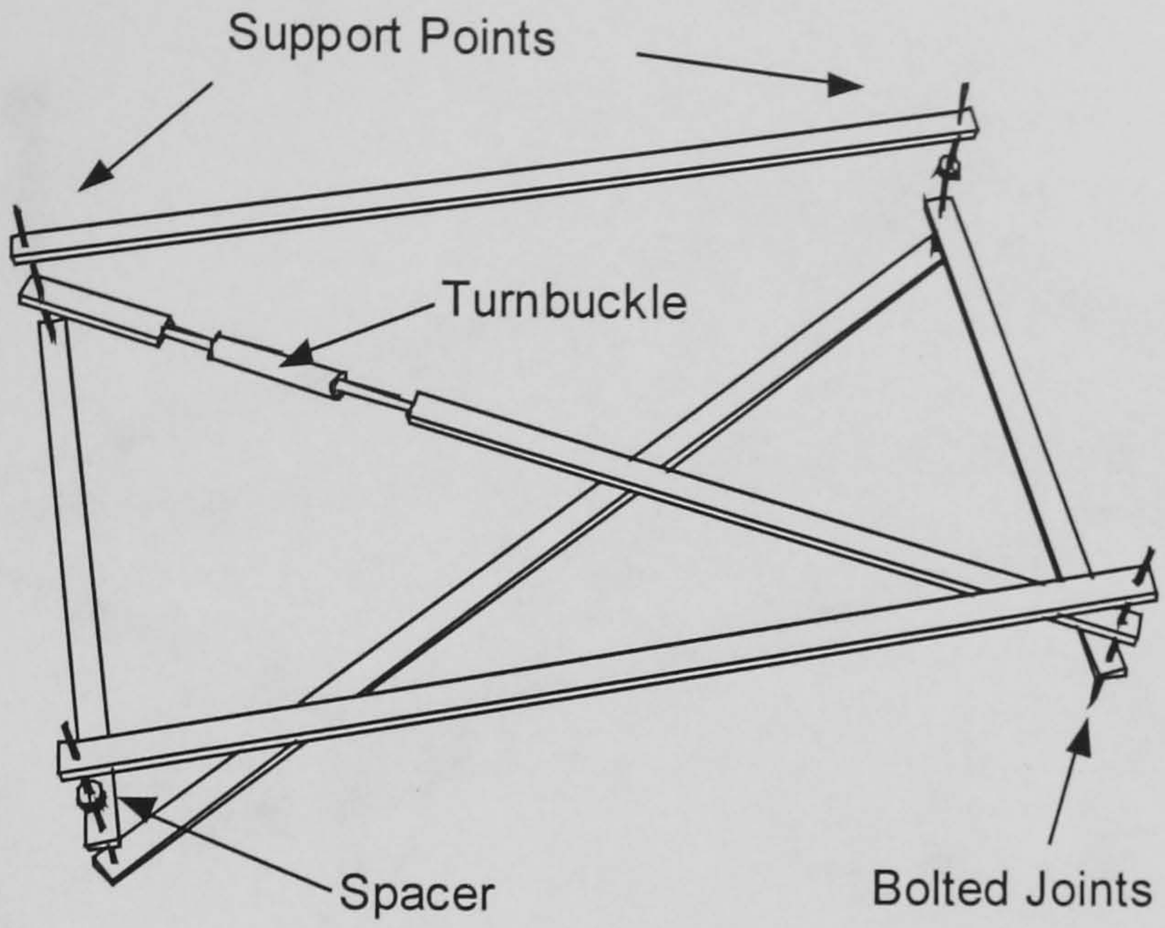

Figure 4.13 - Exploded View of Frame

Figure 4.14 – Front View of Redundant Frame Showing Measurement Points

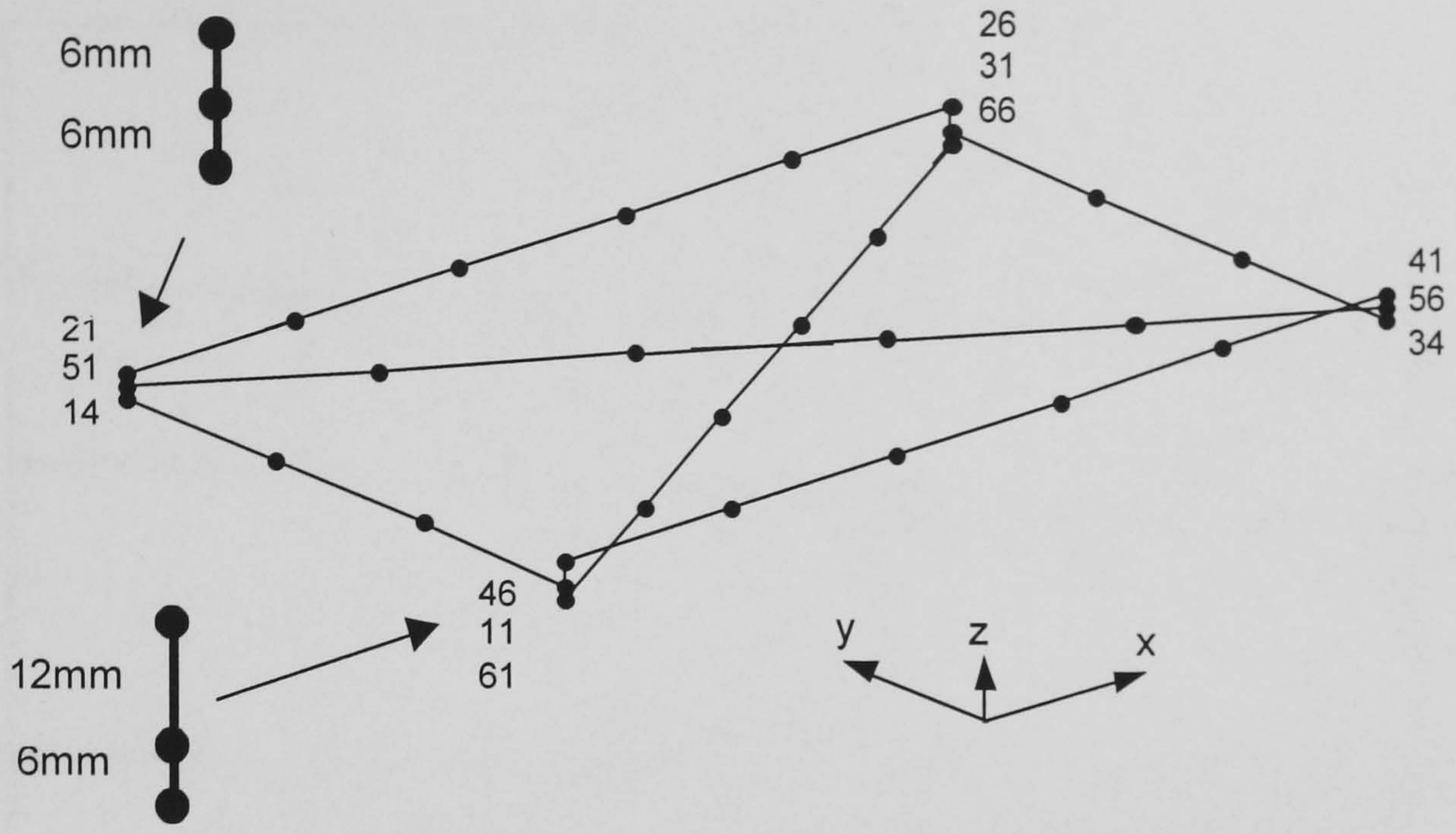

Figure 4.15 – Finite Element Model of Framework

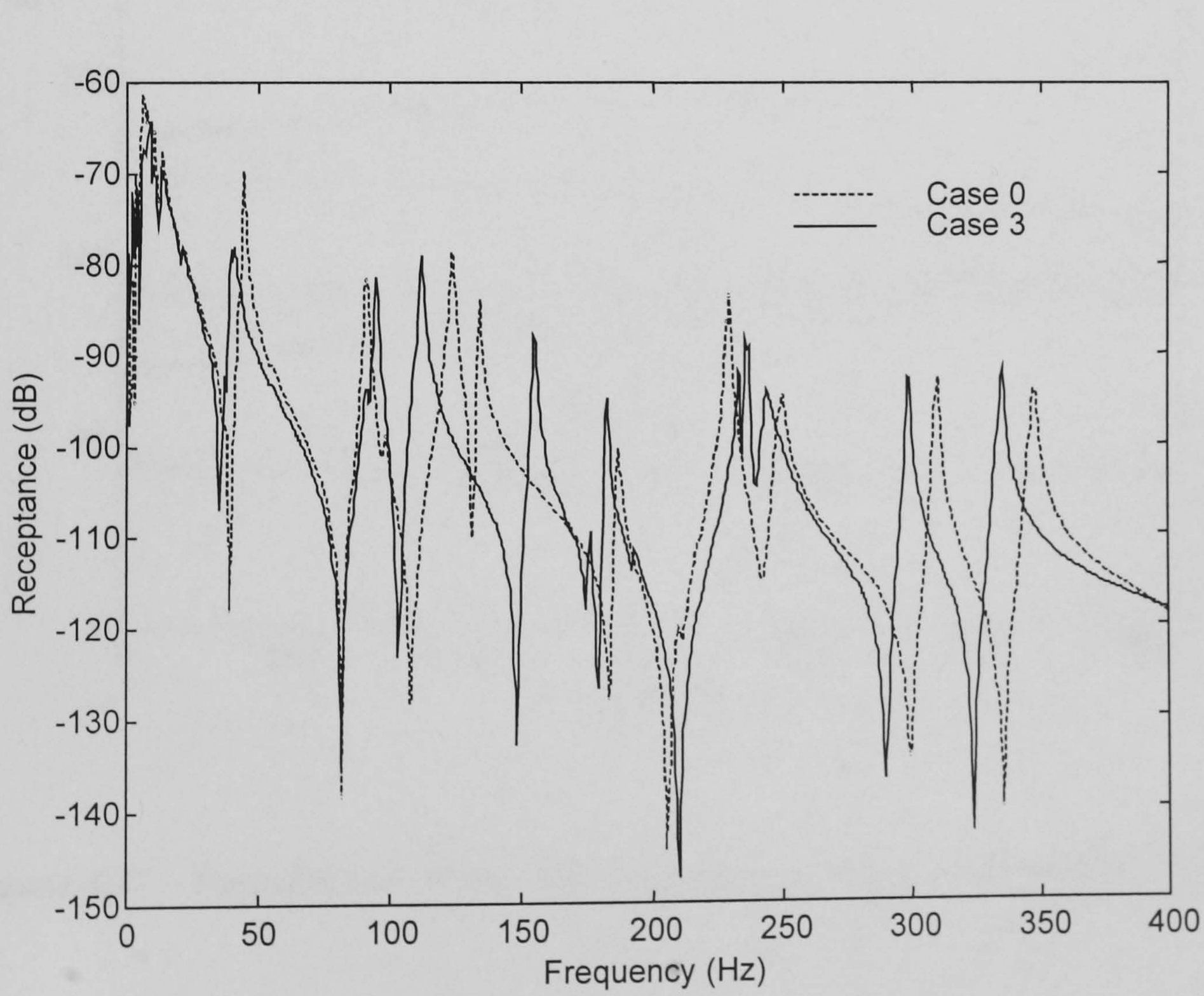

Figure 4.16 – Point Receptance Load Cases 0 & 3

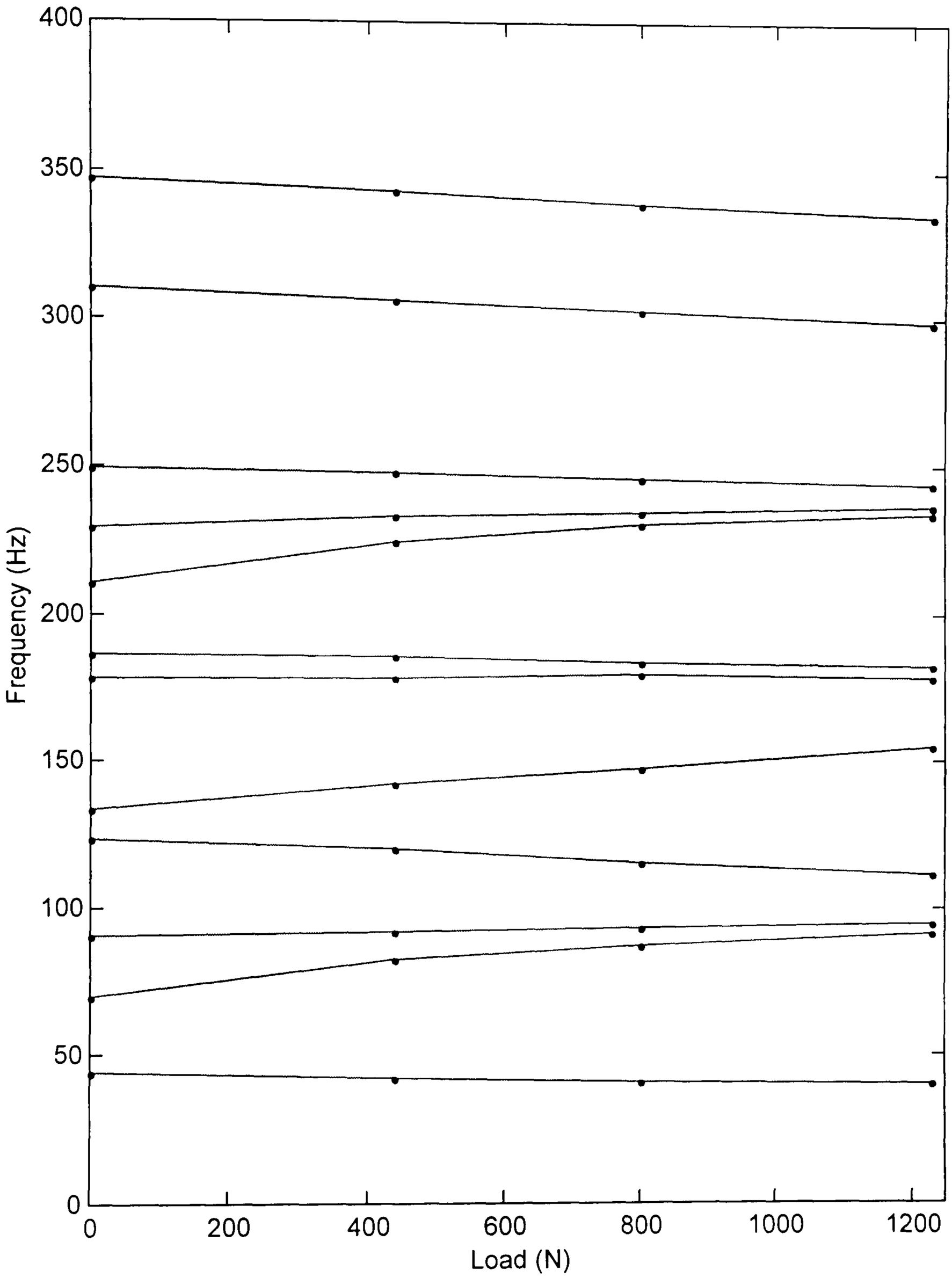

Figure 4.17 – Perturbation of Resonant Frequencies Experimental Observations

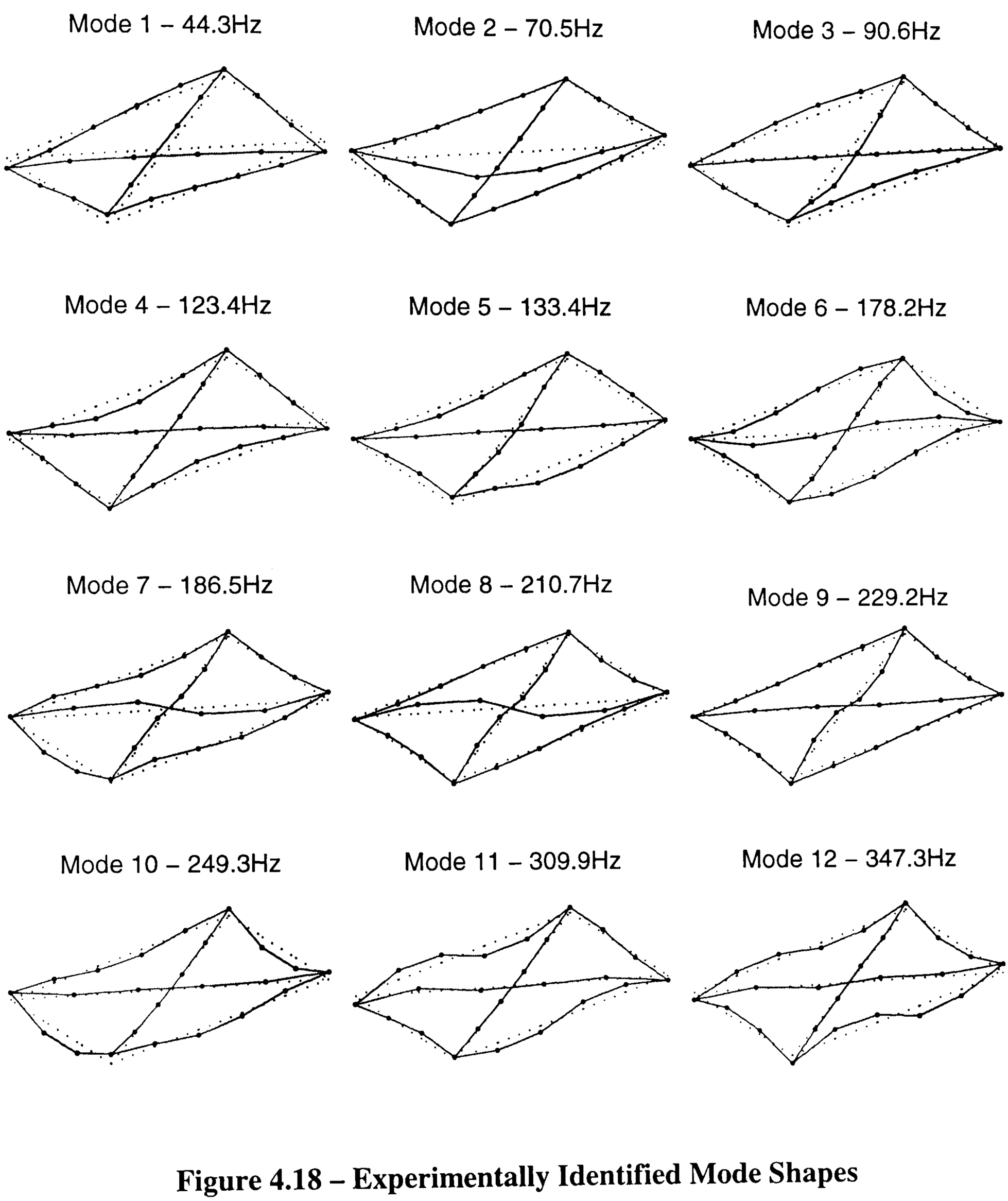

Figure 4.18 – Experimentally Identified Mode Shapes

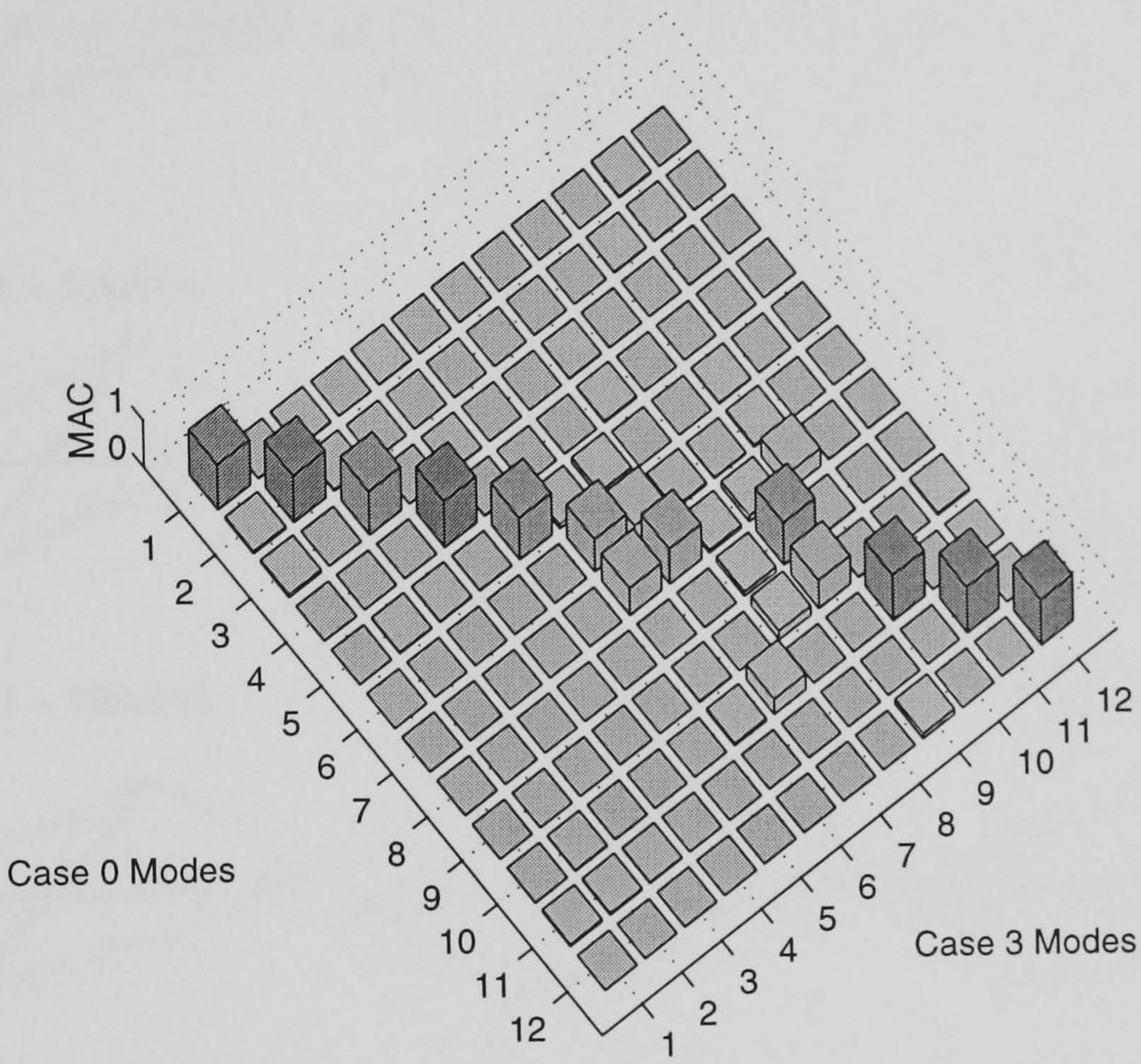

Figure 4.19 – MAC Between Experimental Load Cases 0 and 3

Mode 1 – 46.6Hz

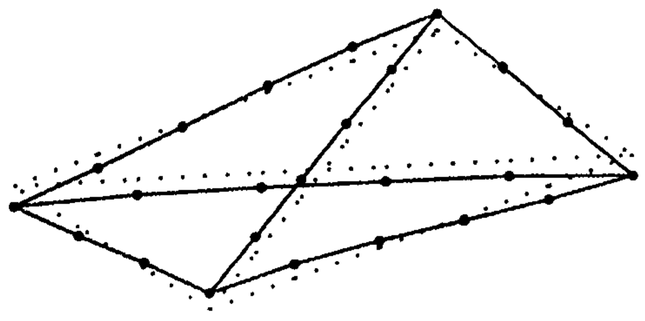

Mode 2 – 87.2Hz

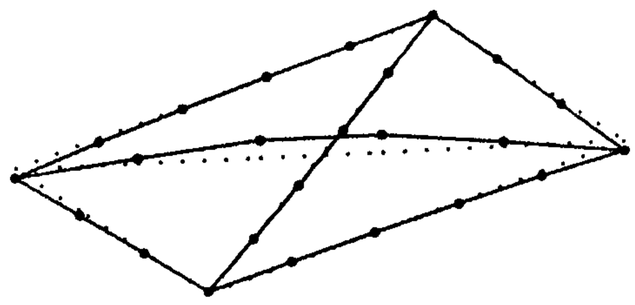

Mode 3 – 94.9Hz

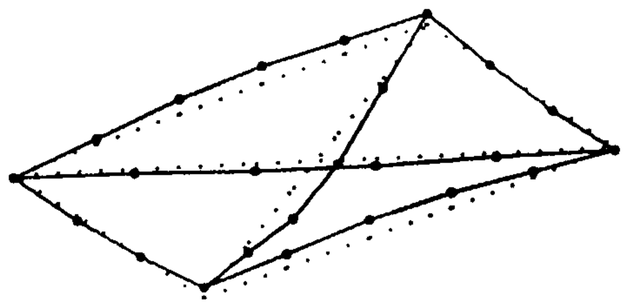

Mode 4 – 129.9Hz

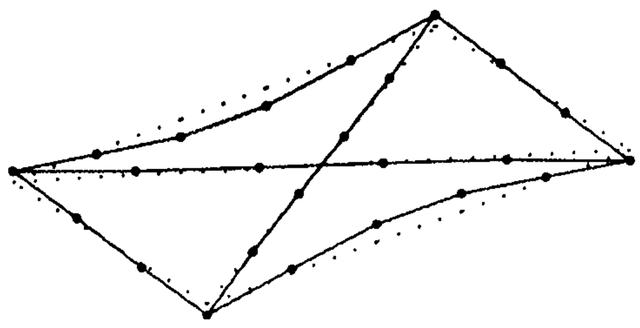

Mode 5 – 140Hz

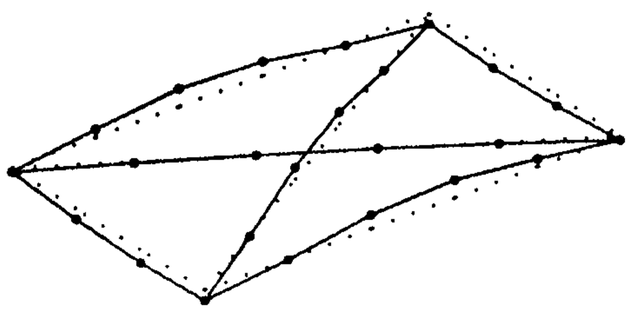

Mode 6 – 186.1Hz

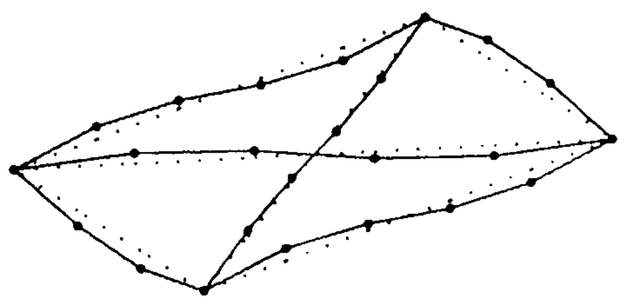

Mode 7 – 199.5Hz

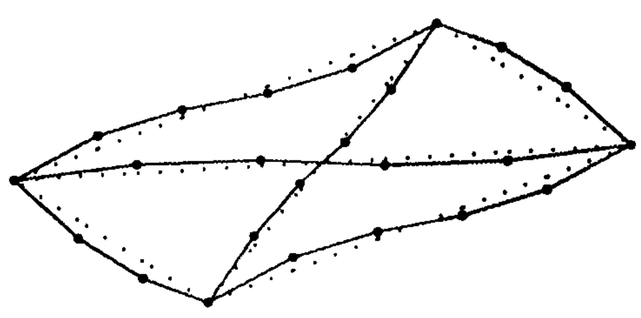

Mode 8 – 213.1Hz

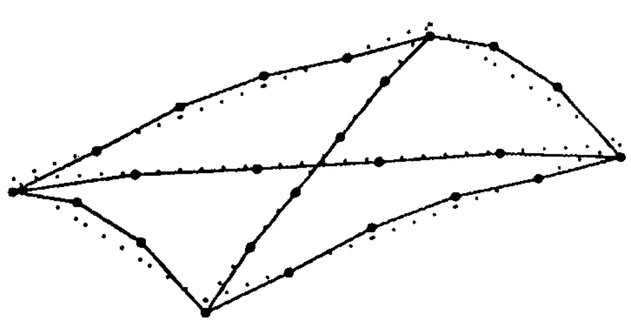

Mode 9 – 226.8Hz

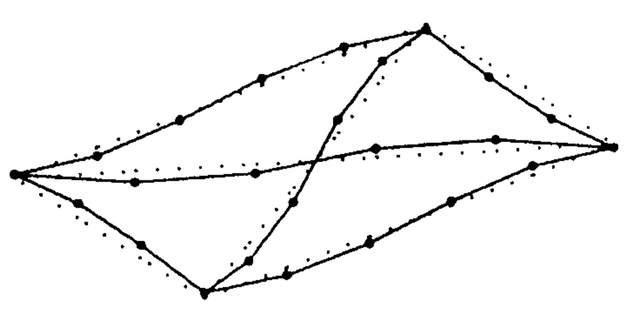

Mode 10 – 239Hz

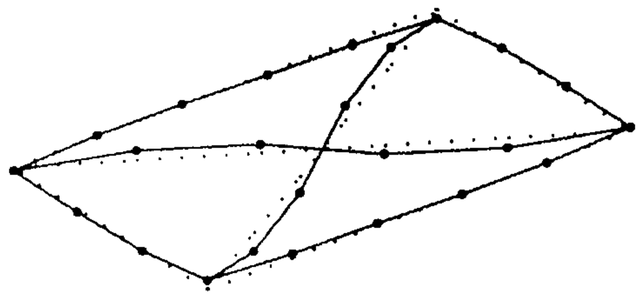

Mode 11 – 245.5Hz

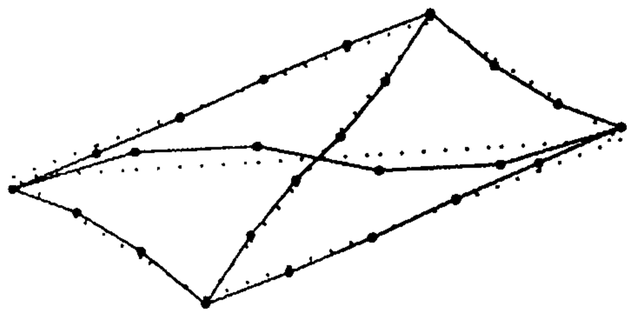

Mode 12 – 271.1Hz

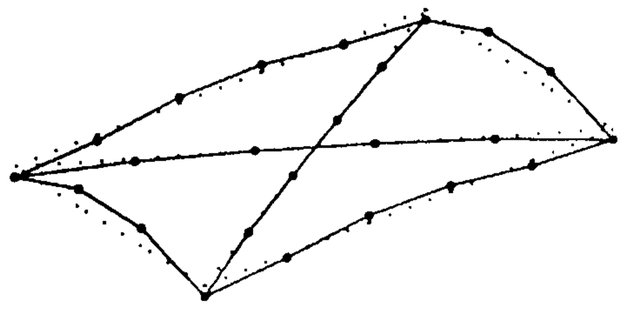

Mode 13 – 302.3Hz

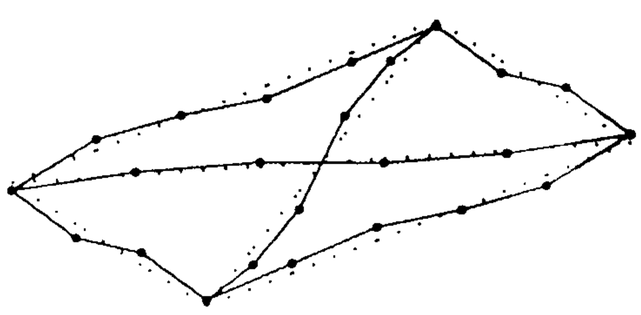

Mode 14 – 331Hz

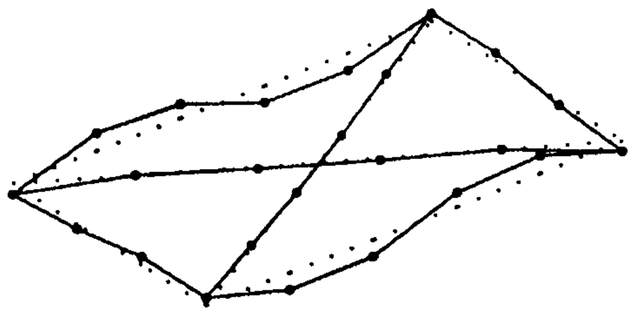

Mode 15 – 368Hz

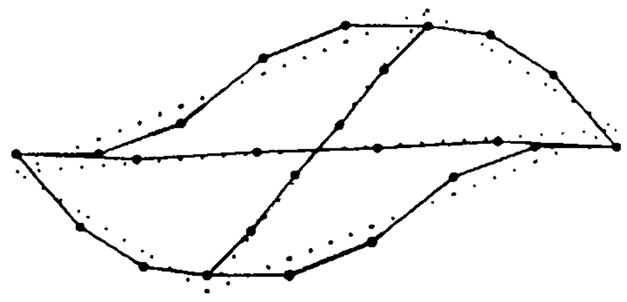

Figure 4.20 - Finite Element Mode Shapes

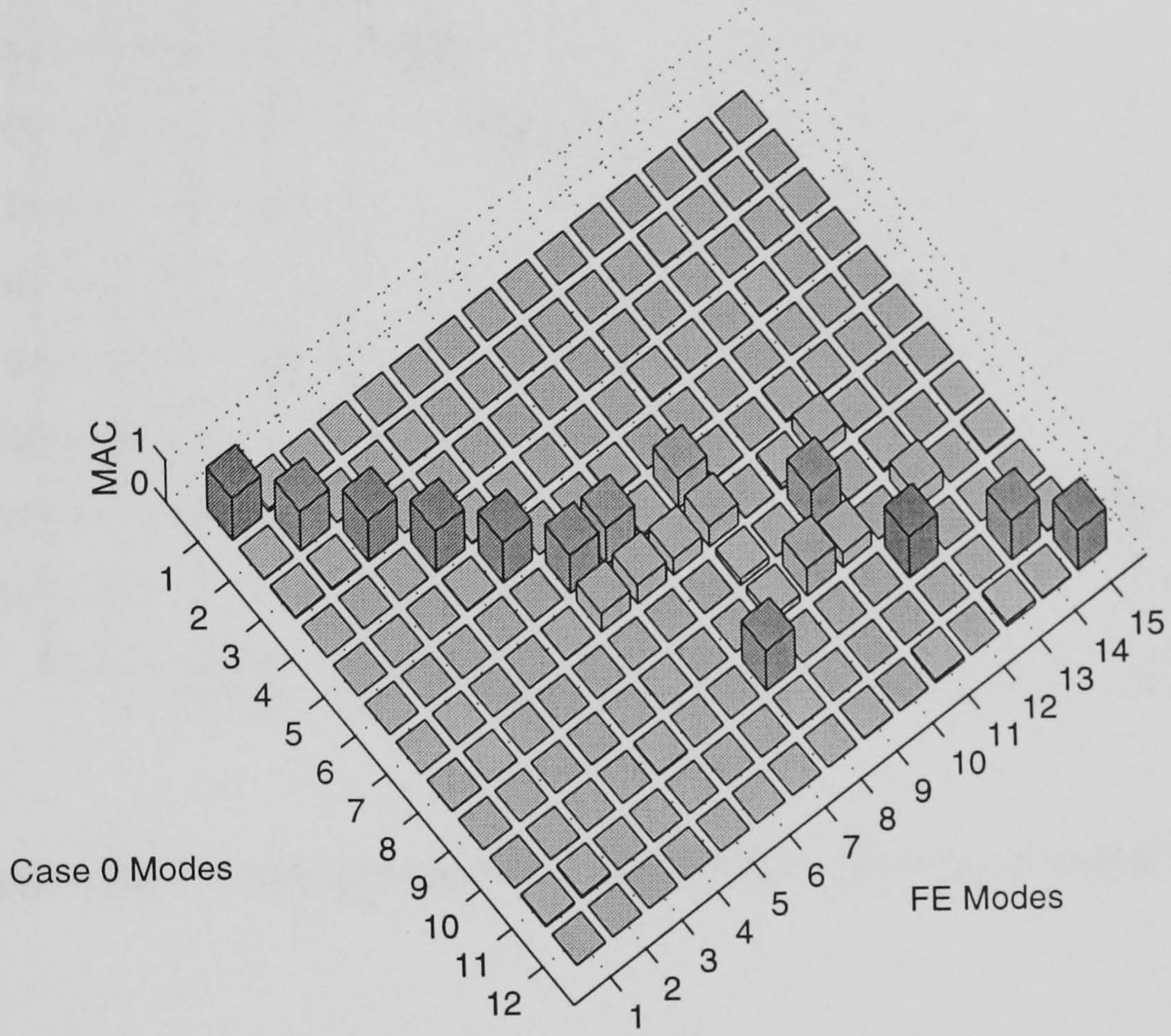

Figure 4.21 - MAC Between Experimental Case 0 Modes and FE Prediction

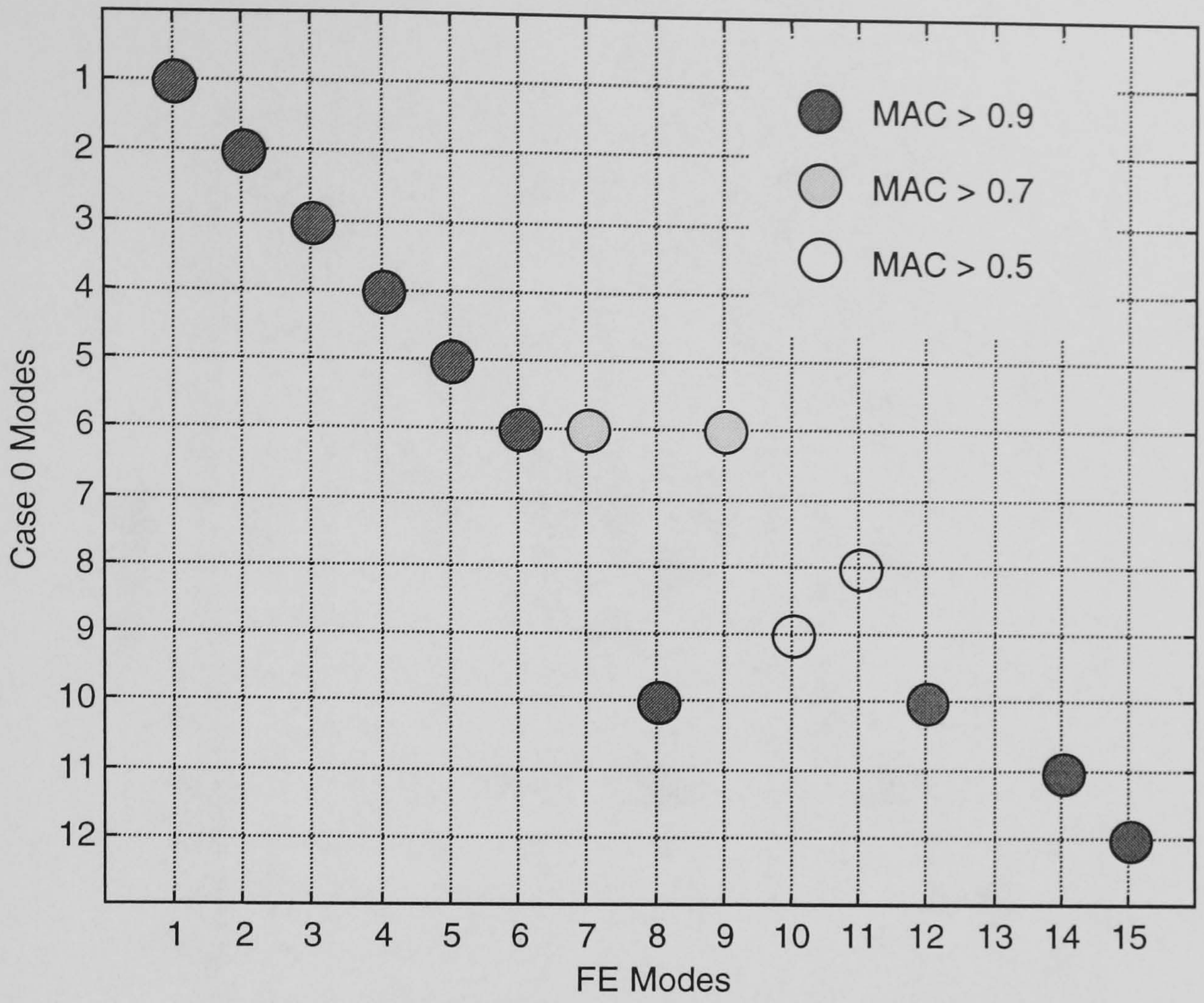

Figure 4.22 – Correspondence of Modes Between Case 0 and FE Models

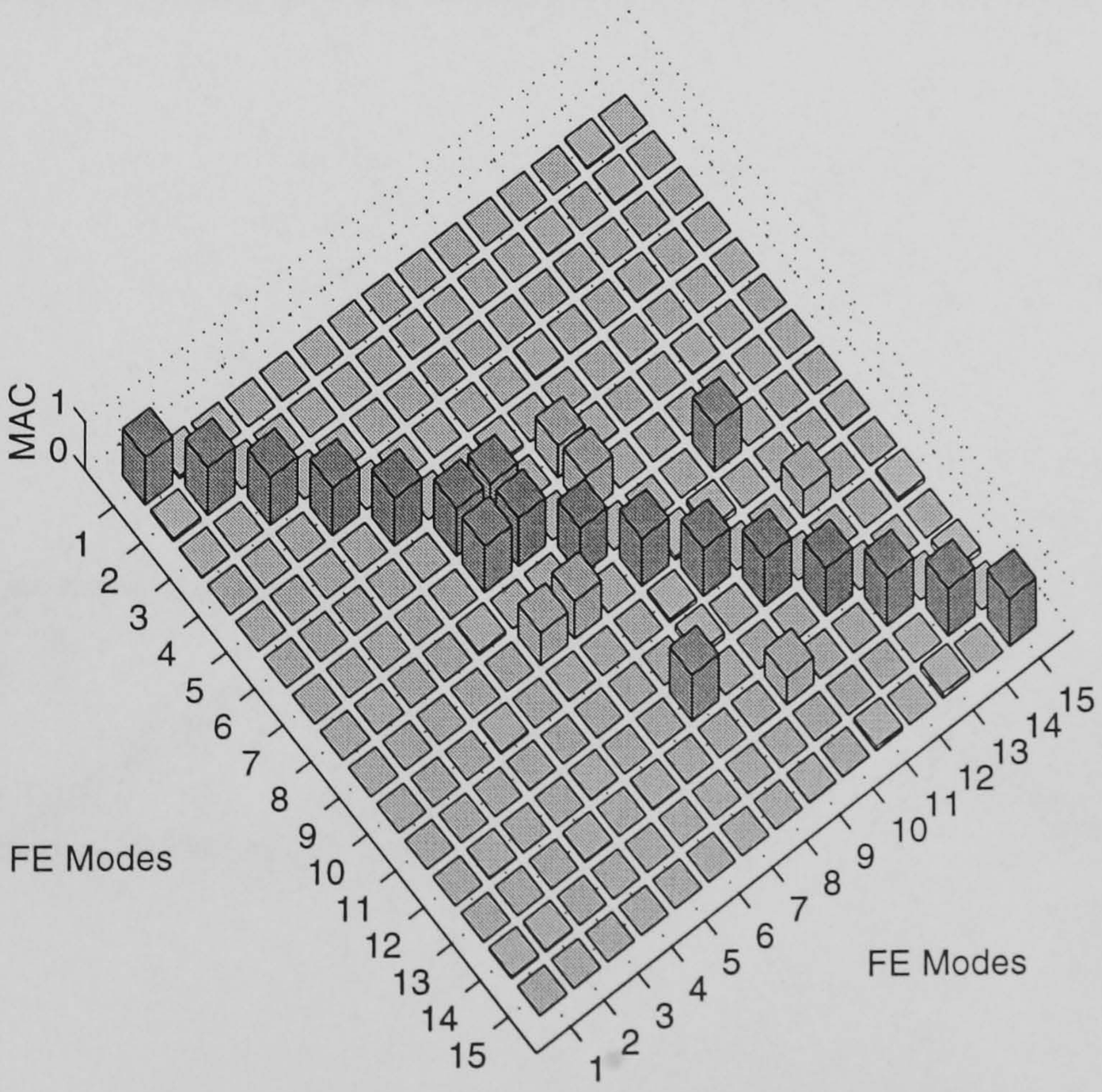

Figure 4.23 – Auto-MAC of FE prediction of First Fifteen Modes of Vibration

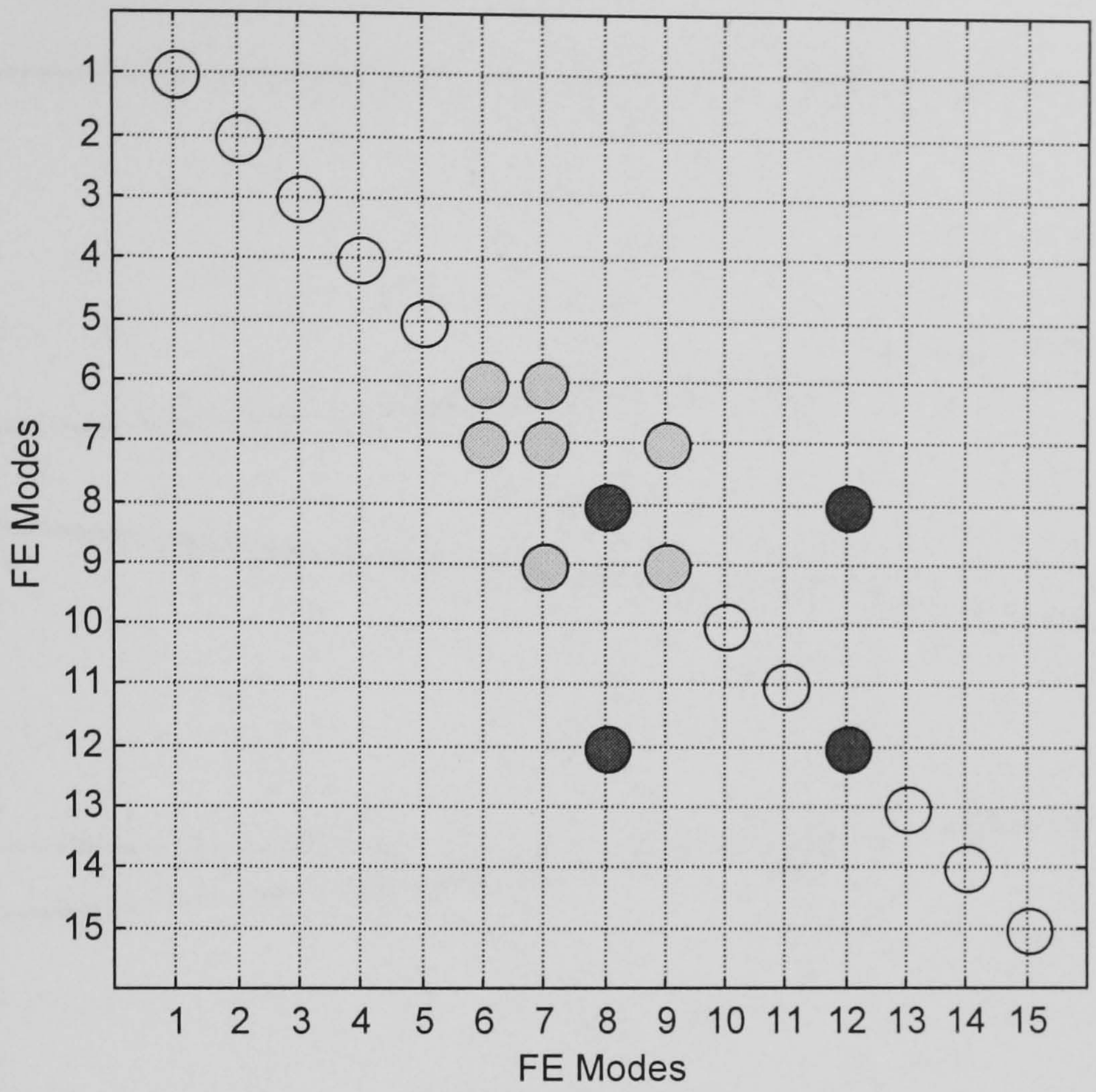

Figure 4.24 – Closely Correlating Modes (MAC > 0.8) in FE Model

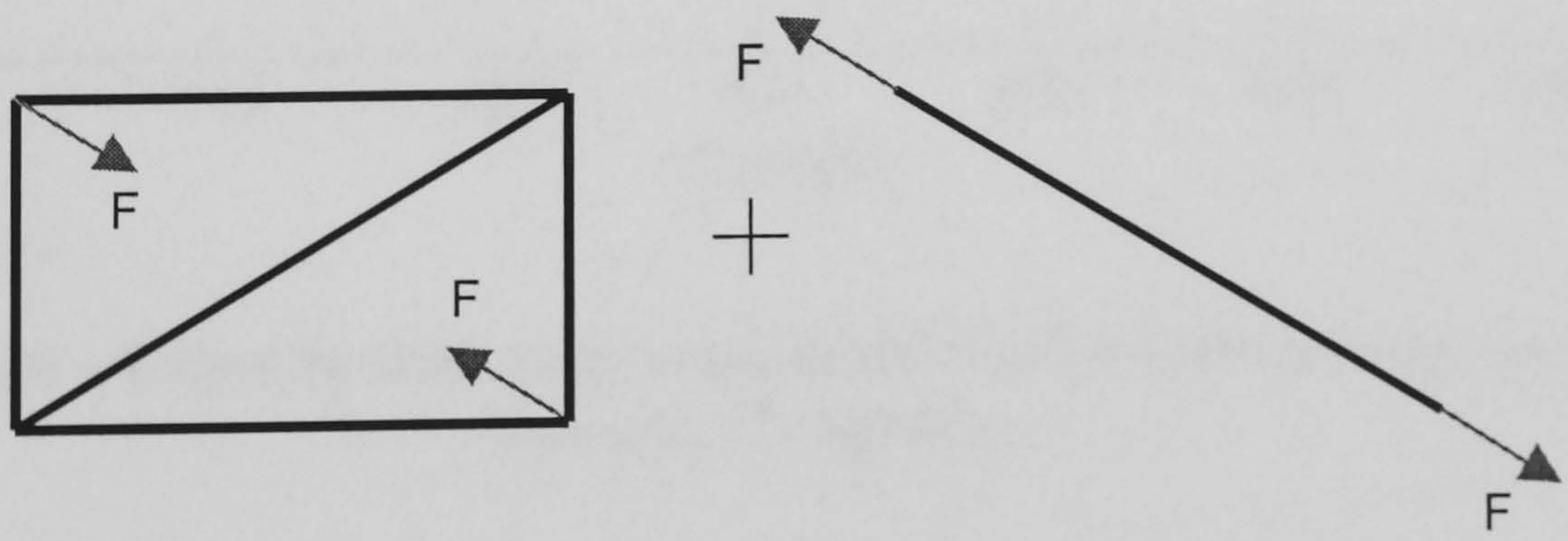

Figure 4.25 - Construction of FE Model

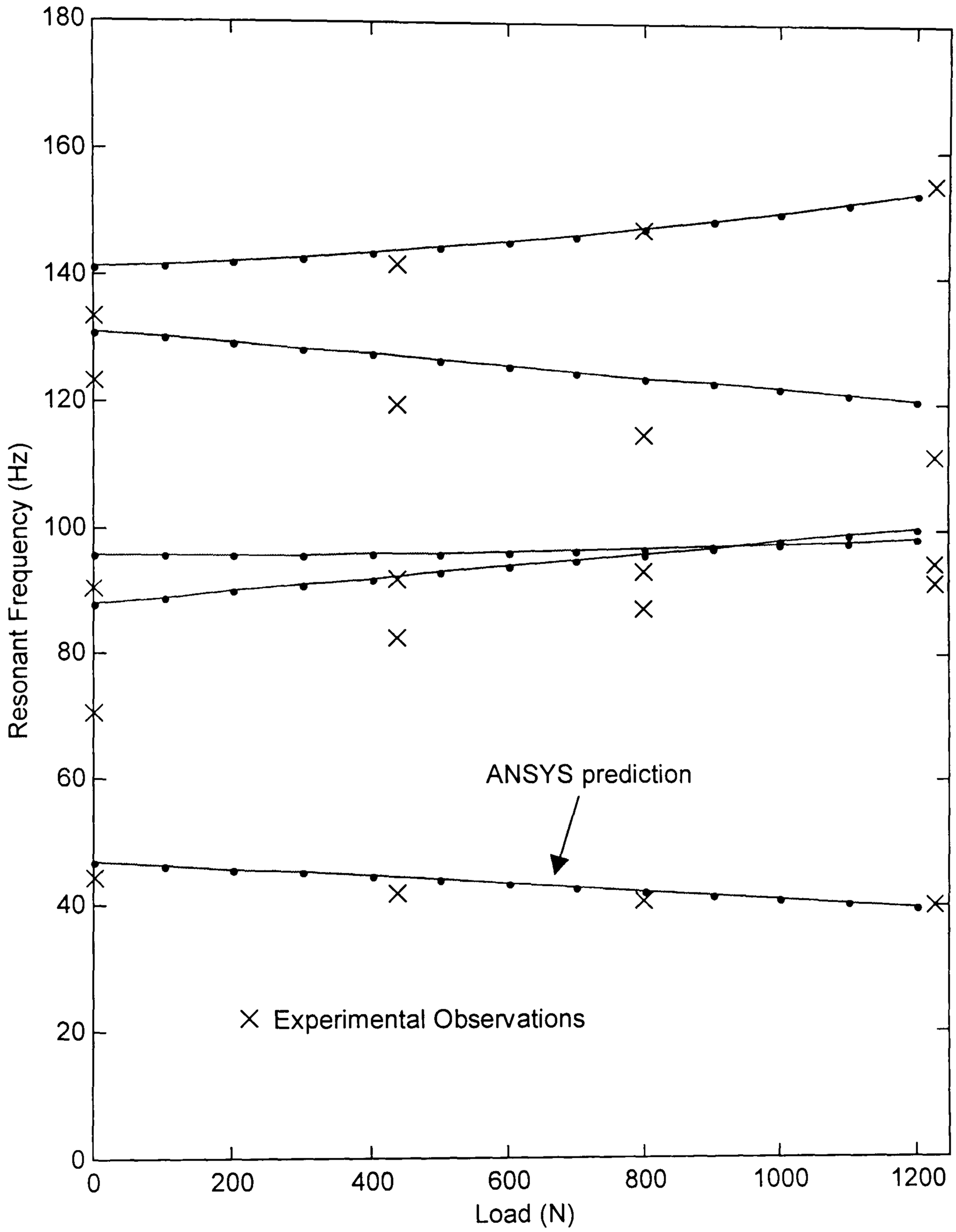

Figure 4.26 – Experimental And Analytical Relationship Between Load and Resonant Frequency

CHAPTER 5

MODEL UPDATING OF LOAD-DEPENDENT STRUCTURAL PROPERTIES

5.1 Introduction

Chapters 3 and 4 have dealt with the theory underlying the changes to structural matrices resulting from structural loading. In addition the practical aspects of identifying axial load distribution and making changes to structural matrices from essentially static data have been investigated. It is observed that resonance frequencies are liable to change as a result of loading and that some success can be gained in matching the dynamic response of loaded structures from static load identification using traditional techniques. The earlier chapters introduce a *static updating* step prior to dynamic testing. The approach is to alter element structural matrices to be a close representation of the structure undergoing subsequent dynamic testing.

In particular, chapter 3 shows how the changes to structural matrices resulting from static nonlinear geometry effects are taken into account by relatively simple changes to structural matrices at an elemental level. Stress stiffening is effectively included by the addition to the elemental structural matrices of a term which is a function of both the geometry of the element and the axial[25] force. Deformation effects manifest themselves in the form of elemental rigid body rotations.

The initial static updating step is effective in cases where it is possible either to determine the loading point(s) and magnitude(s) directly, or decide whether enough information is available to infer these parameters. In practice it is likely that structural loading cannot be easily directly determined. Motivated by a need to address this difficulty, this chapter explores the possibility of casting the stress stiffening and

---

[25] Membrane forces in the case of stress stiffened plates.

element rotation terms as updating parameters. The goal is to include the deformed characteristics of the structure under test which could be encapsulated in a finite element model directly using dynamic measurements. These quantities will be henceforth referred to as *load-dependent updating parameters*. The load-dependent parameters could further be included with the updating parameters which might be chosen in a typical updating procedure. This approach opens the possibility of including both *transient* and *permanent* differences between the finite element model and the prototype structure in a single step. Figure 5.1 compares the two approaches to the inclusion of load dependent effects graphically.

The two new updating parameters namely the elemental stress stiffening and elemental rigid body rotation are considered separately in the two following sections (5.2 and 5.3). The practicality of implementing each type of updating parameter is examined with respect to the eigenvalue sensitivity approach to model updating described in chapter 2. Section 5.4 compares the load-dependent updating parameters to currently popular updating parameters and in particular so-called generic parameters which can be thought of as allowing the most general possible representation of a particular element type.

Note that the application of the updating parameters is explained and demonstrated in terms of beam type elements. Their usefulness is examined with respect to sensitivity methods of model updating. Where appropriate the possibility of applying the techniques to different element types and other model updating strategies are referred to in the discussion.

5.2 Updating of Stress Stiffening Effects

It has already been shown in chapter 3 that stress stiffening effects can be included in finite element models by the addition of extra components to elemental stiffness matrices. This occurs in situations where elements form part of a structure which is sufficiently slender that axial load may effect the vibration characteristics. It has further been seen that stress stiffening effects the stability and dynamic behaviour of elementary

structures. This is well known and exploited. However, the relationship between loading and dynamic behaviour in more complex structures is less easily characterised without turning to finite element modelling. This method is effective in allowing changes in dynamic behaviour of structures as a result of loading to be ascertained (see chapters 3 and 4). Performing the reverse process of assessing structural loading from dynamic frequency shifts in complex structures however, has hitherto only been possible in the most elementary of cases. This section investigates the formulation of a relationship between changes in stress stiffening of individual elements and changes in resonant frequency. From this basis stress stiffening can be calculated from the modal properties by an iterative process.

5.2.1 Theory

Starting with the premise that the correct (updated) structural stiffness[26] matrix can be constructed in terms of the *a priori* model by

$$[K]^U = [K]^A + [\Delta K]. \tag{5.1}$$

where the superscripts U and A represent the updated and initial (*a priori*) stiffness matrices respectively. The usual assumption that the updated stiffness matrix is a function of a set of updating parameters $p_1, p_2, \ldots, p_{n_p}$ is adopted here. This can further be expressed as a Taylor expansion about the initial stiffness matrix in powers of p. The updated stiffness to the first order is given by

$$[K]^U = [K]^A + [\Delta K] = [K]^A + \sum_j \delta p_j \frac{\partial}{\partial p_j}[K]^A + O\left(p_j^2\right). \tag{5.2}$$

If the *a priori* stiffness matrix is considered as being built from a set of both unloaded and loaded component elemental matrices it can be expressed as

---

[26] A similar derivation can be constructed for the mass matrix, in this case however only changes to the stiffness matrix are required.

$$[K]^A = \sum_{j=1}^{n_{elems}} \left([K]_{e_j}^z + [K]_{e_j}^{ss} \right), \tag{5.3}$$

where the superscripts z and ss refer to the original/zero load elemental matrices and stress stiffened matrices respectively. This requires that the axial load present in an element - which is implicit in the stress stiffening term - is available. Recasting the original stiffness matrix in terms of a set of factors $p_1, p_2, \ldots, p_{n_{elems}}$ upon the stress stiffening terms results in a stiffness matrix given by

$$[K]^A = \sum_{j=1}^{n_{elems}} \left([K]_{e_j}^z + p_j [K]_{e_j}^{ss} \right). \tag{5.4}$$

Differentiating with respect to p_j gives

$$\frac{\partial [K]^A}{\partial p_j} = [K]_{e_j}^{ss}. \tag{5.5}$$

from which it can be seen that the second and higher derivatives are zero.

The similarity of the choice of the stress stiffening component of the stiffness matrix of a loaded structure with the use of elemental stiffness is thus evident. As with using the overall elemental stiffness as an updating parameter comparing equations (5.2) and (5.4) it is seen that the relationship between the updated structural matrix and the updating parameter becomes exact

$$[\Delta K] = \sum_j \delta p_j [K]_{e_j}^{ss}. \tag{5.6}$$

Noting that the stress stiffness matrix has axial load as a factor and defining $[\hat{K}]_e^{ss}$ as the *normalised* stress stiffness. Substituting in equation (5.4) leads to the parameter p_j correctly representing the value of load, that is

$$[K] = \sum_{j=1}^{n_{elems}} \left([K]_{e_j}^z + p_j [\hat{K}]_{e_j}^{ss} \right). \tag{5.7}$$

Recalling that the sensitivity of a system eigenvalue λ_i to changes in an updating parameter p_j set out chapter 2 (equation (2.49)) is given by

$$\frac{\partial \lambda_i}{\partial p_j} = \{\phi\}_i^T \left(\frac{\partial}{\partial p_j}[K] - \lambda_i \frac{\partial}{\partial p_j}[M] \right) \{\phi\}_i , \tag{5.8}$$

substituting (5.5) into (5.8) leads to

$$\frac{\partial \lambda_i}{\partial p_j} = \{\phi\}_i^T [K]_{e_j}^{ss} \{\phi\}_i \tag{5.9}$$

where $\{\phi\}_i$ is the mass normalised mode shape (eigenvector) of the i^{th} mode. The sensitivity of n_{modes} eigenvalues to n_p parameter values can be expressed as

$$\begin{bmatrix} \frac{\partial \lambda_1}{\partial p_1} & \frac{\partial \lambda_1}{\partial p_2} & \cdots & \frac{\partial \lambda_1}{\partial p_{n_p}} \\ \frac{\partial \lambda_2}{\partial p_1} & \frac{\partial \lambda_2}{\partial p_2} & & \\ \vdots & & \ddots & \\ \frac{\partial \lambda_{n_{modes}}}{\partial p_1} & & & \frac{\partial \lambda_{n_{modes}}}{\partial p_{n_p}} \end{bmatrix} \begin{Bmatrix} \delta p_1 \\ \delta p_2 \\ \vdots \\ \delta p_{n_p} \end{Bmatrix} = \begin{Bmatrix} \delta \lambda_1 \\ \delta \lambda_2 \\ \vdots \\ \delta \lambda_{n_{modes}} \end{Bmatrix} \tag{5.10}$$

or in matrix, vector form as

$$[S]\{\delta p\} = \{\delta \lambda\} \tag{5.11}$$

where the rows of $[S]$ and $\{\delta \lambda\}$ should provide sufficient information to produce a good estimate of the unknown changes in updating parameter $\{\delta p\}$. The pseudo-inverse of the sensitivity matrix can be determined in a *least-square* sense using singular value decomposition (see section 2.4 in chapter 2). In addition the changes in parameter value can be ascertained by pre-multiplying the right hand side of (5.11) by the pseudo inverse of the sensitivity matrix

$$\{\delta p\} = [S]^+ \{\delta \lambda\}. \tag{5.12}$$

A useful result of using SVD is that the Frobenius norm of the residual

$$R = \| \{\delta \lambda\} - [S]\{\delta p\} \| \tag{5.13}$$

is minimised. The best estimate of the $\{\delta p\}$ for the given $\{\delta\lambda\}$ are gained by an iterative process described in chapter 2, where the $(k+1)^{th}$ set of updating parameter are given by

$$\{p\}_{k+1} = \{p\}_k + \{\delta p\}_k . \tag{5.14}$$

The magnitude of the changes in parameter

$$mag = |\{\delta p\}| \tag{5.15}$$

at a particular step in the updating iterations is used to measure convergence. Convergence occurs when this value falls below a defined threshold. Given that the updating parameters here are closely related to structural loading, the choice of threshold becomes one of setting the accuracy to which loads must be determined.

From equation (5.9) it is seen that the terms of the sensitivity matrix need to be updated for each iteration. Only the mode shape terms $\{\phi\}$ are changed at each iteration, the stress stiffening term $[K]^{ss}$, itself not being a function of any of the updating parameters $\{p\}$. This implies the *a priori* finite element model requires changes to only stress stiffening parameters to bring it into agreement with experimental data, if the variation between the changes in values of $\{\phi\}$ prevent updating from occurring in a single step. This further suggests that the mode shapes of the small framework of chapter 4 which were found to vary considerably under loading would produce less robust convergence upon correctly identified stress stiffening parameters.

In chapter 3 it was shown that stress stiffening has the effect of perturbing resonant frequencies by linear quantities rather than factoring them. Thus, the sensitivity of eigenvalues to stress-stiffening updating parameters will not increase with each mode, instead the terms of the sensitivity matrix will be of the same order. The result is a set of well conditioned equations where the higher resonant frequencies will not necessarily dominate the updating problem. Conversely, if other sources of error in the initial FE model of a structure cause increasingly large perturbations to higher order resonant frequencies but are not update-able, alterations to elemental loads are unlikely to be able

to reconcile analytical predictions of dynamic behaviour with the dynamic measurements.

Note that the method described for assessing the effects of load in a structure strives to estimate the set of loads which best match observed experimental dynamic data. This does not necessarily lead to a set of loads that are physically realistic. Exactly the same problem faces *any* choice of updating parameters. This is a criticism often levelled at model updating since it is often very difficult to verify whether the changes suggested are valid. In the case of loading, however, the physical relevance of the updating parameter allows the engineer more insight into veracity of the updated model.

While the stress stiffening technique offers the prospect of identifying axial loads present in slender elements, a formulation of the stress stiffening matrix for the element must be obtainable. As the introductory chapter indicates, this thesis concentrates upon the example of two and three dimensional beams for which the stress stiffening matrix is readily available. These element types are heavily used in modelling engineering structures and exclusively in the case of structural frameworks. Note that the technique is applicable to any other element for which a stress stiffening matrix can be derived.

5.2.2 Practical Application of Stress Stiffening Updating

The theory outlined in the previous section is of considerable practical significance. It offers the prospect of identifying axial loads in framed structures under arbitrary loading conditions from dynamic measurements. The usefulness of this technique is investigated in the following sections by means of two case studies.

5.2.2.1 Identification of Force Magnitude in Axially Loaded Beam

Consider in the first instance the narrow plate model which has already been thoroughly investigated throughout this thesis. The task of identifying an unknown axial load from experimental dynamic observations - while trivial - is a useful starting point. The case study is similar to that described in section 3.2.4 of chapter 3, the configuration of the

simulated experiment is shown in figure 5.2. Since all elements are identical and the beam experiences only axial load, a single updating parameter is required to account for the stress stiffening effects. The overall stiffness is included as a second updating parameter with which to compare the new parameter. The experimental data were synthesised without any other sources of error between the FE and "experimental" data. The stiffness of the experimental model was set at 20% greater than the original FE model and an axial load of 5kN was applied. Figure 5.3 shows the receptance of both sets of data up to 400Hz, which contains all of the hallmarks of two structures with different stiffnesses. Commencing from the finite element model without stress stiffening effects included, the sensitivities of the first two eigenvalues lead to the following expression from which the two parameter values can be ascertained

$$\begin{bmatrix} 1.57\times10^{5} & 7.42 \\ 1.19\times10^{6} & 2.78 \end{bmatrix} \begin{Bmatrix} p_k \\ p_{ss} \end{Bmatrix} = \begin{Bmatrix} -1.17\times10^{3} \\ 1.35\times10^{5} \end{Bmatrix}, \tag{5.16}$$

where the updating parameters are defined as[27]

$$[K]_U = (1+p_k)[K]^z + p_{ss}\left[\hat{K}\right]^{ss}. \tag{5.17}$$

This two degree of freedom configuration affords some insight into the applicability of stress stiffening. Figure 5.4 shows the two linear equations of (5.16) as lines which meet at the solution point for p_k and p_{ss}. This approach to demonstrating conditioning of sets of equations in two unknowns was previously used by Waters [54]. The conditioning of sets of equations is analogous to the angle between the sets of lines. improving as the lines become perpendicular. Based on this criterion it is observed that the conditioning of the equations enables an accurate solution to be obtained. The conditioning of the sets of equations deteriorate with higher order modes. In other words it is more difficult to determine accurately both stress stiffening and overall stiffening effects using high order frequencies. This is explained in light of the fact that changing the overall stiffening of the bar results in increasingly large perturbations to

---

[27] The stress stiffening matrix is formulated for a unit load and is thus normalised; represented with a hat.

resonant frequencies which will dominate when compared to the perturbations caused by stress stiffening effects. This observation implies that where changes to elemental stiffening (or density) are likely to require inclusion in a sensitivity based updating procedure, the information from the lower order modes should be used primarily to update the stress stiffening effects.

From equation (5.16) it can also be seen that the sensitivities associated with the overall stiffness are a number of orders of magnitude greater than those associated with the stress stiffening updating parameter. The problem of ill-conditioning arising from the size of sensitivity terms can be alleviated by factoring the stress-stiffening matrix. This is achieved by a scaling factor which essentially represents an estimation of the order of magnitude of the force to be identified. In this case if the updating parameters are defined as

$$[K]_U = p_k[K]^z + 1000\,p_{ss}[\hat{K}]^{ss}, \tag{5.18}$$

the second column of the sensitivity matrix in equation (5.16) is factored by the same amount and the conditioning of the problem is thus improved. In physical terms this process is the same as estimating the initial load in a structure. If more than one stress-stiffening updating parameter is used, any set of initial parameter (element load) values can be chosen to assist with the conditioning of the problem.

To assess the effect of noise[28] and choice of frequencies for updating, multiple updating runs were performed with artificial errors of up to 5% imposed upon the experimental eigenvalues. The pertubation to eigenvalues used to simulate experimental data are employed to test the resilience of the updating procedure to noise. In practice noise will largely arise from innacuracies in recorded time series data as well as errors arising from the modal identification process.

---

[28] Noise is defined in this thesis so as to include all effects which result in the data from an experimental test not agreeing with the predictions of a finite element model which are not accounted for when altering the finite element model to match the experimental data.

Three sets of simulations were defined by the number of modes used to update the FE model and comprised respectively; the first two, four and eight modes. The results from the three sets are shown as differently shaded circles in figure 5.5. As one would expect all of the results are distributed about the correct result, but the more modes used to in the updating process, the less accurate the estimation of the loading parameter. The level of accuracy in estimation of the stiffness updating parameter does not seem to be affected by the number of modes used to update the finite element model. At first sight this result might seem counter-intuitive. It is usually the maxim that the more information about structural dynamics i.e. modes available, the better the chances of success in performing a model update. The reason for the decrease in effectiveness of the updating process to identify the loading in the beam with number of modes introduced can be explained by the choice of the noise model. Multiplying the correct values of resonant frequencies by a factor of up to 5% causes increasingly large absolute shifts in frequency. It is the experience of the author that noise introduced due to errors in signal processing etc. does not exhibit this phenomena. This assertion is backed up by results presented in the chapter 6. If instead a random absolute value is applied to the system eigenvectors the result is very different. Figure 5.6 shows the result perturbing the experimental eigenvalues by adding random values, the magnitude of the added value was chosen such that the perturbation to the first eigenvalue was up to 5% as before, corresponding to a shift of up to 14Hz on the resonant frequencies. It is seen that the convergence upon the correct parameter values is excellent and moreover that using higher order modes improves the ability of the updating scheme to identify these points.

To summarise, the likelihood of success in using stress-stiffening as an updating parameter appears to lie in the amount of divergence of modal perturbation with frequency. An additional factor is the extent to which this perturbation is caused by parameters which can be changed in the updating process. An initial survey of the data

available from a test structure will quickly allow an engineer to assess the likelihood of success of updating the stress-stiffening parameters.

If experimentally identified resonant frequencies from a loaded structure are found to diverge from the unloaded finite element model but experimentally identified resonant frequencies are available for a different load step, there is a likelihood that the experimental frequency perturbation can be used to identify relative load levels.

5.2.2.2 Identification of Loads in Small Framework

The framework structure introduced in the previous chapter allows the usefulness of the load identification method to be ascertained in a situation where the relationship between structural loading and perturbation to resonant frequencies is not intuitive.

The finite element model of the framework (see figure 4.14) consists of 34 elements, 26 of which represent the 6×15mm spars which make up the framework with the remaining 8 representing the non-coincidence of the 6 spars of the framework. If n_{modes} resonant frequencies are identified and we wish to identify n_{loads} elemental axial loads starting with an initial load distribution defined by $p_1, p_2, \ldots, p_{n_{loads}}$ the following equation is solved iteratively

$$[S]_{n_{modes} \times n_{loads}} \{\delta p\}_{n_{loads}} = \{\delta \lambda\}_{n_{modes}}. \tag{5.19}$$

It is both sensible and reasonable to decrease the number of δp_i to identify by assuming that the load in certain sets of elements or substructures will be the same. In this case equation (5.19) is reduced to

$$[\{\{S\}_{1a} + \{S\}_{1b} + \ldots\} \quad \ldots] \begin{Bmatrix} \Delta p_{spar1} \\ \Delta p_{spar2} \\ \vdots \end{Bmatrix} = \{\Delta \lambda\}, \tag{5.20}$$

where the subscripts *1a, 1b, ...* for instance refer to the elements which constitute spar 1. The same procedure is undertaken for all six spars of the framework leading to six

independent loading-related parameters to be identified. The numbering scheme is reproduced in figure 5.7.

It is intuitive that the best initial estimation of load within a structure will lead to the best likelihood of convergence on the correct loading values. At the other extreme most flexibility would be offered if very little information about the load state is required beforehand. The importance of the initial estimate of the loading is investigated by means of the framework case study.

In the following simulations the "experimental" eigenvalues are simulated using the finite element model described in chapter 4 with the axial load in each spar given in table 5.1, the loads were chosen to represent the load present in a 2D, pinned idealisation of the framework where a tensile load of 1kN is imposed on one of the diagonal members.

Spar	Load (N)
1	-515
2	-857
3	-515
4	-857
5	1000
6	1000

Table 5.1 – "Experimental" Force Distribution

The stress stiffening components were incorporated directly into the finite element model outside of the finite element package allowing the effect of structural deformity arising from loading to be ignored for the time being. The first 15 non-rigid body resonant frequencies for this case are shown in table 5.2 with the absolute and percentage frequency shift also presented.

Frequency (Hz)			
Unloaded	Loaded	Absolute Increase (Hz)	Percentage Increase
46.6	39.3	-7.3	-15.6
87.2	96.5	9.3	10.6
94.9	98.7	3.7	3.9
129.9	120.3	-9.6	-7.4
140.0	138.2	-1.9	-1.3
186.1	186.7	0.6	0.3
199.5	197.2	-2.3	-1.2
213.1	210.0	-3.1	-1.4
226.8	230.2	3.4	1.5
239.0	249.3	10.2	4.3
245.5	254.8	9.3	3.8
271.1	264.6	-6.5	-2.4
302.3	299.2	-3.1	-1.0
331.0	321.7	-9.3	-2.8
368.0	359.1	-9.0	-2.4

Table 5.2 – Change in Natural Frequencies Due to Loading

The perturbations to natural frequencies are seen not to show any systematic trends. It is further observed that the frequency shifts are in both directions. While there is much similarity between some of the mode shapes (see chapter 4), the mode pairs shown in table 5.2 are known to correlate with each other.

Taking the entirely unloaded structure as the initial model, the first set of stress-stiffening parameters are thus set to zero. The sensitivity matrix of the 15 natural frequencies shown above to the six updating parameters evaluated about the zero-load case is shown graphically in figure 5.8. The sensitivity of higher order modes to changes in load in the six spars are seen to be larger than their lower order counterparts, but not dramatically so. Comparing the sensitivity matrix and the finite element mode shapes shown in figure 4.22 confirms that the distribution of strain energy in each mode shape relates clearly to the sensitivity of the associated resonance to the added stiffness

in that area. For instance the flexure of spar 5 is characterised by mode 2. This manifests itself as a high sensitivity of mode 2 to changes in the stress stiffening of that particular spar.

The values of the six updating parameters after 10 iterations of the updating process are shown in table 5.3. The tension loads are seen to have been exactly identified and the loads in the compression members are estimated to within approximately 10% of the target value. Figure 5.9 shows the identified loads are converging upon their "experimental" counterparts.

Spar	Theoretical Load (N)	Identified Load (N)
1	-515	-475
2	-857	-902
3	-515	-579
4	-857	-800
5	1000	1000
6	1000	1000

Table 5.3 – Identified Load After Ten Iterations, No Initial Knowledge of Loading

The correct value of the loads in the diagonal are quickly converged upon which can be explained by the preponderance of modes which are sensitive to these particular parameters. The first step of the iteration of the updating process is seen to overestimate three of the spar loads substantially with subsequent steps producing convergence upon the correct values.

Applying the additive noise perturbation model described in the previous section whereby a random value between –10 and 10 Hz is applied to each frequency point yields a reasonably good estimation of the loading present in the structure. Twenty different target sets of data with different noise models were prepared as the experimental data and the updating procedure was invoked with no initial knowledge of load. Fifteen natural frequencies were used to characterise the loaded structure. Ten iterations of the updating process were performed and the twenty sets of identified loads

are shown in figure 5.10. Clearly the load in the diagonal members are updated most robustly with useful estimates of the loading in the vertical and horizontal members also gained.

The preceding discussion has assumed that no initial knowledge of the loading is available. In practical situations while fully instrumenting a structure might prove impractical, some estimation of the loading might be possible. If for instance, the stress in one or more members of the framework is available then two benefits will arise:

(i) reduction in number of unknowns to identify; and

(ii) more insight into the correct solution will lead to an improved chance of identifying the correct loading.

As we might expect from the previous results, the most valuable contribution to the conditioning of the updating problem is made by a knowledge of the loads upon which convergence is slowest. Figure 5.11 shows the result of performing the load identification four times with known loading in respectively members 1, 2 and 5 compared to the zero initial load situation, the loads in members 3, 4 and 6 converge in the same manner as their counterparts, their omission from figure 5.11 is only to aid clarity. As anticipated, a knowledge of either of the compression loads is seen to dramatically improve the convergence upon the target loads.

The significance of this observation is that a formulation of the sensitivity of eigenvalues to elemental axial load gives insight into which member should be instrumented to enable the most successful identification of loading. A simulated study would allow this information to be gained. However, this is a somewhat involved not to mention computationally expensive procedure. A more rapid estimate of which elements should have their loading identified experimentally can be gained from a consideration of the pseudo-inverse of the sensitivity matrix. The magnitude of the terms in the rows in this matrix give an indication of the 'lack of sensitivity' of elements to modal changes. Hence elements giving rise to large values of the "Element-wise

inverse sensitivity magnitude" or EISM provide the best candidates for determination of loading by other means. Figure 5.12 shows the value of the EISM for each of the six spars of the current case study for the sensitivity matrix constructed for {p}=0. The spars experiencing compression are seen to exhibit much higher values than spars 5 and 6 indicating that independently identified loading in these members would be most helpful.

5.2.3 Implementation Using Commercial Software

The finite element modelling, eigen-solutions and subsequent analysis for the two brief case studies (in sections 5.2.2.1 and 5.2.2.2) were performed entirely in the MATLAB [14] environment. This offers the ideal conditions for investigating and developing updating techniques. In practice however, a specialist commercial finite element package would be used to generate the initial finite element model.

The method lends itself well to implementation in "real life" provided that the following information is available from the finite element software and can be exported to third party software:

(a) elemental structural matrices;

(b) location of elements in global matrices; and

(c) stress stiffening modification to elemental matrices.

The method proceeds in exactly the same way as the overall elemental mass and stiffness would be updated. The modification to the approach is that the elemental stress stiffening matrices are required instead of the elemental mass and stiffness matrices.

5.3 Updating of Deformation Properties

In some circumstances, load induced alterations to dynamic behaviour can be taken into account largely or entirely by the stress stiffening effects described in the previous

section. The preceding chapters have shown, however, that structural deformity also plays a role in altering resonant frequencies. Chapter 3 and 4 indicate that in terms of the finite element model, changes to geometry can be accounted for by rigid body rotation of individual finite elements. The transformation from the unloaded and undeformed finite element structural model to the deformed model is an involved process even if the location and magnitude of structural loading is known. If the loading - and hence deformations - must be inferred indirectly, the process can be very computationally intensive. This is particularly relevant for elements with more degrees of freedom than the 2D beam. There is the additionally onerous requirement that a wide range of static measurements are required.

The motivation therefore for a method of identifying structural deformations from dynamic measurements is very clear. To this end a method is presented whereby the sensitivity of measured dynamic data to changes in elemental rotation are derived. The method is validated using the simple narrow plate example which has been used frequently in this thesis.

An extension to this procedure whereby groups of elemental rotations whose inter-relationship is known is developed and tested by means of a simulated case study.

The introduction of rigid body rotation updating parameters has been motivated by the requirement to model the effects of loading to structures. However, it is important to note that the methods introduced in the following sections can be used to update structural deformity arising from *any* source. In other words, these parameters allow the possibility that the finite element model can be released from the constraints of the initial spatial choice of node points.

5.3.1 Eigenvalue Sensitivity to Rigid Body Rotation

The transformation which rotates the structural matrices of a two dimensional beam element while conserving length and other properties is given by

$$[K]_e^{rot} = [G]^T [K]_e^z [G] \tag{5.21}$$

and

$$[M]_e^{rot} = [G]^T [M]_e^z [G], \tag{5.22}$$

where

$$[G(\theta)] = \begin{bmatrix} \cos(\theta) & \sin(\theta) & 0 & 0 & 0 & 0 \\ -\sin(\theta) & \cos(\theta) & 0 & 0 & 0 & 0 \\ 0 & 0 & 1 & 0 & 0 & 0 \\ 0 & 0 & 0 & \cos(\theta) & \sin(\theta) & 0 \\ 0 & 0 & 0 & -\sin(\theta) & \cos(\theta) & 0 \\ 0 & 0 & 0 & 0 & 0 & 1 \end{bmatrix}. \tag{5.23}$$

The notation $[G(\theta_j)]$ will be used to represent the rotation of the j^{th} element. The superscripts on the elemental stiffness matrices represent the matrices before and after rotation. The initial matrix given the superscript z need not represent the basic elemental formulation, this represents any element in an *a priori* finite element model.

The transformation is, of course, the same as that which converts elemental to global co-ordinates described in chapter 2 and is implicit in finite element coding. Note that only a single parameter is required to facilitate the transformation in two dimensions. A further two parameters are required in three dimensions.

To enable the use of the elemental rotation as a (dynamic) updating parameter it is necessary to establish a relationship between the rotation of one or more elements and some measurable dynamic properties of a structure. The crucial stage in the use of both the eigenvalue and response function sensitivity methods is to establish the rate of change of the stiffness and mass matrices with respect to an updating parameter p_j, that is

$$\frac{\partial}{\partial p_j}[K] \tag{5.24}$$

and

$$\frac{\partial}{\partial p_j}[M]. \tag{5.25}$$

If a set of parameters θ_j upon which the formulation of the global stiffness and mass matrices depend are defined as the update-able parameters, the global mass and stiffness matrices are constructed from the transformed elemental matrices thus

$$[K]=\sum_{j=1}^{n_p}[G(\theta_j)]^T[K]_{e_j}[G(\theta_j)]+\sum_{a=1}^{n_e-n_p}[K]_{e_a} \tag{5.26}$$

and

$$[M]=\sum_{j=1}^{n_p}[G(\theta_j)]^T[M]_{e_j}[G(\theta_j)]+\sum_{a=1}^{n_e-n_p}[K]_{e_a}\,, \tag{5.27}$$

where n_p is the number of elements to update and n_e is the total number of elements. The second summation in each case represents the contribution of elements which are not rotated by any of the θ_j.

Differentiating the expression for the transformed stiffness matrix of equation (5.26) with respect to the j^{th} elemental rotation leads to

$$\frac{\partial}{\partial\theta_j}\left([G]^T[K][G]\right)=\frac{\partial[G]^T}{\partial\theta_j}[K][G]+[G]\frac{\partial[K]}{\partial\theta_j}[G]+[G]^T[K]\frac{\partial[G]}{\partial\theta_j}, \tag{5.28}$$

where the dependence of $[G]$ upon θ_j is omitted for the sake of brevity. To simplify this expression the substitution

$$[H(\theta_j)]=\frac{\partial}{\partial\theta_j}[G(\theta_j)] \tag{5.29}$$

is made, from which it can easily be demonstrated that

$$[H(\theta_j)]^T=\frac{\partial}{\partial\theta_j}[G(\theta_j)]^T. \tag{5.30}$$

Substituting (5.29) and (5.30) into (5.28) and further noting that the basic stiffness matrix $[K]_e$ is not itself a function of the rotation θ_j gives

$$\frac{\partial}{\partial\theta_j}[K]=\frac{\partial}{\partial\theta_j}\left([G]^T[K]_{e_j}[G]\right)=[H]^T[K]_{e_j}[G]+[G]^T[K]_{e_j}[H]. \tag{5.31}$$

A similar relationship is derived for the transformation of the mass matrix

$$\frac{\partial}{\partial\theta_j}[M]=\frac{\partial}{\partial\theta_j}\left([G]^T[M]_{e_j}[G]\right)=[H]^T[M]_{e_j}[G]+[G]^T[M]_{e_j}[H]. \tag{5.32}$$

Substituting (5.31) and (5.32) into (5.8) gives

$$\frac{\partial\lambda_i}{\partial\theta_j}=\{\phi\}_i^T\left([H]^T[K]_{e_j}[G]+[G]^T[K][H]-\lambda_i\left([H]^T[M]_{e_j}[G]+[G]^T[M]_{e_j}[H]\right)\right)\{\phi\}_i \tag{5.33}$$

which is the sensitivity of the i^{th} eigenvalue to the rotation of the j^{th} element. Given that this expression can be evaluated for some initial value of θ_j, the familiar iterative approach to estimating the overall changes in a number of such parameters can be embarked upon.

As with the stress stiffening updating procedure described above, information in addition to the elemental matrices is required. In this case the rotational transformation matrix $[G]$ and its derivative $[H]$ are required for as many elements as one wishes to alter the rigid body rotations. Note however that the transformation matrices are general quantities and that the *actual* rotations of elements relative to some axis are *not* required.

For the two dimensional beam the transformation matrix $[H]$ in (5.33) can be found to be

$$[H]=\begin{bmatrix} -\sin(\theta) & \cos(\theta) & 0 & 0 & 0 & 0\\ -\cos(\theta) & -\sin(\theta) & 0 & 0 & 0 & 0\\ 0 & 0 & 0 & 0 & 0 & 0\\ 0 & 0 & 0 & -\sin(\theta) & \cos(\theta) & 0\\ 0 & 0 & 0 & -\cos(\theta) & \sin(\theta) & 0\\ 0 & 0 & 0 & 0 & 0 & 0 \end{bmatrix}. \tag{5.34}$$

As the previous example of updating stress stiffening parameters has suggested, in addition to the information furnished by dynamic measurements a great deal more

information about possible patterns of elemental rotations can be input from a knowledge of the structure. To this end a technique is described in section 5.3.3 which paves the way for updating of groups of elements whose rigid body rotations obey some pre-defined relationship.

5.3.2 Implementation of Elemental Rotation Updating

To investigate the usefulness of the rotational updating parameter, the 650mm long 100mm wide x 5mm deep beam is once again investigated. The validity and some of the aspects of the method are first studied by considering a single updating parameter namely the rotation, ξ, of the sixth of the thirteen two dimensional beam elements shown in figure 5.13. While a very simple transformation, the finite element model thus altered is a reasonable representation of a beam whose ends have been translated. The rotation of this element causes varying amounts of perturbations to the resonant frequencies, the first six of which are shown in figure 5.14. The effect of both positive and negative rotation are seen to be identical which is understandable given the symmetrical nature of the structure's geometry. Accordingly the sensitivity of all of the natural frequencies to the change in rotation, which is the gradient of any of the lines shown in figure 5.14, passes through the origin at zero rotation. The perturbation to the first six frequencies of the structure due to a rotation of this element of 2° is shown in table 5.4. As with the perturbations to resonant frequencies caused by variations in elemental stress stiffening, the modal shifts do not appear to obey any systematic trends. Principally there does not seem to be a trend for the absolute increase in resonant frequency to grow with the order of the identified resonances.

Frequency (Hz)			
Straight	Deformed	Absolute Increase (Hz)	Percentage Increase
62.9	63.3	0.3	0.6
173.5	176.4	2.8	1.6
340.4	342.6	2.2	0.6
563.1	563.9	0.8	0.1
842.4	845.6	3.3	0.4
1179.0	1179.1	0.0	0.0
1574.6	1577.3	2.7	0.2

Table 5.4 – Perturbation to Natural Frequency By Rotating Single Element

Taking the FE model of the straight beam as the initial estimate, so that $\xi = 0$, leads to zero sensitivity values. No estimate of an improved estimation of the updating parameter can therefore be made. If instead, a non-zero value of θ_j is chosen which essentially implies that the initial FE model includes a deformation then it is possible to converge upon an estimate for the rotation of the element which represents the "experimental" data.

Continuing with the example of the beam and formulating the updating sensitivity problem to discover the rotation ξ of the sixth element of the beam from dynamic measurements. The experimental data in the first instance is derived from the case ξ=2°, shown in the second column of table 5.4. Four modes are used to estimate the value of the elemental rotation. As the previous discussion has indicated, a value of ξ = 0 leads to a null sensitivity matrix therefore some initial value is required to solve the equation

$$\{S\}\delta\xi = \{\delta\lambda\}. \tag{5.35}$$

It is intuitive that an initial guess at the value of ξ should be of the same order as the expected alteration. Figure 5.15 shows how the sensitivity of the first four modes to the value of ξ vary. While there do appear to be optimal values for each mode, the choice

of initial parameter does not appear to affect the conditioning of the problem excessively. Commencing with an initial rotation of the sixth element of 5°, the correct value is converged upon quickly as shown in figure 5.16.

An interesting insight into the possibility of correctly identifying shape changes from dynamic data is gained by attempting to update the rotation of two independent elements. Considering the rotations of the fifth and sixth elements of the beam - ξ_5 and ξ_6 - as the update-able parameters and setting the target values as 0° and 2°, and starting with a number of initial values of ξ_5 and ξ_6 leads to four possible solutions. Two of these correspond to the target / experimental value and its symmetrical counterpart while the others correspond to another configuration of the two elemental angles. The two possible positive solutions are shown in table 5.5. Given the proximity of the second choice of update-able element to the first, it is not a surprise that similar frequency perturbations will be observed by rotating the adjacent element. The values of updating parameter which are converged upon depend on the initially chosen values of ξ_5 and ξ_6. Figure 5.17 shows a large range of starting points on the ξ_5 - ξ_6 plane as well as the four pairs of values which match the data closely.

Updating Parameter	Correct	Incorrect
ξ_5	0.00	1.53
ξ_6	2.00	0.05

Table 5.5 – Possible Solutions For Two Elemental Rotations

If more than two updating parameters are chosen, the number of possible solutions increases accordingly. This example graphically demonstrates that if the rotations of individual elements are to be updated, the number and location of elements must be carefully limited to avoid the possibility of many competing solutions whose alteration to the structural form is very similar. An extension from single element transformation to alteration of *profiles* which mitigates against this limitation is described in the following section.

5.3.3 Updating of Deflection Profile Magnitudes

The sensitivity of natural frequencies to rotations of individual elements has been shown to work via a simulated case study which has allowed some of the characteristics of this approach to be investigated. The restricted amount of information available from a comparison of dynamic data limits the number of independent parameters which can be realistically updated. Therefore, with the exception of cases where the orientation of a small number of elements can be seen to characterise structural deformation, the requirement to consolidate elemental deformations into fewer parameters which have a global effect is pressing.

At this point the concept of structural *profiles* are introduced. The profiles describe the relationship which exists between a number of element rigid body rotations such that they can be defined by a *single* parameter. The magnitude of the profile term is arbitrary, the entire profile being factored by a scalar which gives the set of elemental rotations some physical relevance. The rotations of n_η elements, the k^{th} of which is θ_k can be written

$$\begin{Bmatrix} \theta_1 \\ \theta_2 \\ \vdots \\ \theta_{n_\eta} \end{Bmatrix} = \begin{Bmatrix} \eta_1 \\ \eta_2 \\ \vdots \\ \eta_{n_\eta} \end{Bmatrix} p \,, \tag{5.36}$$

where $\eta_1, \eta_2 \ldots \eta_{n_\eta}$ define the profile and p scales the profile to a useful value. The structural finite element is recast to be a function of the profile

$$[K] = \sum_{k=1}^{n_\eta} \left([G(p\eta_k)]^T [K]_{e_k} [G(p\eta_k)] \right) + \sum_{a=1}^{n_e - n_\eta} [K]_{e_a} \tag{5.37}$$

where the second summation represents the set of elements whose rotation is not affected by the profile.

The values of the θ_k for the half period sinusoidal deflection of a beam such as that shown in figure 5.18 and consisting of n elements for example can be determined from

$$\theta_k = \frac{\pi d}{L}\cos\left(\frac{(2k-1)\pi}{2n}\right) \quad k = 1,2,\ldots n_\eta . \tag{5.38}$$

In terms of the notation used in (5.36)

$$p = \frac{d}{L} \tag{5.39}$$

and the profile of the k^{th} element is given by

$$\eta_k = \pi\cos\left(\frac{(2k-1)\pi}{2n}\right) \quad k = 1,2,\ldots n_\eta . \tag{5.40}$$

It should be noted that no functional relationship need exist between the values of η_k; if necessary the values can be defined explicitly. The example of the beam displacing with the sinusoidal characteristic represents the buckled shape of a perfect pin-jointed strut as well as the mode shape corresponding to the first mode of vibration. This is considered in the case study in the following section along with the shape corresponding to the second buckling/vibration mode.

It is clear from (5.36) that p can be considered as an update-able parameter. So for the beam example, if the values of η_k are chosen according to (5.40) and the length of the beam is necessarily considered constant then the central deflection of the beam will essentially be the updating parameter.

A value of $p = 0$ implies no change to the finite element model as before. Moreover as with the single element rotation described in section 5.3.1 the symmetrical nature of the profile of rotations implies that the derivative of the system eigenvalues with respect to p evaluated at $p = 0$ will also be equal to zero. That is

$$\left.\frac{\partial\lambda_i}{\partial p}\right|_{p=0} = 0, \quad i = 1,2,\ldots,n_f . \tag{5.41}$$

For this reason a realistic but non-zero value of the updating must be chosen initially. Given the physical relevance of the parameter it is an easy task to choose this initial value.

Now differentiating equation (5.37) with respect to p gives

$$\frac{\partial}{\partial p}[K]=\sum_{k=1}^{n_\eta}\left(\frac{\partial(\eta_k p)}{\partial p}\frac{\partial}{\partial(\eta_k p)}[K]\right). \tag{5.42}$$

Differentiating $[K]$ with respect to $\eta_k p$ as above in equation (5.31)

$$\frac{\partial}{\partial p}[K]=\sum_{k=1}^{n_\eta}\eta_k\left([H(\eta_k p)]^T[K]_{e_k}[G(\eta_k p)]+[G(\eta_k p)]^T[K]_{e_k}[H(\eta_k p)]\right) \tag{5.43}$$

As before the same procedure must be applied to the mass matrix.

The expression for the sensitivity of the i^{th} resonant frequency to the j^{th} profile updating parameter is given by given by the usual relationship

$$\frac{\partial\lambda_i}{\partial p_j}=\{\phi\}_i^T\left(\frac{\partial}{\partial p}[K]-\lambda_i\frac{\partial}{\partial p}[M]\right)\{\phi\}_i. \tag{5.44}$$

Clearly the same reasoning can be applied to any set of elements whose rigid body rotations form a relationship which approximates to a realistic displacement. Further, any number of parameters which define *profiles* can be used as updating parameters.

Another issue which must be addressed before this technique can be implemented practically is that of symmetry. It is clear that there can exist multiple states of symmetrical displacements which will achieve the same frequency perturbation. If it is important to identify the correct displacement from the set of possible values, several possible avenues are available. The initial values of profile magnitude will influence which solution is converged upon therefore the initial values are chosen such that the shape of the initial finite element model[29] matches the shape if not the magnitude of the observed displacements. In this case then it is likely that the solution will converge upon the correct value. Alternatively the updating process could be started from arbitrary parameter values. The sign of the values are subsequently altered to match known characteristics of the structural displacement.

---

29 This term relates to the finite element model constructed according to the initial updating parameter values.

5.3.4 Implementation of Profile Updating Method

The process of updating the magnitude of pre-defined structural deformations appears to offer a method of taking account of deformations which cause perturbations to resonant frequencies in practice. Before attempting to use this technique on experimental data it is prudent to assess its effectiveness via a carefully controllable case study. As a first step the method will attempt to determine deflection characteristics of the clamped beam described above.

To add an element of realism, the measured initial deformity of the thin plate will be used to generate the "experimental" data. The plate is therefore being assumed to adopt its naturally cambered state even when clamped. The measured deflection of the plate has been described in section 4.2.1 having a maximum deflection of 2.4mm and being neither symmetrical nor sinusoidal. At this stage the deformity of the plate is considered independently of loading i.e. the camber in the plate would still exist if the plate was released from its fixed supports.

If the rotation of the thirteen elements of the initial 13 2D beam element FE model of the thin plate are related by the sinusoid relationship given in equation (5.38) the variation of the first five natural frequencies of the plate with d are shown in figure 5.19. Note that the value of the parameter represents the deflection of the plate in metres. As the previous chapters have led one to expect, the effect of this type of deflected shape strongly influences the first mode of vibration. Note however that if the beam was a part of a larger assembly the effects of this deflection would be more widespread.

This elementary case study allows one important note of caution to be struck. At a certain level of deflection shown clearly in figure 5.20 (approximately 12mm in this situation) the symmetrical mode of vibration which occurs at the lowest frequency in the straight beam increases to exceed the resonant frequency of the first anti-symmetric mode of vibration. The sensitivity of the "new" first modes drops dramatically at this point. The result of choosing as an initial parameter for beam deflection a point beyond

this limit leads to unrealistic beam deflection profiles, an example of which is shown in figure 5.21. This extreme updated solution would of course be rejected, but it serves as a reminder that the physical relevance of updated structural deflections allows the veracity of updated solutions to be determined with some confidence.

Using as an initial estimate of the deflection of the beam any point below the 12mm limit leads quickly to an estimation of the sinusoidal shape which most closely matches the dynamic properties of the deflected experimental the plate. Figure 5.22 shows that the identified sinusoidal shape is a close representation of the measured deflection. Additionally it is seen that convergence upon this solution occurs after around 3 iterations of the updating procedure.

Natural Frequencies (Hz)		
Straight	**Target**	**Updated**
62.95	69.53	69.59
173.55	173.84	173.54
340.38	341.01	340.40
563.12	563.13	563.12
842.37	842.48	842.37

Table 5.6 – Natural Frequencies of Updated Model Compared With Target

Table 5.6 above shows the natural frequencies of the updated model compared to those of the target model from which it can be seen that the first mode of vibration of the updated finite element model is a much closer match of the experimental target data.

It is clear that considering the perturbation to the lowest resonant frequency provides the most useful information with which to identify this type of deflection of the beam. Note however that the same result can be gained from using any combination of modes although in some cases convergence will be extremely slow. The use of an SVD solution to determine the deflection from a number of modes would allow the equation involving the first natural frequency to dominate.

If instead of the profile approach, the standard technique of updating elemental mass or stiffness factors the result would be much the same as the case study presented in chapter 2 section 2.6. Many solutions would be possible depending on the choice of elements to update, but none would be physically justifiable.

The consideration of a second updating parameter to allow the updated model to contain a linear combination of two profiles is now introduced. In the current context the most logical choice of shape is that of a sinusoid of half the period of the previous example. The profile is defined by

$$\eta_k = 2\pi \cos\left(\frac{(2k-1)\pi}{n}\right) \qquad k = 1,2,\ldots n_\eta, \tag{5.45}$$

where once again the updating parameter is takes on the value

$$p = \frac{d}{L}. \tag{5.46}$$

Using two updating parameters p_1 and p_2 relating to the maximum deflections of the two profiles, a slightly improved match to the target dynamic data and the deformed shape is achieved. This is shown in figure 5.23 along with the convergence of the two updating parameters upon their final values. Table 5.7 shows that the prediction of the natural frequency of the second mode - which is most sensitive to the second profile chosen - is improved by incorporating the second profile updating parameter.

Resonant Frequencies (Hz)			
Straight	**Target**	**Updated p_1**	**Updated p_2**
62.95	69.53	69.59	69.53
173.55	173.84	173.54	173.84
340.38	341.01	340.40	340.40
563.12	563.13	563.12	563.12
842.37	842.48	842.37	842.37

Table 5.7 – Improvement to Prediction of Resonant Frequency From Using Two Profiles

Clearly the choice of profiles to update shares some similarities with the Fourier transform, indeed if the beam was modelled with an infinite number of elements, the more profiles chosen by halving the period of the previous profile would allow convergence upon *any* continuous deflected shape.

The relationship between the initial values of the updating parameters and the final values for the two profile parameter case is shown in figure 5.24. As with the case of two single element rotations, there are four possible solutions. The small dots show initial conditions which do not lead quickly to convergence. The two bands of non-converging points relate to structural configurations in which the modes do not share a direct correlation with the correct model due to mode swapping. As the previous section has outlined, the physical relevance of the updated parameters allows a good estimate of the initial parameters.

5.4 Comparison With Established Updating Parameters

The evolution of different types of updating parameters has been thoroughly set out in chapter 2. The diversity of updating parameters is somewhat curtailed by the lack of information available from experimental observations. The under-determination of the updating problem partly explains the continued popularity of updating elemental stiffness and mass values.

The introduction by Gladwell and Ahmadian [42] of the concept of generic elements offers the opportunity of updating generalised elemental parameters such that the updated element is a member of a family of physically realistic elements. To establish the credentials of the updating parameters proposed in this chapter it is prudent at this stage to consider whether they themselves are members of the their "generic" element family. The generic element method will firstly be set out in some detail.

In terms of the changes which must be made to an elemental stiffness or mass matrix to model the prototype model correctly, *a priori* elements are split into two categories: those whose formulation does not include certain important 'effects' and those where all

'relevant effects' are included but their numerical results may be inaccurate. The latter problem is likely to benefit from more accurate changes in conventional updating process. However this level of accuracy in the original FE model somewhat blunts the effectiveness of updating methods.

The generic element method takes a different view. Instead of seeking to change individual elemental parameters to minimise some objective function, the overall elemental form is potentially altered to meet the optimal requirements. Essentially the *mode shapes* of individual elements are altered used as updating parameters.

The changes to a 2D beam to update load effects as described in the previous sections can be shown not to be a members of the generic 2D beam family. Considering firstly the effect of adding a stress stiffening matrix at the elemental level given by

$$[K]_e = EI\begin{bmatrix} 12 & 6 & -12 & 6 \\ 6 & 4 & -6 & 2 \\ -12 & -6 & 12 & -6 \\ 6 & 2 & -6 & 4 \end{bmatrix} + F\begin{bmatrix} 6/5 & 1/10 & -6/5 & 1/10 \\ 1/10 & 2/15 & -1/10 & -1/30 \\ -6/5 & -1/10 & 6/5 & -1/10 \\ 1/10 & -1/30 & -1/10 & 2/15 \end{bmatrix}. \quad (5.47)$$

Considering values of the parameters E, I and F as unity, the elemental matrix can quickly be determined to have rank 3. This in turn implies three straining modes. An element undergoing rigid body rotation in an updating procedure can be quickly shown not to be a member of the family of elements. The rotation of the element will introduce apparent coupling between axial loads and transverse motion with respect to the element's original local axes.

5.5 Concluding Remarks

Based upon experience gained from the previous chapters, two new types of updating parameters have been introduced. The parameters allow the aspects of the finite element which are known to be altered during loading to be included as parameters in a model updating procedure.

A stress stiffening parameter has been shown to provide a means of identifying axial loads in beam elements from the dynamic characteristics of the structure in loaded and unloaded states. The prediction of unloaded behaviour is generated by a finite element model and the identification of elemental loads is performed as part of a more general identification of mis-modelled structural properties.

The validity of the method has been demonstrated by means of two examples based upon beam elements. The likelihood of identification of structural loading is shown not be sensitive to the addition of realistic levels of noise. Divergence of successive differences in resonant frequencies such as would be expected from a mis-modelling of structural mass or stiffness leads to a dominance of the higher order modes and hence a likelihood of poor identification of loading. To this end it is advised that stiffness and mass parameters are included in the updating process and that where identification of loading is of primary importance, lower order modes are given prominence in the solution of the updating equation.

Some independent static measurement of the load within a structure is shown to improve the chance of successfully identifying elemental loading. The choice of location at which loading is specified is shown to be significant in determining the speed and accuracy of the dynamic load identification. A method is presented which indicates the locations at which a knowledge of structural loading are most beneficial to the dynamic load identification method.

Sensitivity of dynamic behaviour to rigid body rotation of individual elements has been investigated. A method for updating individual elemental rotations to change the geometry of a structure effectively has been presented and shown to work in a simulated case study. An attractive extension to this technique has been set out whereby the magnitudes of sets of pre-defined structural deflections can be updated.

The danger of modes "swapping" as a result of parametric changes has been encountered. A case study has shown that swapping of FE modes which are compared with experimental values can have a deleterious effect on the likelihood of updating

success. This issue is not isolated to rigid-body rotation elements. The ability of FE updating techniques to cope with mode swapping is an area for urgent further work.

The changes made to individual beam elements have been shown not to be members of the family of generic beam elements. Thus while offering an attractive means of updating finite elements, it is not possible to take account of load-induced effects using the generic updating parameters. Conversely the updating of generic parameters cannot account for stress stiffening effects and structural deformations.

Broadly the two new types of updating parameters are philosophically different from previous updating parameters and allow the effects of loading to be encapsulated in a finite element model.

The use of rigid body updating parameters in particular offers a new dimension to the attributes of an initial finite element model which can be updated. The use of updating profiles potentially allows changes to the geometry of any or all of the FE model of the test structure. This approach appears to offer a great deal of potential and should be the subject of future work.

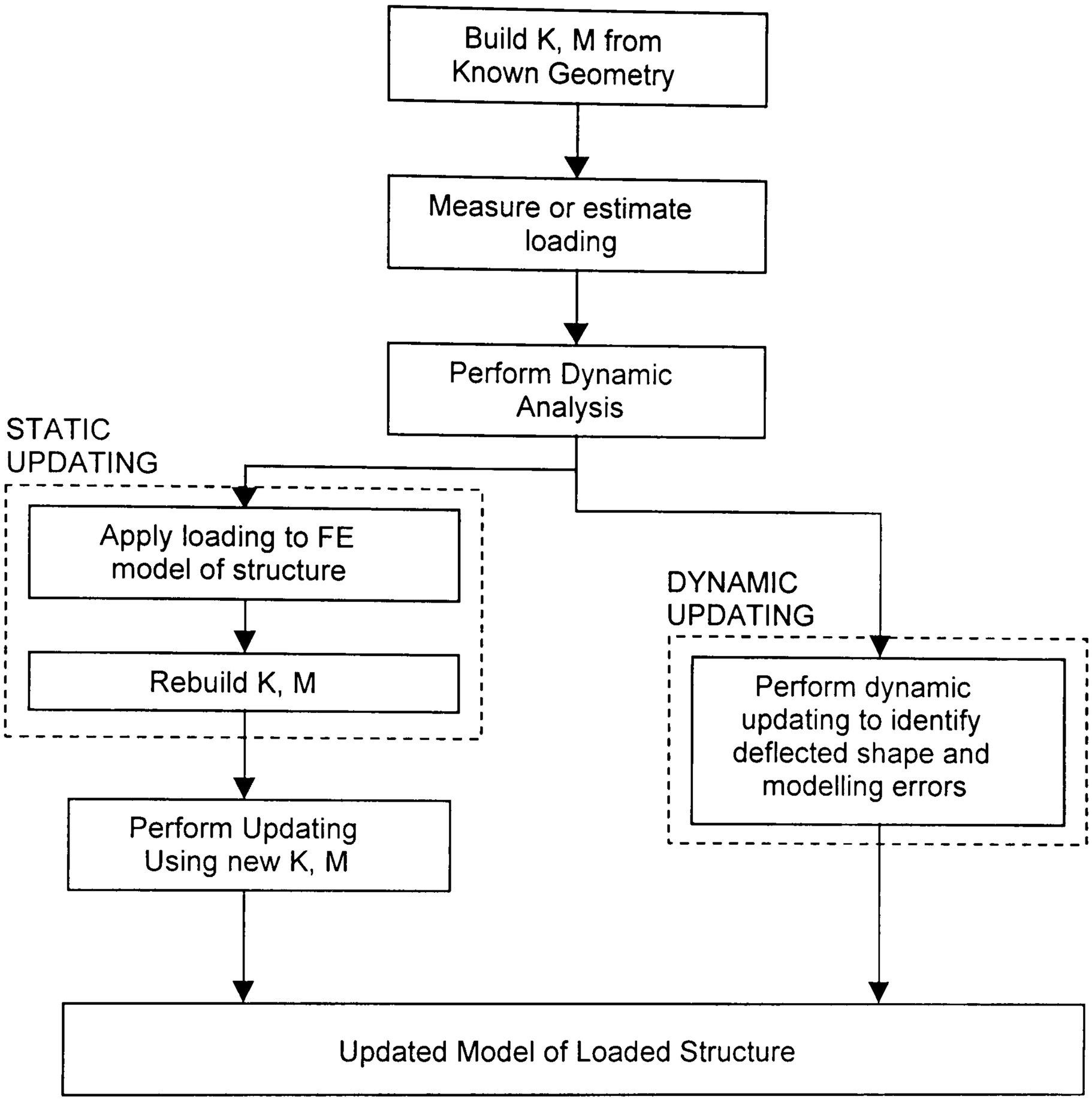

Figure 5.1 – Static vs. Dynamic Approaches to Updating

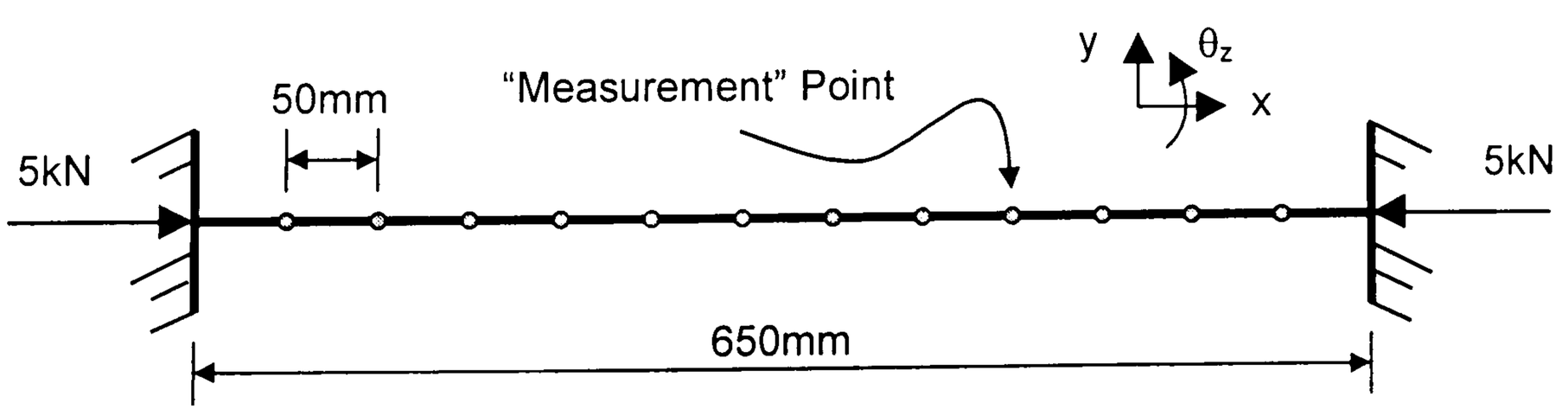

Figure 5.2 - Fixed-Fixed 13 Element Beam

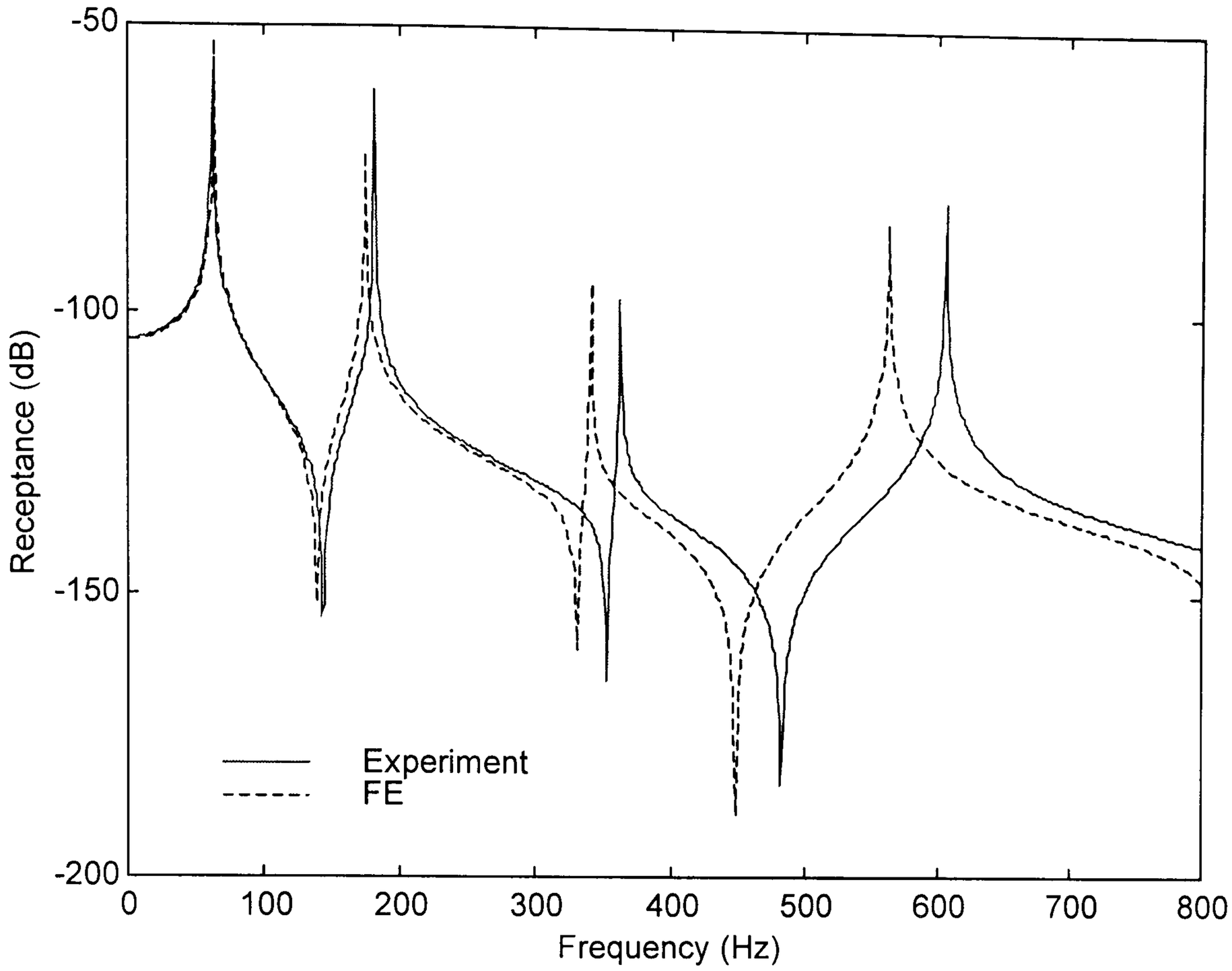

Figure 5.3 – Receptance of "Experiment" from FE Model

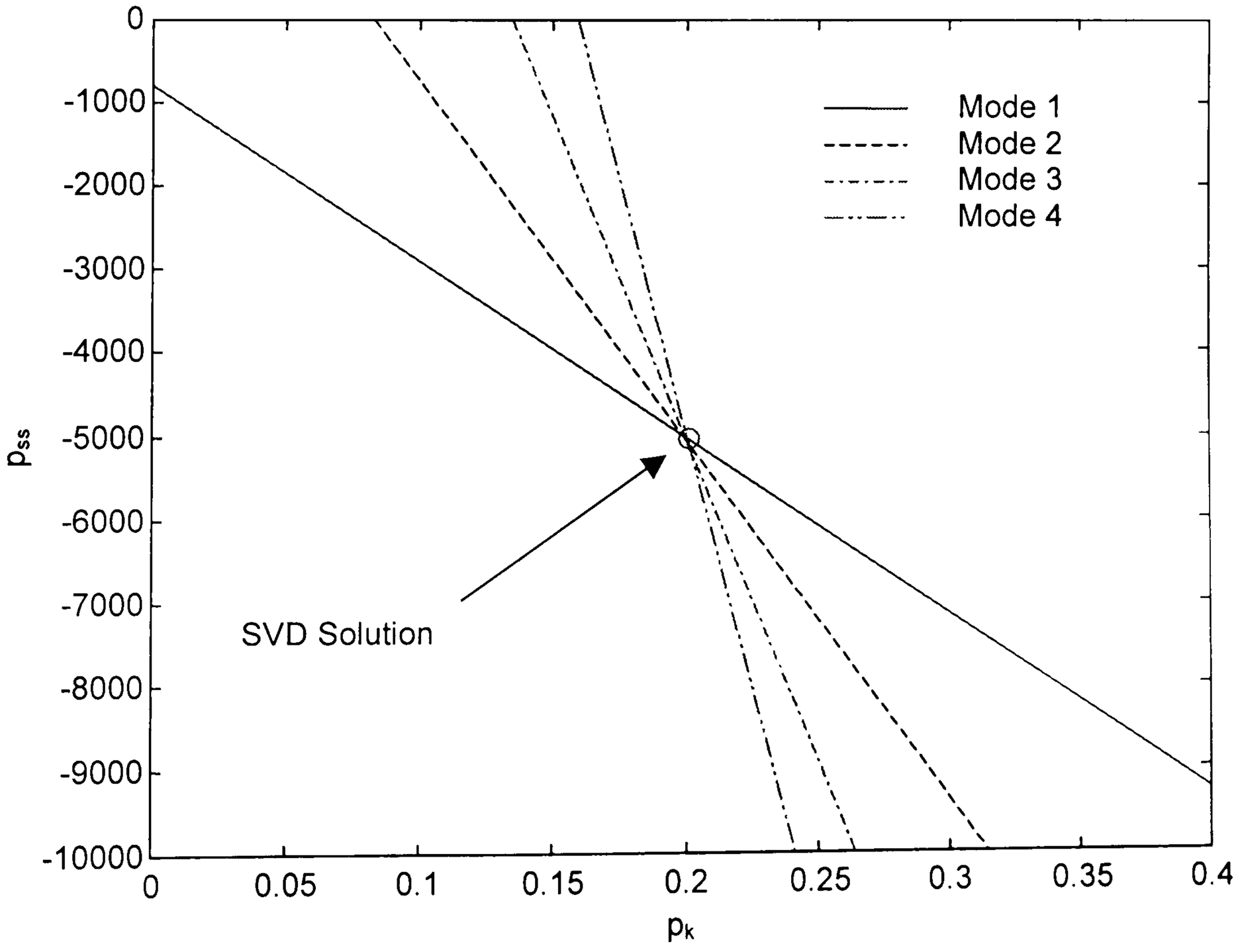

Figure 5.4 – Identification of Stiffness and Stress Stiffening Using Two Modes

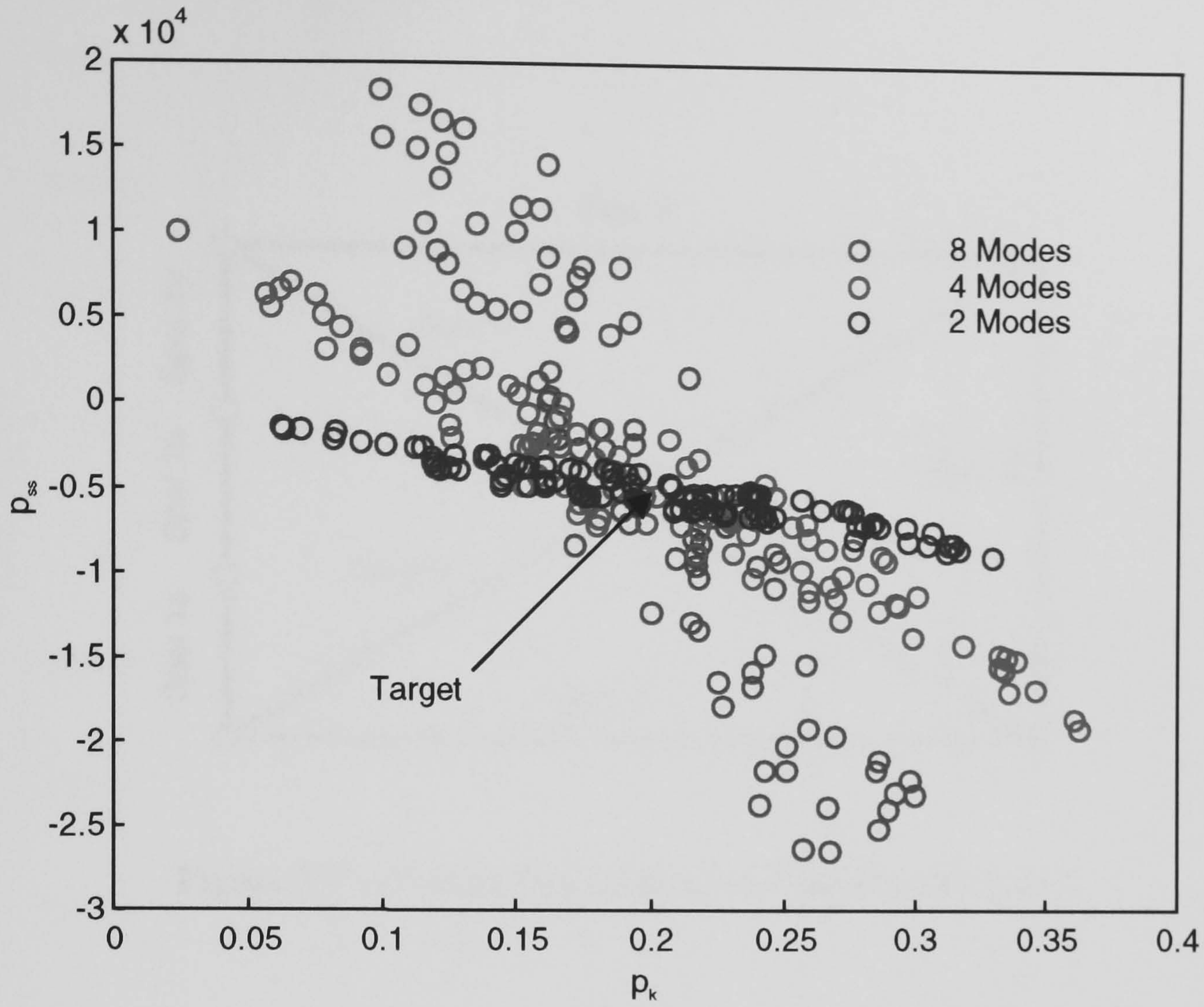

Figure 5.5 – Effect of Multiplicative Noise & Eigenvalue Choice on Updating

Figure 5.6 – Effect of Additive Noise and Eigenvalue Selection on Updating Success

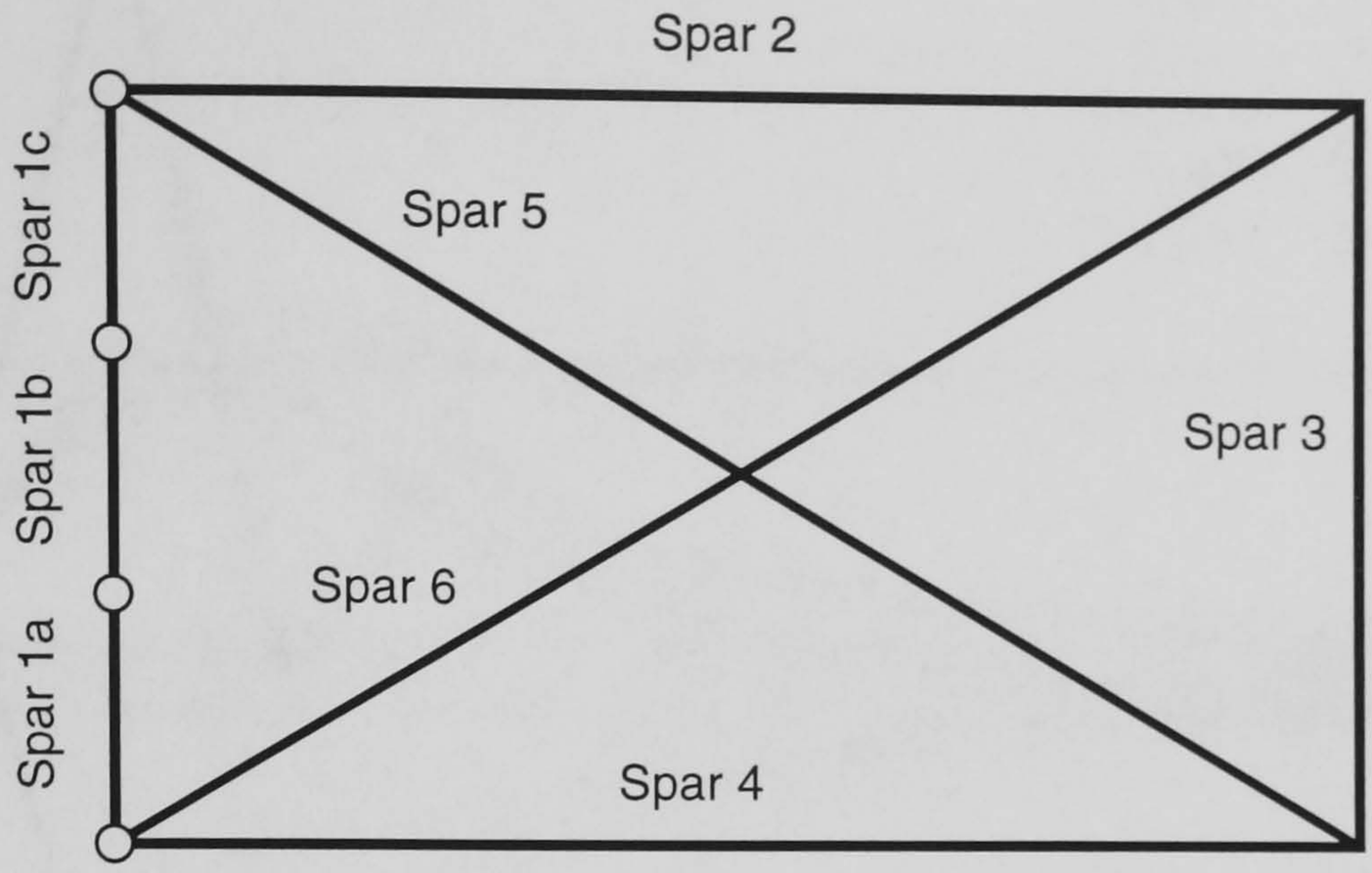

Figure 5.7 – Numbering System for Framework Spars

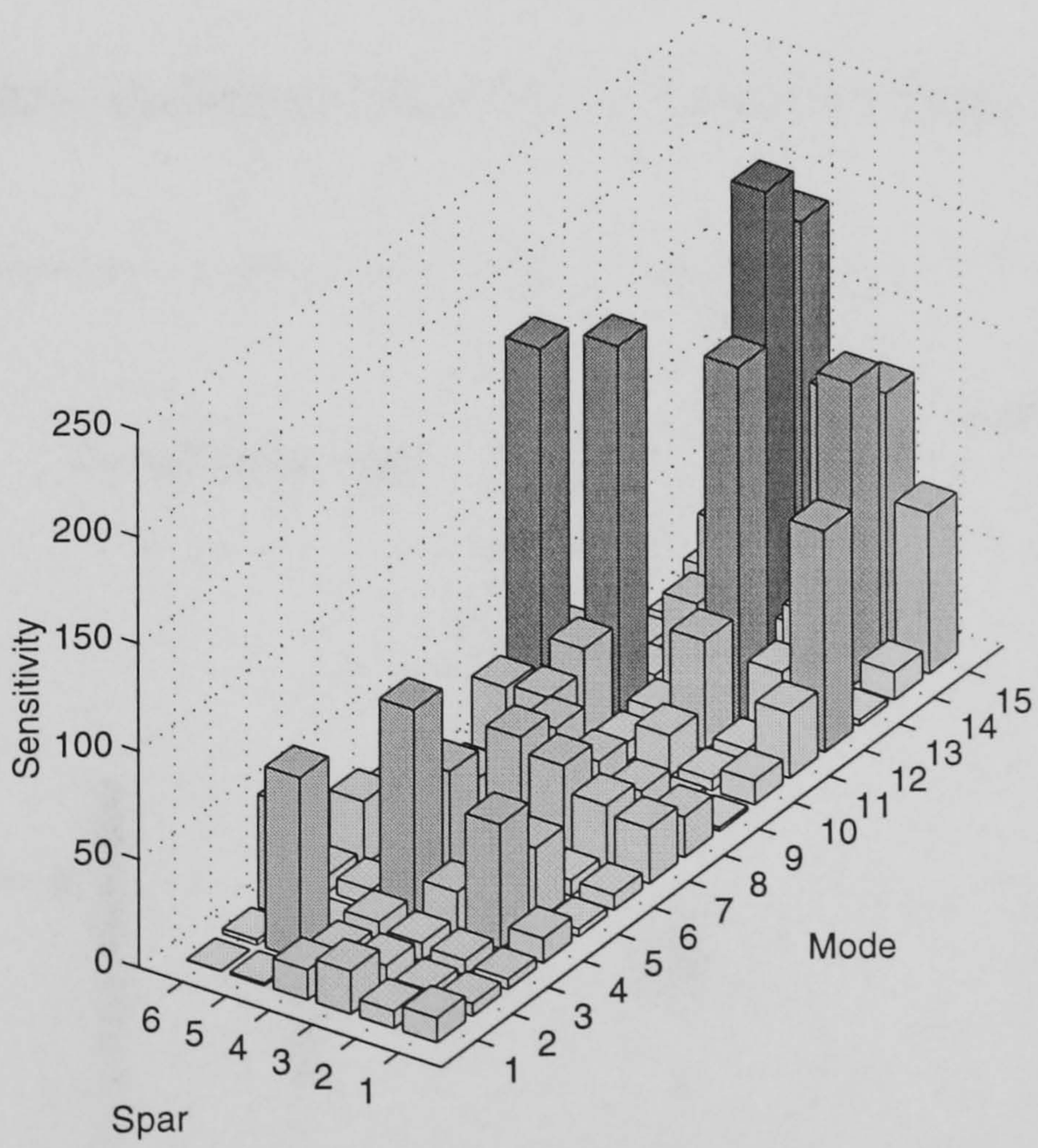

Figure 5.8 – Sensitivity Matrix, {p} =0

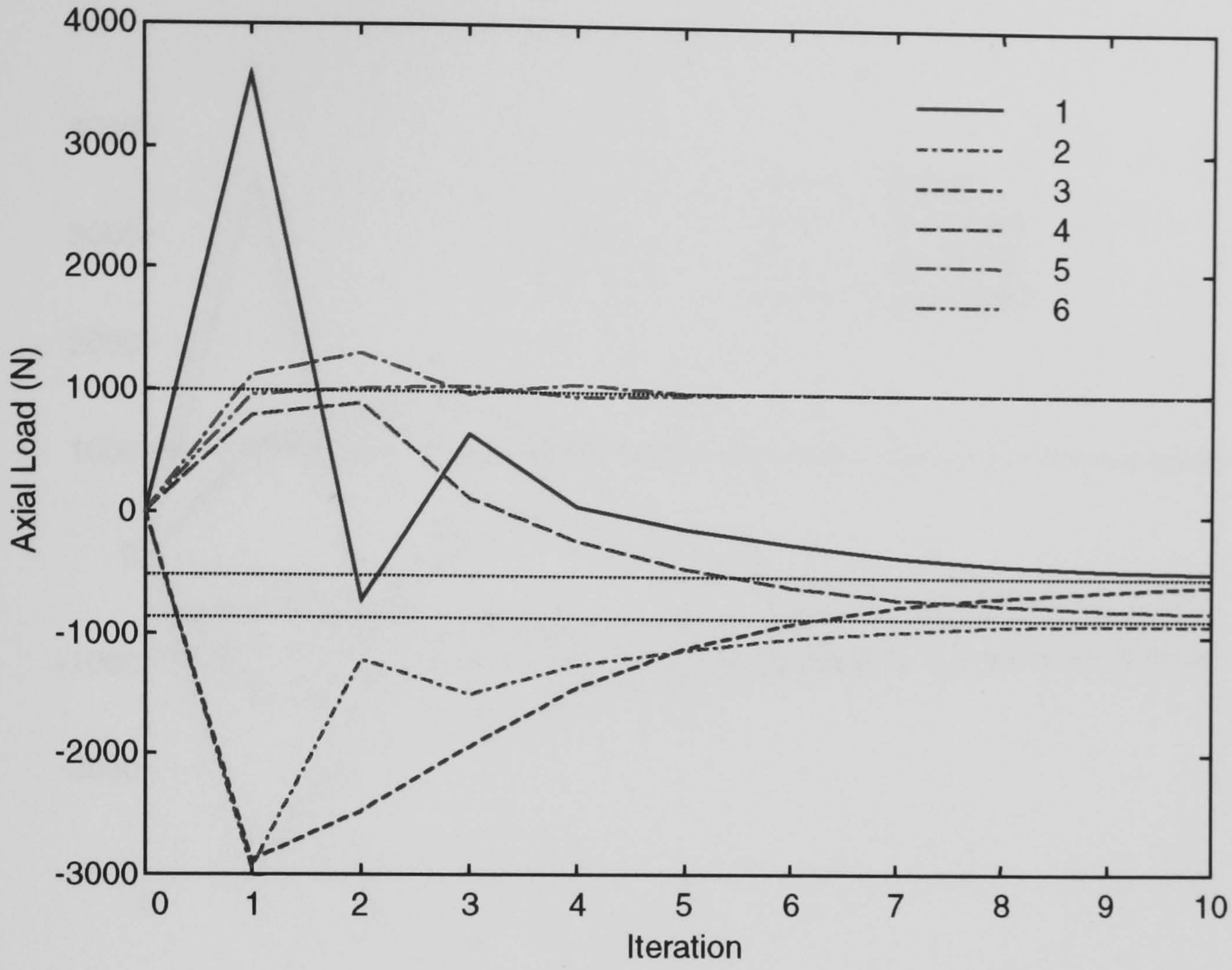

Figure 5.9 – Identified Loads From No Initial Knowledge of Loading

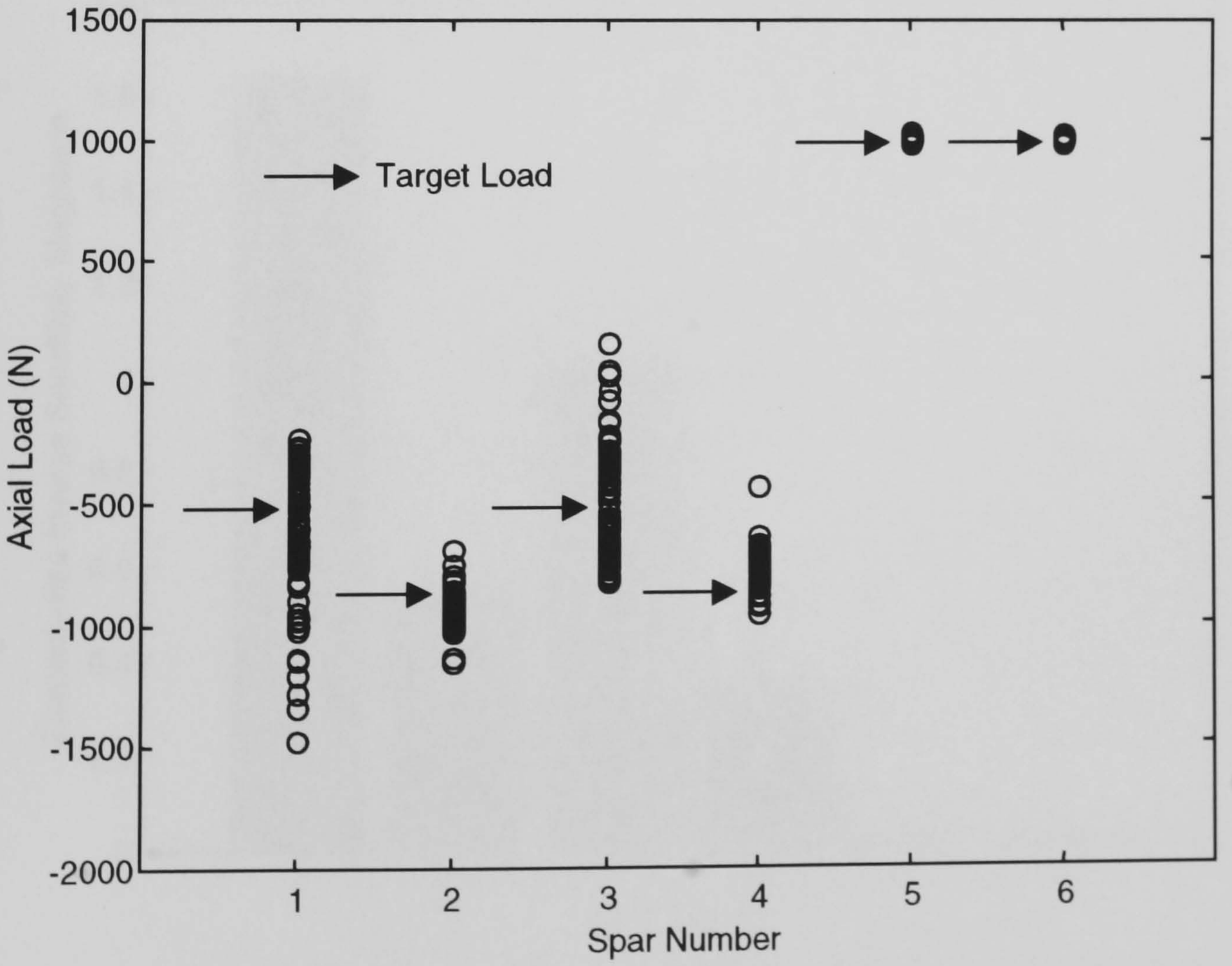

Figure 5.10 – Loads Identified From Noisy Experimental Data

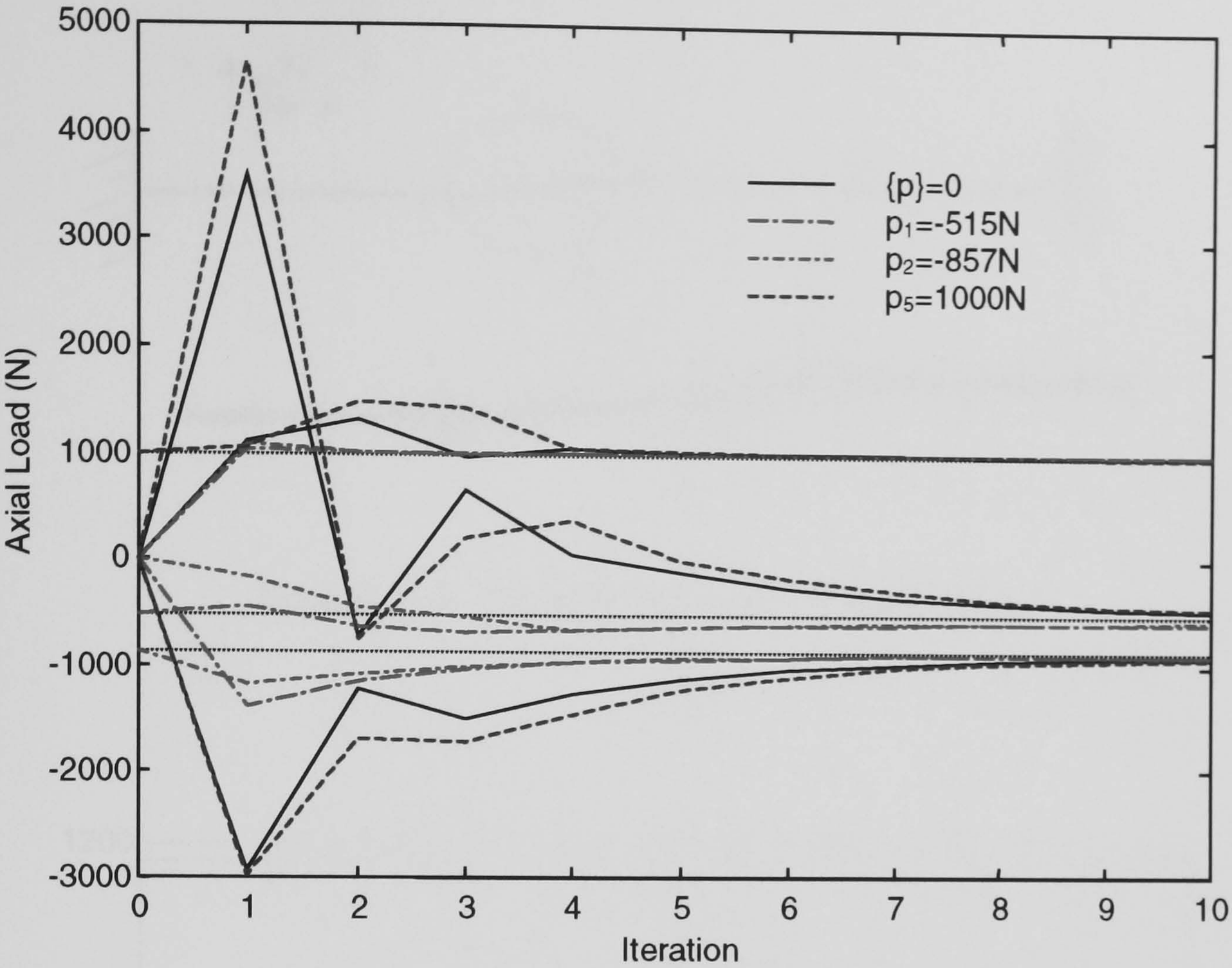

Figure 5.11 – Load Identification With Various Initial Condition

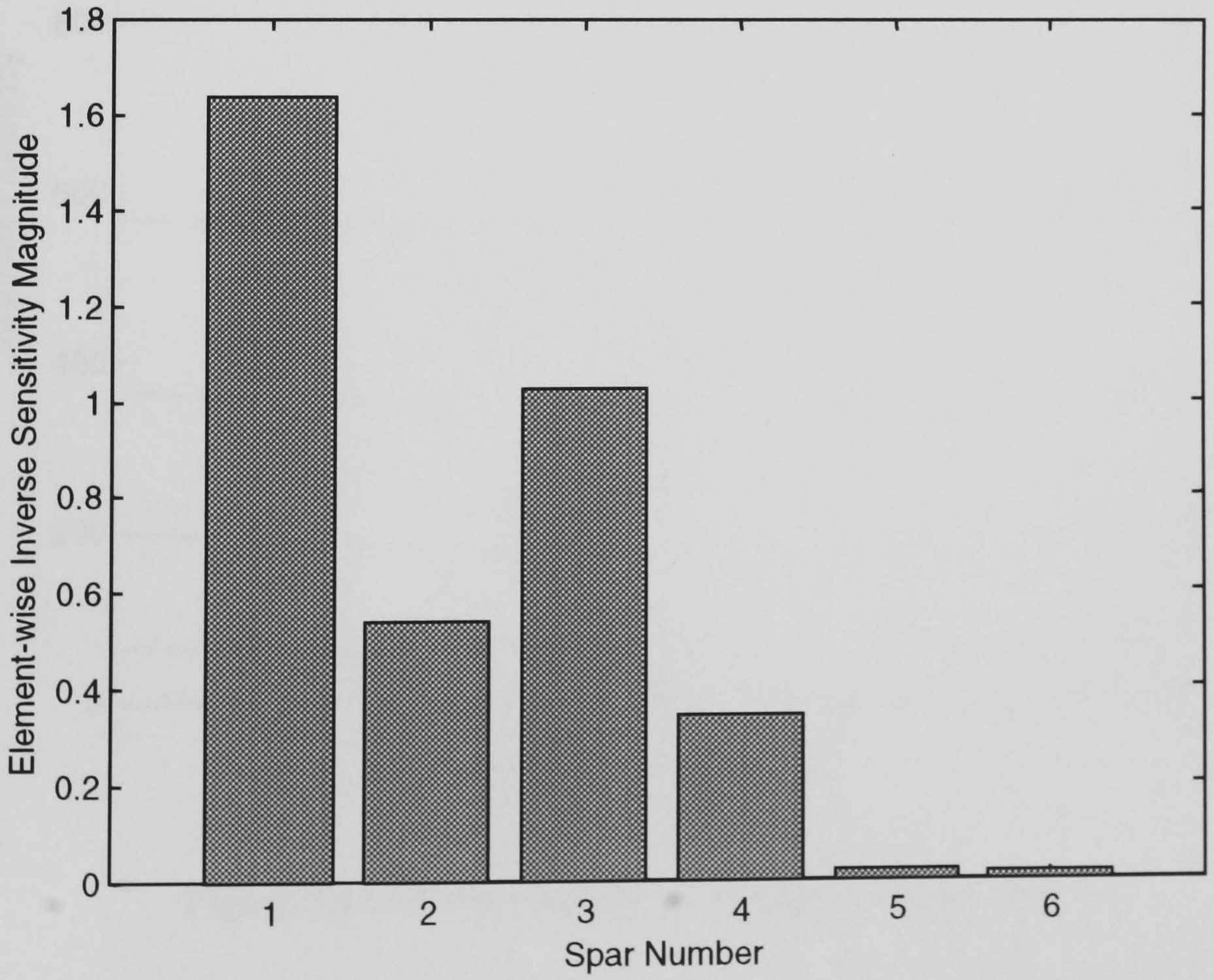

Figure 5.12 – EISM to Estimate Spar For Static Load Determination

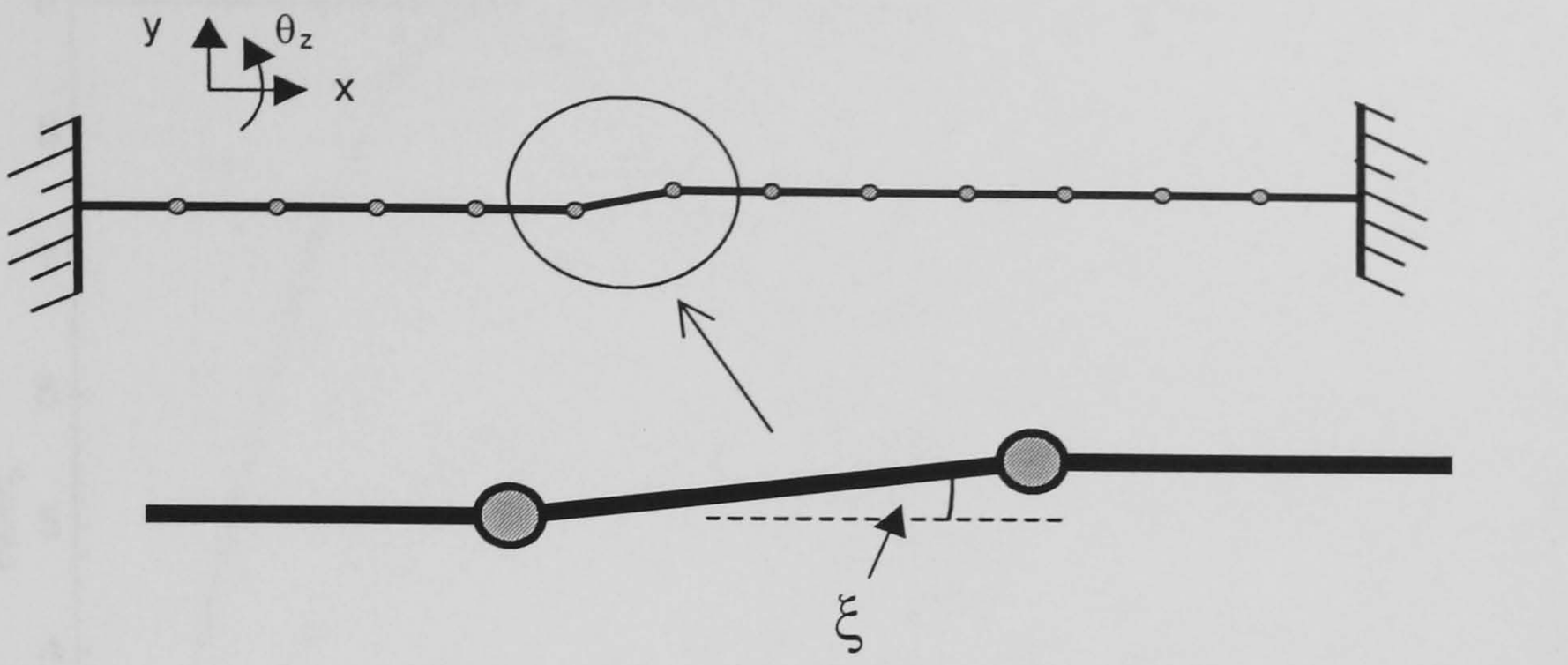

Figure 5.13 - Rotation of Single Beam Element

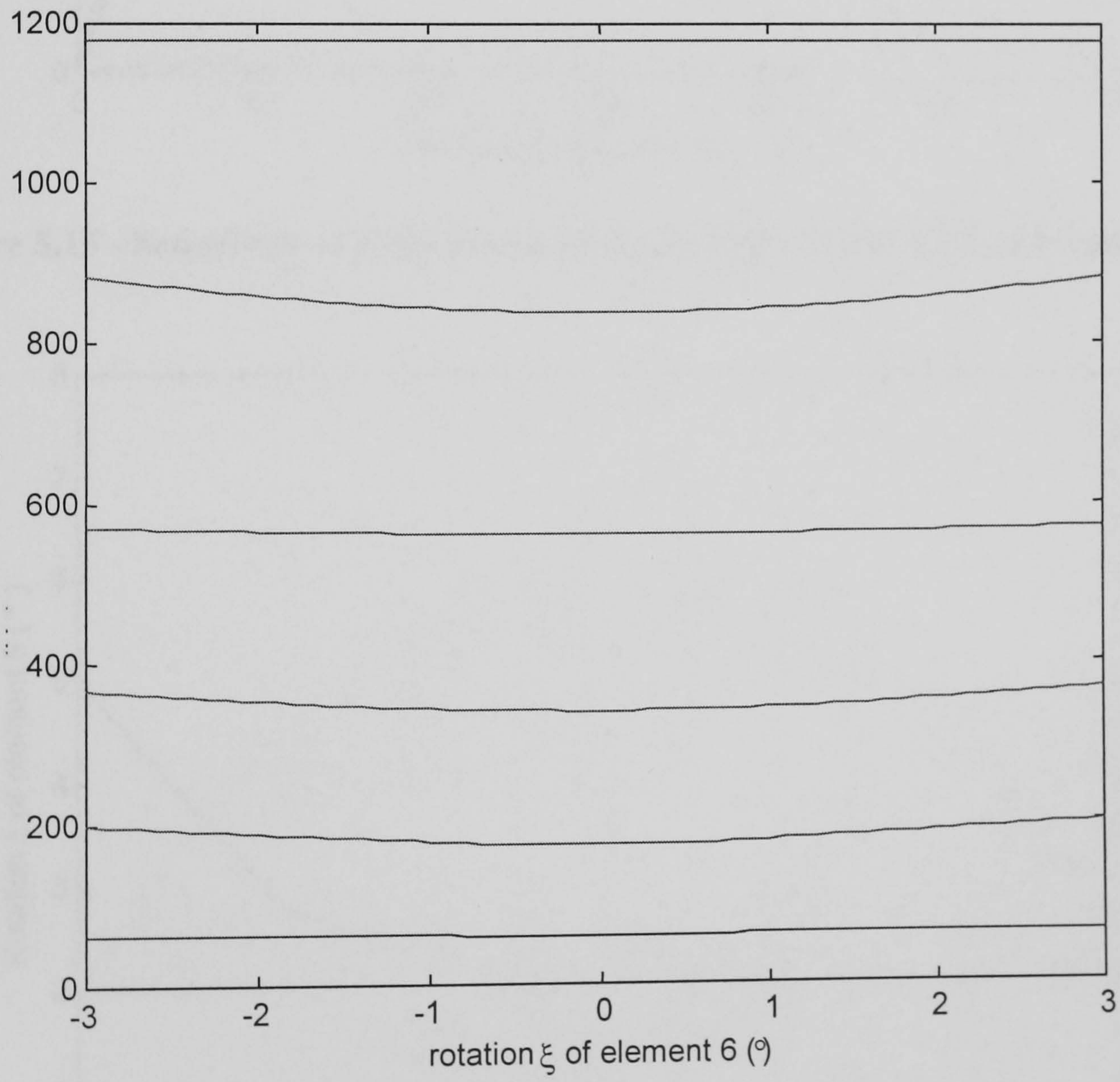

Figure 5.14 - Perturbations to Resonant Frequencies

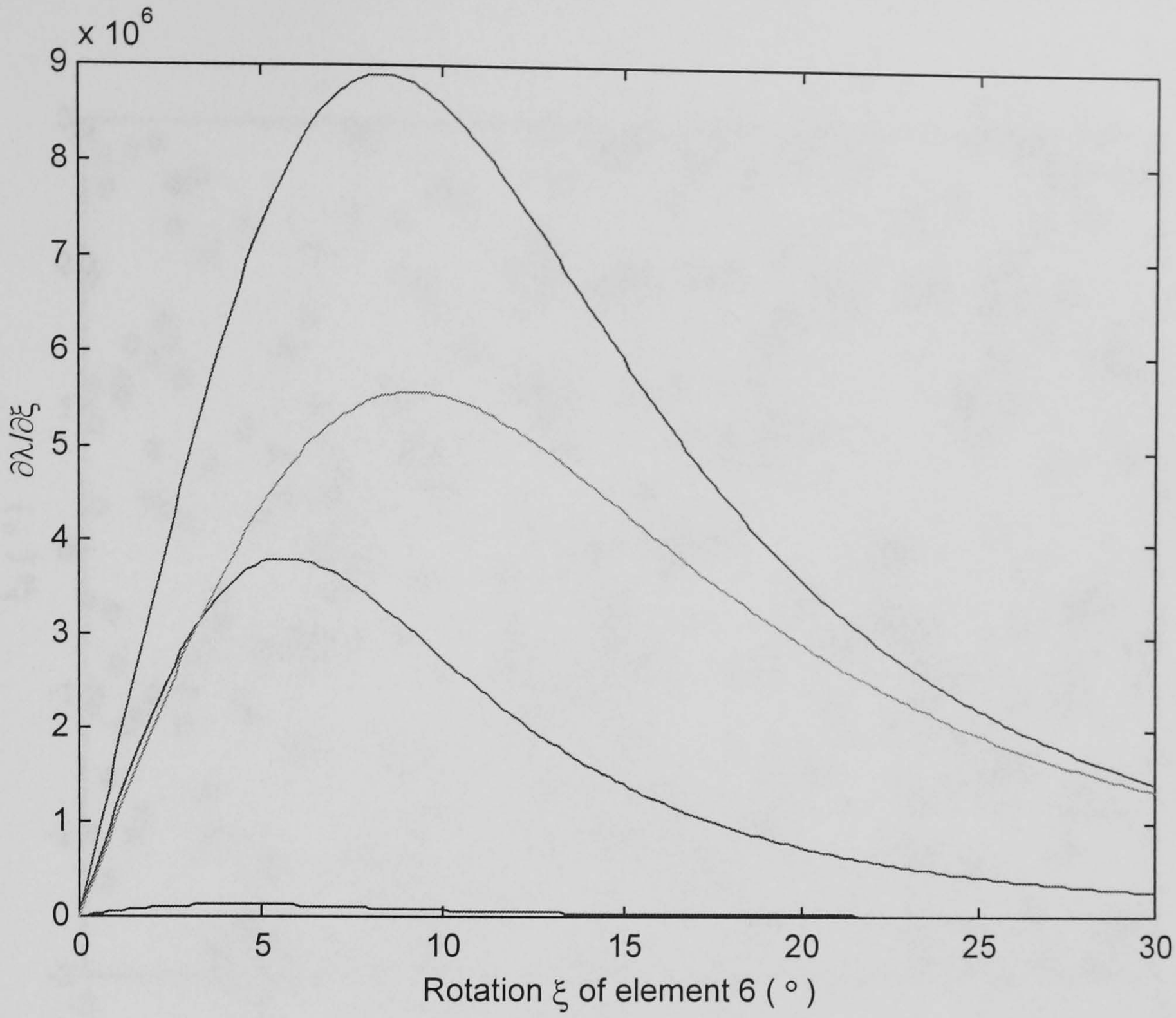

Figure 5.15 - Sensitivity of Four Resonant Frequencies to Rotation of Element Six

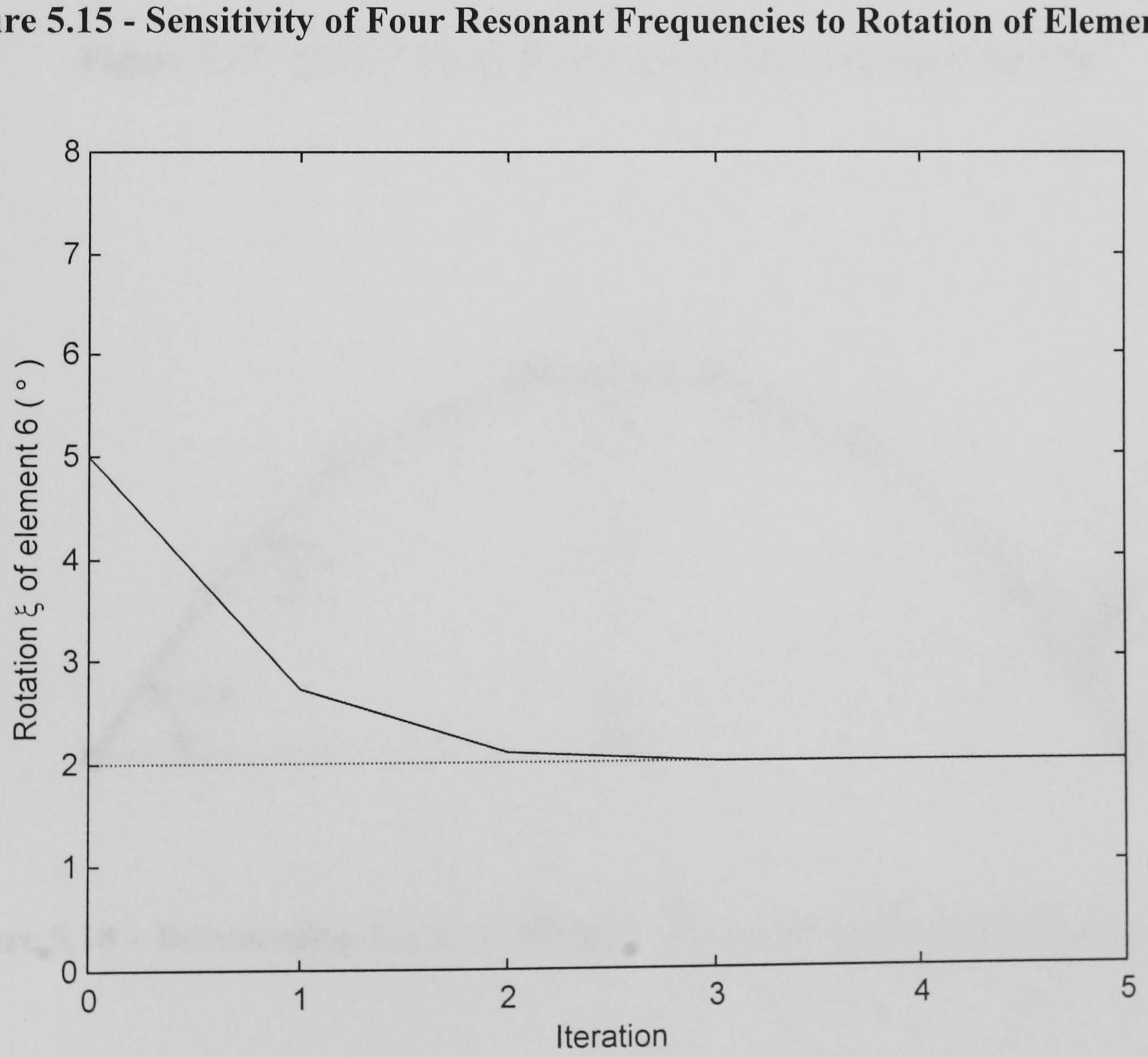

Figure 5.16 – Convergence Of Element Rotation on "Experimental" Value

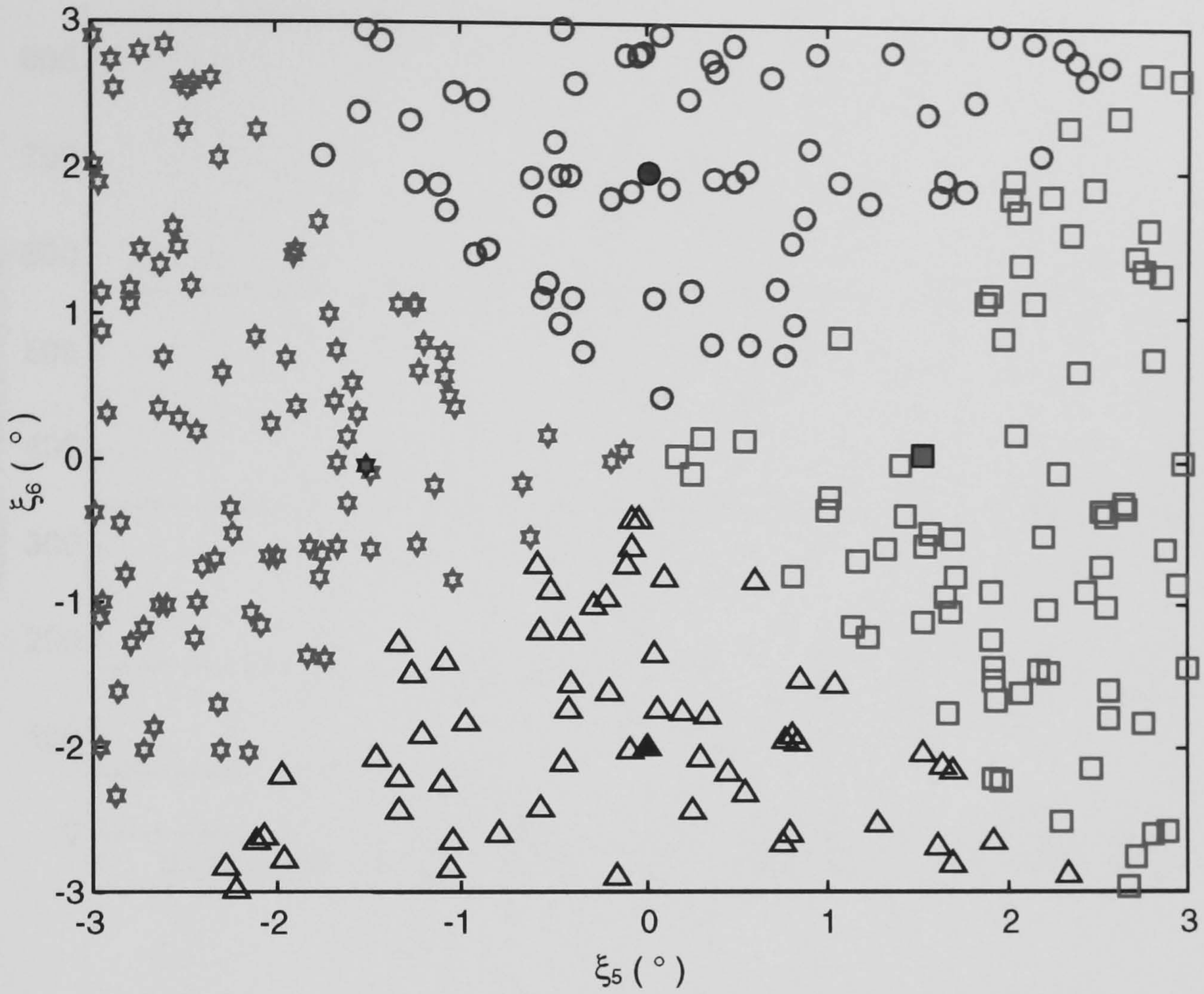

Figure 5.17 – Four Possible Solutions to Two Parameter System

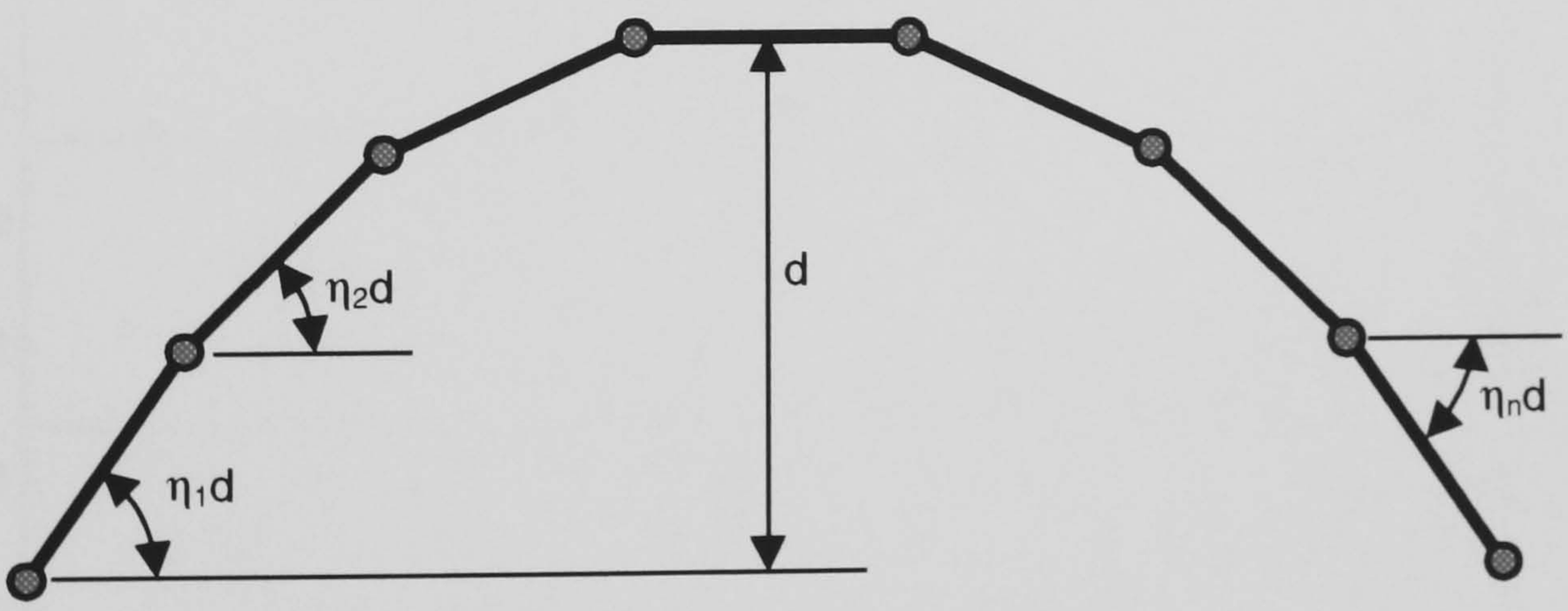

Figure 5.18 – Relationship Between Element Rotations and Central Displacement

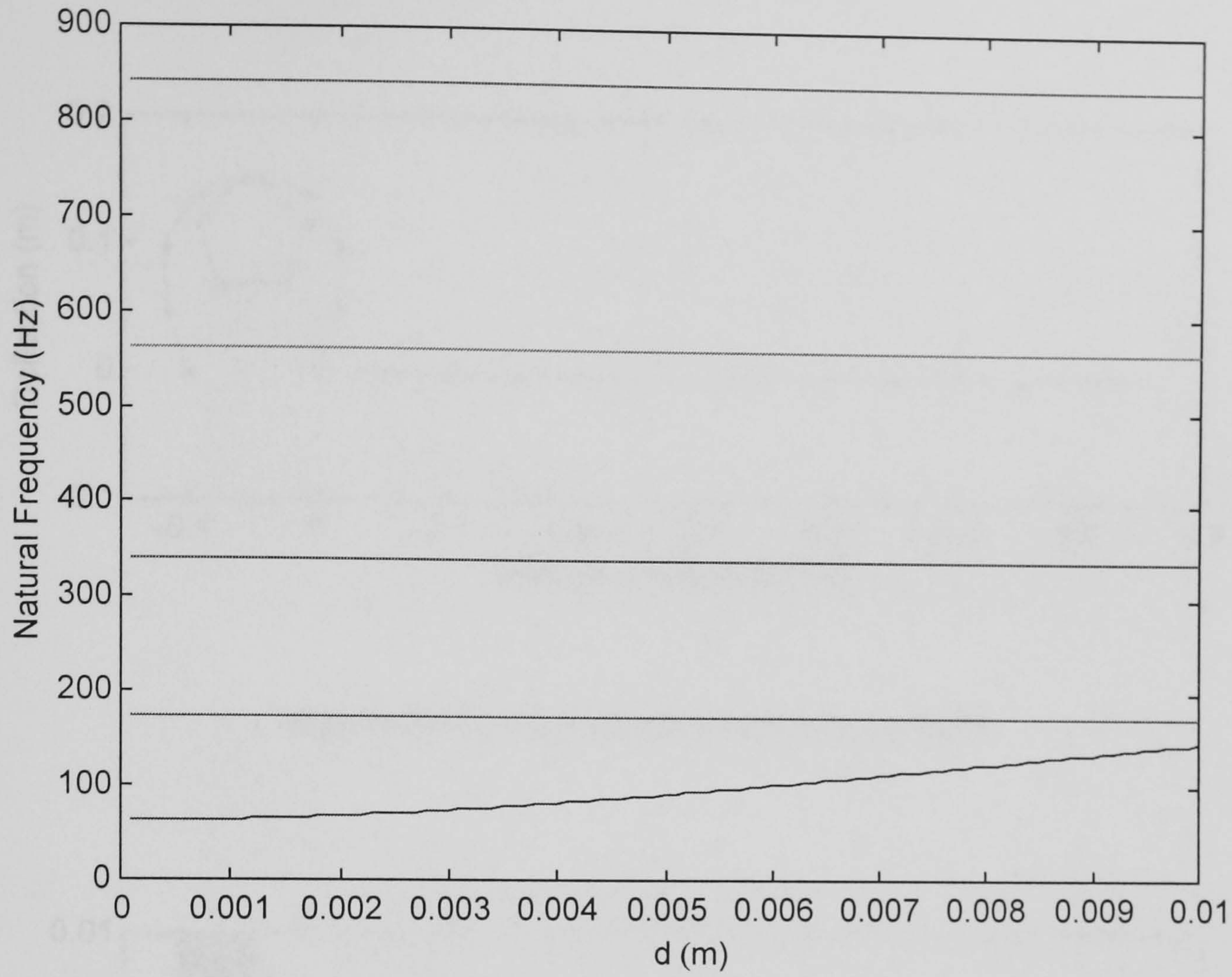

Figure 5.19 – Effect of Sinusoidal Static Displacement on Resonant Frequency

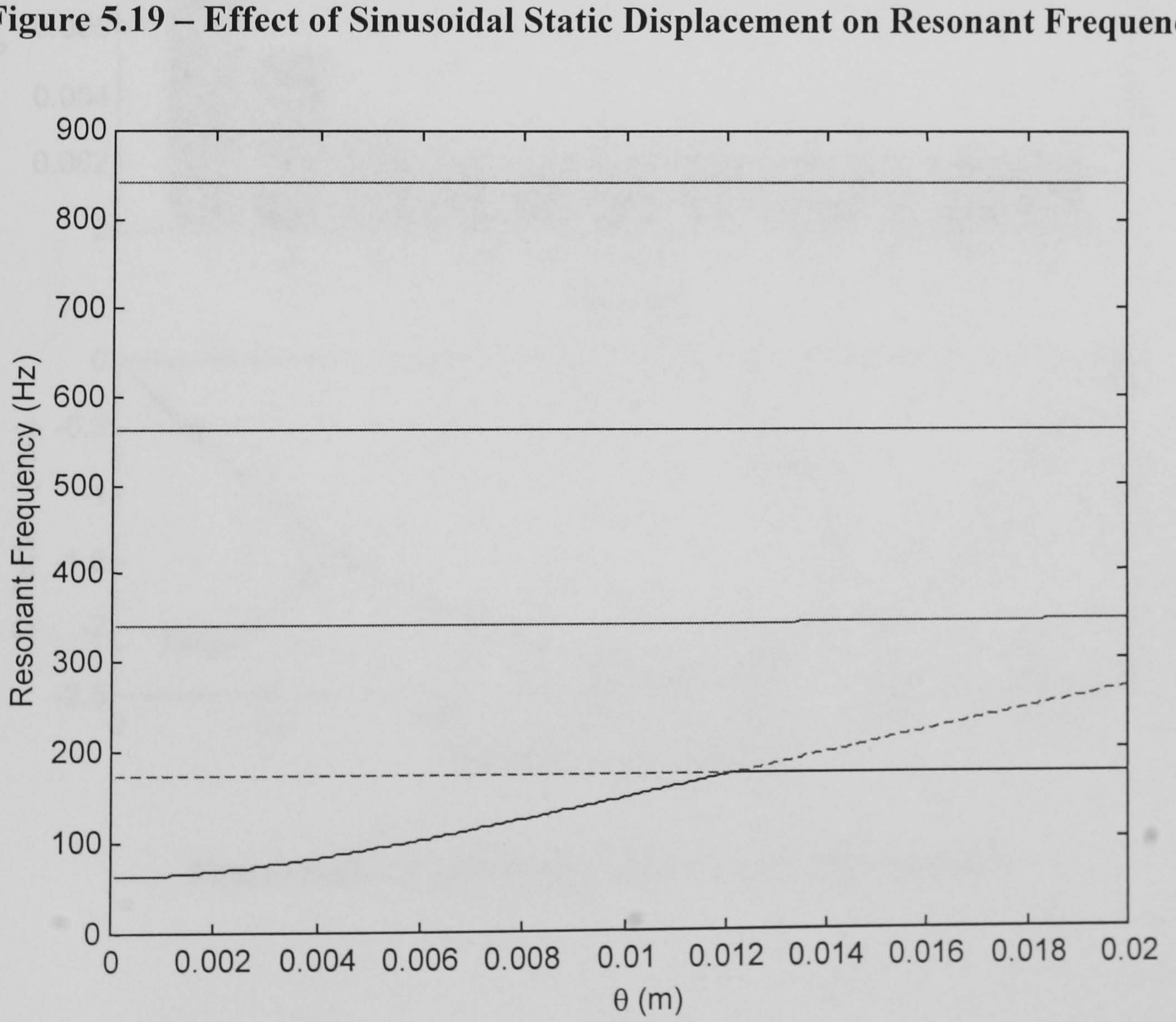

Figure 5.20 – Mode Swapping With Large Displacement

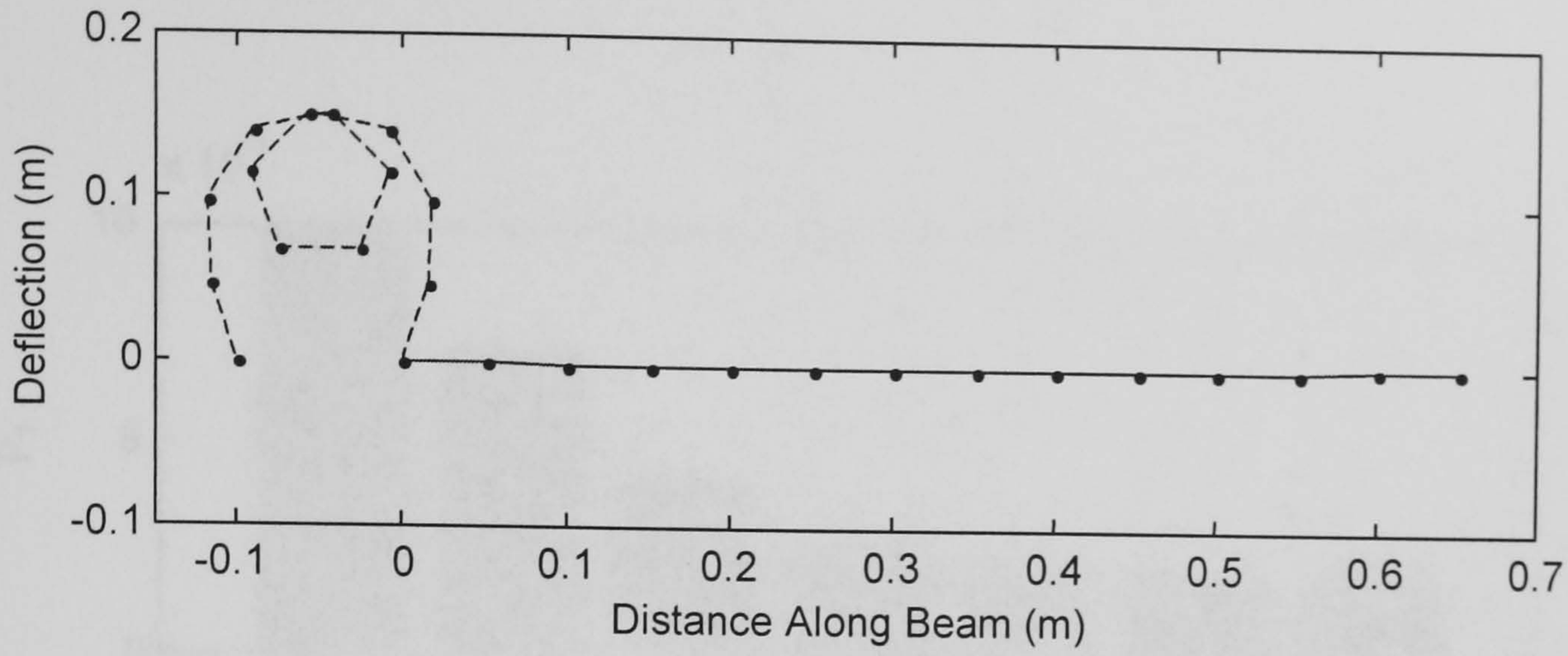

Figure 5.21 – Updated Solution $\theta_{initial}$=0.02

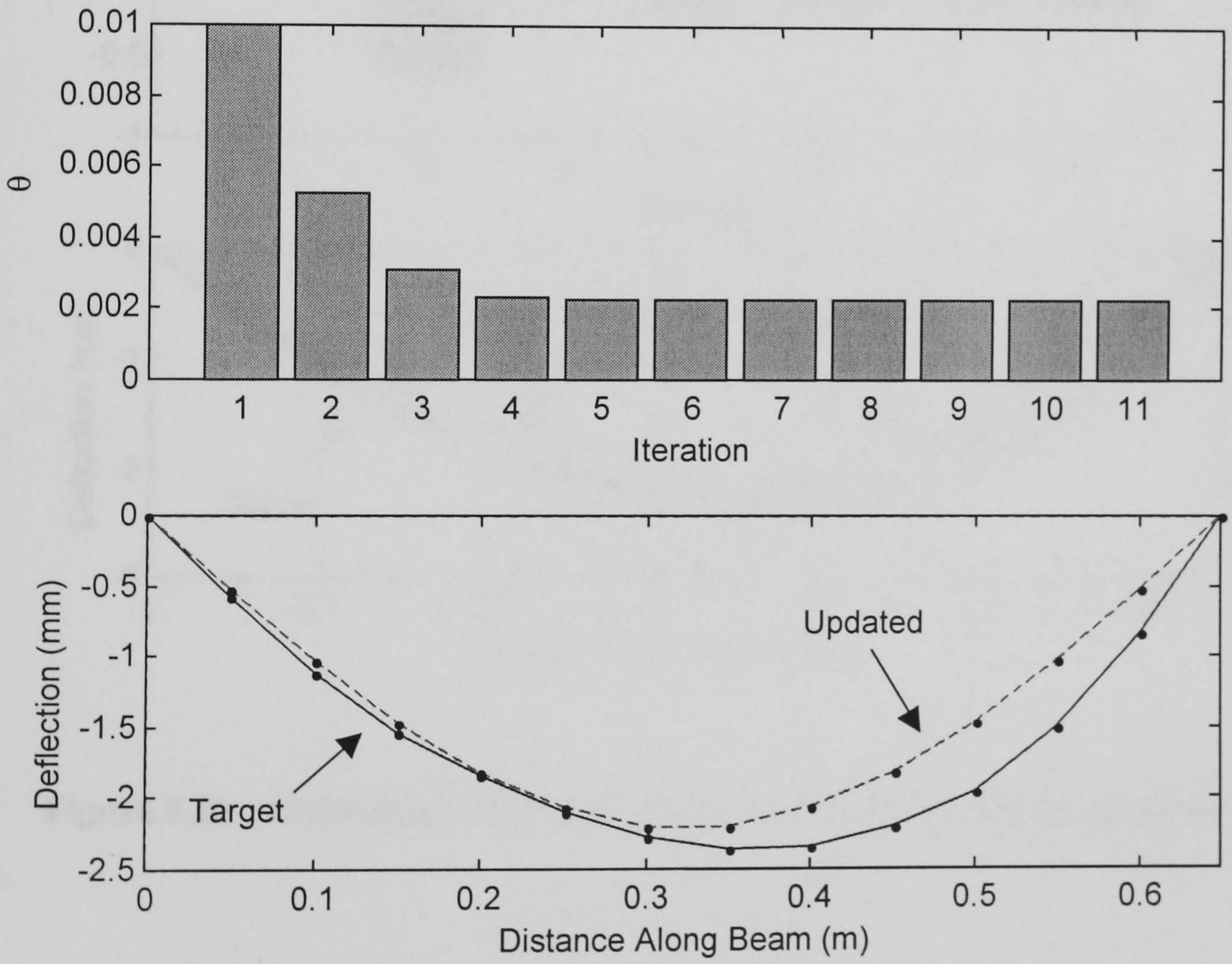

Figure 5.22 – Convergence Upon "Best Fit" Solution

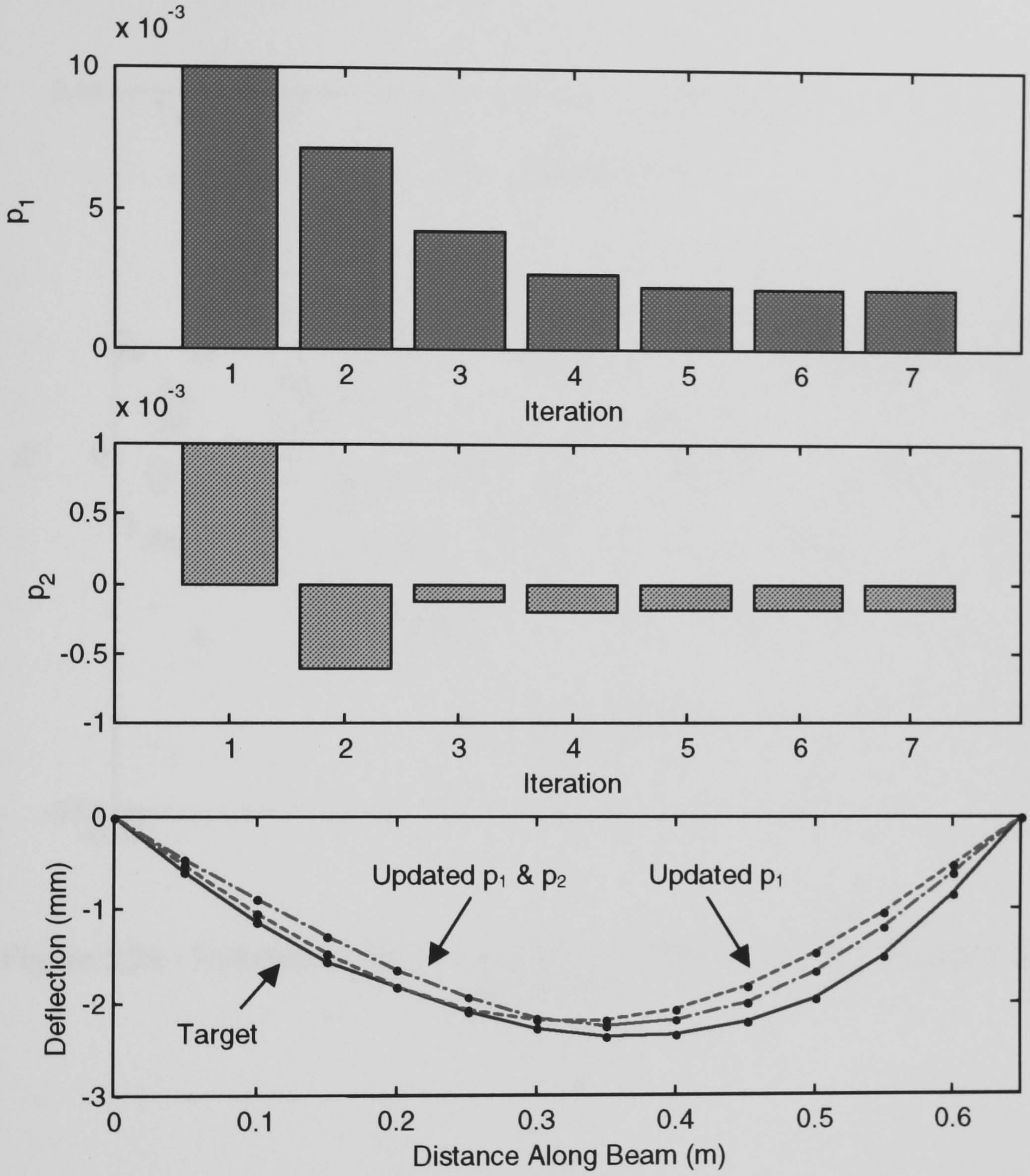

Figure 5.23 - Converged Solution Using Two Profile Updating Parameters

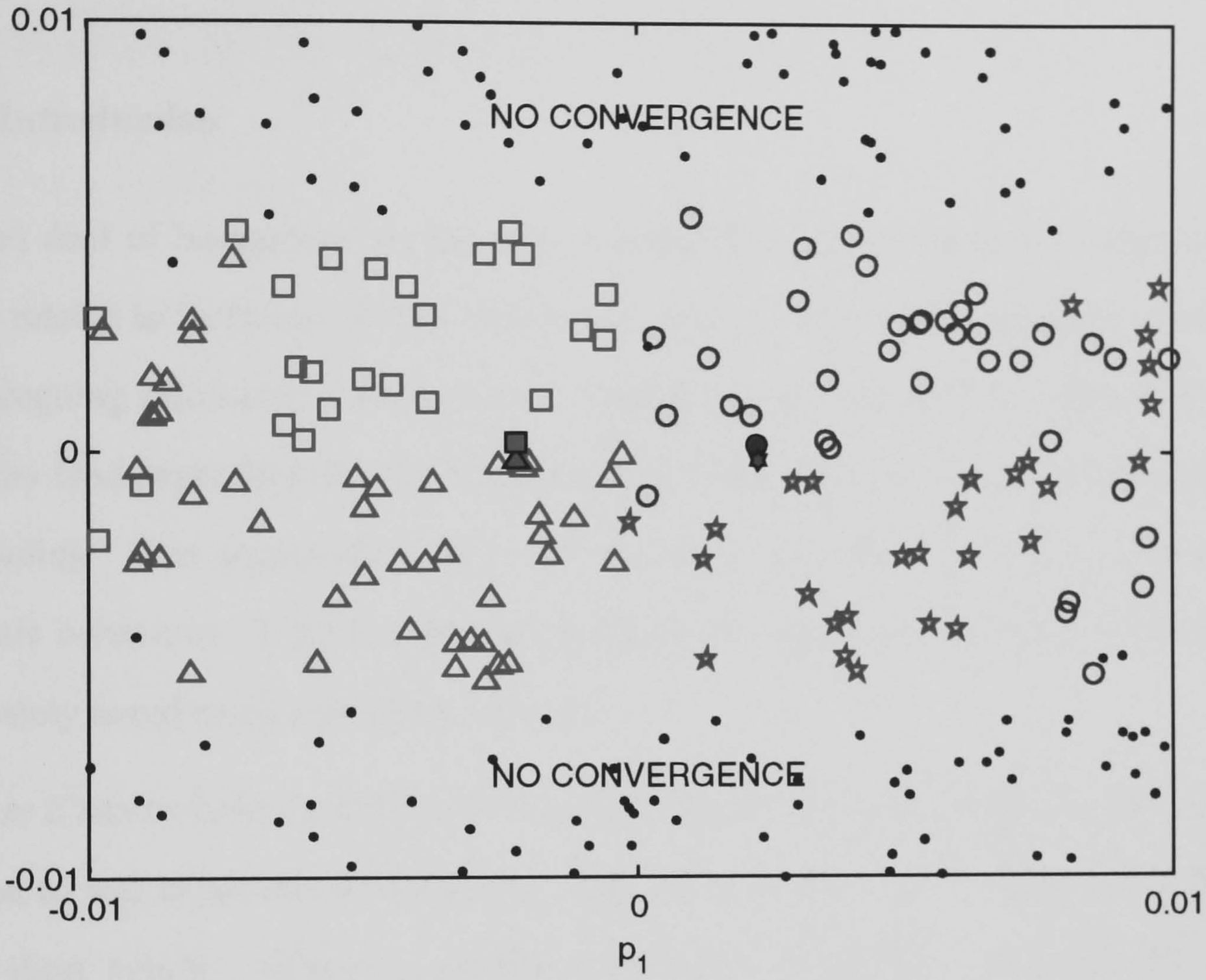

Figure 5.24 - Updated Solution Using Two Profile Parameters; Various Initial Deflections

CHAPTER 6

EXPERIMENTAL UPDATING OF LOADED STRUCTURE

6.1 Introduction

A good deal of background to the area of identification of structural loading and the issues related to inclusion of these effects in finite element models has been covered in the foregoing discussion. The previous chapter has specifically investigated methods whereby load dependent updating parameters allow structures to be updated to account for loading. This potentially allows the possibility of identifying loading levels from dynamic behaviour. However, the practicalities of using these parameters can only be adequately tested using a practical test case.

Chapter 2 has reviewed a number of reported cases of updating techniques having been applied to real experimental situations. The observation was that success has been in quite short supply. Given the extensive literature devoted to finite element model updating, the amount of effort expended in applying the techniques to real experimental data has until recently been relatively low. This chapter intends to redress the balance by presenting the results of tests upon an experimental structure. Three identical structures have been tested extensively in different load conditions. This has led to a large amount of information from which conclusions can be drawn about the certainty with which the dynamic behaviour can be characterised. The experimental data are augmented by a new finite element model built "from scratch" whose material properties have been validated at several stages of its construction.

Both dynamic and static load measurements have been taken from the set of test structures under several sets of loading. These allow the predictive accuracy of a statically updated finite element model to be determined.

The effectiveness of dynamically updating the model using parameters set out in the previous chapter is finally investigated. The large amount of information about the structure which is available makes it possible to draw conclusions about the correctness of the updated model. The availability of data from several identical structures allows some insight into the effect of variability in construction.

6.2 Experimental Details

The test structures consist of three frames similar in nearly all respects to the one described in chapter 4. The experimental procedure for testing the three new frameworks is broadly similar to that set out in chapter 4 to which the reader is referred for further details.

6.2.1 Description of Test Specimen

The new frames differed from the previously described frame in two important respects. Firstly the new frames employed a different - slightly more slender - design of turnbuckle. Secondly, and more importantly, the corners of the frame were spot welded; effectively fixing the joints. Experience from the first frame suggested that the level of torqueing of the bolts of the first frame introduced some uncertainty concerning the fixity of the frame in terms of the static load. To improve the chance of successfully modelling the structure under static loading this unknown was effectively removed.

The new frames were labelled B, C and D. The original frame, where necessary, is referred to as frame A.

6.2.2 Testing Procedure

Each of the frames B, C and D were tested under 4 levels of loading. The first loading regime in each case was intended to relate to the zero-load state. The loading instances will be referred to as cases 0, 1, 2 and 3. Cases 1, 2 and 3 were induced by shortening the adjustable spar number 5 (shown in figure 6.1) using the turnbuckle. The load

increments were intended to be approximately equal. The tests reported on frames B. C and D were conducted under identical experimental conditions.

At each level of loading, mobility measurements[30] were determined between the excitation point at node 26 – shown on figure 6.1 - and the response of each of the other visible points in the out of plane direction. All other experimental details are identical to those described in section 4.3.2.

6.3 Measured Loading on Three Frames

The strain gauging positions for frames B, C and D are shown in figure 6.2. Frame B was extensively gauged to help to compare the loading present in the structure with that predicted by finite element modelling. The measured axial load in the adjustment spar for each frame and each load case are shown in table 6.1. As with the tests on frame A described in chapter 4, the zero-load case is defined by a noticeable slacking in the turnbuckle. The load steps are seen to be approximately 500N.

Load Case	Force (N)		
	Frame B	Frame C	Frame D
0	0	0	0
1	449	514	616
2	1135	1066	1161
3	1618	1488	1604

Table 6.1 – Identified Load in Adjustment Spar

Frame B boasts some twenty four strain gauges and allows the distribution of load in the structure to be determined. Figure 6.3 shows the axial load identified in each gauging point upon frame B for load case 2. The data are compared to a simple resolution of forces resulting from a tensile load of 1135N acting along the centre line of the

---

[30] Recall that all responses in this thesis are presented as receptance.

adjustable spar. Despite the fact that the connections of the frame have been effectively fixed and the structure is not strictly planar, the results give a good match.

The strain gauges upon frame B also allow the bending moment at several discrete locations around the frame to be determined. From figure 6.4 it is seen that a significant bending moment is developed in each of the spars with the exception of the adjustable spar. The data further shows that the structure acts symmetrically in that pairs of similar spars display closely matching behaviour. This observation is exploited in section 6.8 when choosing load-dependent parameters to update. The choice of location of strain gauges allows the bending in the principal axis of the spar section to be determined. The fixed nature of the joints of the framework implies that the spars are likely to experience other components of bending as well as torsional loading. Figure 6.5 for instance shows the distribution of bending moments of spars 1 and 2 from which it can be seen that large proportions of the maximum moments are carried at the corners.

During static loading, spars 2 and 4 are observed to deflect most significantly with spar 6 also experiencing a noticeable bow. A highly exaggerated view of the deflected shape under loading via shortening of spar 5 is shown in figure 6.6 from which spars 2, 4 and 6 are seen to deflect in the positive z-direction with spars 1 and 2 deflecting by a small amount in the opposite direction. The deflections of each of the spars were measured manually relative to a straight edge run between the corners of the frame under a load in spar 5 of 1930N (corresponding to two complete revolutions of the turnbuckle), the results are set out in table 6.2.

Spar	Central Deflection (mm)
1	-1
2	9
3	-1
4	10
5	0
6	9

Table 6.2 – Measured Frame Deflections Under 1930N Load

While this method for determining deflected shape is rather crude – accuracy is certainly no better than the nearest millimetre – an outline knowledge of relationship between load and deflection is useful in the validation of the finite element model of the structure (section 6.7.1).

6.4 Modal Analysis

Modal analysis was once again performed on all of the sets of data using the global method [58] implemented in the ICATS [87] suite of modal analysis software. The data was processed by the author and, for comparison, independently by an experienced modal analyst.

6.4.1 Mode Identification

Since the ANSYS finite element model developed in chapter 4 indicated 15 modes in the 0-400Hz range compared with 12 that had been identified in the modal analysis of frame A, a much more rigorous search for resonant frequencies was performed. The result of this strategy was that up to fourteen modes were identified. As before, the level of loading was found to influence significantly the contribution of certain modes to the response.

The twelve sets of data arising from the four load cases upon three structures were independently analysed by an experienced modal analysist. He found consistently fewer modes than the author as well as different numbers of modes from the same structure in different load cases. Table 6.3 shows the number of modes identified by the author and the independent analyst.

		Load Case			
	Frame	0	1	2	3
Author	B	13	12	14	13
	C	10	12	12	13
	D	10	12	12	11
Analyst	B	10	9	10	11
	C	9	11	11	11
	D	9	9	12	12

Table 6.3 - Number of Modes Identified

The modes identified independently represent a good estimate of the number of modes which would have been identified without the insight provided by the previous analysis and testing described in chapter 4.

Several trends become apparent through analysing the large volume of data available. For instance the second identifiable mode becomes easier to identify with large loading. Conversely the fourth mode is observed to become less easy to identify with increasing load. As with the tests on frame A described in chapter 4, modes 2 and 3 converge upon one another in terms of both frequency and mode shape at higher loading levels.

It is observed that sets of tests on the three frames under four different levels of loading reveal a total of around 50 modes. Given that similarity between about half of the identified modes is strongly influenced by the loading, the task of correlating all of the modes is an extremely onerous one! To compare every mode shape with every other shape for each of the tests would require in excess of 50 MAC [57] calculations each of which produces a matrix containing over 100 elements.

Some more insight into the nature of the dynamic behaviour is given by figure 6.7. This shows the complete set of receptances taken for load case 2 of frame B, the frequencies at which resonance was identified are shown as vertical dotted lines. It is seen that while many of the modes are dominant system modes, others are local to only a proportion of the responses.

The complete set of mode shapes and resonant frequencies for frame 2, load case B which yielded the most information are shown in figure 6.8. A set of tables containing the full set of resonant frequencies identified by the author are presented in appendix B.

By comparing each of the sets of experimental modes with each other using the MAC, a subset of the modes are found to have both been identified in each load case and to correlate with each other and the ANSYS FE model of the structure. Figure 6.9 shows for example, the values of the MAC between the experimental readings from load case 2 of frame B and the initial ANSYS FE model that exceed 0.9. The seven ever-present "consistent" modes common to all of the experimental data and for which mode shapes do not change excessively are shown as shaded. These are seen to correspond to modes 1 to 5 and modes 14 & 15 of the original ANSYS FE model. This "consistent" set of modes are identified to reduce the confusion which has been seen to arise from the modes shapes being sensitive to load. This in turn allows concise comparison between each set of experimental data and the finite element model.

The remainder of the experimentally identified modes and the other eight modes predicted by the finite element model whose correspondence is less clear are nonetheless important characteristics of the system. As such these should clearly not be overlooked. Further insight into the nature of the "inconsistent" modes is gained by comparison with a statically updated finite element model described in section 6.7.3.

6.4.2 Perturbation to Resonant Frequencies Under Loading

The relationship between the "consistent" modes identified previously and loading for each of the three frames is shown in figure 6.10, from which several interesting

observations can be made. The response to loading for each framework appears to be very similar. Several modes are systematically different from the corresponding modes on the other frames. Mode 5 of frame B for instance is approximately 4Hz lower than the response of frames C and D. The offset is almost certainly due to permanent differences between the two structures a factor which must be accounted for by conventional permanent updating parameters.

The absolute and percentage increase in resonant frequency from the zero loading to the maximum loading upon each of the three frames for the seven consistent modes are shown in table 6.4.

	Frame B – 1618N		Frame C – 1488N		Frame D – 1604N	
FE Mode	Abs Increase (Hz)	% Increase	Abs Increase (Hz)	% Increase	Abs Increase (Hz)	% Increase
1	-8.73	-19.14	-7.06	-16.00	-8.37	-18.54
2	25.66	37.19	23.13	32.53	22.74	31.41
3	3.94	4.27	4.13	4.53	5.00	5.43
4	-14.21	-11.35	-13.07	-10.34	-15.25	-12.15
5	19.96	15.37	21.42	15.99	24.09	18.13
14	-9.50	-3.02	-9.32	-2.93	-8.93	-2.84
15	-18.55	-5.24	-11.09	-3.20	-14.57	-4.15

Table 6.4 – Absolute and Percentage Increase in Experimentally Identified Resonance Frequencies

The resonance frequencies as before are seen to shift significantly in both absolute and percentage terms. An attempt to validate a finite element of a structure against these data is clearly folly unless the temporary effects of the loading upon the structure are taken into account.

6.4.3 Variability of Results

The construction of 3 identical frames allows some insight into the variability of results arising from differences in construction. Figure 6.11 shows the receptances

corresponding to the point mobilities taken from frames B, C and D under zero-loading. It is seen that there is generally good agreement especially of the lower order modes. Table 6.5 shows the resonant frequencies of the seven "consistent" modes identified from all four frames with zero load induced in the frame. The bracketed values indicate the result of independently applying the modal identification procedure.

	Frequency (Hz)				
FE Mode	**Frame A**	**Frame B**	**Frame C**	**Frame D**	**Max Abs. Difference**
1	44.3	45.6 (45.4)	44.1 (44.1)	45.1 (45.1)	1.5
2	70.5	69.0	73.3	70.0	4.3
3	90.6	92.2 (92.1)	91.2 (91.2)	92.1 (92.4)	1
4	123.4	125.3 (126.1)	126.4 (126.4)	125.5 (125.6)	1.1
5	133.4	129.9 (130.1)	134.0 (133.9)	132.9 (133.1)	4.1
14	309.9	315.0 (315.1)	318.4 (318.3)	314.0 (314.2)	8.5
15	347.3	353.8 (353.8)	346.5 (346.5)	350.7 (350.7)	7.3

Table 6.5 - Comparison of Resonance Frequencies Between Unloaded Frames

The prediction of these seven modes are seen to be reasonably consistent. The results from frame A contribute most to the spread of results. The influence of the variety of identified values shown in table 6.5 on finite element model updating are investigated in section 6.8.3.

6.5 Construction and Validation of MATLAB FE Model

The interest in updating parameters of the model indicates the utility of modelling the structure independently of a commercial FE package. In this way a great deal more flexibility over manipulation of the structural elemental matrices is possible. With this in mind, a new model of the structure was built in MATLAB [14].

The intention was to attempt to use experimental data to compare with the finite element model predictions of the frame structures in some detail. Therefore, it is important to have confidence in the parameters chosen for the finite element model. While model

updating is itself intended to correct mistakes made in the model, it is generally accepted that as close agreement between the initial set of data as possible must be sought before embarking upon further refinements.

To establish the dynamic behaviour of the material without the complications of joints etc., a piece of the 6mm by 15mm material constituting the framework was tested in free-free conditions. The specimen was 400mm long and from the same batch of material which was used to construct the test frames.

The beam was also modelled in MATLAB using 3D beam elements using the parameters set out in table 6.6. The dimensions of the structure were measured accurately and the structure weighed to estimate the density. Text book values were taken for Young's elastic modulus and the shear modulus [88]. The local axes for the beam are defined in figure 6.12. The measured mass of the force transducer (20 grams) was placed at the excitation point.

Parameter		Value	Directly Measured ?
Label	Name		
E	Young's Modulus	2.11×10^{11} Nm^{-2}	×
ρ	Density	7770 kgm^{-3}	✔
A	Cross Section Area	8.895×10^{-4} m^2	✔
I_{zz}	Second Moment of Area About z-axis	2.7×10^{-10} m^4	✔
I_{yy}	Second Moment of Area About y-axis	1.69×10^{-10} m^4	✔
J	Polar Moment of Area	8.084×10^{10} m^4	✔
G	Shear Modulus	8.1×10^{10} Nm^{-2}	×

Table 6.6 – Parameters Used in Finite Element Modelling of Frames

The identified values of the three bending frequencies shown are set out in table 6.7. The second column shows the frequencies predicted by using elements of length 100mm with the following column showing the results of modelling the beam with double the number of elements. The last two columns show the result of modelling the beam

without the transducer mass and the classical closed form solution for vibrations of a free-free regular beam. It is seen that these are very close and that the second and third bending modes are sensitive to the added mass.

	Frequency (Hz)			
Measured	FE 4 elements	FE 8 elements	FE 4elements no added mass	Closed Form
194	199.1	198.9	199.3	200.8
527	530.1	527.6	552.1	553.7
1030	1040.5	1035.0	1083.5	1085

Table 6.7 – Identified and Analytical Bending Frequency Estimates

In the light of these observations, it seems reasonable to accept that the parameters chosen are close enough. The remaining error is likely to derive from the interaction of the structure with the shaker mechanism.

6.6 Initial Correlation

The previous ANSYS FE model of the framework structure helped to establish that changes made by a finite element model to account for loading. This enabled the dynamic properties of loaded structures to be modelled *qualitatively*. Some mismatch was seen to exist between the finite element model and the zero-load experimental data. While building an improved FE model the opportunity was taken to consider the reasons for the mismatch between zero-load experimental readings and the initial FE model.

Table 6.8 shows the initial FE estimate from the new model[31] of the seven consistent modes. The results from frame B, zero-loading are also shown as well as the absolute and percentage difference between the experimental and analytical results.

---

31 This almost identical to the predictions of the original ANSYS model. The only differences arise from geometric properties having been measured with more accuracy in the second case.

FE Mode	FE (Hz)	Experimental Frame B (Hz)	% Increase	Abs Increase (Hz)
1	46.59	45.60	-2.1	-1.0
2	87.24	69.01	-20.9	-18.2
3	94.94	92.17	-2.9	-2.8
4	129.88	125.3	-3.6	-4.6
5	140.05	129.9	-7.3	-10.2
14	331.04	315.0	-4.8	-16.0
15	368.03	353.8	-3.9	-14.2

Table 6.8 – Comparison of Zero-Load Resonant Frequencies; FE and Frame B

The finite element prediction is an overestimate in all cases one might expect and arises as a result of the discretised nature of the finite element approximation to the prototype structure. There are however several parameters which were chosen somewhat arbitrarily during the construction of the finite element model. The variation in their value is likely to influence the prediction of dynamic behaviour.

One such parameter is the spacer element chosen to represent the non-coincidence of the structural spars. This is likely to have a large effect on the dynamic behaviour of the frameworks. Given that the spacer is modelled as a short beam, the radius of the beam appears the most suitable parameter to change.

The turnbuckle in spar 5 has hitherto not been explicitly modelled. However, as increased accuracy is required of the finite element model, this area of the structure stands out as a likely source of error in the finite element model. This view is lent more weight by the relatively inaccurate prediction of the resonant frequency of mode 2 which consists predominantly of bending of spar 5 (see figure 4.20).

Since the turnbuckle is a relatively complex part of the structure, it is difficult to be certain about how to account for its effect. The solution chosen was firstly to change the location of node points on the adjustment spar so that one element represented the turnbuckle. The turnbuckle was then modelled as a beam with circular cross section which allowed the radius of the section to be chosen as a variable parameter.

It is a simple task for a model of this size to alter these two parameters in an iterative fashion to assess the likelihood that they are the chief causes of error between the finite element model and the experimental observations. The values of the two radii producing the closest match with the experimental data were found to be 2.5mm and 10.8mm for the turnbuckle and spacer respectively. Table 6.9 shows the seven consistent natural frequencies predicted by the new model compared to both the original ANSYS model and the experimental results. As previously described the modes were paired using the MAC. The fit with the experimental data is much better with the biggest error in mode two which might be expected since the representation of the turnbuckle while optimised is still heavily simplified.

FE Mode	Experimental	ANSYS	Abs Increase	MATLAB FE	Abs Incease
1	45.60	46.59	-1.0	44.35	-1.25
2	69.01	87.24	-18.2	76.55	7.55
3	92.17	94.94	-2.8	92.99	0.82
4	125.27	129.88	-4.6	124.54	-0.73
5	129.87	140.05	-10.2	127.21	-2.66
14	315.04	331.04	-16.0	318.69	3.65
15	353.82	368.03	-14.2	350.96	-2.86

Table 6.9 – Effect of Optimising Spacer and Turnbuckle Characteristics

The manually adjusted MATLAB finite element model is seen to show a closer match with experimentally determined data and this model was used in the subsequent analysis described in the following sections.

6.7 Static Updating of Load Dependent Properties

The process of static updating has been described in the previous chapters. The approach involves the identification of loading from static measurements such that its effect upon dynamic behaviour can be accounted for in a finite element model. As with the example of the thin plate described in chapter 4, the direct identification of the

applied loading is not necessarily possible. An initial step is required to identify the loads which should be applied to the finite element model. In the case of the small framework, however, the source of the loading is known and only the magnitude remains to be identified. The loading is induced into the frame by shortening spar five which contains a turnbuckle device. Strain gauges were used to identify the loading in this spar. The use of the directly identified load to alter the finite element model is investigated in this section.

The MATLAB FE model which benefited from the improvements described in the previous section was taken as the initial model. There are a number of levels of complexity to which *already known* loads can be applied, these have been covered in chapter 3 and consist of:

(a) applying loading in a single static step and rebuilding the structure using the deflected shape;

(b) as (a) but include stress stiffening effects;

(c) apply load in a number of steps, at each stage including the stress stiffening component from the previous stage; and

(d) use a 'Full' nonlinear geometrical analysis such that the stress stiffening component and the deformity are updated a number of times[32].

These approaches are set out more clearly in table 6.10.

---

[32] This can be achieved by an incremental approach in which large number of small steps are used or by an iterative scheme where equilibrium of external and internal loading is achieved at each level of loading. the results will converge upon the same correct solution although the iterative approach is likely to less computationally intensive.

Analysis	Stress Stiffening	Deformation Effects	Fast / Innacucurate	Slow / Accurate
(a)		✔	✔	
(b)	✔	✔	✔	
(c)	✔			✔
(d)	✔	✔		✔

Table 6.10 – Four Approaches to Static Updating

Analysis (d) is the most accurate analysis which includes both stress stiffening and large deformation effects. At the other extreme analysis (b) takes account of both effects but in the quickest but least accurate way possible. Analysis (a) allows the effect of only deformation effects to be considered. Analysis (c) allows a comparison with (d) to be drawn to assess the relative influence of stress stiffening and large deflection.

6.7.1 Verification of Measured Displacement

Section 6.3 has set out the measured deflection of frame B under a measured applied load of 1930N. A useful first step in choosing which load model to employ is to compare the predicted deflections with the measured ones. It is seen that the deflections predicted by using analyses (a) and (b) will be similar and equal to the deflection yielded by solving for displacements in a single static step. The results of this analysis are shown in table 6.2.

Spar	Central Deflection (mm)			
	measured	(a),(b)	(c)	(d)
1	-1	-0.3	-0.4	-0.6
2	9	6.4	7.6	8.7
3	-1	-0.3	-0.4	-0.6
4	10	6.4	7.6	8.7
5	0	0.0	0.0	0.0
6	9	8.3	8.1	7.8

Table 6.11 – Measured Frame Deflections

The finite element results which were expected to be the most accurate (analysis (d)) agree to a satisfying degree with the measured results especially recalling that the measured values were only accurate to within approximately 1mm. The difference in analysis (c) from (b) results from the static effect of the change to the stiffness of the structure due to loading.

The ability to predict static deflection is closely related to the ability to model stress effects which can be directly measured. Where the loaded state of a structure must be determined indirectly in this way, several iterations of a nonlinear approach will be required. The number of iterations required depends on the flexibility of the structure and the amount of loading.

6.7.2 Frequency Perturbations From Different Analysis Approaches

The previous section has shown that the four different levels of accuracy demanded of the finite element model result in different predictions of the static structural behaviour in the form of the out of plane deflections of the six spars. The four statically updated model types also display different modal properties. Table 6.12 shows the absolute frequency shifts from the zero load resonant frequencies for the seven consistent modes under a load of 1kN.

	Δ frequency (Hz)				
FE Mode	**(a)**	**(b)**	**(c)**	**(d)**	**(d)-(c)**
1	0.45	-6.17	-6.63	-6.06	0.57
2	0.63	14.29	13.49	14.35	0.86
3	-3.45	2.52	2.95	2.46	-0.49
4	-0.03	-8.15	-8.14	-8.09	0.05
5	-0.13	9.79	4.08	11.42	7.34
14	-1.47	-8.66	-7.18	-8.05	-0.87
15	-0.62	-7.17	-6.56	-7.17	-0.61

Table 6.12 – Resonant Frequency Shifts Resulting From Four Statically Updated Models

The clearest observation is that the stress stiffening has the most profound effect upon frequency perturbation. The results from analysis (a) show the frequency shifts resulting only from deflection while perceptible are generally far outweighed by the stress-stiffening effects. Analysis (b) is essentially the quickest way of including both stress stiffening and deformity effects and is seen to be a reasonable approximation to the results of the full analysis (d). Analysis (c) allows insight into the effect of coupling stress-stiffening and large deflection. The difference between the results produced by analyses (c) and (d) – shown in table 6.12 – indicates the effect of the large deflection upon the consistent modes. It is seen that the effect is marginal except in the case of FE mode 5 where the perturbation is very much larger.

A great deal more insight into the interaction of stress stiffening and large deformation effects is gained from figure 6.14 which shows the result of using methods (c) and (d) over a wide range of loads. Several of the modes (for instance 1,2,3) where the lines are practically overlaid indicate that the stress stiffening effect dominates the frequency shift with loading. Four or five of the modes - most dramatically mode 6 - are seen to be very significantly influenced by the large deformation effect.

The reason for the unexpectedly large influence of deformation effects upon mode 5 now becomes clear. The dashed boxes in figure 6.14 shows that in between loads of 0 and 1kN, the (solid) line which represents the effect of only stress stiffening on mode 6 has dropped below mode 5. The correct value for the increase in mode 5 is 11.02.

This plot along with the experience gained in correlating experimental and FE mode shapes leads an important observation. The modes of vibration which are least affected by changes to the deflected shape of the structure are the modes which have already been identified as consistent. This has several repercussions. Choosing closely correlating FE-experimental mode pairs from loaded structures leads to use of modes which are mainly affected by stress stiffening effects. For this reason, stress stiffening updating parameters will be concentrated upon in the experimental updating case study in section 6.8. Additionally, to identify mode shifts which are sensitive to changes in

structural deformed shape the MAC appears to be inadequate. Figure 6.14 clearly shows modal trends but the previous experience (mainly in chapter 4) is that mode shapes change a great deal over the range of loading shown. As section 6.4.1 has concluded, applying the current practice of identifying correlating mode pairs using the modal assurance criterion leads to around half of the identified modes being disregarded. Since the experimental modal information is scarce, not being able to make use large portions of it presents a very serious limitation the overall value. An urgent requirement therefore exists to enable correlation of pairs of modes whose mode shapes have been affected by loading.

6.7.3 Comparison of Statically Updated Model With Dynamic Data

The value of identified consistent experimental frequencies at the measured load levels are overlaid upon the full-nonlinear MATLAB FE in figure 6.15. The prediction of the zero-load resonant frequencies as well as the perturbations arising from the loading are seen to be better than the previous attempt in chapter 5 (figure 4.26).

Of the seven modes previously singled out since they appeared to show consistent correlation between experimental and finite element modes under loading, six modes (1, 2, 3, 4, 14 and 15) show very close agreement with their finite element counterparts. Indeed the finite element prediction *at all load levels* lies within the variation observed between the nominally identical frames. This observation gives confidence in the finite element model of the structure as well as the changes made to account for the loading. Under loading, the fifth experimentally identified mode appears to correspond more closely to the sixth FE mode. This thesis is confirmed by considering the MAC between the MATLAB FE modes and the experimental modes. The result for frame B at an applied load of 514N in the region is denoted by the dashed box in figure 6.15. This shown in table 6.13 and indicates that the fifth experimental mode correlates with the sixth experimental mode.

		Exp	
		4	5
FE	4	0.98	0.01
	5	0.15	0.74
	6	0.01	0.97

Table 6.13 –MAC Between Experimental Frame B and FE Modes Under Applied Load of 514N

The difficulty in correctly correlating modes is illustrated very clearly by considering the MAC. An overhead view is shown in figure 6.16 with closely correlating modes identified in figure 6.17. This has been calculated between the original FE model described in chapter 4 and the "improved" finite element model which has benefited from the changes described in section 6.6. The enhancement to the model is principally the inclusion of the turnbuckle. Of most interest is the observation that several of the modes in the improved model do not correspond with any from the original model. This is a surprising observation given that only relatively minor modifications were made to change the finite element model.

The previous section has outlined that problem that some of the mode shapes are susceptible to change under loading. The MAC has therefore been seen to be inadequate in matching some loaded mode shapes with unloaded counterparts. Another route to correlating experimental and finite element modes is in a load-case by load-case manner. This strategy uses the mode shapes identified at a certain load level to compare with the finite element model subjected to this level of loading. The MAC between the experimental and FE mode shapes of the four load cases of frame B are shown in figure 6.18 through figure 6.21. This approach is seen to allow a better degree of insight into modal correlation. Generally the graphs MAC calculations give the highest number of correlated mode pairs with the least ambiguity. The number of closely correlating modes is however seen to vary with loading with the fewest correlated mode pairs at the highest level of loading.

The results of the MAC calculations between statically updated FE model and experimental data are summarised clearly in figure 6.22. The correlating modes are shown as stars and the modes which do not allow correlation are shown as dots. In the cases that correlating modes do not match with the closest line the correspondence is shown with an arrow. The experimental modes corresponding to the FE modes 7 and 8 are found with some success. Further work is required to investigate how the FE model can better be matched with the remaining modes.

6.8 Dynamic Updating Of Framework Structure

The previous section gives considerable insight into the relationship between resonant frequencies, stress stiffening and structural deformation resulting from application of load to the framework structure. The changes made to the structure to account for the loading effects allow the perturbation of a number of the resonant frequencies to be predicted with a good deal of accuracy. The satisfying level of agreement of the modes least affected by deformation gives confidence in going ahead with the reverse process of attempting to identify the stress-stiffening properties of the finite element model from frequency perturbations.

Updating of the stress stiffening effects which are seen to be the principal effect in altering the dynamic behaviour under loading are is considered in the following sections.

6.8.1 Updating of Stress Stiffening

The preceding discussion, particularly chapter 3, has shown that to account for load effects in a finite element model the structural deformation must be included in the model. It has been seen in section 6.7 that stress stiffening have more effect on the modal perturbations in this particular case. As a first step towards updating of load dependent properties using *real* experimental data, the following sections investigate the

possibility of identifying loading by updating parameters related to the stress stiffening in individual elements as described in chapter 5.

Before embarking upon the updating procedure several decisions must be made. These can be summarised as:

(a) how many parameters are to be updated? i.e. number of independent loads to identify;

(b) how many and which shifts in resonant frequency to use;

(c) what is the initial value of updating parameter to be used?; and

(d) what amount of measured load information to be included.

At first glance, (c) and (d) clearly share some similarity. The former however is required educated guesswork to identify order of magnitude estimation of loading to be used as an initial value and the latter relates to the situation where loading in certain members may be measured explicitly.

6.8.1.1 Initial Investigation

Given that the position of loading is known, it is possible to derive a simple relationship between the load in each strut and the applied load. In the most basic case therefore it is possible to summarise the loading in terms of a single parameter. At the opposite extreme, the axial load in each element could be derived. The latter approach would require up to 34 independent parameters to be altered. This would have to be achieved from a maximum of 14 pieces of information offered by the differences in frequency between the finite element model and experimental measurements in the frequency range 0-400Hz. Two possible compromise approaches appear to offer the most sensible approach. The first is to attempt to identify the load in each of the six spars separately. A slightly simplified approach - given the near symmetry of the frameworks - is to attempt to identify the three *pairs* of identical loads in the vertical, horizontal and

diagonal spars. Given the limited number of correlating modes this approach will be used here.

The experience from the previous section suggests that most information can be gained from those corresponding to the FE modes 1, 2, 3, 4, 14 and 15. This is based upon the ability to correlate these modes with the FE model as well as the observation that these modes are not affected by deformation effects.

To reduce the amount of information presented to manageable levels, the identification of loading in load case 2 on frame B will be considered. This is appropriate since the dynamic data from this particular configuration has been shown to contain the most information.

Figure 6.23 shows the result of updating the three independent stress stiffness parameters using the resonant frequencies from load case 2 on frame B. The modal data corresponds correspond to the finite element modes 1, 2, 3, 4, 14 and 15. The top plot is the *residual*, R, at each iteration given by

$$R = \left\| \{\lambda\}_{FE_k} - \{\lambda\}_{\exp} \right\|_2 . \tag{6.1}$$

where $\{\lambda\}_{FE_k}$ are the eigenvalues arising from the finite element model at the k^{th} updating iteration and $\{\lambda\}_{\exp}$ are the corresponding experimentally-identified eigenvalues. It is recalled that the i^{th} eigenvalue is related to the corresponding observed resonant frequency f_i in Hertz by

$$\lambda_i = (2\pi f_i)^2 . \tag{6.2}$$

The residual indicates that at each step of the updating process the resonant frequencies of the finite element model become a closer match of the experimental model. The updated frequencies are shown in table 6.14 along with the initial FE values and the experimental values *for the modes which were updated.*

	Frequency (Hz)			Δ frequency (Hz)	
FE Mode	Experimental	Initial FE	Updated FE	Initial - Experimental	Initial – Updated
1	39.69	44.19	36.18	4.49	-3.51
2	89.95	76.90	90.00	-13.05	0.05
3	94.57	92.72	94.31	-1.85	-0.26
4	115.43	124.11	113.81	8.68	-1.62
14	308.85	318.17	308.99	9.32	0.14
15	341.55	349.96	341.72	8.41	0.16

Table 6.14 – Resonance Frequencies of Updated Model

The middle plot of figure 6.23 indicates that the changes to perturbations required at each step of the updating process converged quickly to zero. The convergence of each updating parameter upon its final value is shown in figure 6.24. The data raise an unusual issue in that the experimental case shows more robust convergence than its simulated counterpart described in chapter 5. This can be seen by comparing figure 6.24 for example with figure 5.9. The improved convergence can best be explained by the fact that only a subset of the modes is used in the experimental study. This has been based on some insight into their usefulness.

Moving on to the identified loads, the measured loads in each spar for load case 2 are shown in the third plot of figure 6.23 against the identified values. The identification of the load in the compression members (1 through 4) is more successful than that in the tension members. The percentage difference from the measured values are shown in table 6.15.

Spar	Measured Axial Load (N)	Identified Axial Load (N)	% Difference (Increase)
1	-483.24	-511.69	5.89
2	-891.88	-902.49	1.19
3	-708.61	-511.69	-27.79
4	-808.84	-902.49	11.58
5	1135.59	547.71	-51.77
6	1007.07	547.71	-45.61

Table 6.15 – Measured and Identified Axial Load; Frame B, Load Case 2

While the updated finite element data is not a perfect match with the measured values. the updated model is a good deal closer to representing the structure in the loaded configuration. To this extent, the validation and updating procedure described previously can be said to have been verified as being successful. This is a far from routine observation in model updating!

The inaccuracies in the loads identified by the updating process are likely to be due to a number of factors. For instance:

(1) frequency perturbations caused by mis-modelling of initial finite element model;

(2) not including the correct updating parameters to account for permanent errors;

(3) not including the effects of deformity; and

(4) insufficient independent stress stiffening updating parameters.

Despite the great care with which the initial FE model was built, it is the opinion of the author that the first two point are the most important factor in influencing the likelihood of success in identifying loads. The two effects are closely inter-related and while being almost completely unavoidable, present the biggest obstacle to *any* model updating scheme with *any* set of updating parameters.

In addition the inaccuracy associated in the identification of resonant frequency as well as the errors attendant to the measurement of load conspire to bring about difference between updated load parameters and measured values.

6.8.1.2 Updating With Offset

With the comments of the previous paragraphs in mind a method of decreasing the effects of permanent errors in the initial finite element model is presented here. That is to treat the difference between the initial finite element model and the zero load experimental resonant frequencies as a permanent offset. The magnitude of which the updating process should not seek to minimise. In terms of system eigenvectors, the offset is given by

$$\{\Delta\lambda\} = \{\lambda\}^z_{FE} - \{\lambda\}^z_{\exp} \tag{6.3}$$

where.., the difference in eigenvalue which we hope to minimise is given by

$$\{\delta\lambda\} = \{\lambda\}_{FE_k} - \{\lambda\}^z_{FE} + \{\lambda\}^z_{\exp} - \{\lambda\}_{\exp} \tag{6.4}$$

compared with

$$\{\delta\lambda\} = \{\lambda\}_{FE_k} - \{\lambda\}_{\exp}, \tag{6.5}$$

used previously.

Applying this method with the same data described in section 6.8.1.1 leads to results shown in figure 6.25. Quick convergence is once again achieved. As one would expect the overall residual at the final iteration is rather larger than in the previous step. This comes about since the updating procedure is not *allowed* to converge as closely on the experimental data from the loaded case. The overall estimation of loading in the spars is well within the realms of possibility. However, it is a rather worse match of the measured data than the previous updating scenario. The percentage differences are shown in table 6.16.

Spar	Measured Axial Load (N)	Identified Axial Load (N)	% Difference (Increase)
1	-483.2	-1967.6	307.2
2	-891.9	-659.6	-26.1
3	-708.6	-1967.6	177.7
4	-808.8	-659.6	-18.5
5	1135.6	840.1	-26.0
6	1007.1	840.1	-16.6

Table 6.16 – Measured and Identified Axial Load Using Frequency Offset Method

The load in the horizontal and diagonal members have been closely matched but at the expense of a heavy overestimation of the load in the vertical spars. It is still justifiable to say that a model updated thus is more useful than the original finite element model for predicting the dynamic behaviour of the frame undergoing the specified loading. The values of identified load are not better than those predicted by the standard method described in the previous section.

The apparent lack of success of this method is likely to be due to the good quality of the initial finite element model. It is the opinion of the author then that this method should reduce some of the problems related to mismatch of the zero-load FE model and experimental results in cases where the initial agreement of the FE model and experimental data is not perfect.

6.8.1.3 Effect of Eigenvalue Selection

The previous two examples give confidence in the usefulness of the method in practice. Also they are based on sensible choices of updating parameter and eigenvalue selection. They show that the method is sufficiently robust to start from a point of no prior knowledge of structural loading. To allow further insight into the issues relating to applying the technique to real data, a large number of case studies have been run with different choices of eigenvalue used to characterise the change in dynamic behaviour. Once again the experimental data from frame B load case 2 is used for illustrative

purposes. Figure 6.22 reveals that 10 of the experimental modes correlate with the finite element model at this level of loading. However, minimising the difference between all ten modes and their finite element counterparts is found to produce a prediction of the loading in each spar shown in table 6.17 which while plausible, is not a good agreement with the measured data.

Spar	Measured Axial Load (N)	Identified Axial Load (N)
1	-483.2	-1336
2	-891.9	-753
3	-708.6	-1336
4	-808.8	-753
5	1135.6	677
6	1007.1	677

Table 6.17 – Measured and Identified Axial Load Using 10 Correlating Modes

To assess which modes are most useful in producing the correct results based on the measured loading in the structure, the updating procedure was implemented 210 times. Every combination of four eigenvalues from the possible population of 10 was used to provide the target for the updating process. The three updating parameters related to the load in the vertical, horizontal and diagonal members were once again set as the only parameters to be updated. The updating used the experimental data with no initial knowledge of the load known. Of the 210 runs 135 produced converging solutions, the criterion being that the residual vector had dropped below 10 within 10 iterations.

Load sets were defined to be useful if each fell between zero and twice the value of the corresponding measured load. The reasoning was that any change to the stiffness matrix corresponding to a set of loads meeting this criterion produces a finite element model which is a better representation of the loaded structure than the initial finite element model.

Of the 135 converged sets of loads, 47 solutions proved useful. Figure 6.26 shows the number of times each of the 10 possible modes is a member of the 47 sets of 4

eigenvalues which lead to a successful updating outcome. It is seen that modes 7 and 8 feature far less often than the remaining 8 modes. The consistent modes defined in section 6.4.1 fare particularly well in addition to FE modes 6 and 10. Referring back to figure 6.14 reveals that all of the modes which lead to the most accurate answers are not affected by deformity.

This observation confirms that if purely stress stiffening effects are to be determined from a structure undergoing loading, the modes whose shapes change least should be used in preference to those whose shape is changed considerably by the loading effects.

The use of the 8 modes which have been identified as most useful leads to identified loads shown in table 6.18.

Spar	Measured Axial Load (N)	Identified Axial Load (N)
1	-483.2	-578
2	-891.9	-893
3	-708.6	-578
4	-808.8	-893
5	1135.6	577
6	1007.1	577

Table 6.18 – Identified Loads Using Best 8 Modes

The final residual is found to be lower than any of the 210 updating runs which gives considerable confidence in the results.

6.8.2 Updating of Permanent and Transient System Parameters

The ultimate test of whether it is possible to include the load-dependent properties in parallel with other permanent changes is to attempt such a process on experimental data. For the current example, the most rigorous test of the method lies in identifying the remaining sources of error in the finite element model. These errors are in addition to those not identified in the initial phase of model correction (section 6.6). While a

worthy goal, several factors lead the author to believe that this is not the route to be taken in validating the method. The first is the erosion in the amount of useful data arising from discounting modes whose inter-correlation varies with loading. Additionally a difficulty exists in explicitly identifying further sources of error in the finite element model. This is coupled with the problem of incorporating suitable updating parameters into the updating process. Instead it is proposed that a known error be imposed in the initial finite element model In this way it is possible to assess very clearly to what extent the error can be identified simultaneously with the identification of the load dependent parameters.

To this end a mis-estimation of the overall stiffness is introduced into the initial finite element model. The stiffness is decreased to 95% of the value which was used to gain reasonably good agreement with experimental results. The updating process described in section 6.8.1.1 was repeated but with an extra updating parameter, p_k, introduced to factor the initial stiffness such that the updating stiffness matrix is given by

$$[K]^U = p_k [K]^A . \tag{6.6}$$

Initially no mis-estimation of the stiffness was imposed upon the initial FE model and in a second instance the initial stiffness was decreased by 5%. Table 6.19 shows that the updated stiffness is slightly lower (in fact by about 1.5%) than the initially chosen value, since the initial value of 2.11×10^{11} Nm^{-2} is a text book value, a real value of 2.08×10^{11} Nm^{-2} is well within the realms of possibility. Referring back to the validation of the finite element model in section 6.5, table 6.20 shows the result of setting E=2.08×10^{11} Nm^{-2}.

Updated Parameters	Measured / Known (N)	Identified using p_k (N)	Identified without p_k (N)
Spar 1 Axial Load	-483.24	-273.80	-511.69
Spar 2 Axial Load	-891.88	-720.44	-902.49
Spar 3 Axial Load	-708.61	-273.80	-511.69
Spar 4 Axial Load	-808.84	-720.44	-902.49
Spar 5 Axial Load	1135.59	546.10	547.71
Spar 6 Axial Load	1007.07	546.10	547.71
Stiffness Factor	1	0.99	-

Table 6.19 – Identified Loading and Stiffness Using Experimental Data

The match of the updated stiffness with the measured values is arguably better than the original values. The "residual", defined here by

$$R = \left\| \{\lambda\}_{exp} - \{\lambda\}_{FE} \right\|_2 \tag{6.7}$$

of the (higher accuracy) eight element model using the updated stiffness is 2.24×10^5 compared to the residual using the original FE model of 4.15×10^5. This provides a an indication that the updated stiffness is a better representation of the practical stiffness than the original value. This observation gives a strong independent endorsement to the value of the updated stiffness.

Updating of the stiffness results in different values of load in the spars are converged upon. Very little effect on the identified values in the diagonal spars is found while the load in the vertical spars (1 and 3) is different from the previously identified value shown in column 3 of table 6.19.

	$E=2.11\times10^{11}$ Nm^{-2}		$E=2.08\times10^{11}$ Nm^{-2}	
Measured Frequency (Hz)	**FE 4 elements Frequency (Hz)**	**FE 8 elements Frequency (Hz)**	**FE 4 elements Frequency (Hz)**	**FE 8 elements Frequency (Hz)**
194	199.1	198.9	197.8	197.5
527	530.1	527.6	526.3	524.0
1030	1040.5	1035.0	1033.1	1027.8

Table 6.20 – Comparison of Updated Stiffness With Validated Result

Since the results derive from a specific set of experimental readings and are sensitive to the eigenvalues compared. It is impossible to be more general than to say that the measured static load data allows the updated model to be a better representation of the loaded structure than the original finite element model.

The deliberate mis-estimation of the stiffness in the initial finite element model allows a quantitative judgement of the ability of the set of updating parameters to update transient load-dependent parameters. These have been considered alongside permanent errors. The first column of table 6.21 shows that an increase in stiffness of 4% is required. This, when applied in conjunction with the 1.5% mis-estimation of stiffness in the "correct" initial FE model, matches closely with the additional imposed error.

Updated Parameters	**Identified using p_k (N)**	**Identified without p_k (N)**
Spar 1 Axial Load	-170.94	357.58
Spar 2 Axial Load	-789.23	-378.89
Spar 3 Axial Load	-170.94	357.58
Spar 4 Axial Load	-789.23	-378.89
Spar 5 Axial Load	531.21	529.46
Spar 6 Axial Load	531.21	529.46
Stiffness Factor	1.04	-

Table 6.21 – Identified Loading and Stiffness Using Experimental Data 95% Stiffness

Identified axial loads once again differ from previously identified values but continue to be a useful estimate of the actual loading. The second column of table 6.21 shows that there is considerable mis-estimation of loads in the vertical spars. This observation lends weight to the advice of chapter 5 that if stiffness properties are in error these must be included in an updating procedure for load dependent parameters to be identified accurately.

Also of note in the data presented in this section is that the parameter related to load in the vertical spars is most sensitive to mis-estimation of stiffness in the finite element model. Additionally, the identification of load in the diagonal spars is particularly robust - as was first predicted in chapter 5.

6.8.3 Updating Using All Experimental Results

The previous sections have concentrated on the use of experimentally derived data from frame B. This frame has allowed the initial comparison of measured and predicted loads. Load case 2 was used in particular since it provides most modal information. Using the insight gained in these studies, updating was performed using the modal information from all twelve experimental cases. The six modes corresponding to the FE modes 1, 2, 3, 4, 14 and 15 were used as the input. As before three loads corresponding to the loads in the vertical, horizontal and diagonal spars were identified.

Figure 6.27 shows the loads identified for frame B for load cases 1 to 3 as well as the corresponding measured values. The identification of the loads for cases 2 and 3 are seen to be qualitatively similar to the measured values with the identified loading of case 1 not corresponding well. A closer examination reveals that the trend in the identified data is consistent in each case. This suggests that the inaccuracy in the prediction of load arises from *consistent* factors. As the previous sections have suggested, the offset upon the load predictions is likely to be due to the mismatch between the zero-load experimental and FE data.

The identified loads for frames C and D for three load cases are shown in figure 6.28. No information was available about the axial load in the horizontal and vertical spars of these frames with which to compare the identified values directly. However recalling that the load steps are roughly equal (table 6.1)and that the frames are built to the same specification, the load distribution would be expected to be similar to that of frame B. The results show similar behaviour to those from frame B. Once again the loads are seen to display a regular trend while an initial offset appears generally to skew the predictions. The effect of the initial offset is to reduce the effectiveness of identification especially at low load levels.

6.9 Concluding Remarks

This chapter has presented results from a comprehensive modal analysis and FE modelling of a small structure. The various steps undertaken to achieve a successful update are shown in full to enable transparency of the procedure.

The experiment has shown that an identical structure under different loads can display sets of dynamic characteristics which are very different from one another. Different numbers of resonant frequencies have been identified from the same structure under varying loading. Certain mode shapes have been found to be altered dramatically under loading making the task of correlating modes from loaded structures with the FE model arduous.

A consideration of a subset of the identified modes whose inter-correlation was good and which could be matched with FE modes has led to useful results. These modes have been designated as “consistent”. The consistent modes have been found to include the first five fundamental modes of the structure.

A finite element model of the structure has been built from first principals and validated. This has produced closer agreement with experimental data than the initial ANSYS FE model described previously.

Static updating of the structure has been carried out using measured loads and taking account of both stress stiffening and deformation effects is seen to produce a very close agreement with experimental results for the "consistent" modes. A study of the stress stiffening effects separately from large deformation effects has shown that the modes of vibration whose resonant frequencies are most affected by large deformation effects experience the most dramatic changes to their mode shapes.

A statically updated finite element model has shown that clear trends in the resonant frequency can exist while corresponding mode shapes alter. The change in mode shapes can be sufficient that the MAC deteriorates considerably. The requirement for a new technique which allows modes which correspond under load but whose mode shapes alter has been identified. Such a technique would pave the way for the profile updating scheme outline in chapter 5 to be implemented practically.

The experimental data has been successfully used to update the stress-stiffening of the structure. Levels of structural loading have been identified from measured dynamic data. Static measurement of loading has allowed an independent check upon the validity of updating parameters.

Convergence of the three stress-stiffening updating parameters upon final values has been seen to be both quick and robust. Loads have been successfully identified from no a priori knowledge of the structural loading. This leads to confidence that the technique could act as a stand-alone method to identify structural loading from dynamic measurements.

The overall stiffness of the structure has been updated simultaneously with the stress-stiffening parameters. A plausible value for the change to the stiffness was found along with realistic loading values.

The initial mismatch between the finite element model and experimental data has been seen to affect the identified load values. The loads identified from the three sets of experimental data have demonstrated this phenomenon clearly. The sets of identified

loads from the three experimental frames have been seen to vary linearly with the known applied load increments. The values of the identified load however have shown that the changes to stress stiffening are not the only parameters that are in error.

A technique whereby the initial difference in the FE and experimental modes is removed from the overall perturbation under load has been introduced. For the specific experimental case considered the technique did not improve upon the original method. However it is the opinion of the author that in the general case this method will allow loading to be identified in structures where the initial finite element model does not correlate well with the loading.

The results of performing a great number of updating runs using different experimental eigenvalues have been presented. A large proportion of the runs have been shown to produce successful convergence upon a useful result. While not producing unique solutions, the results have been shown to be useful representations of the loaded structure.

The usefulness of each of the correlating modes in identifying stress stiffening parameters has been investigated. The mode shapes identified as not varying significantly under loading have been shown to be amongst the most useful. The use of these modes has been shown to produce the most accurate prediction of structural loading.

In summary, the following steps should be taken to identify loading in practice using the stress stiffening method:

(i) ensure that the initial FE model is an accurate representation of the structure;

(ii) include at least one stiffness updating parameter in addition to the axial load parameters;

(iii) use modes whose mode shapes correlate clearly with the initial FE model in the updating procedure;

(iv) if zero load experimental data are available (or can be derived) the offset removal method should be considered;

(v) provide as much information as possible from static measurements;

(vi) keep some static load measurements to check the updated solution; and

(vii) minimise the number of parameters to update by exploiting known relationships between axial loads.

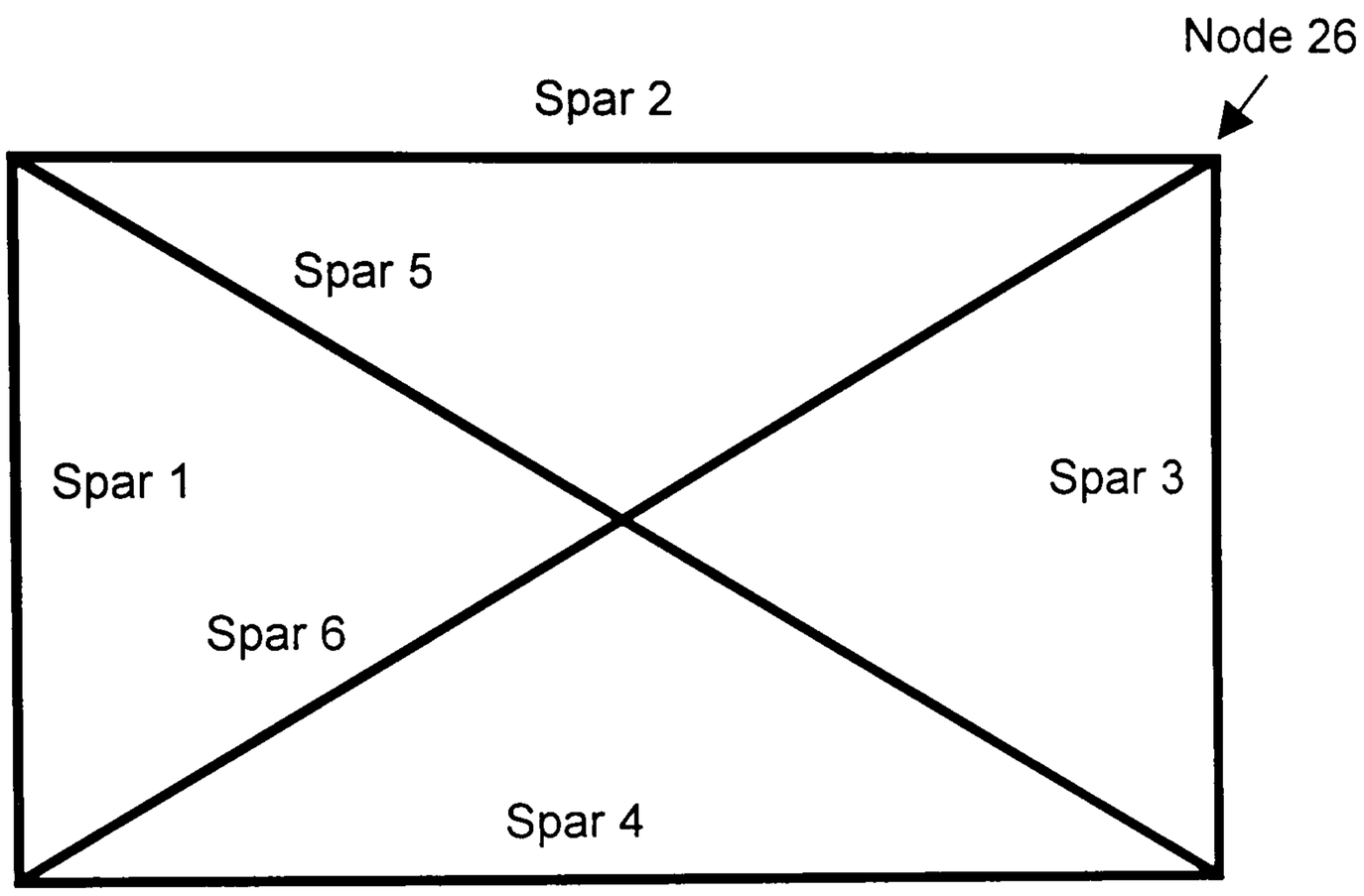

Figure 6.1 – Spar Numbering Convention and Excitation Node

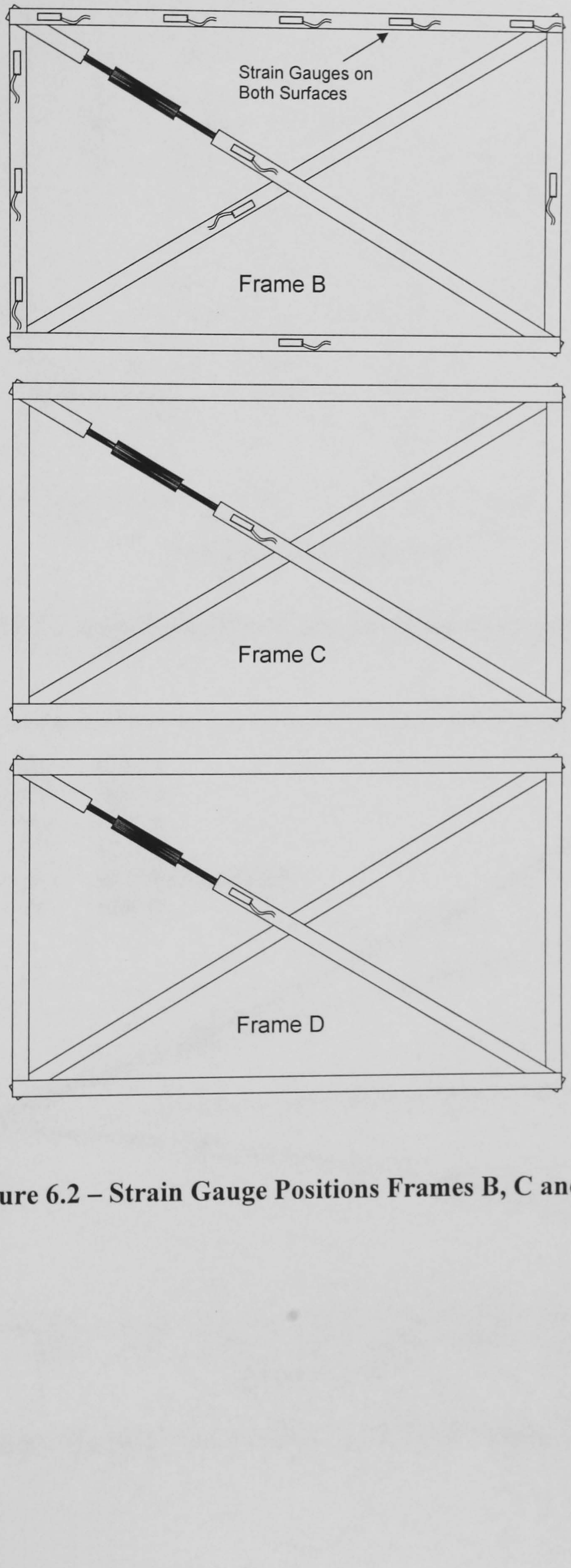

Figure 6.2 – Strain Gauge Positions Frames B, C and D

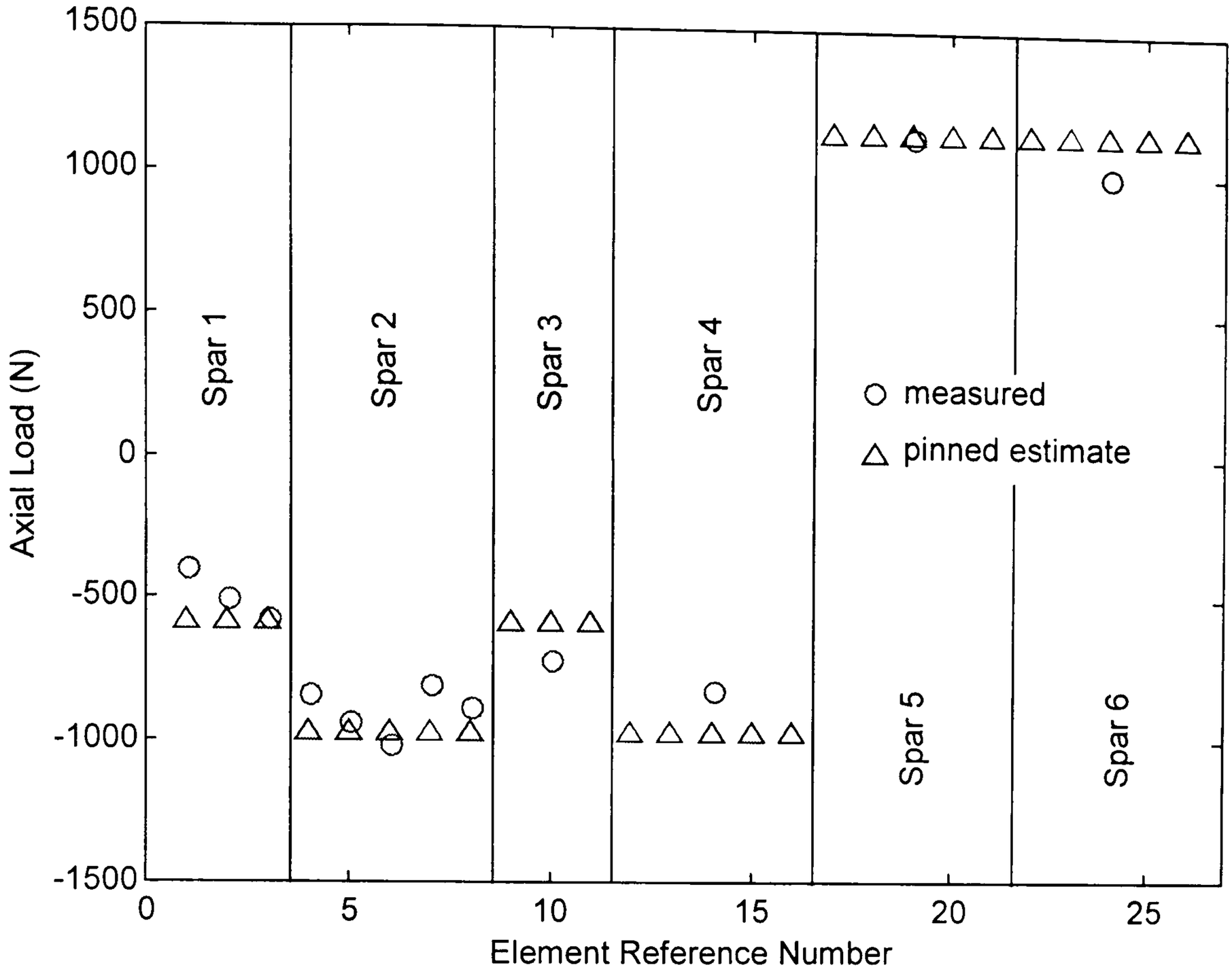

Figure 6.3 – Axial Load Distribution in Frame B, Load Case 2

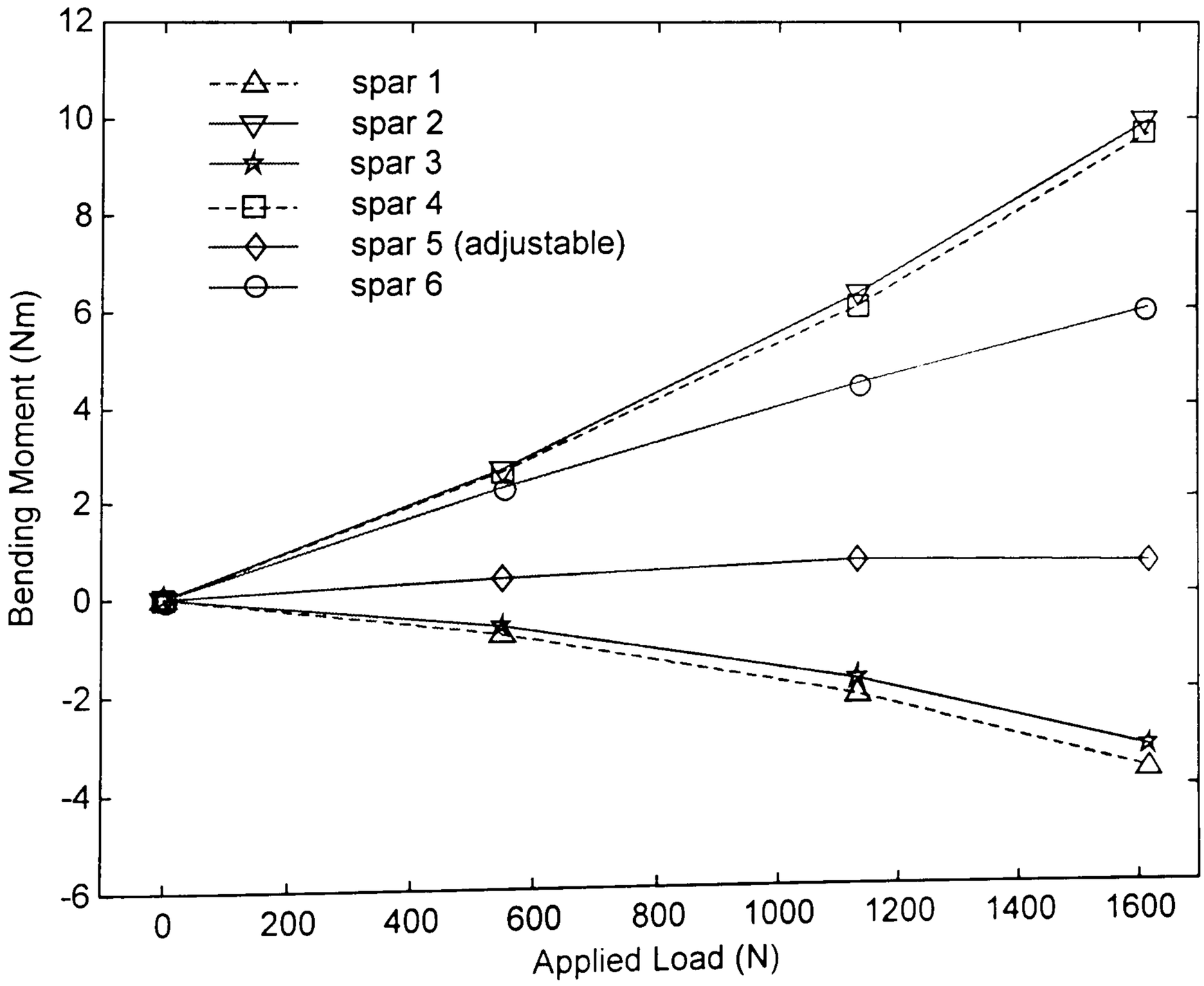

Figure 6.4 – Bending Moments at Centre of Six Spars, Frame B

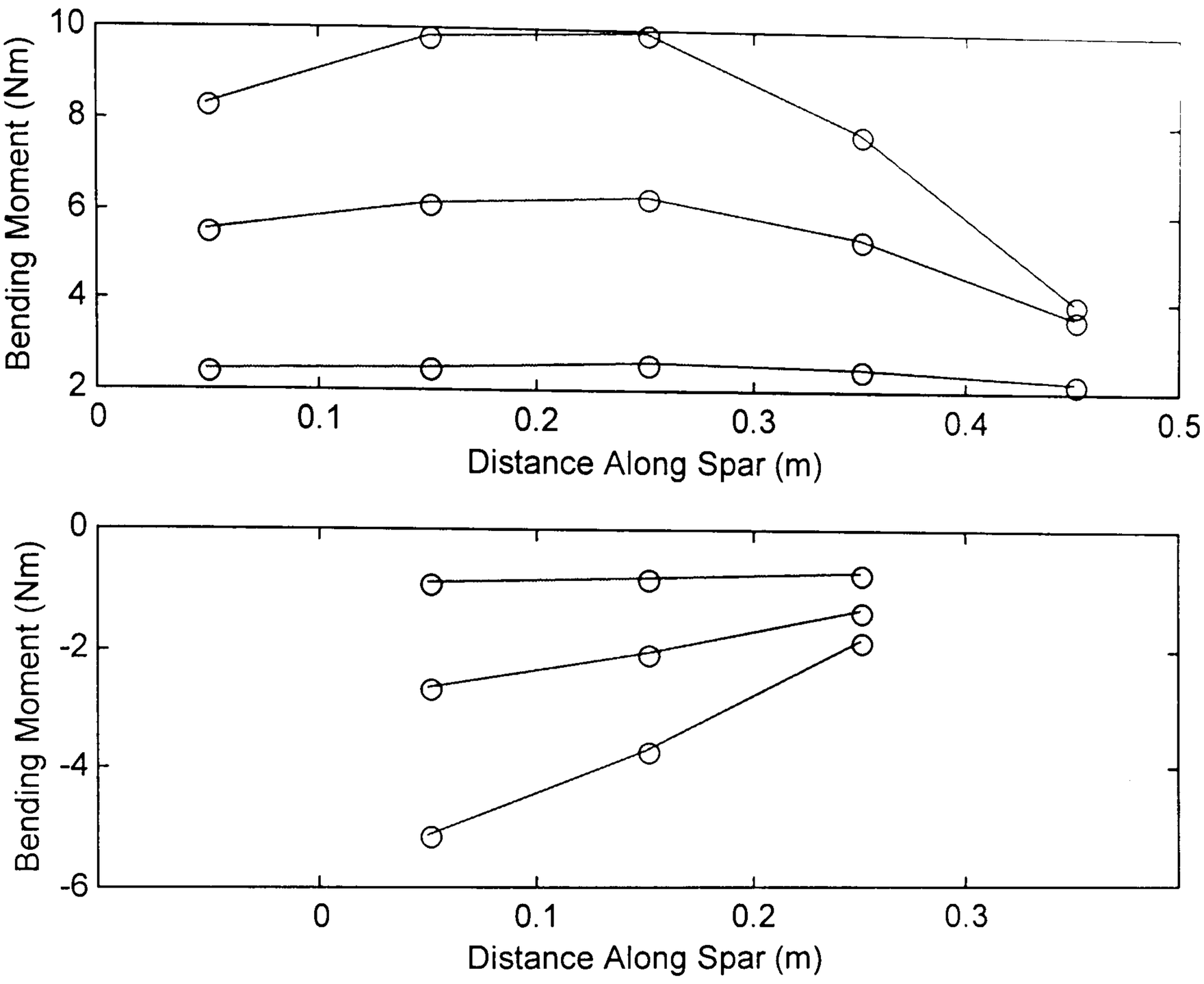

Figure 6.5 – Bending Moment Distribution Spars 1 and 2

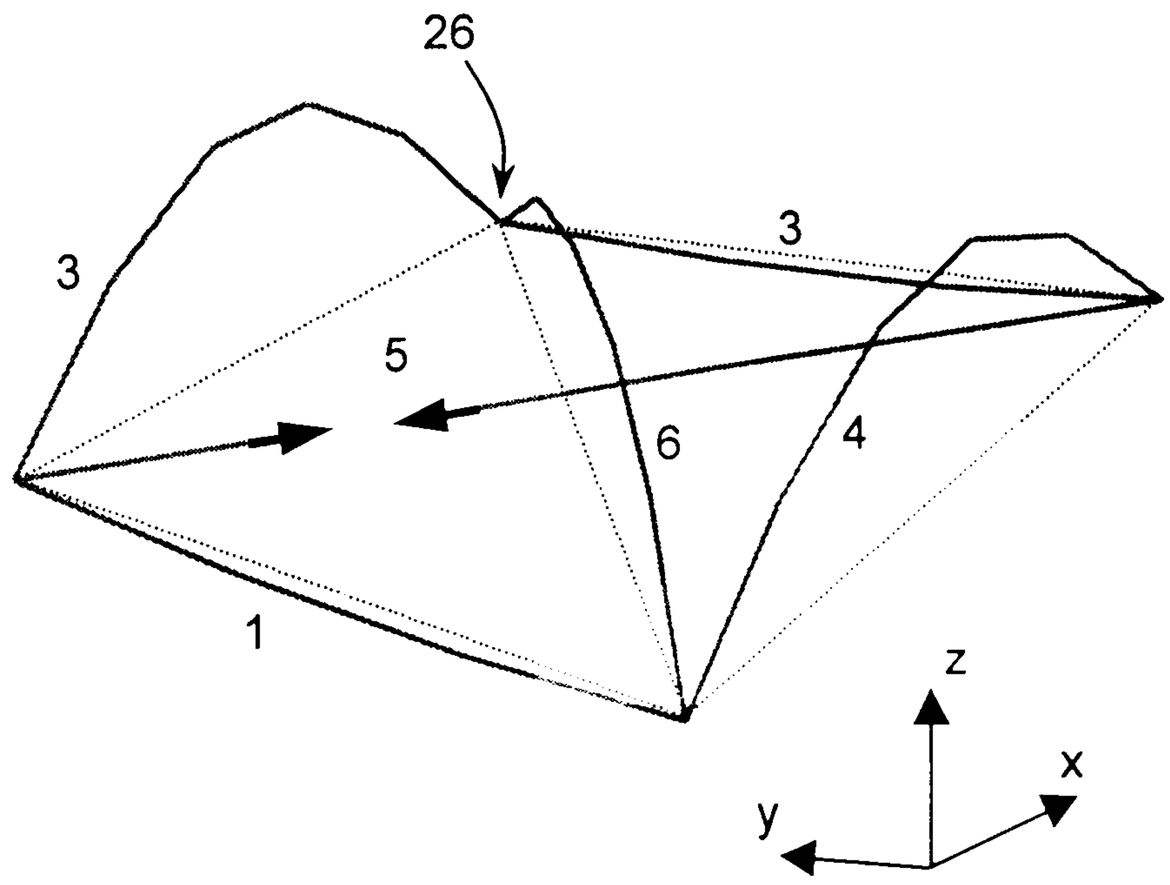

Figure 6.6 – Exaggerated Static Deflected Shape

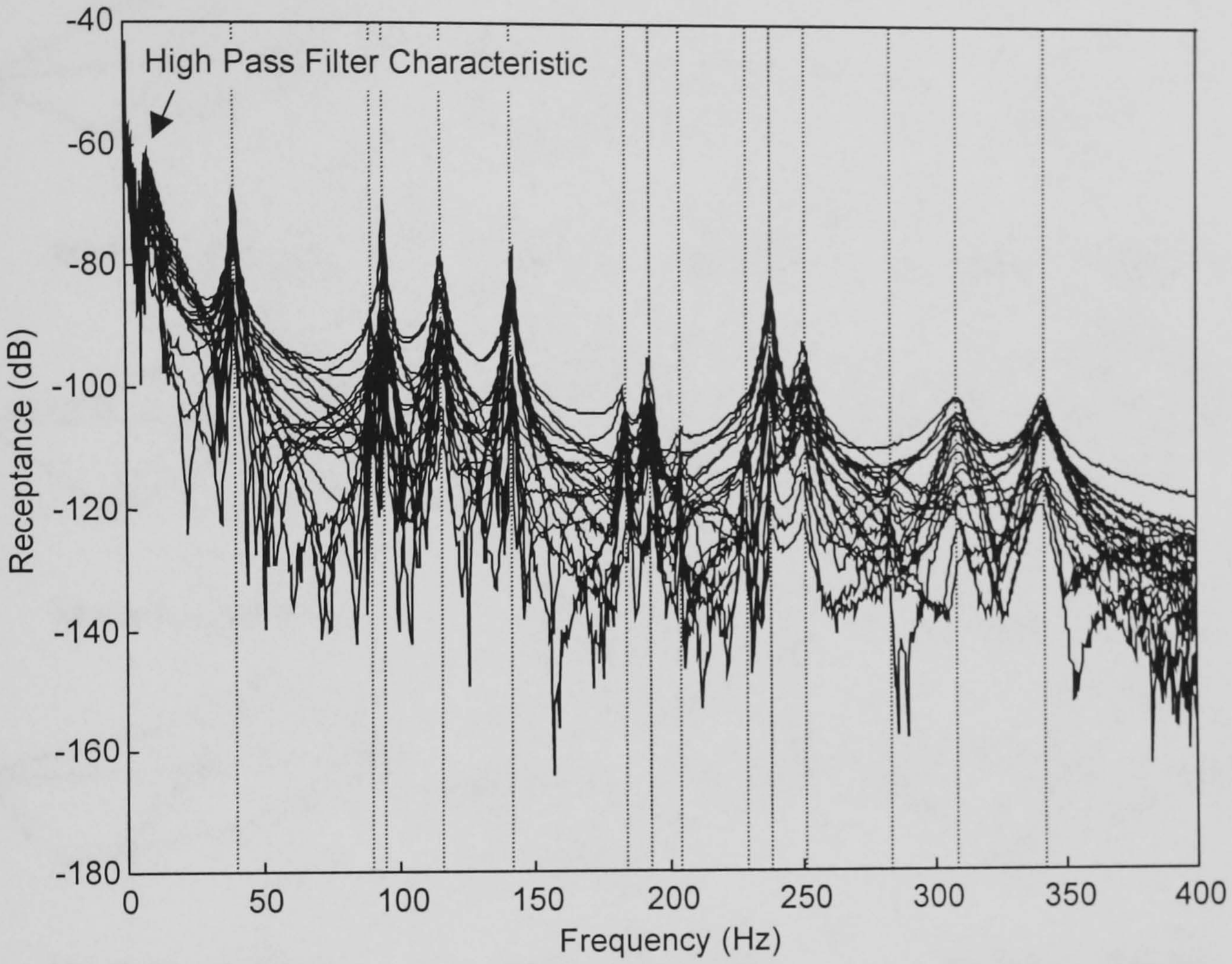

Figure 6.7 – All Measured Responses Frame B, Case 2

Mode 1 – 39.7Hz

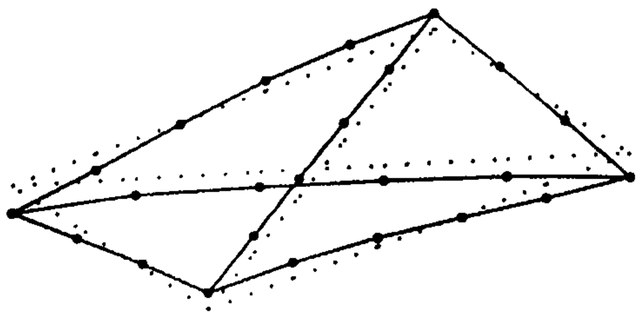

Mode 2 – 89.9Hz

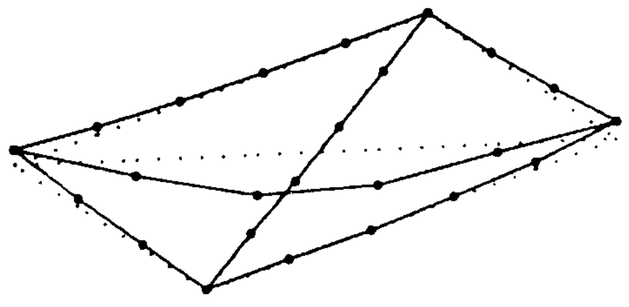

Mode 3 – 94.6Hz

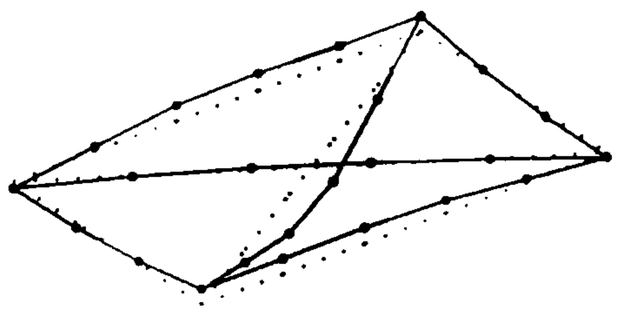

Mode 4 – 115.4Hz

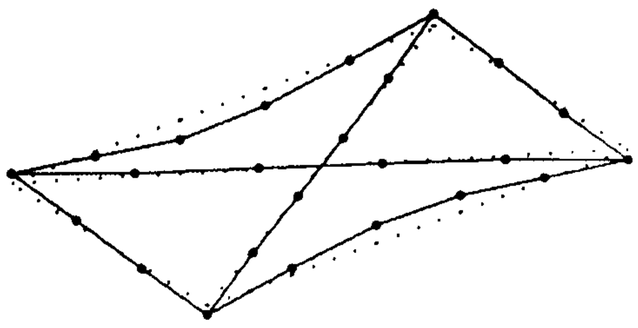

Mode 5 – 141.8Hz

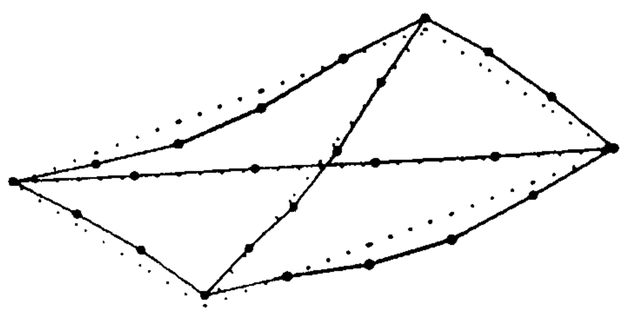

Mode 6 – 184.2Hz

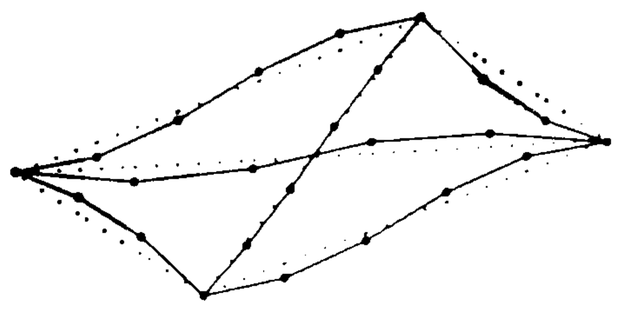

Mode 7 – 192.9Hz

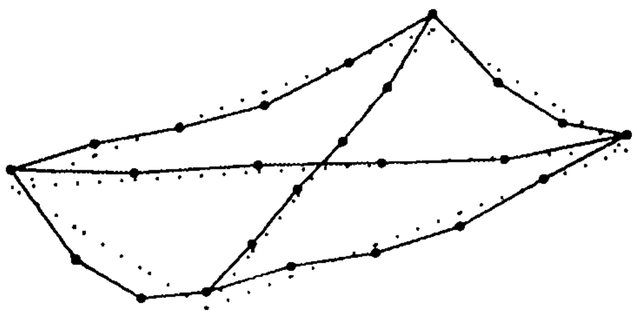

Mode 8 – 204.2Hz

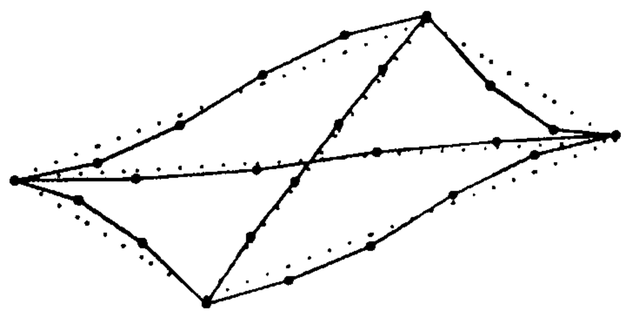

Mode 9 – 229.1Hz

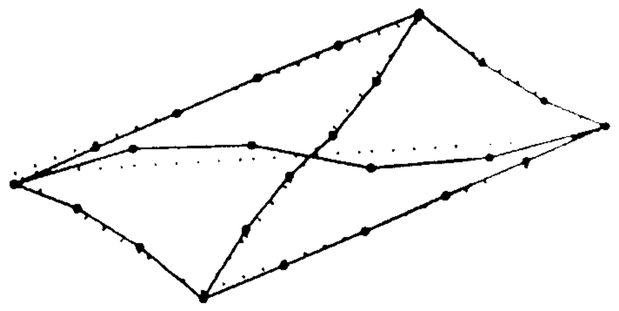

Mode 10 – 238.3Hz

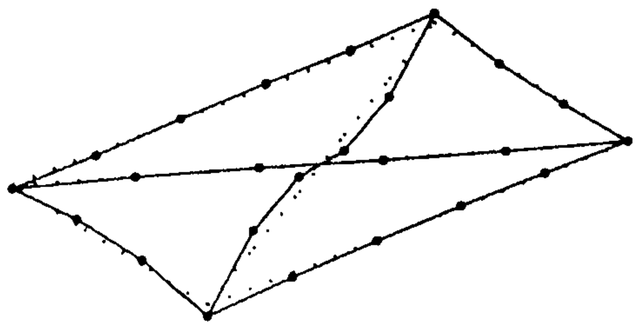

Mode 11 – 250.9Hz

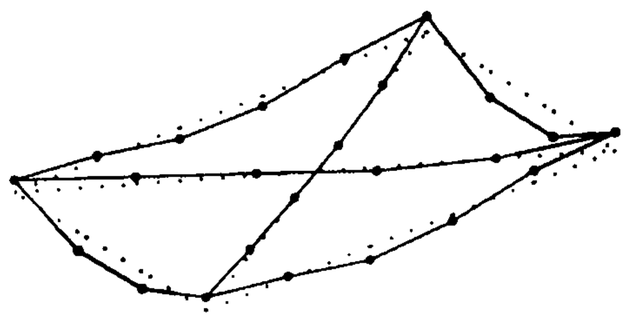

Mode 12 – 283.7Hz

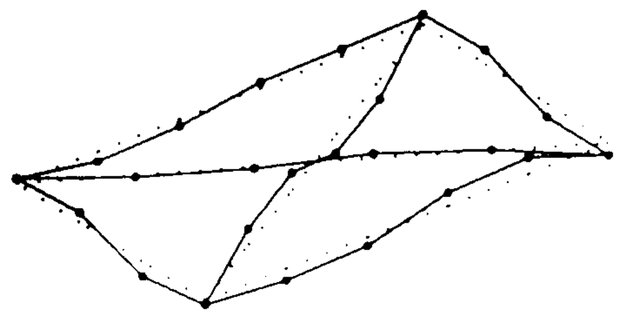

Mode 13 – 308.8Hz

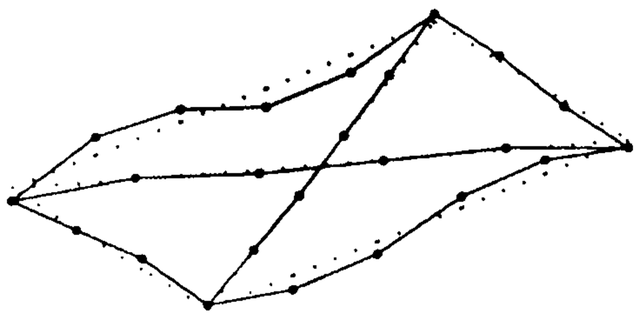

Mode 14 – 341.6Hz

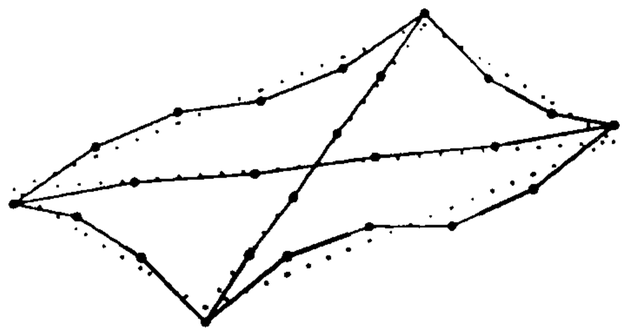

Figure 6.8 – Fourteen Identified Resonant Frequencies; Frame B Load Case 2

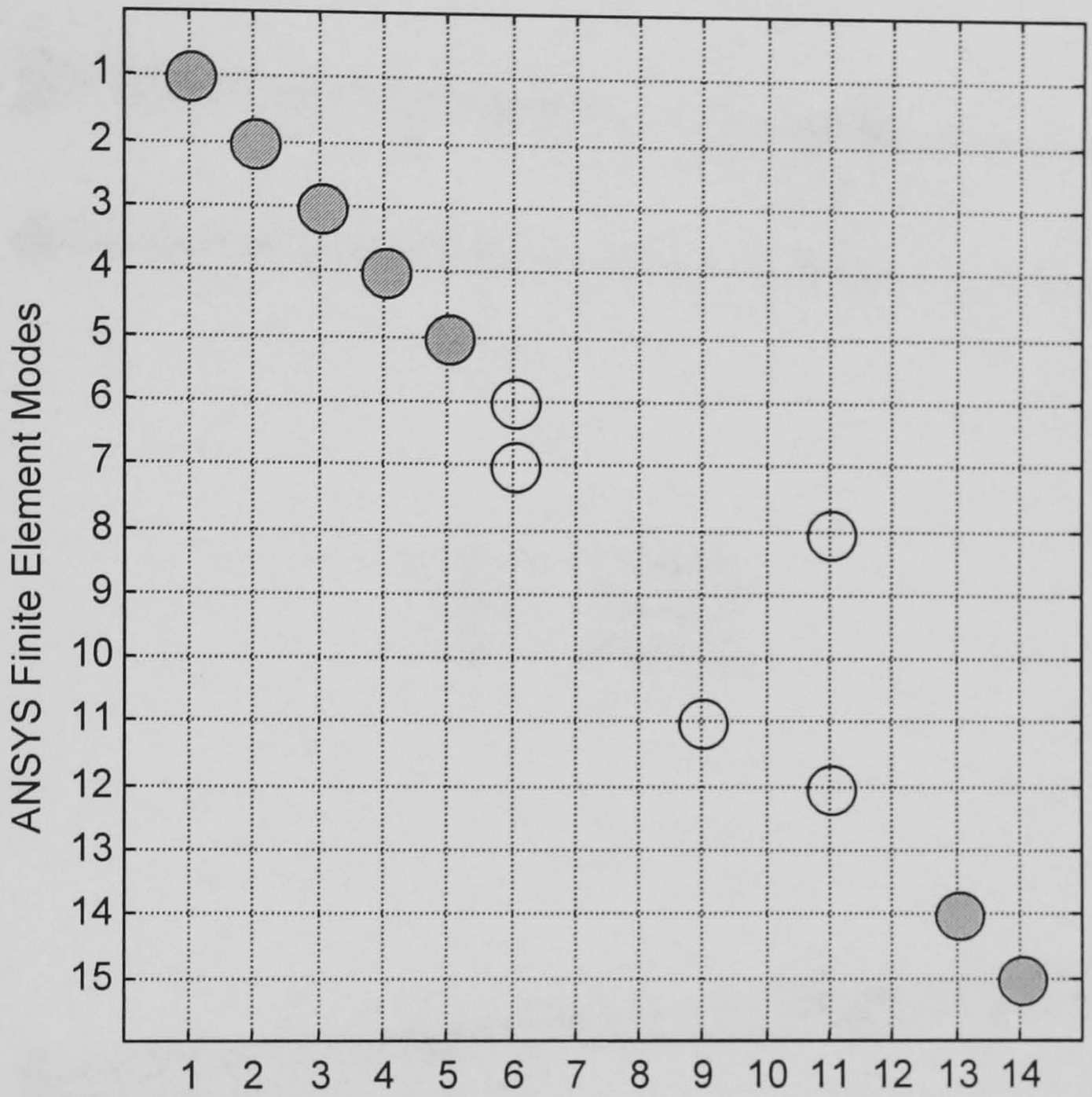

Figure 6.9 – MAC > 0.8 Between FE and Experimental Modes, Zero Load

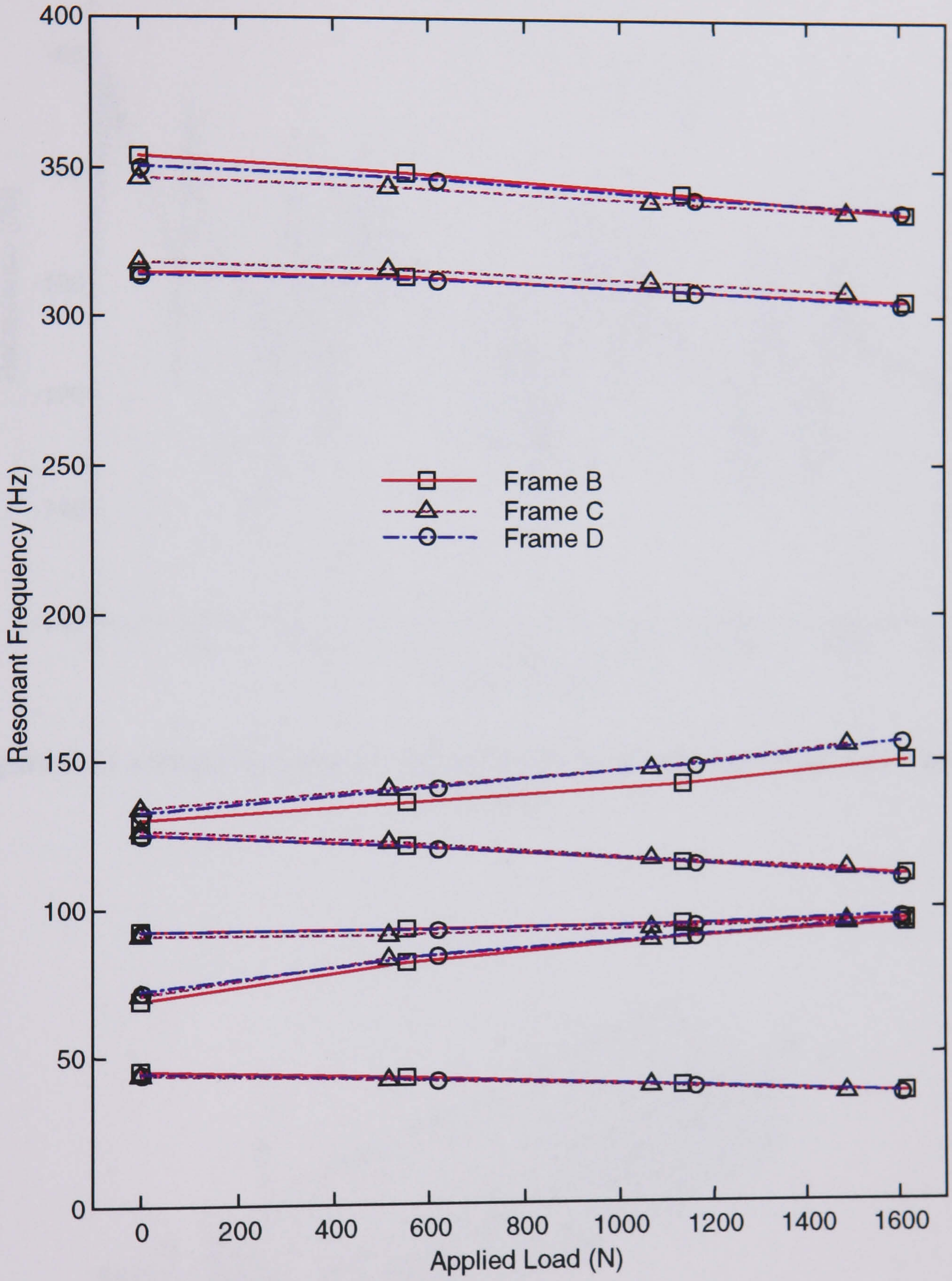

Figure 6.10 – Modal Perturbation Under Loading, Three Independent Cases First Five Modes

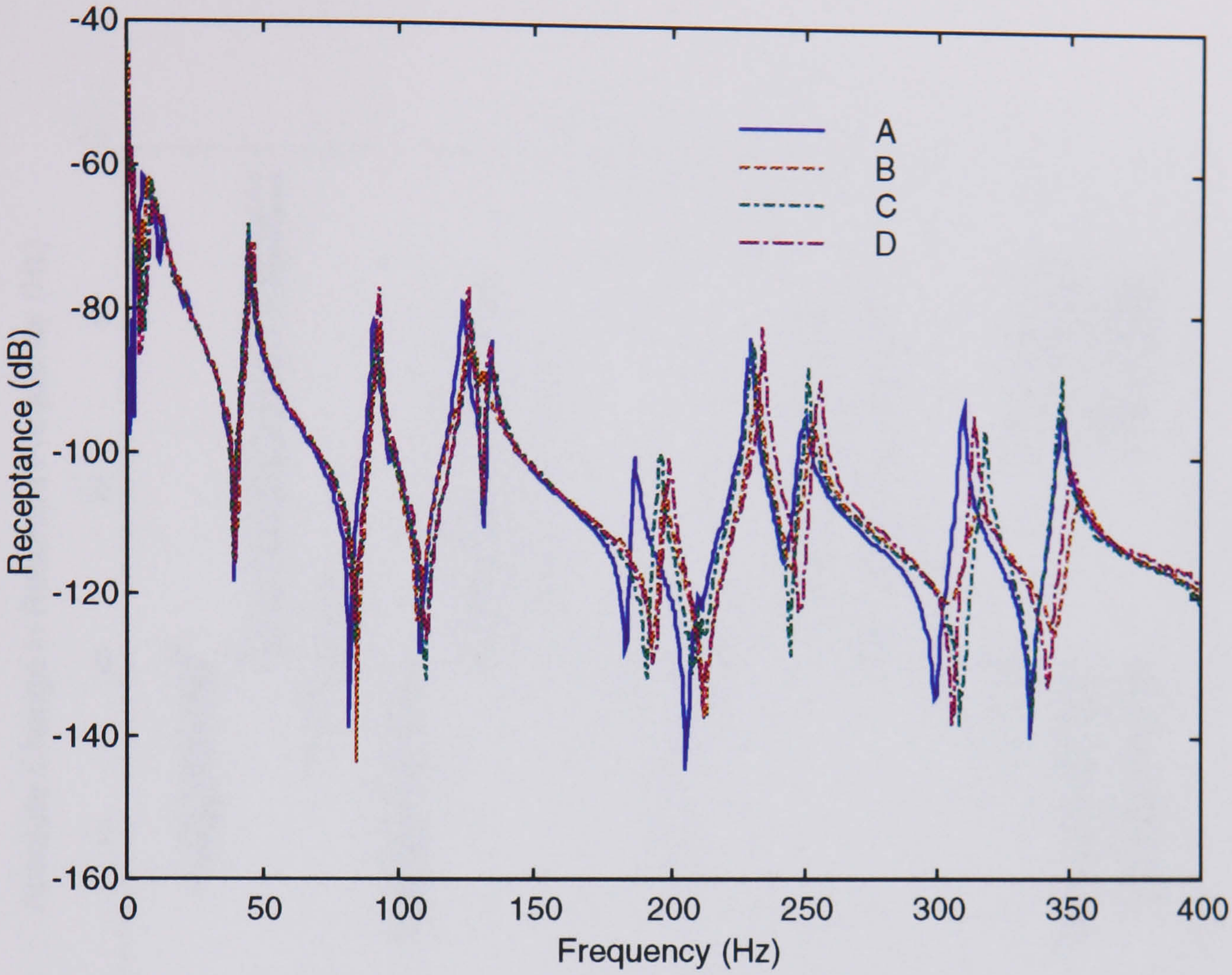

Figure 6.11 – Point Receptances From Three Nominally Identical And Unloaded Frames

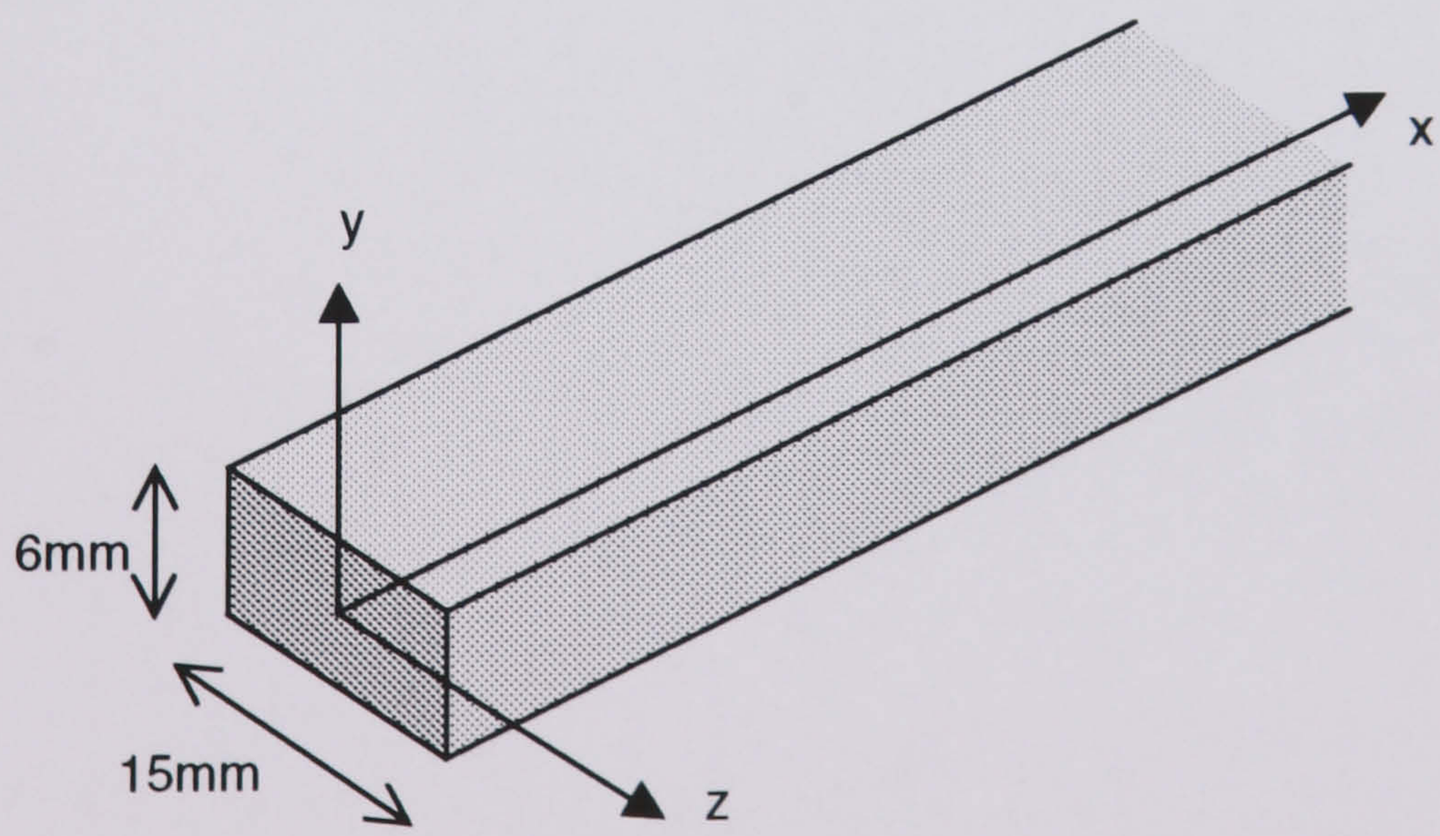

Figure 6.12 – Local Axis Definition

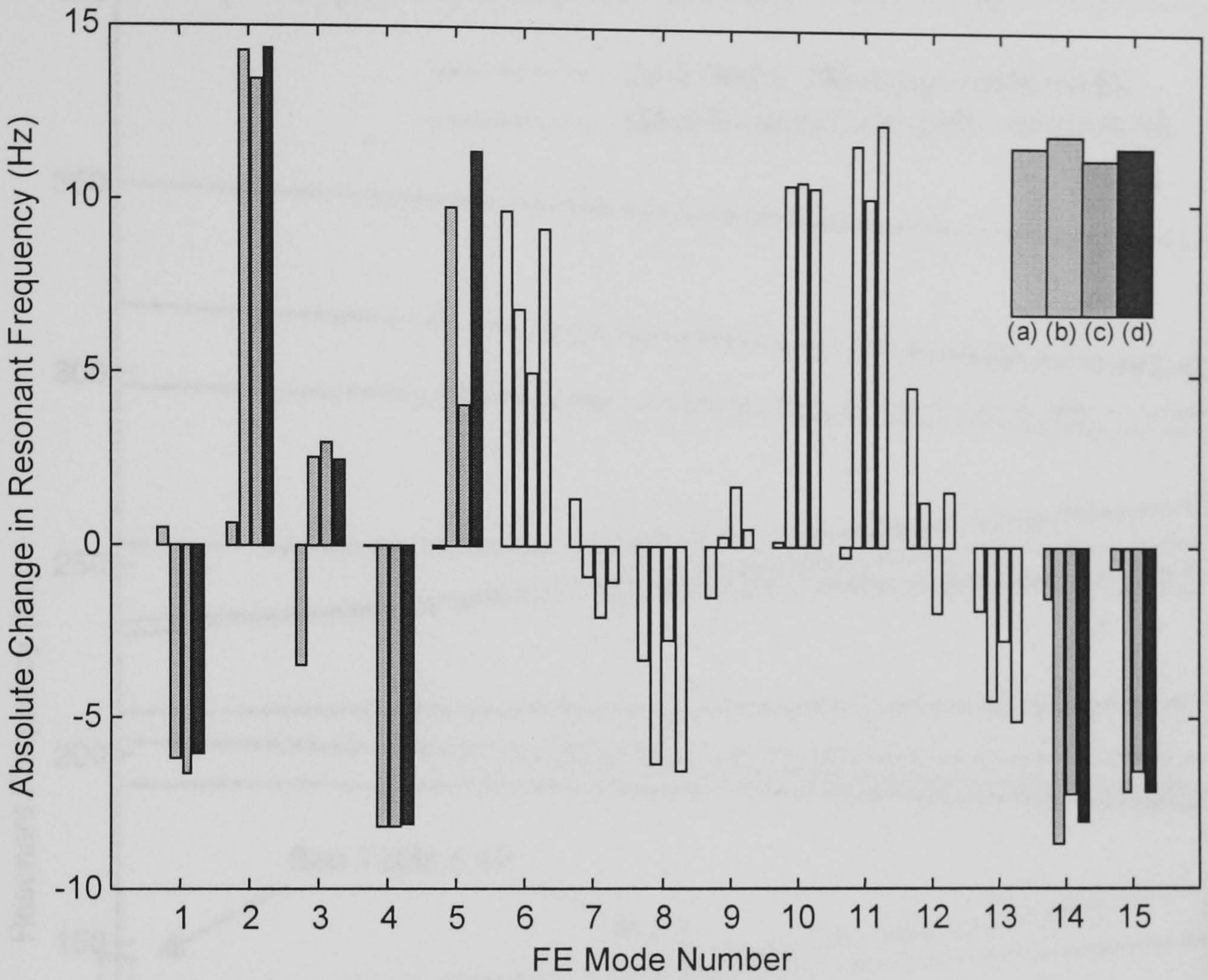

Figure 6.13 - Modal Perturbations Using Different Loading Models; 1kN Applied Load

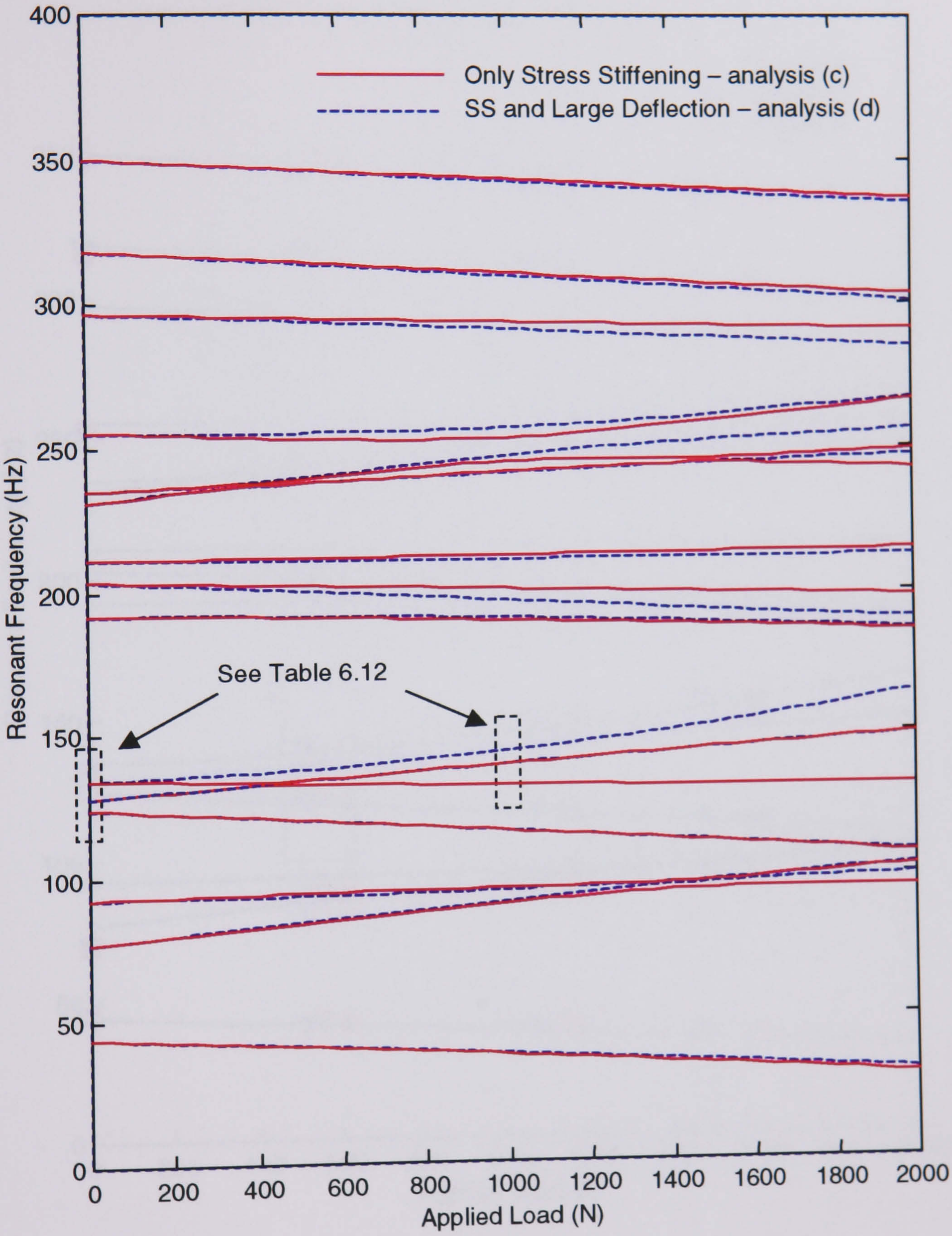

Figure 6.14 –Stress Stiffening and Large Deformation Effect on Resonant Frequencies

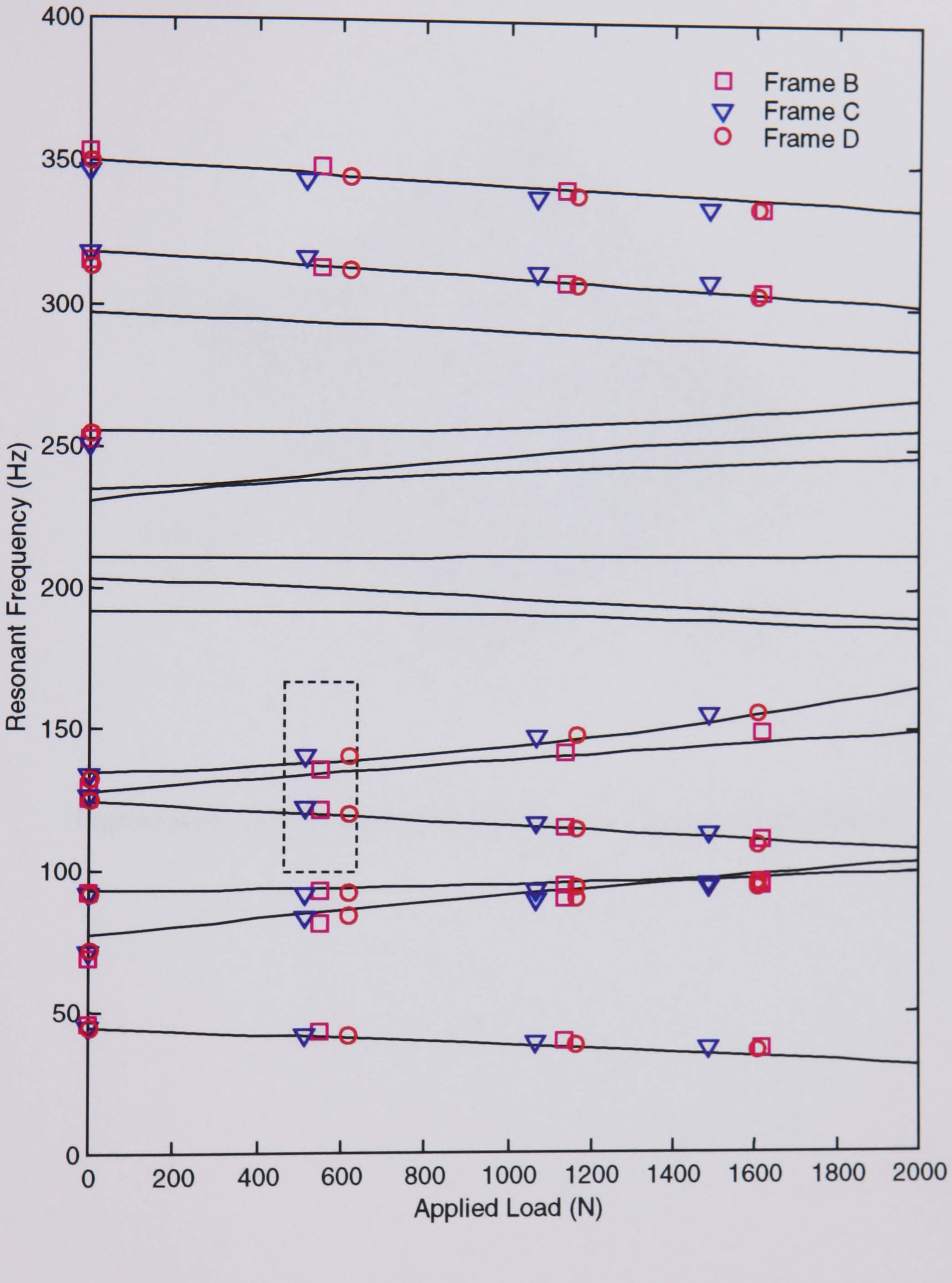

Figure 6.15 – FE and Experimental Load vs., Frequency Relationship

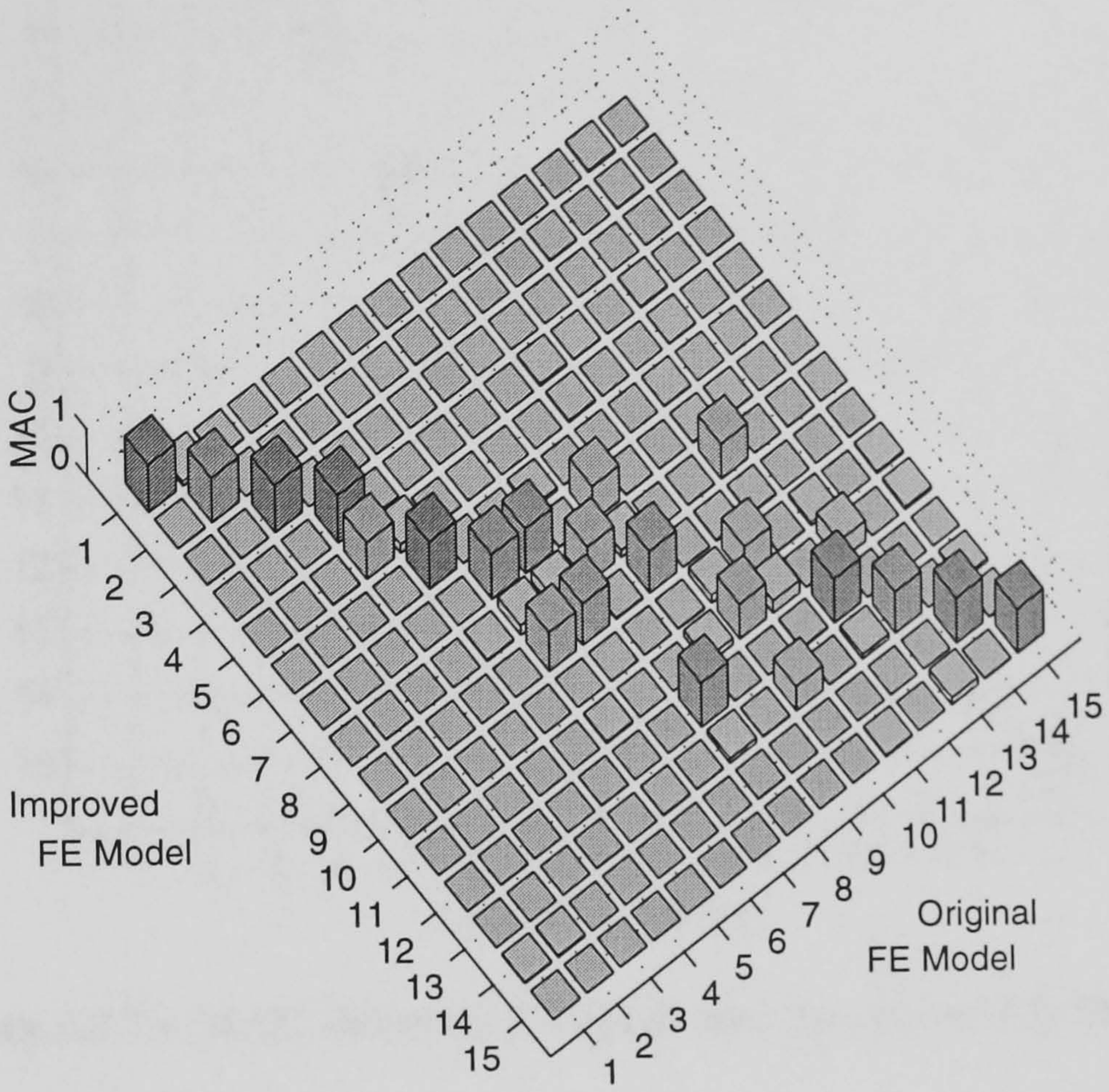

Figure 6.16 – MAC Between Original and Improved FE Models

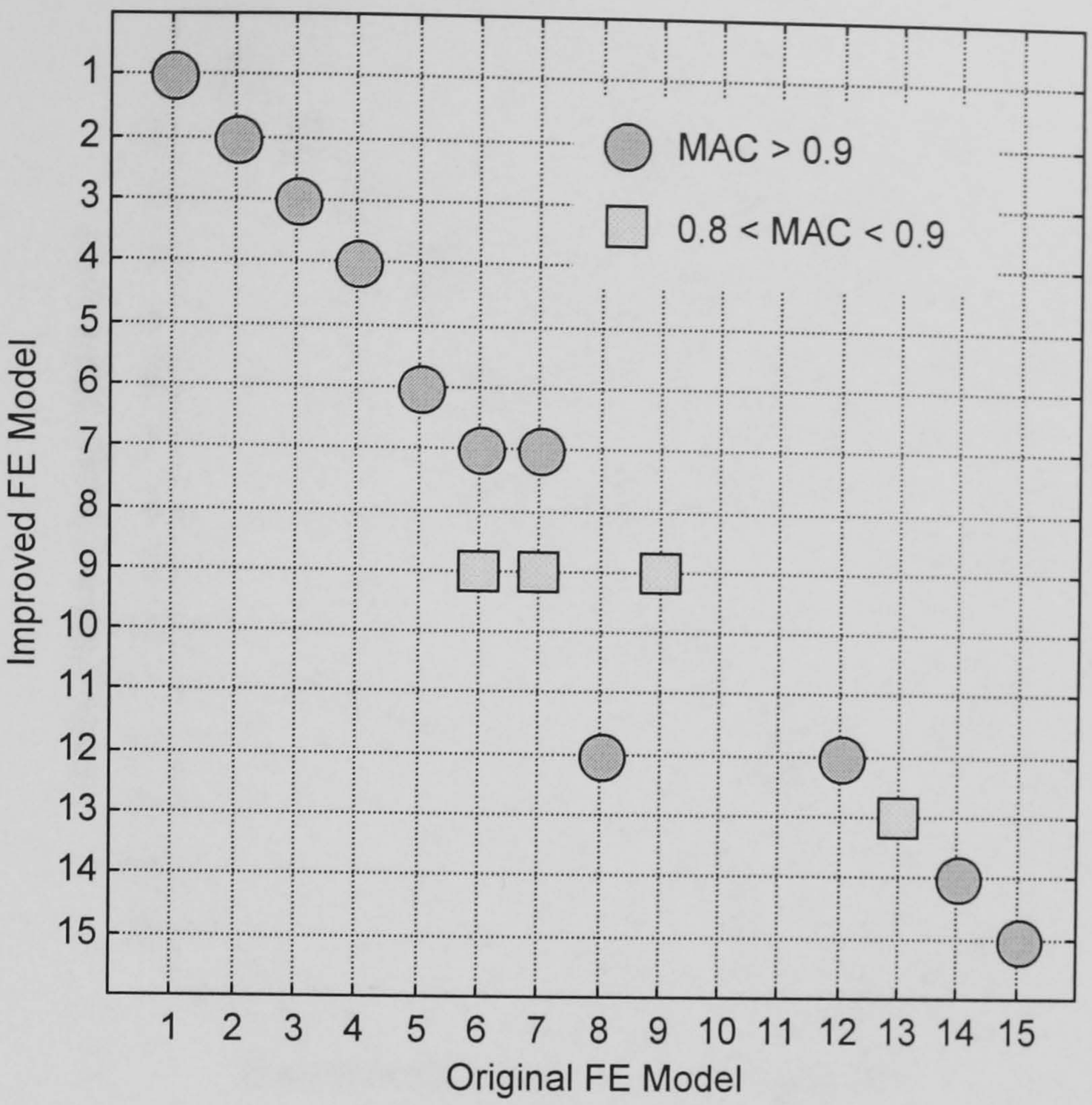

Figure 6.17 – MAC Between Original and Improved FE Models

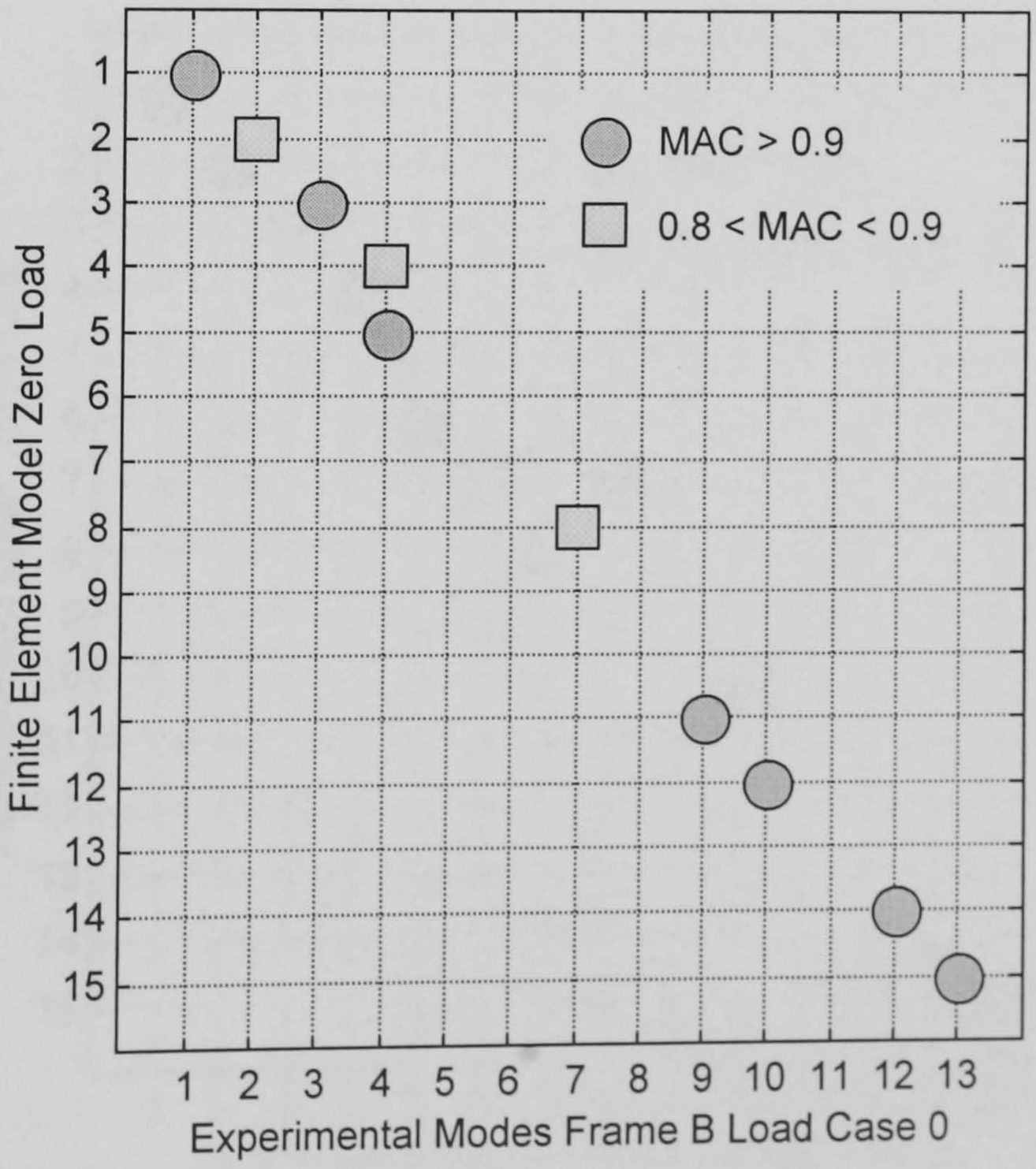

Figure 6.18 – MAC Between FE and Frame B; Zero Load

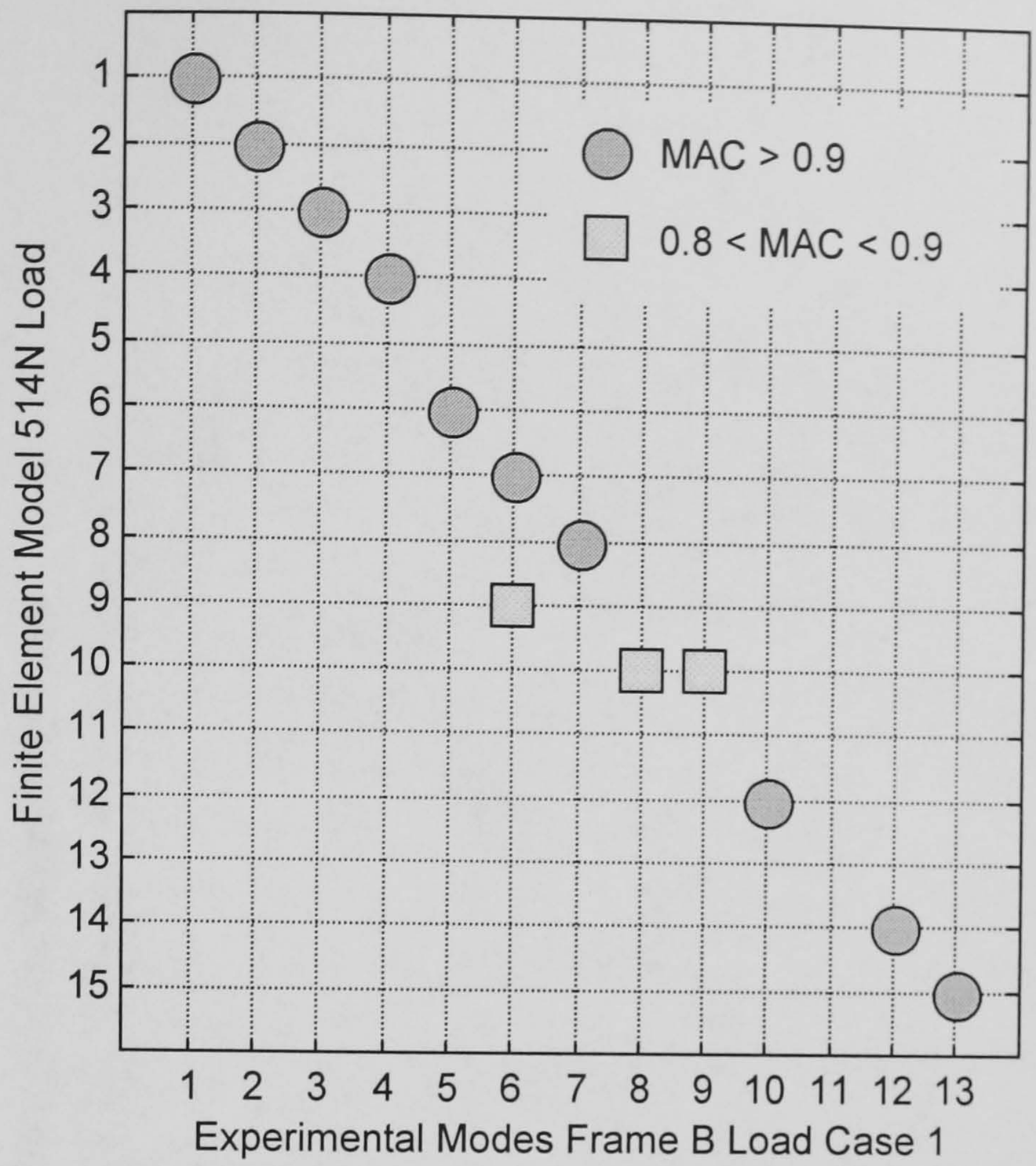

Figure 6.19 – MAC Between FE and Frame B; 514N Load

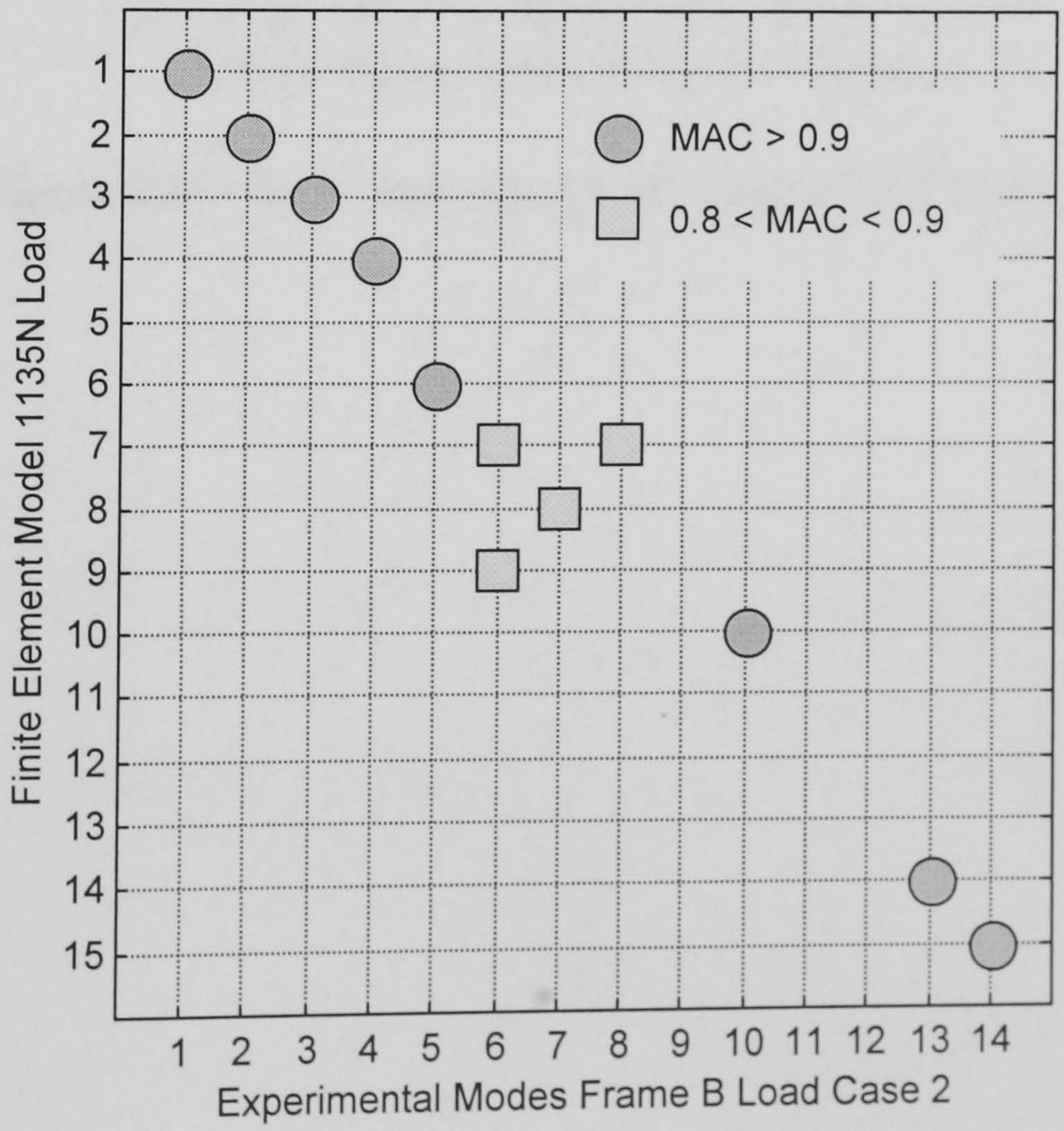

Figure 6.20 – MAC Between FE and Frame B; 1135N Load

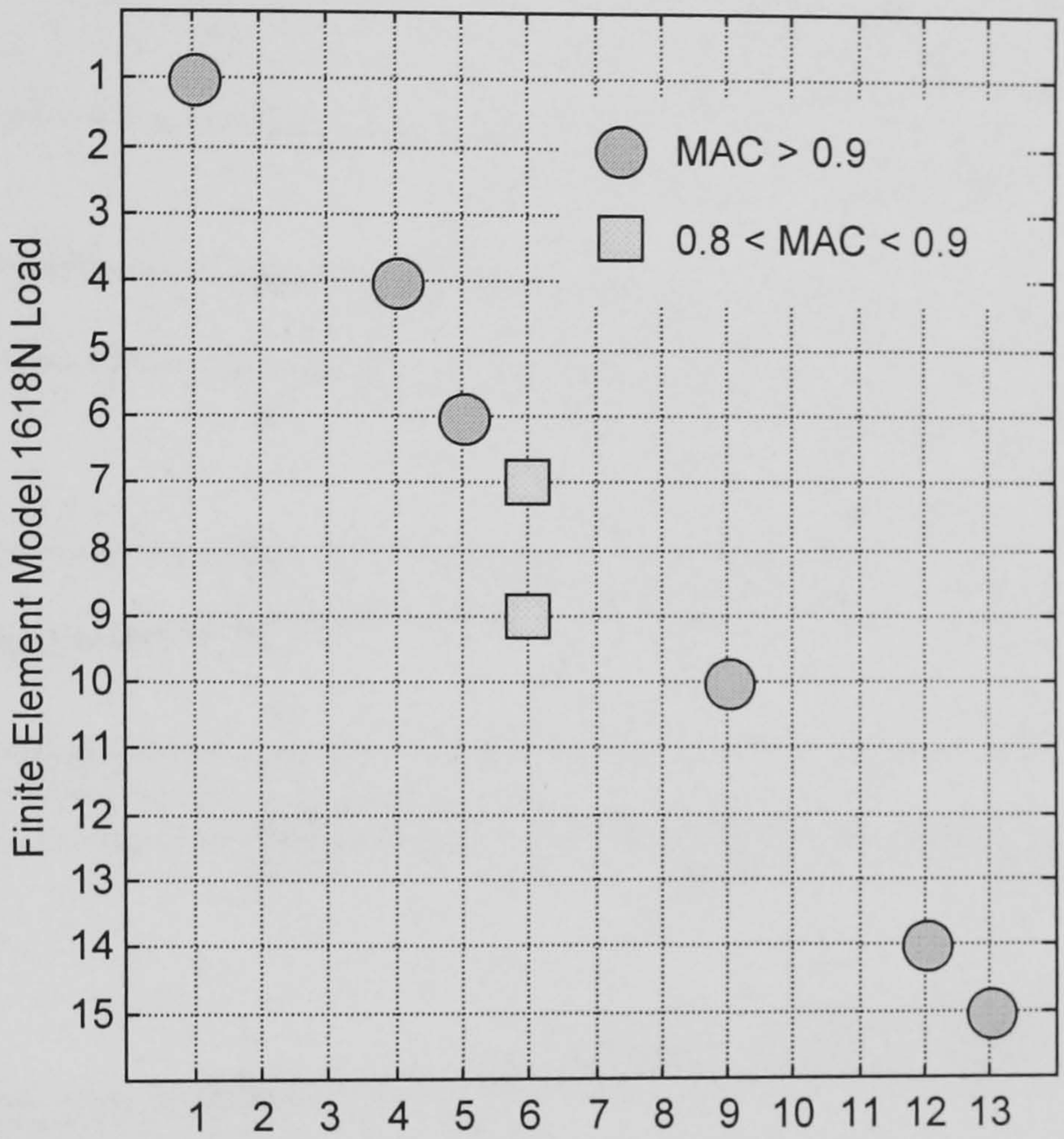

Figure 6.21 – MAC Between FE and Frame B; 1618N Load

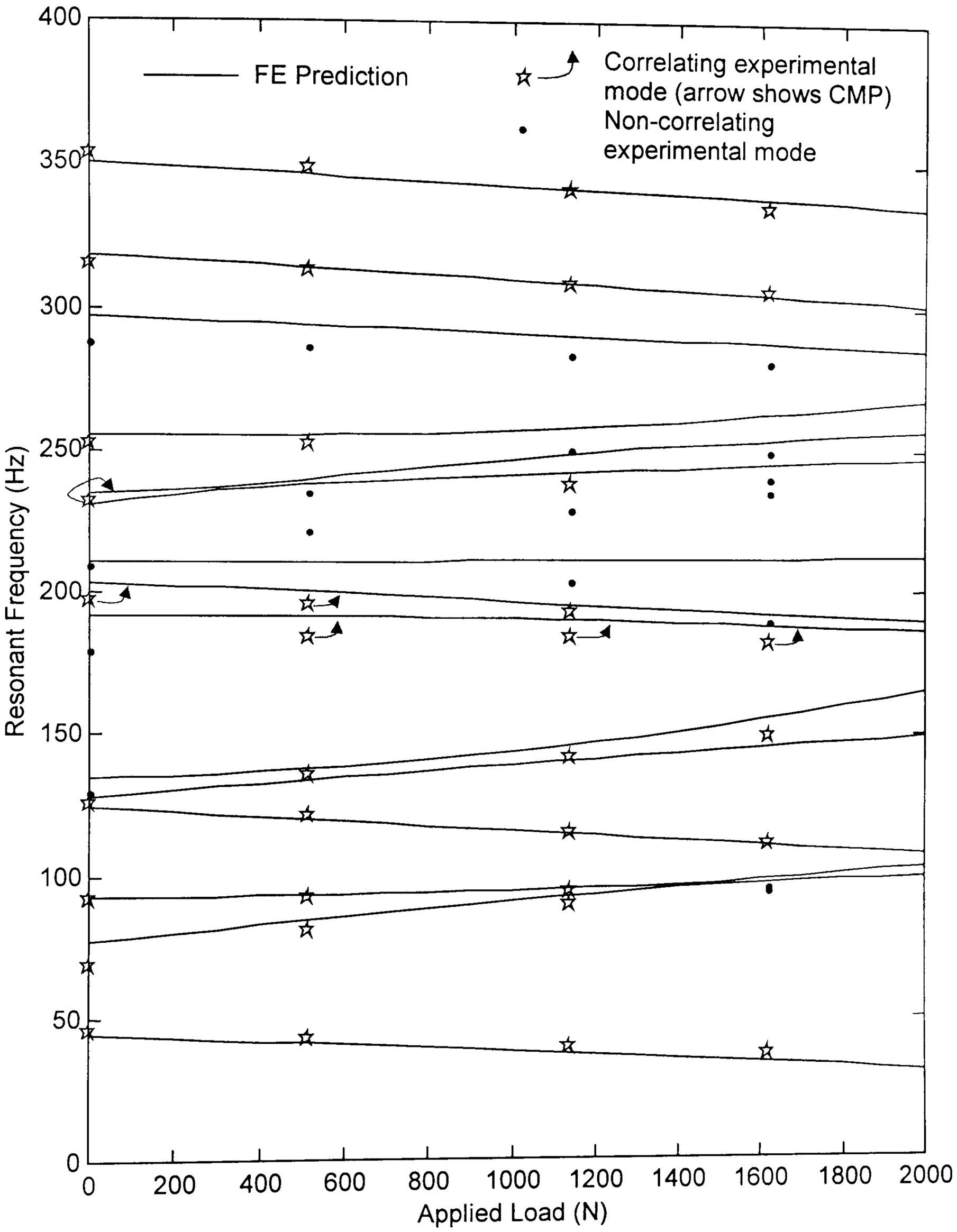

Figure 6.22 – FE and Frame B; Load vs. Frequency Relationship

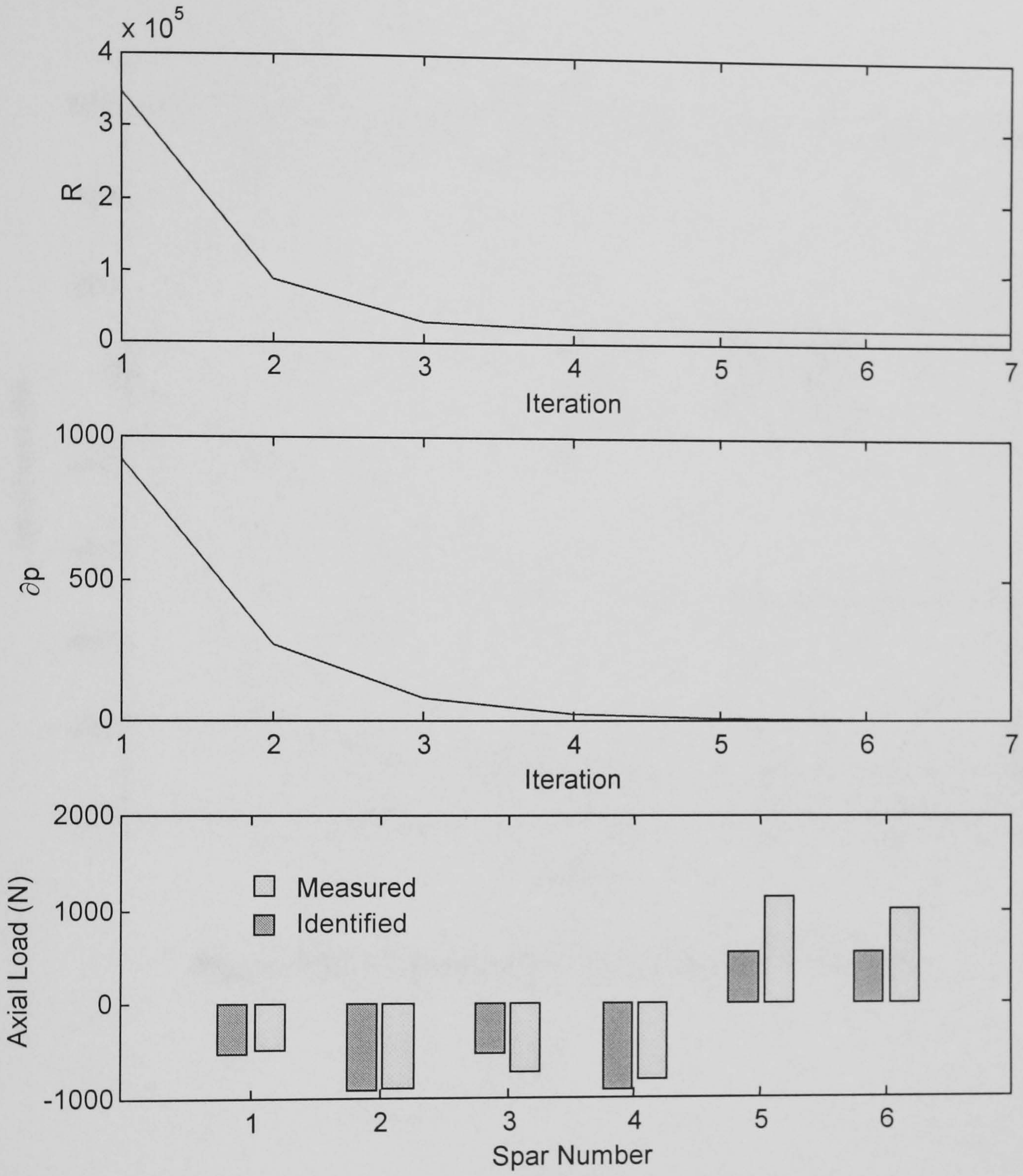

Figure 6.23 – Updated / Identified Loads

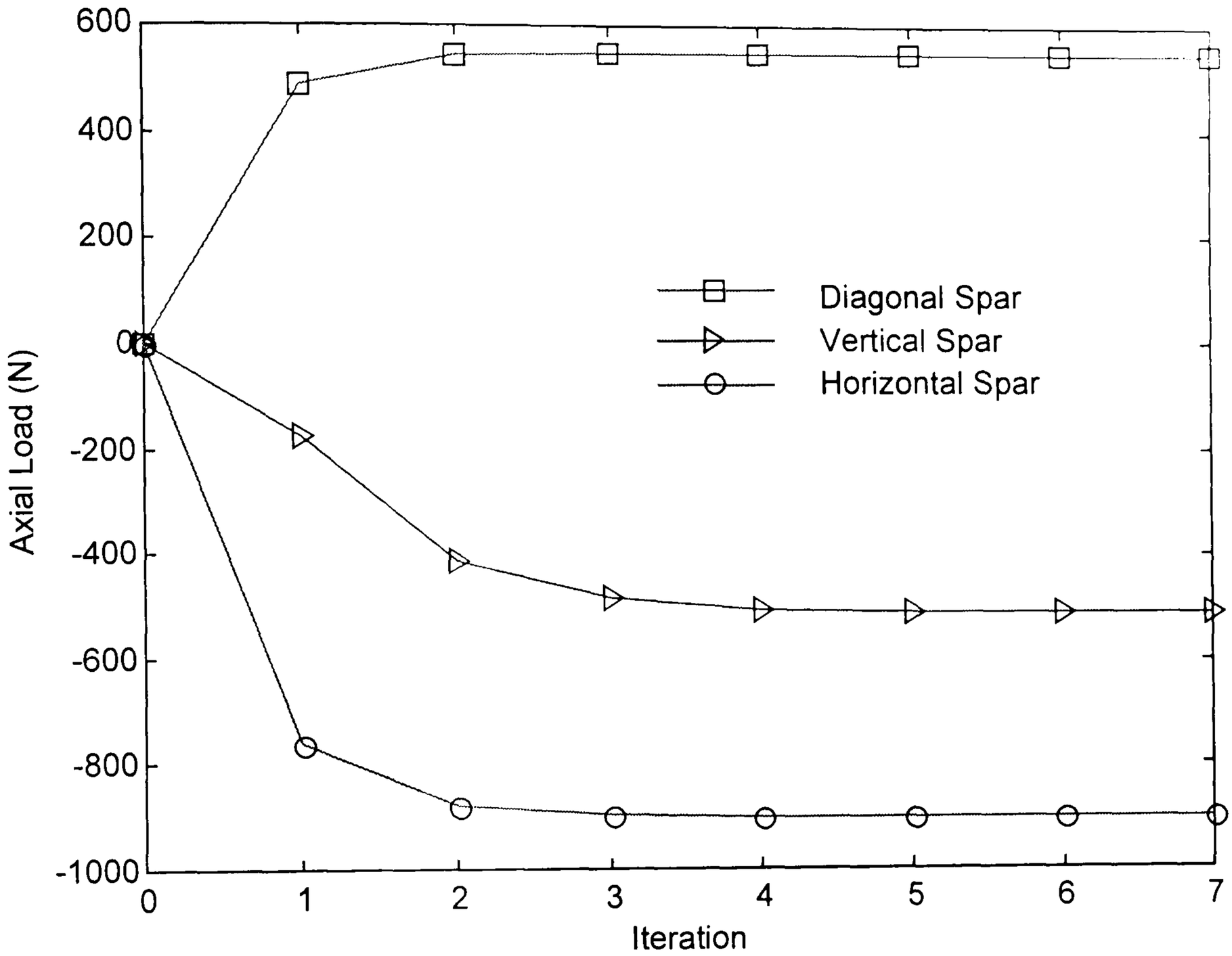

Figure 6.24 – Convergence Upon Identified Loading

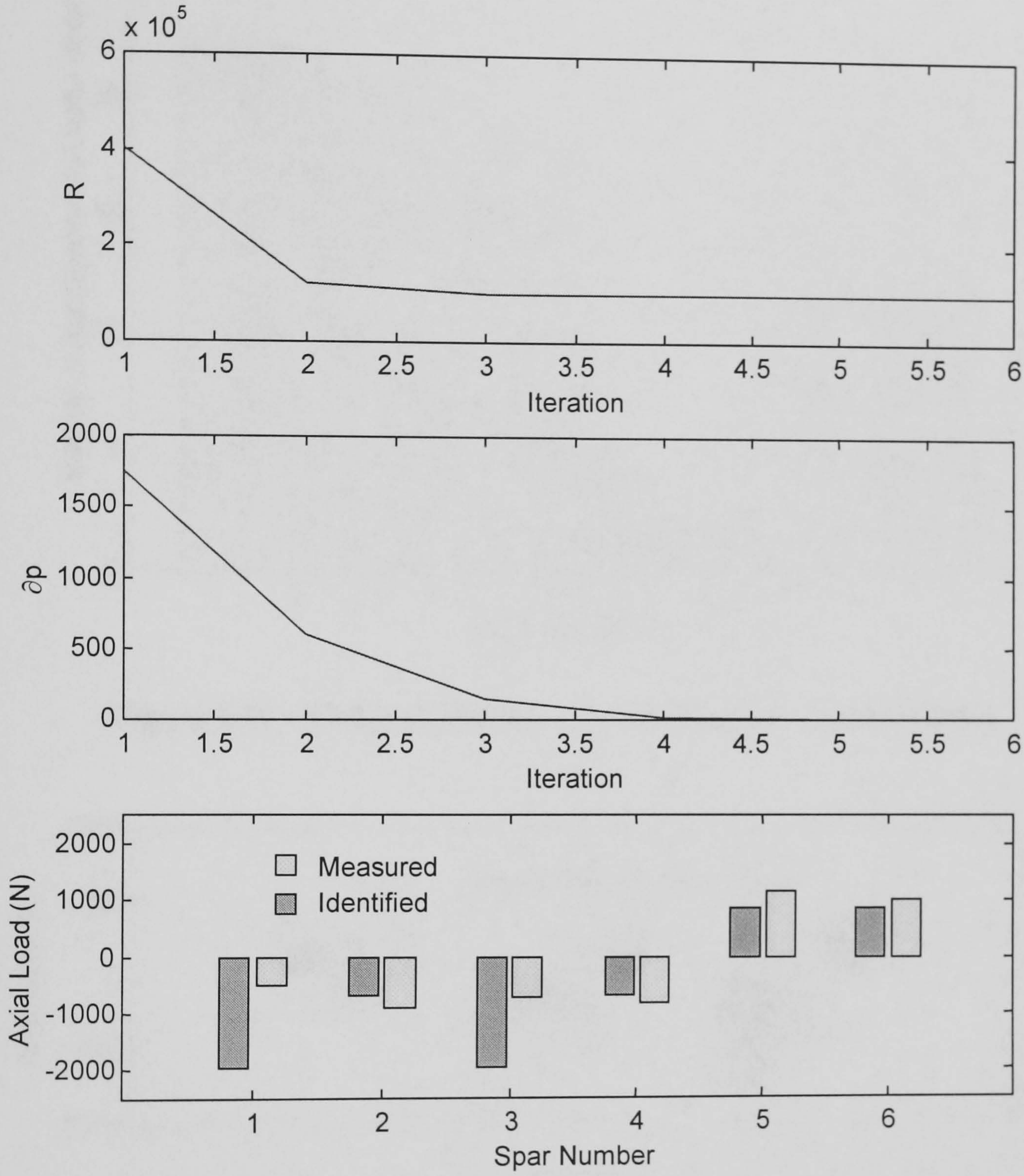

Figure 6.25 – Updated Parameters After Removing Zero Load Offset

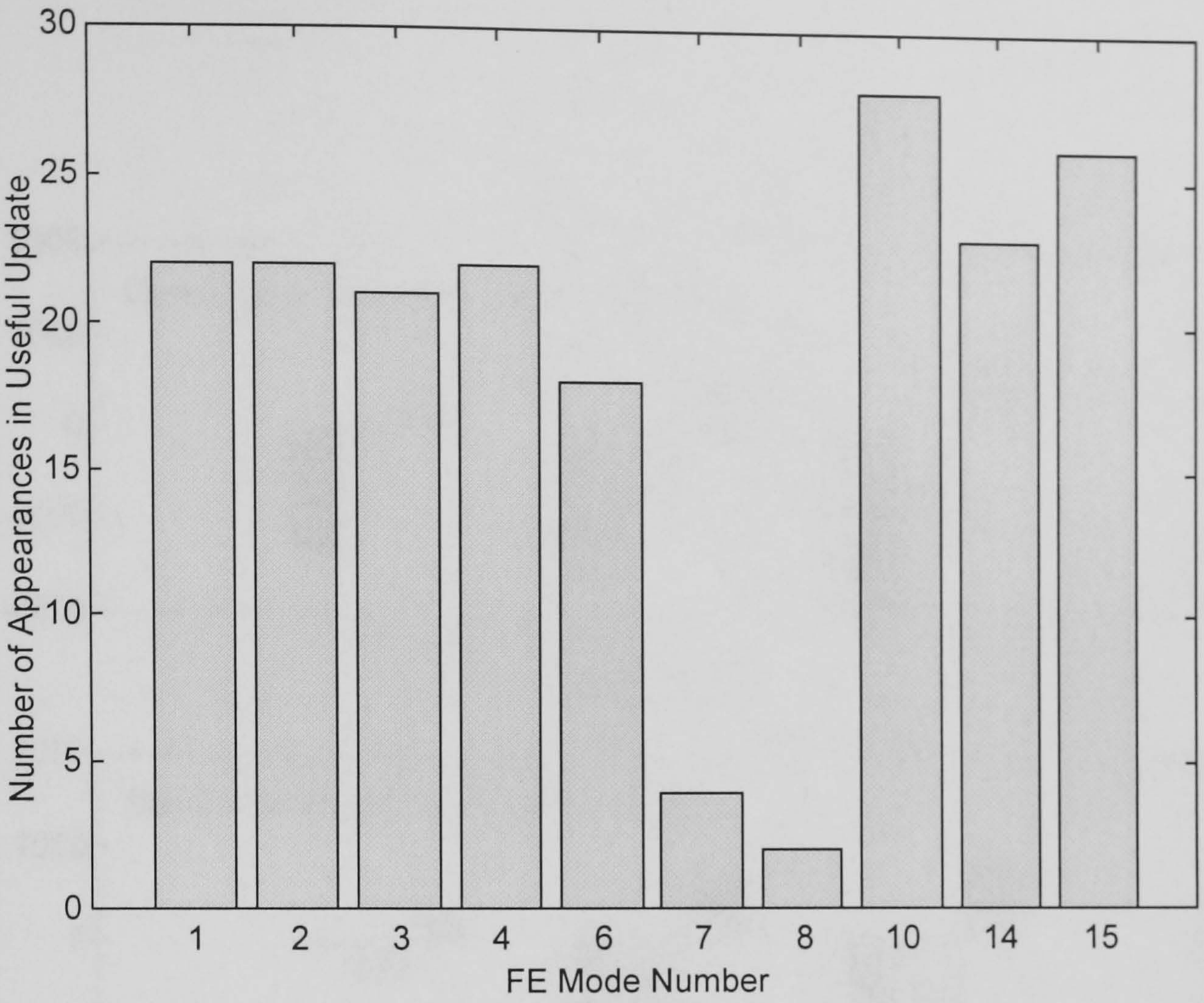

Figure 6.26 – Utility of Modes in Producing Converged Solution

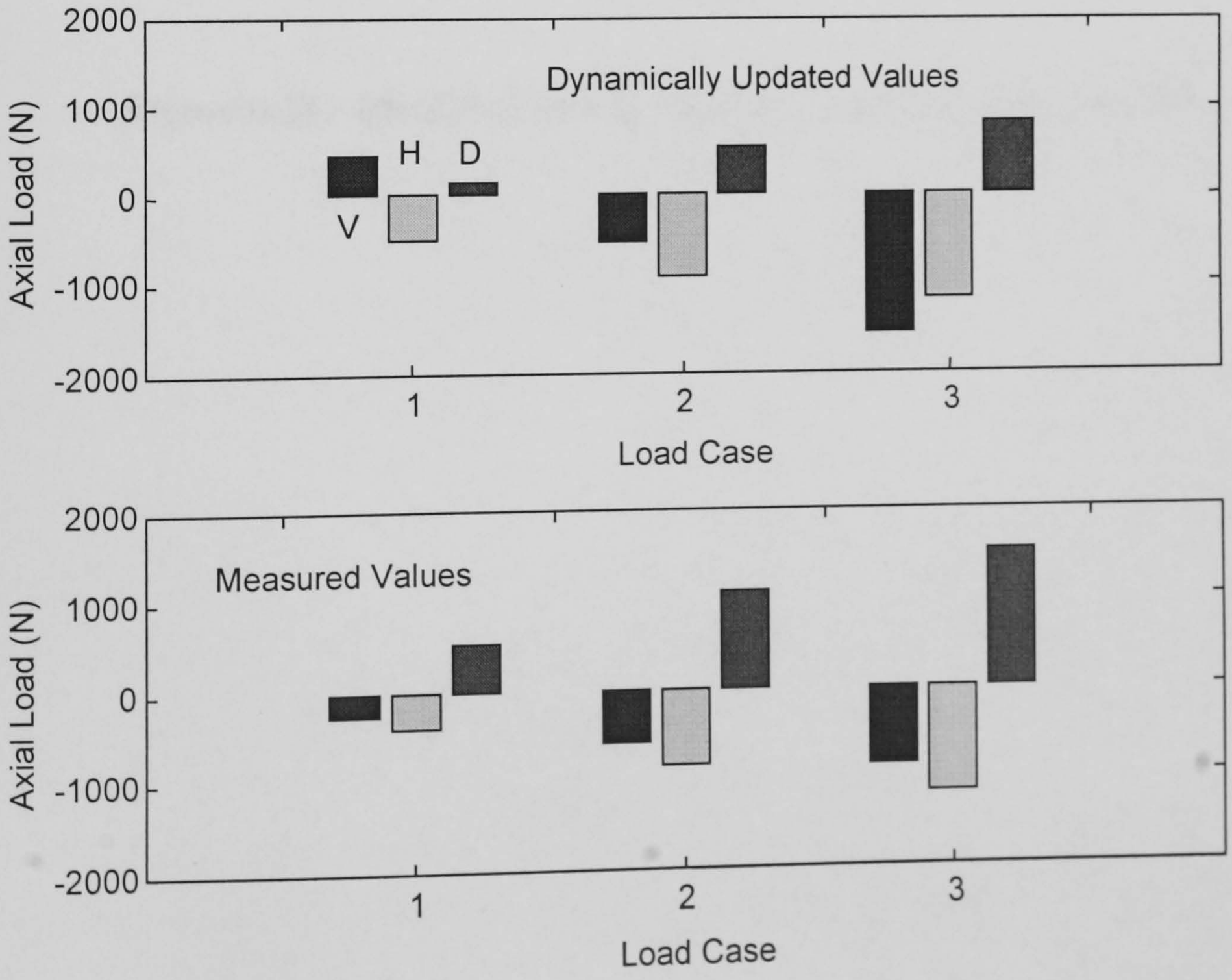

Figure 6.27 – Identified and Measured Loads; Frame B Load Cases 1-3

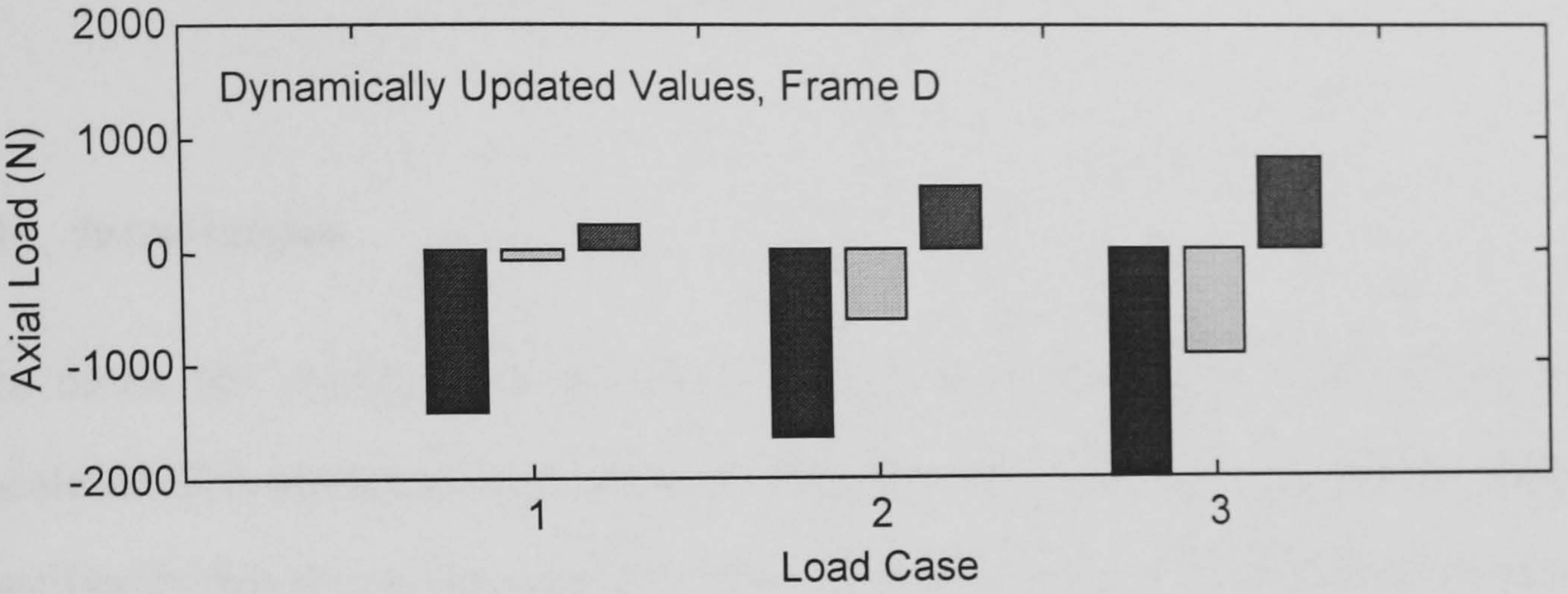

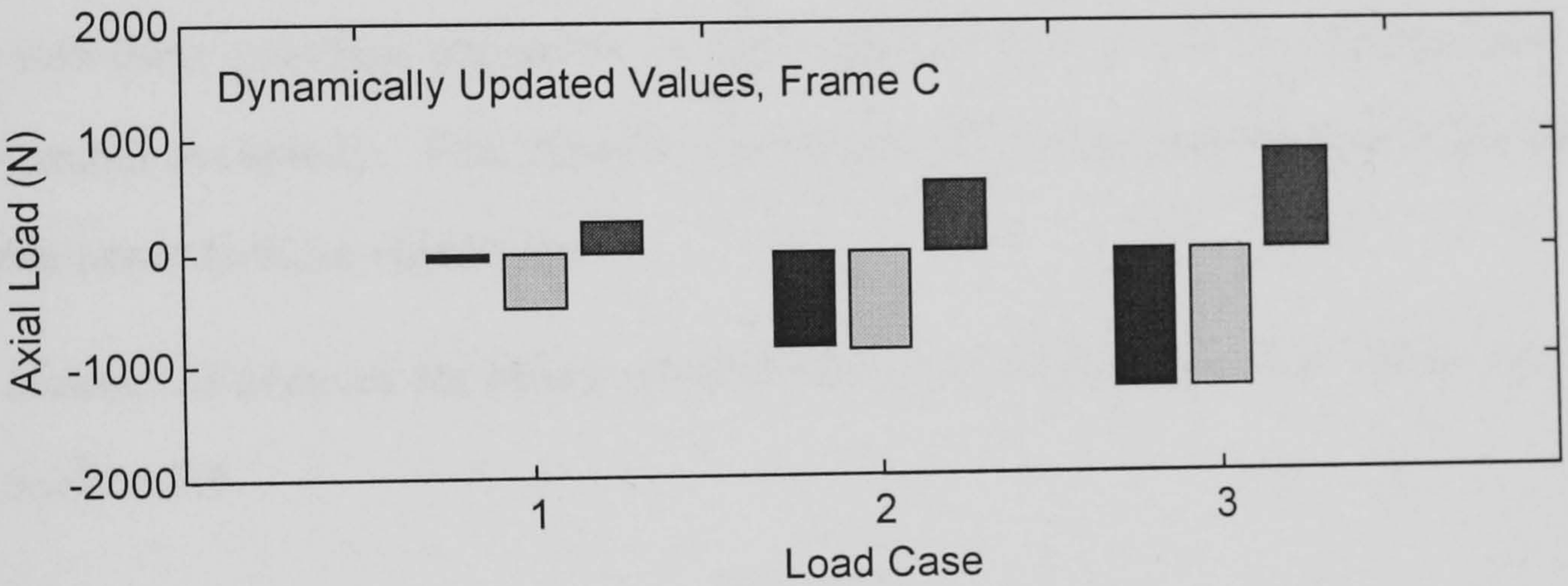

Figure 6.28 – Identified Loads; Frames C and D, Load Cases 1-3

CHAPTER 7

CONCLUSIONS

7.1 Introduction

The thesis has chiefly been motivated by the observation that little success has been encountered in updating finite element models using experimentally derived data. More specifically this thesis has sought to investigate the effect of loading upon structures and to introduce practical measures to allow finite element models to represent loaded structures accurately. This chapter summarises the contributions which this thesis has made towards these objectives.

A number of avenues for future research been opened by this thesis. These are outlined in section 7.6.

7.2 Literature Review

A review of literature related to the consideration of variability of experimental modal data has been presented. The received wisdom when comparing finite element predictions of dynamic behaviour with experimental observations, all of the error is assumed to exist in the former.

Recent consideration of variations in experimental dynamic observations has concentrated upon different behaviour arising from nominally identical structures. Few, if any authors, have studied the factors influencing time variant (transient) changes in dynamic behaviour from a single structure.

In addition to work presented in this thesis, independent observations of time varying modal characteristics have been quoted. The phenomenon has been seen to affect both

in-situ structures which are exposed to the elements and uncertain boundary conditions as well as carefully controlled laboratory based measurements.

A review of model updating technologies has been presented. Particular attention has been paid to attempts to use measured experimental data to update an initial finite element model of the structure automatically. Success has been seen to be extremely limited. While convergence upon a plausible updated model has in some cases been possible, serious doubts about the justification for and uniqueness of the updated solutions remain.

The evolution in different updating parameter types has been reviewed. Parameters that do not preserve the physical meaning of the initial finite element model have become discredited. Factors upon the mass and stiffness of individual elements or groups of elements have been popular for a number of years and continue to be so. Updating of geometric element properties has recently been suggested. In some cases finite elements are customised to model a particular structural component. The new elements are characterised by one or two parameters which can be updated. The concept of generic elements has been introduced in the last few years. This approach allows a great deal of flexibility in elemental changes with relatively few updating parameters. However, the constraint exists that the updated element is a member of the same *family* of elements as the initial element.

7.3 Effect of Load on Structures

Two case studies have produced results which conform to the expectation that dynamic loading is influenced by the level of static load. The perturbations to resonant frequencies under controlled loading are found to be significant. The extent of changes to the dynamic data taken from a loaded structure could result in erroneous parameter changes in a subsequent finite element model validation or updating exercise.

The effect of load has been shown to affect mode shapes greatly. This occurs to the extent that the modal assurance criterion between the "same" mode from a loaded

structure and from loaded experimental data indicates very little or no similarity between mode shapes.

Analysis in this thesis has shown that the resonant frequencies whose mode shapes are dramatically altered by loading effects are themselves most affected by deformation effects.

7.4 Static Updating of Loaded Structures

Static updating of structures has been defined in this thesis as follows: using measured data to characterise loading to a structure to alter the attributes of a finite element model. The goal of this approach is to generate a better representation of the loaded structure for dynamic prediction purposes.

This thesis has advocated the use of existing nonlinear geometric techniques for finite model alteration. The methods have been successfully used to match measured stresses closely with nonlinear distributions. The changes made to finite element models by nonlinear geometry techniques have also been used to match dynamic prediction of the FE model with experimental values. The method has produced a very close dynamic match of correlating modes in a situation where the load applied to the test structure is directly measurable.

The problem of identifying zero-load experimental dynamic baseline data has been introduced. A simple method to determine an estimate for the zero-load experimental data from loaded dynamic and static measurements has been presented. The technique has been shown to give satisfactory results in an experimental case study. The method is particularly suited to situations were static and dynamic measurements from structures can be taken routinely. Since developments in sensor technologies make this a likelihood, the method of identifying zero-load experimental dynamic behaviour in practice seems to be a strong and useful possibility.

7.5 Dynamic Updating of Loaded Structures

The study of static updating of loaded structures revealed that changes to the finite element model to represent loaded behaviour consisted principally of two factors namely stress stiffening and deformation. These can be included at an elemental level by addition of a stress stiffening matrix and rigid body elemental rotations.

This thesis has introduced the two elemental changes as dynamic updating parameters. Their inclusion into the sensitivity method of model has been set out. The parameters can be updated alongside traditional parameters to enable the transient effects of loading to accounted for in a test structure.

The usefulness of these parameters has been tested by means of several simulated case studies. Updating of stress stiffening has been shown to be able to identify loading successfully from no *a priori* knowledge of load levels, even under realistic levels of (additive) noise. Statically measured load information is shown to improve the success of load identification. A method has been presented which allows the engineer to decide which part(s) of a structure to instrument to provide the most useful information for dynamic updating.

The changes to resonant frequencies arising from stress stiffening effects has been shown to cause perturbations of a similar order to all resonant frequencies. The result is that the sensitivity matrix is well conditioned. It is noted that other factors such as mis-estimation of overall stiffness can cause increasingly large perturbations to resonant frequencies. To update stress stiffening parameters successfully, these other parameters should be also taken into account. Generally lower order modes have been seen to be most useful for updating stress stiffening parameters.

Updating of rigid body elemental rotations has been introduced. This technique has been shown by means of an experimental case study to correctly identify structural deformations. The method has been shown to require an initial estimate of the deformation.

An enhancement to the method whereby the rigid body rotation of a number of elements is updated has been presented. Updating of the so-called *profiles* has been shown to be useful in characterising the magnitude of pre-determined deflected shapes. The method shows great promise but further work is required to allow modes affected by deformation effects to be correlated satisfactorily.

An experimental case study has been presented in which stress stiffening parameters are updated. Experimental static load measurements allowed the correctness of identified loads to be examined. As with any updating scheme, the updated solution has been found to be a function of the parameters to be updated and the modes of vibration considered. A set of guidelines have been set out for choice of these parameters based on the experimental experience. Following these suggestions useful predictions of the level of loading in the experimental structure have been found.

7.6 Future Work

All of the methods described in this thesis have been developed, demonstrated and tested with respect to beam elements. The methods are not specific to this type of element. The opportunity exists to test the usefulness of updating load-dependent properties on structures consisting of a larger variety of element types.

The method of updating rigid body rotation profiles represents a general technique to modify structural form. This method offers an exciting new direction for model updating and should be pursued.

Related to this goal is the requirement to correlate resonant frequencies whose mode shapes differ greatly under loading. Finite element modelling of small incremental loading allows correlation of modes to be determined analytically but the author knows of no method for successfully correlating experimental modes taken at discrete load levels.

The work in this thesis has concentrated upon using the eigenvalue sensitivity method of model updating. A clear research opportunity exists to investigate the use of the new updating parameters with other updating methods.

7.7 Epilogue

This thesis has identified the effect of loading upon structures as an important factor that influences structural dynamic characteristics. This effect should be taken into account when validating and updating finite element models of structures from experimental data.

Two types of updating parameters which are philosophically different from traditional parameters have been introduced. These parameters both complement and expand the scope of existing finite element updating technologies. It is hoped that the new direction offered to model updating will help to improve the success of applying the technique to practical situations.

REFERENCES

1 **Clough R. W. Penzien J.**
Dynamics of Structures
McGraw-Hill, Inc., 1975, ISBN 0-07-113241-4

2 **Ewins D. J., Imregun M.**
State-Of-The-Art Assessment of Structural Dynamic Response Analysis Models (DYNAS)
Shock and Vibration Bulletin, Vol. 51, No. 3, 1981

3 **Maguire J.**
A Correlation Benchmark for Dynamic Analysis
Proceeding, Second International Conference "Structural Dynamics Modelling" Test, Analysis and Correlation, 1995, pp 1-12

4 **Ewins D. J.**
Modal Testing Theory and Practice
Research Studies Press

5 **Fregolent A., D'Ambrogio W., Sestieri A.**
Correlating A Finite Element Model With Tests From a Set of Sample Structures
Proceeding, Second International Conference "Structural Dynamics Modelling" Test, Analysis and Correlation, 1995, pp 53-63

6 **Ziaei-Rad S., Imregun M.**
On The Accuracy of Required Experimental Data for Finite Element Model Updating
Journal of Sound and Vibration, Vol. 196, No. 3, 1996, pp 323-336

7 **Imregun M., Ewins D. J., Hagiwara I., Ichikawa T.**
A Comparison of Sensitivity and Response Function Based Updating Techniques
Proceedings of the 12th International Modal Analysis Conference , 1994, pp 1390-1400

8 **Carne T. G., Dohrmann C. R.**
Support Conditions, Their Effect on Measured Modal Parameters
Proceedings of the 16th International Modal Analysis Conference, 1998, pp 477-483

9 **Woon C. E., Mitchell L. D.**
Variations in Structural Dynamic Characteristics Caused By Changes in Ambient Temperature: 1. Experimental
Proceedings of the 14th International Modal Analysis Conference, 1996, pp 263-274

10 **Alampalli S.**
Influence of In-Service Environment On Modal Parameters
Proceedings of the 16th International Modal Analysis Conference, 1998, pp 111-118

11 **Forward R,**
Picostrain Measurements with Piezoelectric Transducers
Journal of Applied Physics, Vol. 51, No. 11, 1980, pp 5600-5603

12 **Dosch J J,**
Piezoelectric Strain Sensor
Proceedings of the 17th International Modal Analysis Conference, 1999, pp 537-542

13 **Todd M D, Chang C C, Johnson G A, Vohra S T, Pate J W, Idriss R L,**
Bridge Monitoring Using a 64-Channel Fiber Bragg Grating System
Proceedings of the 17th International Modal Analysis Conference, 1999, pp 1719-1725

14 **MATLAB**
Version 5.2
The Mathworks, Inc., 1997

15 **CALFEM**
Version 3.2
Department of Structural Mechanics, LTH, Lund University, 1996

16 **ANSYS**
Version 5.4
Swanson Analysis Systems Inc., 1997

17 **Lieven N. A. J., Ewins D. J.**
Call for Comments: A Proposal for Standard Notation and Terminology in Modal Analysis
International Journal of Experimental Modal Analysis, Vol. 7, No. 2 1992, pp 151-156

18 **Courant R.**
Variational Methods for the Solution of Problems of Equilibrium and Vibrations
Bulletin of the American Mathematical Society, Vol. 49, 1943, pp. 1-23

19 **Turner M. J., Clough R. W., Martin H. C., Topp L. J.**
Stiffness and Deflection Analysis of Complex Structures
Journal of the Aeronautical Sciences. Vol. 23, No. 9, 1956, pp 805-823

20 **Argyris J. H., Kelsey S.**
Energy Theorems and Structural Analysis
Butterworths, London, 1960

21 **Clough R. W.**
The Finite Element In Plane Stress Analysis
Proceedings of the 2nd ASCE Conference on Electronic Computation, Pittsburgh, USA, pp 345-378

22 **Zienkiewicz O.C., Taylor R.L.**
The Finite Element Method
McGraw-Hill, 1986, ISBN 0-07-084072-5

23 **Bathe K-J.**
Finite Element Procedures in Engineering Analysis
Prentice-Hall, 1982, ISBN 0-13-317305-4

24 **Cook R. D.**
Finite Element Modelling for Stress Analysis
John Wiley & Sons, Inc. 1994 ISBN 0-471-10774-3

25 **Przemieniecki J. S,**
Theory of Matrix Structural Analysis
McGraw-Hill. Inc. 1968 ISBN 07-050904-2

26 **Cook R. D.**
Concepts and Applications of Finite Element Analysis
John Wiley & Sons, Inc. 1974 ISBN 0-471-16915-3

27 **Natke H. G.**
Updating Computational Models in the Frequency Domain Based on Measured Data; A Survey
Probabilistic Engineering Mechanics, Vol. 3, pp 28-35

28 **Imregun M., Visser, W. J.**
A Review of Model Updating Techniques
Shock and Vibration Digest, Vol. 23, pp 28-35

29 **Mottershead J. E., Friswell M. I.**
Model Updating in Structural Dynamics: A Survey
Journal of Sound and Vibration, Vol. 167, No. 2, 1993, pp 347-375

30 **Friswell M. I., Mottershead J. E.**
Finite Element Model Updating in Structural Dynamics
Kluwer Academic Publishers, 1995, ISBN 0-7923-3431-0

31 **Berman A., Nagy E.J.**
Improvement of a Large Analytical Model Using Test Data
AIAA Journal, Vol. 21, No. 8, 1983, pp 1168-1173

32 **Baruch M.**
Optimization Procedures to Correct Stiffness and Flexibility Matrices Using Vibration Tests
AIAA Journal, Vol. 16, No. 11, 1978, pp 1208-1210

33 **Levin R. I., Lieven N. A J., Waters T. P.**
Required Precision and Valid Methodologies for Dynamic Finite Element Model Updating
ASME Journal of Vibration and Acoustics, Vol. 120, No. 3, 1998, pp 733 - 741

34 **Wittrick W. H.**
Rates of Change of Eigenvalues with Reference to Buckling and Vibration Problems
Journal of the Royal Aeronautical Society. Vol. 24, 1962, 590-591

35 **Lin R. M., Ewins, D. J.**
Model Updating Using FRF data
Proceedings, 15th International Seminar on Modal Analysis - KULeuven, 1990, pp 141 - 162

36 **Fritzen C., Kiefer T.**
Localization and Correction of Errors in Finite Element Models Based on Experimental Data
Proceedings of the 17th International Seminar on Modal Analysis , 1992, pp 1581-1596

37 **Imregun M, Visser W. J.**
A technique to Update Finite Element Models Using Frequency Response Data
Proceedings of the 9th International Modal Analysis Conference , 1991, 462-468

38 **Ratcliffe M. J.**
Identification and Application of Measured Frequency Domain Data For Structural Dynamics
PhD Thesis, University of Bristol, UK. 1997

39 **Mottershead J. E, Friswell M. I., Ng G. H. T., Brandon J. A.**
Model Updating of Joints and Constraints
Mechanical Systems and Signal Processing. Vol. 10, No. 2, 1996, pp 171-182

40 **Mottershead J. E., James S.**
Updating Parameters for the Model of a Three Storey Aluminium Frame
Proceedings of the 16th International Modal Analysis Conference, 1998, pp 8-11

41 **Ahmadian H., Mottershead J. E., Friswell M. I.**
Parameterisation and Identification of a Rubber Seal
Proceedings of the 16th International Modal Analysis Conference, 1998, pp 558-564

42 **Gladwell G. M. L., Ahmadian H.**
Generic Elements Suitable for Finite Element Model Updating
Mechanical Systems and Signal Processing, Vol. 9, no. 6, 1995, pp 601-614

43 **Golub G. H., Van Loan C.F.**
Matrix Computations
John Hopkins University Press, 1989, ISBN 0-85312-130-3

44 **Maia N. M. M.,**
Fundamentals of Singular Value Decomposition
Proceedings of the 9th International Modal Analysis Conference, 1991, pp 1515-1521

45 **Cafeo J. A., Dogget S. J., Feldmaier D. A., Lust R. V., Nefske D. J., Shung H. S.**
A Design-of-Experiments Approach to Quantifying Test-to-Test Variability for a Modal Test
Proceedings of the 15th International Modal Analysis Conference, 1997, pp 598-604

46 **Cafeo J. A., Feldmaier D. A., Dogget S. J**
Considerations to Reduce Modal Analysis Test Variability
Proceedings of the 16th International Modal Analysis Conference, 1998, pp 470-476

47 **Balmès E.**
Predicted Variability and Differences Between Tests of A Single Structure
Proceedings of the 16th International Modal Analysis Conference, 1998, pp 558-564

48 **De Clerck J. P.**
Using Singular Value Decomposition to Compare Correlated Modal Vectors
Proceedings of the 16th International Modal Analysis Conference, 1998, pp 1022-1029

49 **Hoff C., Natke H. G.**
Correction of a Finite Element Model By Input-Output Measurements with Application to a Radar Tower
International Journal of Experimental Modal Analysis, Vol. 4, 1989, pp 1-7

50 **Imregun M., Ewins D. J., Hagiwara I., Ichikawa T.**
Updating the Finite Element Model of a Box Like Structure Using the Response Function Method
Proceedings of the 11th International Modal Analysis Conference , 1993, pp 434-443

51 **Lammens S., Heylen W., Sas P.**
Model Updating Using Experimental Frequency Response Functions: Case Studies
Proceeding, First International Conference "Structural Dynamics Modelling" Test, Analysis and Correlation, 1993, pp 195-204

52 **Imregun M., Sanliturk K. Y., Ewins D. J.,**
Finite Element Model Updating using Frequency Response Function Data - II. Case Studies on a Medium-Size Finite Element Model
Mechanical Systems and Signal Processing. Vol. 9, No. 2, 1995, 203-221

53 **Imregun M., Agardh L.,**
Updating of The Finite Element Model of a Concrete Highway Bridge
Proceedings of the 12th International Modal Analysis Conference, 1994, pp 1321-1328

54 **Waters T. P.**
Finite Element Model Updating Using Frequency Response Functions
PhD Thesis, University of Bristol, UK. 1995

55 **Mottershead J.**
Finite Element Model Updating - Case Studies
Automotive Modelling and NVH, 1997, pp. 51-63

56 **Imamovic N.**
Validation of Large Structural Dynamics Models Using Modal Test Data
PhD Thesis, Imperial College, 1998

57 **Allemang R. J., Brown D. L.**
A Correlation Coefficient For Modal Vector Analysis
Proceedings of the 1st International Modal Analysis Conference , 1983, pp 110 - 116

58 **Fillod R., Lallement G., Piranda J., Raynaud J. L.**
Global Method of Identification
Proceedings of the 3rd International Modal Analysis Conference, 1985, pp 1145-1151

59 **Dobson B. J.**
A Straight-Line Technique for Extracting Modal Properties From FRF Data
Mechanical Systems and Signal Processing. Vol. 1, No. 1, 1987, pp 29-40

60 **MaiaN. M. M., Silva J. M. M. (eds.)**
Theoretical and Experimental Modal Analysis
Research Studies Press Ltd., 1997, ISBN 0 86380 208 7

61 **Blevins R. D.**
Formulas for Natural Frequency and Mode Shape
Van Nostrand Reinhold 1979 ISBN 0-89874-791-0

62 **Mottershead J. E., Goh E. L., Shao W.**
On The Treatment of Discretisation Errors in Finite Element Model Updating
Proceedings, 17th International Seminar on Modal Analysis - KULeuven, 1992, pp 1245-126

63 **Friswell M. I., Mottershead J. E.**
Best Practice in Finite Element Model Updating
International Forum on Aeroelasticity and Structural Dynamics, Vol. 2, 1995, pp 1-11

64 **Williams F. W.**
An Approach to the Nonlinear Behaviour of the Members of a Rigid Jointed Plane Framework With Finite Deflections
Quarterly Journal of Mechanics and Applied Mathematics, Vol. 17, 1964, pp 451-469

65 **Euler L.**
Mechanica Sive Motus Scientia Analytice Exposita
St Petersburg, 1736

66 **Lurie H.**
Lateral Vibrations as Related to Structural Stability
Journal of Applied Mechanics, Vol. 19. 1952 pp 195-204

67 **Stephens B. C.**
Natural Vibration Frequencies of Structural Members as an Indication of End Fixity and Magnitude of Stress
Journal of the Aeronautical Sciences, Vol. 4, 1936. pp 54-56

68 **Lurie H.**
Effective End Restraint of Columns by Frequency Measurements
Journal of the Aeronautical Sciences, Vol. 19 , 1951 pp 21-22

69 **Plaut R. H., Virgin L. N.,**
Use of Frequency Data to Predict Buckling
Journal of Engineering Mechanics, Vol. 116, 1990. pp 2330-2335

70 **Warburton G. B.**
The Dynamical Behaviour of Structures
Pergamon Press Ltd., 1976, ISBN 0-08-020364-7

71 **Massonnet C.**
Le Voilement des Plaques Planes Sollicitees dans leur Plan
Final report of the International Association for Bridge and Structural Engineering, 1948, Liege

72 **Gallagher R. H., Padlog J.**
Discrete Element Approach to Structural Stability Analysis
AIAA Journal, Vol. 1, no 6 1963. pp 1437-1439

73 **Ryu J., Kim S-S., Kim S-S.**
A Criterion on Inclusion of Stress Stiffening Effects in Flexible Multibody Dynamic System Simulation
Computers and Structures, Vol. 62, no 1 1997. pp 1035-1048

74 **Greening P. D., Lieven N. A J.**
The Effect of Pre-Load and Associated Deformation On The Stability of A Simple Updating Problem
Proceedings of the 15th International Modal Analysis Conference , 1997, pp 434-443

75 **Turner M. J., Dill E. H., Martin H. C., Melosh R. J.**
Large Deflections of Structures Subjected to Heating and External Loads
Journal of the Aero/Space Sciences, 1960. pp 97-127

76 **Jennings A.**
Frame Analysis Including Change of Geometry
Proceedings of the ASCE, Journal of the Structural Division, 1968 vol. 94 pp 627 644

77 **Rankin C. C., Brogan F. A.**
An Element Independent Corotational Procedure for the Treatment of Large Rotations
Journal of Pressure Vessel Technology. Vol. 108, 1986 pp 165-174

78 **Bergan P. G., Clough R. W.**
Convergence Criteria for Iterative Processes
AIAA Journal, Vol. 10, No. 8, 1972, pp 1107-1108

79 **Lamb H.,**
On The Flexure and the Vibrations of a Curved Bar
The Proceedings of the London Mathematical Society, XIX, 1889. pp 365-376

80 **Den Hartog J. P.**
The Lowest Natural Frequencies of Circular Arcs
Philosophical Magazine, Vol. 5, 1928. pp 400-408

81 **Cook S. E., Ventura C. E.**
Dynamic Strain Measurement of The Lindquist Bridge
Proceedings of the 17th International Modal Analysis Conference, 1999, pp 1707-1712

82 **Greening P. D., Lieven, N. A. J., Vann A. M.**
Effect of a Pre-Load on the Dynamic Properties of a Simple Structure
Proceedings of the 2nd International Conference "Structural Dynamics Modelling: Test, Analysis and Correlation, Cumbria, 1996 pp 391-401

83 **Nelder J. A., Mead R.**
A Simplex Method for Function Minimization
The Computer Journal. Vol. 7, 1996 pp 308-313

84 **Link M.**
Updating of Analytical Models – Basic Procedures and Extensions
Main Lectures and Papers, NATO Advanced Study Institute: Modal Analysis and Testing, Sesimbra, Portugal, May 1998, pp 335-355

85 **Heylen W., Lammens S.**
FRAC: A Consistent Way of Comparing Frequency Response Functions
Proceedings of Identification in Engineering Systems, Swansea, 1996 pp 48-57

86 **Lieven N. A. J., Ewins D. J.**
Spatial Correlation of Mode Shapes, the Co-ordinate Modal Assurance Criterion
Proceedings of the 6th International Modal Analysis Conference, 1988, pp 690-695

87 **ICATS**
Imperial College Analysis and Testing Software
Imperial College, London, UK.

88 **Jackson N., Ravindra K. D. (eds.)**
Civil Engineering Materials
The Macmillan Press Ltd., 1976, ISBN 0-333-46501-6

APPENDIX A

FINITE ELEMENT FORMULATION

A method for deriving elemental stiffness matrices from assumed displacement fields is given below, the method described is general for all elements. While this derivation is available in many text books the terminology and nomenclature vary a great deal and a concise understanding of the theory underlying the formation of finite element matrices is very valuable.

The displacement at the point

$$\{x\} = \begin{Bmatrix} x \\ y \\ z \end{Bmatrix} \tag{A.1}$$

is given by

$$\{u\} = \begin{Bmatrix} u \\ v \\ w \end{Bmatrix}, \tag{A.2}$$

where $u = u(x)$ etc.

The six components of strain at some point are given by the vector

$$\{\varepsilon\} = \begin{Bmatrix} \varepsilon_x \\ \varepsilon_y \\ \varepsilon_z \\ \varepsilon_{xy} \\ \varepsilon_{yz} \\ \varepsilon_{zx} \end{Bmatrix}, \tag{A.3}$$

similarly the vector of stresses is

$$\{\sigma\} = \begin{Bmatrix} \sigma_x \\ \sigma_y \\ \sigma_z \\ \sigma_{xy} \\ \sigma_{yz} \\ \sigma_{zx} \end{Bmatrix}. \tag{A.4}$$

Defining the displacements of n discrete co-ordinates in some direction

$$\{\Delta\} = \begin{Bmatrix} \Delta_1 \\ \Delta_2 \\ \Delta_3 \\ \vdots \\ \Delta_n \end{Bmatrix} \tag{A.5}$$

where the nodal displacements of a single element will be expressed with the subscript e $\{\Delta\}_e$.

The overall nodal force vector is:

$$\{F\} = \begin{Bmatrix} F_1 \\ F_2 \\ F_3 \\ \vdots \\ F_n \end{Bmatrix}, \tag{A.6}$$

the elemental force in local elemental co-ordinates is $\{\mathrm{F}\}_e$, n in this case is the number of elemental degrees of freedom.

The strain energy is given by:

$$\int \{\varepsilon\}^T \{\sigma\} dV \tag{A.7}$$

and force displacement relationship:

$$\{F\}_e = [K]_e [\Delta]_e \tag{A.8}$$

Using a virtual work argument equating work done by external forces $\{F\}_e$ in moving virtual displacements $\{\hat{\Delta}\}_e$ with its internal work in creating virtual strains $\{\hat{\varepsilon}\}$ gives

$$\int_V \{\sigma\}^T \{\hat{\varepsilon}\} dV = \{\hat{\Delta}\}_e^T \{F\}_e . \tag{A.9}$$

The stresses and strains are related by

$$[\sigma] = [E][\varepsilon], \tag{A.10}$$

where [E] is the *material property matrix* which for an isotropic material can be shown [89] to be

$$[E] = \frac{E}{(1-2\gamma)(1+\gamma)} \begin{bmatrix} 1-\gamma & \gamma & \gamma & 0 & 0 & 0 \\ & 1-\gamma & \gamma & 0 & 0 & 0 \\ & & 1-\gamma & 0 & 0 & 0 \\ & & & \frac{1}{2}-\gamma & 0 & 0 \\ & & & & \frac{1}{2}-\gamma & 0 \\ sym & & & & & \frac{1}{2}-\gamma \end{bmatrix} \tag{A.11}$$

where E is the Young's elastic modulus and γ is Poisson's ratio both of which are properties of the material. The relationship between strain and displacement is given by

$$\{\varepsilon\} = [\partial]^T \{u\} \tag{A.12}$$

where $[\partial]$ is a matrix of differential operators:

$$[\partial] = \begin{bmatrix} \frac{\partial}{\partial x} & 0 & 0 & \frac{\partial}{\partial y} & 0 & \frac{\partial}{\partial z} \\ 0 & \frac{\partial}{\partial y} & 0 & \frac{\partial}{\partial x} & \frac{\partial}{\partial z} & 0 \\ 0 & 0 & \frac{\partial}{\partial z} & 0 & \frac{\partial}{\partial y} & \frac{\partial}{\partial x} \end{bmatrix} \tag{A.13}$$

The elemental stiffness matrix for a particular element is characterised by a shape function $[N]_e$. This relates the general displacement to the displacement of elemental degrees of freedom.

$$\{u\} = [N]_e \{\Delta\}_e \tag{A.14}$$

Combining equations (A.8) - (A.13) gives

$$\{\hat{\Delta}\}_e^T \{F\}_e = \{\hat{\Delta}\}_e^T \left(\int_V \left([\partial][N]_e^T [E][\partial]^T [N]^e \right) dV \right) \{\hat{\Delta}\}_e \tag{A.15}$$

substituting

$$[B] = [\partial]^T [N] \tag{A.16}$$

where [B] is known as the *strain-displacement matrix* and recalling that the nodal displacements are arbitrary, equation A.15 gives

$$\{F\}_e = [K]_e \{\Delta\}_e, \tag{A.17}$$

where $[K]^e$ is the elemental stiffness matrix and is hence given by

$$[K]_e = \int_V \left([B]^T [E][B] \right) dV \tag{A.18}$$

Elemental strain can be found from (A.12) and (A.14)

$$\{\varepsilon\} = [\partial]^T ([N][\Delta]) \tag{A.19}$$

substituting (A.16) into (A.19)

$$\{\varepsilon\} = [B][\Delta] \tag{A.20}$$

APPENDIX B

EXPERIMENTALLY IDENTIFIED MODES

Tables B.1, B.2 and B.3 show the resonant frequencies identified under different load conditions from frameworks B, C and D respectively. Note that the rows of the tables do not necessarily represent correspondence of modes.

	Load Case			
Mode	**0**	**1**	**2**	**3**
1	45.60	42.86	39.69	36.87
2	69.01	81.5	89.95	94.67
3	92.17	92.99	94.57	96.11
4	125.27	121.27	115.43	111.05
5	129.87	136.01	141.78	149.83
6	179.69	184.59	184.23	182.08
7	197.41	195.60	192.87	190.05
8	209.61	221.52	204.22	235.60
9	231.96	235.19	229.10	240.24
10	252.71	252.64	238.28	249.66
11	288.23	286.38	250.85	281.32
12	315.04	313.42	283.67	305.54
13	353.82	348.50	308.85	335.27
14			341.55	

Table B.1 – Identified Resonant Frequencies (Hz); Frame B

	Load Case			
Mode	**0**	**1**	**2**	**3**
1	44.13	41.96	39.21	37.07
2	91.18	82.96	89.26	94.24
3	126.43	91.25	93.01	95.31
4	133.98	122.33	116.82	113.36
5	196.30	140.56	147.47	155.40
6	209.84	184.28	183.92	183.27
7	230.04	194.42	192.12	189.92
8	250.80	219.33	225.87	200.93
9	318.37	233.63	236.55	232.02
10	346.49	253.36	251.98	239.03
11		316.57	312.02	251.28
12		343.71	338.70	309.05
13				335.40

Table B.2 – Identified Resonant Frequencies (Hz); Frame C

	Load Case			
Mode	**0**	**1**	**2**	**3**
1	45.14	42.06	39.24	36.77
2	92.14	84.51	90.48	95.15
3	125.47	93.11	94.72	97.15
4	132.87	120.54	115.41	156.97
5	184.04	136.56	148.62	182.54
6	199.15	141.23	184.21	190.77
7	234.36	185.74	193.44	237.56
8	255.40	196.88	230.53	241.43
9	314.02	237.18	239.52	251.79
10	350.74	254.94	252.69	305.09
11		313.03	308.72	336.17
12		346.17	340.19	

Table B.3 – Identified Resonant Frequencies (Hz); Frame D